Physiological and molecular approaches to better understand early events triggered by water deficit in Arabidopsis roots

Yunji Huang

THÈSE POUR OBTENIR LE GRADE DE DOCTEUR DE L'INSTITUT AGRO MONTPELLER ET DE L'UNIVERSITE DE MONTPELLIER

En Biologie, Intégrations, Diversité Adaptative des Plantes (BIDAP)
École doctorale GAIA – Biodiversité, Agriculture, Alimentation, Environnement, Terre, Eau
Institut des Sciences des Plantes de Montpellier (IPSiM)

Approches physiologiques et moléculaires pour mieux comprendre les évènements précoces déclenchés par le déficit hydrique dans la racine d'Arabidopsis

Présentée par Yunji HUANG
Le 26 octobre 2023

Sous la direction de Christophe MAUREL
Et l'encadrement de Yann BOURSIAC

Devant le jury composé de

Mme. Marie-Béatrice Bogeat-Triboulot, Chargée de Recherche, Nancy	Rapporteur
M. Benoît Landrein, Chargé de recherche CNRS, Lyon	Rapporteur
Mme. Leslie Sieburth, Full professor, University of Utah Salt Lake City	Examinatrice
M. Thierry Simonneau, Directeur de recherche INRAE, Montpellier, Président du Jury	Examinatrice
M. Yann BOURSIAC, Chargé de recherche INRAE, Montpellier	Encadrant de thèse

UNIVERSITÉ DE MONTPELLIER

L'INSTITUT agro Montpellier

Abstract

Water availability stands as one of the most important limiting factor influencing crop productivity. Unraveling the mechanisms governing plant perception of water deficit has become crucial for agriculture, particularly in the context of frequent drought events due to climate change. Plant water potential is primarily composed of two biophysical parameters, the turgor potential (P) and the osmotic potential (Π), that will determine water movements in the soil-plant-atmosphere continuum. Here, decline in external Π and P reduction caused by mild water deficit (MWD, where cortical cells in the elongation zone of the primary root maintained turgidity) were considered as input signals, while early changes in gene expression was taken as a readout. To study the whole-genome transcriptional responses to variations in Π and P, water deficit was induced by treatments of the root with various osmolytes: NaCl, sorbitol, polyethylene glycol 8000 and ethylene glycol (EG), into the hydroponic solution. To further explore the regulatory mechanism of gene expression, we observed the effects caused by the transcriptional inhibitor cordycepin and genetic knockouts of components of mRNA decay pathways. Finally, we aimed at developing Π- and P- reporters, for which we used the regulatory elements (promoter and 3'UTR) of Π- and P- correlated genes to drive the expression of reporters.

Transcriptomic analysis revealed a few Π- and P- correlated genes. Under MWD treatments, the diffusing solute EG provoked less P reduction, thereby allowing us to distinguish quantitative correlations to Π from correlations to P. A P-correlated *At1G64640* (*ENODL8*) and Π-correlated gene *At3G14440* (*NCED3*) were studied in more details. Extending the correlations to more severe treatments and over time showed that plasmolysis of cortical cells altered their response pattern, and that *ENODL8* was probably a true P-correlated gene under MWD treatments, while *NCED3* only exhibited a quantitative response to changes in P in the first 30 min. Manipulating their promoter activity and mRNA degradation showed that both *ENODL8* and *NCED3* expressions were regulated by water deficit at both transcriptional and post-transcriptional levels.

Studying Sluc signals in transgenic plants expressing a *pNCED3::Sluc-3'UTR* construct in response to water deficit demonstrated that this construction could be used as an osmo-reporter in Arabidopsis. Analyzing correlations between Sluc signal and Π or P suggested that, during a long-term treatment, Sluc signal in plants report changes in the external Π, while at the early stage of treatments (30-60 min), Sluc signal report variations in P caused by MWD. Combined with the promoter activity of *ENODL8*, our findings suggest that the perception site may be located in the elongation and meristem zones under MWD, and in the hypocotyl and cotyledons under SWD. Treating plants expressing the osmo-reporter with fluridone, an inhibitor of ABA synthesis and ISX, a compound impairing cell wall integrity showed that initiation of its response was independent of those.

In conclusion, our work showed that reduction of P and Π caused by water deficit governs gene expression at both transcriptional and post-transcriptional levels. We also provide two reliable P- and Π- marker genes, and developped an "osmo-reporter".

Key words: Water deficit, Arabidopsis, water potential, turgor potential, osmotic potential, osmosensing, genetic reporter, promoter, mRNA decay

Résumé

La disponibilité de l'eau constitue l'un des facteurs limitants les plus importants influençant la productivité des cultures. Démêler les mécanismes régissant la perception du déficit hydrique par les plantes est devenu impératif pour l'agriculture, en particulier dans le contexte de fréquentes sécheresses dues au changement climatique. Le potentiel hydrique des plantes est principalement composé de deux paramètres biophysiques, le potentiel de turgescence (P) et le potentiel osmotique (Π), qui vont déterminer les mouvements de l'eau dans le continuum sol-plante-atmosphère. Ici, la diminution du Π externe et la réduction du P provoquée par un léger déficit hydrique (MWD, où les cellules corticales de la zone d'élongation de la racine primaire maintenaient la turgescence) ont été considérées comme des signaux d'entrée, tandis que les premiers changements dans l'expression des gènes ont été considérés comme des signaux de sortie. Pour étudier les réponses transcriptionnelles du génome entier aux modifications de Π et P, un déficit hydrique a été induit par des traitements de la racine avec divers osmolytes : NaCl, sorbitol, polyéthylène glycol 8000 et éthylène glycol (EG), dans la solution hydroponique. Pour explorer le mécanisme de régulation de l'expression des gènes, nous avons observé les effets provoqués par la cordycépine, un inhibiteur de la transcription, et l'inactivation génétique des composants des voies de dégradation de l'ARNm. Enfin, nous avons cherché à développer des rapporteurs de Π- et P-, pour lesquels nous avons utilisé les éléments régulateurs (promoteur et 3'UTR) des gènes corrélés Π- et P- pour piloter l'expression des rapporteurs.

L'analyse transcriptomique a révélé quelques gènes corrélés aux Π et P. L'EG, un composé qui diffuse rapidement dans la cellule, nous a permis de distinguer les corrélations quantitatives avec Π des corrélations avec P. Un gène *At1G64640* (*ENODL8*) corrélé à P et un gène *At3G14440* (*NCED3*) corrélé à Π ont été étudiés plus en détail. Les corrélations avec des traitements plus sévères et au fil du temps ont montré que la plasmolyse des cellules corticales modifiait leur dynamique de réponse, et qu'*ENODL8* était probablement un véritable gène corrélé à P tandis que *NCED3* ne présenterait une réponse quantitative aux changements de P que durant les premières 30 minutes. La manipulation de leur activité promotrice et de la dégradation de l'ARNm a montré que les expressions d'*ENODL8* et de *NCED3* étaient régulées par un déficit hydrique aux niveaux transcriptionnel et post-transcriptionnel.

L'étude des signaux Sluc dans des plantes transgéniques exprimant une construction *pNCED3 :: Sluc-3'UTR* en réponse à un déficit hydrique a démontré que cette construction pourrait être utilisée comme osmo-rapporteur chez Arabidopsis. L'analyse des corrélations entre le signal Sluc et Π ou P a suggéré que, lors d'un traitement à long terme, le signal Sluc dans les plantes signale le Π externe causé par le déficit hydrique, tandis qu'au début du traitement (30 à 60 min), le signal Sluc signale des variations de P. Combinés à l'activité promotrice d'*ENODL8*, nos résultats suggèrent que le site de perception pourrait être situé dans les zones d'élongation et de méristème sous MWD, et dans l'hypocotyle et les cotylédons sous SWD. Le traitement des plantes exprimant l'osmo-rapporteur avec du fluridone, un inhibiteur de la synthèse d'ABA, et d'ISX, qui altère l'intégrité de la paroi cellulaire, a montré que l'initiation de sa réponse était indépendante de ces facteurs.

En conclusion, nos travaux ont montré que la réduction de P et Π provoquée par un déficit hydrique régit l'expression des gènes aux niveaux transcriptionnel et post-transcriptionnel. Nous fournissons également deux gènes marqueurs P et Π fiables, ainsi qu'un « osmo-rapporteur ».

Mots clés: Déficit hydrique, Arabidopsis, potentiel hydrique, potentiel de turgescence, potentiel osmotique, osmosensibilité, rapporteur génétique, promoteur, dégradation de l'ARN messager.

Remerciements

Bienvenue enfin, le moment des remerciements, le calme après la tempête. C'est avec une grande émotion que je m'apprête à prononcer quelques mots, certes non exhaustifs, pour remercier les personnes qui, de près ou de loin, m'ont accompagné sur ce beau chemin.

Tout d'abord, je tiens à remercier les rapporteurs de ma thèse, Marie-Beatrice Bogeat-Triboulot et Benoit Landrein, qui ont pris le temps de lire et d'examiner mon manuscrit. Je souhaite également exprimer ma gratitude envers les autres membres du jury, Thierry Simonneau et Leslie E Sieburth, pour avoir accepté d'évaluer mon travail.

Je tiens également à remercier les membres de mon comité de thèse, Sandrine Ruffel, Gabriel Krouk, François Parcy et François Tardieu, qui ont suivi mon travail de thèse au cours des quatre dernières années, m'aidant à établir les objectifs de ma recherche et m'encourageant dans la réussite de mes travaux.

Un grand, grand merci va tout particulièrement à mon directeur de thèse, Christophe Maurel, et à mon superviseur direct, Yann Boursiac. En eux, j'ai trouvé de formidables mentors. Je remercie Christophe pour ses sourires ensoleillés chaque jour, ainsi que pour ses précieux conseils et discussions lors des réunions de laboratoire. Je remercie Yann pour toutes les heures passées à débriefer dans son bureau (parmi les moments les plus enrichissants), pour toute l'aide apportée concernant la langue française, pour m'avoir enseigné à développer ma pensée scientifique et à avoir plus confiance en mes idées. Je tiens également à le remercier d'avoir accepté le défi de m'apprendre à écrire en anglais, ce qui s'est avéré être un moment très agréable pour moi, au cours duquel j'ai pu beaucoup apprendre. Compte tenu de la longue liste de personnes à remercier, je n'en dirai pas plus, même s'il y aurait de nombreuses autres leçons à souligner.

J'aimerais maintenant prendre le temps de remercier les membres de l'équipe AQUA en constante expansion ! Tout d'abord, je tiens à remercier mes camarades de laboratoire Mattia Adamo et Louai Rishmawi. Merci pour votre soutien scientifique, moral et quotidien, merci de m'avoir aidé et d'avoir conversé avec moi. En particulier, merci à Mattia de m'avoir aidé à trouver un appartement approprié et de s'être occupé de moi lorsque j'étais malade. J'ai hâte de vous retrouver en Chine. Merci à Amandine Crabos pour son soutien technique infaillible, en particulier pour sa grande contribution à la détection du transcriptome et de la pression de turgescence dans notre premier article. Merci à Colette Tournaire pour ta patience et ta gentillesse tout en m'aidant à résoudre les problèmes. Merci à Philippe Nacry d'avoir toujours pris le temps de répondre à toutes mes questions plus ou moins diverses. Merci à Xavier Dumont, toujours plein d'énergie et prêt à la transmettre. Merci à Alexandre Martinière pour ses précieux conseils et discussions, ainsi que pour ses visites dans notre bureau, "ah, juste pour voir Lucille" ;). Merci à Fabrice Bauget pour son aide et sa gentillesse. Merci à Enric Zelazny pour ses précieux conseils et sa gentillesse. Merci à Véronique Santoni pour ses conseils scientifiques et sa disponibilité. Merci à Lionel Verdoucq pour ses questions spirituelles et sa gentillesse. Merci à Jeonghua pour sa gentillesse et nos conversations quotidiennes. Merci à Kasir pour sa gentillesse et nos discussions. Merci à Arthur pour son aide dans l'analyse des images de luciférase, sa gentillesse et ses conseils. Merci à Laura pour son soutien technique, sa gentillesse et nos bonnes conversations. Merci à Armelle pour tout son soutien et sa gentillesse. Merci à Hela pour sa disponibilité et ses informations. Merci à Anas pour ses cours d'arabe et sa gentillesse. Merci à Jessica pour sa gentillesse.

Un grand merci à mes collègues de bureau. Tout d'abord, il y avait Marija, ma première voisine de bureau. Merci pour tous les conseils, le soutien et les moments de détente bien mérités. Ensuite, est venue Virginia. Merci pour ta curiosité, ta convivialité et tes suggestions. Puis est arrivée Lucille (celle qu'Alex cherche désespérément). Un merci spécial à Lucille, nous sommes des "camarades" dans les tranchées et avons passé plus de trois ans ensemble au bureau. Je suis très heureux que nous ayons rédigé nos thèses en même temps, cela a rendu tout

cela plus amusant. Merci aussi de m'avoir emmené à l'hôpital lorsque j'étais malade en pleine nuit (hhh, grâce à l'aide de ton gentil petit ami aussi). Et enfin, Omar est arrivé, mon dernier voisin de bureau, avec son grand sourire et sa gentillesse infaillible, pour compléter cette petite famille qui se soutient mutuellement chaque jour.

Un grand merci à mes compatriotes et collègues, Jing, Fei, Xue Lian et Mei Jie, qui m'ont soutenu dans les expériences, les discussions, l'analyse des données et la vie quotidienne. Vous êtes mes amis les plus proches en France et mes meilleurs amis dans cette vie. En particulier, un immense merci au couple Jing et Fei (j'ai raté leur mariage en Chine pendant que j'écrivais ma thèse), nous nous sommes connus il y a huit ans et avons étudié pour un master dans le même laboratoire. Merci pour votre compagnie, votre générosité et votre chaleureux accueil quand je suis arrivé en France.

J'aimerais maintenant remercier l'équipe technique de l'IPSiM sans laquelle il aurait été difficile de faire pousser les plantes en chambre de culture et en serre. Je tiens à remercier Hugues, Rogatien, Jeff, Thierry et Jose pour leurs sourires, leur gentillesse et leur aide. Et merci à Franck d'avoir été le premier à déchiffrer mon français pour faire des achats au magasin et pour être si amical.

Un grand merci à Carine et Tou-Cheu pour leur disponibilité infaillible et leur gentillesse, pour m'avoir enseigné la microscopie, le clariostar et la caméra CCD, et pour m'avoir conseillé sur le développement de protocoles et de techniques. Merci aux doctorants et aux autres membres non permanents de l'IPSiM qui rendent l'environnement de travail agréable, solidaire et stimulant !

En bref, un grand merci à toute l'équipe de l'IPSiM, qui au fil des ans est devenue ma deuxième maison (ou plutôt ma première si l'on considère que j'ai passé beaucoup plus d'heures ici que chez moi) et qui n'aurait pas été la même sans les formidables personnes qui y vivent. Merci d'avoir rendu ce travail agréable et de m'avoir permis de me former à la fois sur le plan scientifique et personnel. Je pars avec l'affection de nombreuses personnes et de nombreux bons souvenirs. Je n'oublierai jamais ce merveilleux voyage en France.

首先，感谢我亲爱的祖国和我们伟大的中国共产党，您养育了千千万万的中华儿女，给予我们全方位的支持。感谢国家留学基金委员提供的留学资金，以及后续的支持和帮助。感谢父母，姐姐和姐夫对我博士生涯的理解，支持和帮助，尤其感谢姐姐和姐夫帮我照顾年迈的父母，让我能够专心致志的攻读博士学位，您们都是我最可爱的人。他们远在千里之外，跨越欧亚大陆，四年未成回家，我十分的思念您们。感谢我的 8 年老友和同事周婧师姐和高飞师兄的鼎力支持和帮助。感谢李雪莲师姐和王宇师兄，李美洁师妹和其他在法国相遇的师兄弟师姐妹，感谢你们的陪伴和支持。感谢我在中国的好朋友和老朋友，谢谢你们给我的帮助和支持！在本节中，我不会讲太多细节，但你们已经知道你们对我有多重要。

谨以此论文献给我未来的子孙

Table of Content

Abbreviations

ABA: Abscisic acid

ACC: 1-Aminocyclopropane-1-carboxylic acid

CW: Cell wall

CWI: Cell wall integrity

CWD: Cell wall damage

DCC: Differentiated columnella root cap cells

EG: Ethylene glycol

FRET: Förster resonance energy transfer

IAA: Indole-3-acetic acid

IDRs: Intrinsically disordered protein regions

ISX: Isoxaben

LR: Lateral root

Luc: Luciferase

MeJA : Methyl jasmonate

MWD: Mild water deficit

MPPR : mature part of primary root

P: Turgor potential

PEG: Polyethylene glycol

PM: Plasma membrane

PR: Primary root

Sluc: Short-lived version of luciferase

SOV: SUPPRESSOR OF VCS

SWD: Severe water deficit

VCS: VARICOSE

Π: Osmotic potential

Π-All: Π under all the conditions

Π-Turgid: Π under conditions where cortical cells maintained turgid

Ψ: Water potential

General Introduction

1. Background

Plants face various environmental challenges, including both biotic stresses, such as herbivore gnawing and pathogen attacks, and abiotic stresses, such as extreme temperatures and light, nutrient deficiency and water deficit (Suzuki et al., 2014). Animals respond to environmental changes by either escaping or employing tools. However, a single plant individual lacks the ability of using tools and is firmly rooted in a singular geographic region determined by its germination site. Consequently, plants must rapidly sense environmental changes and adapt by tuning the balance of resources allocation between growth and stress tolerance, or they won't be able to complete their life cycle. One axis in plant biology is to understand how plants can sense their environment.

Among environmental factors, water is one of the most limiting for plant growth and development. Water deficit is a common component overlapping with others during many abiotic stresses, such as salinity and drought (Osakabe et al., 2014). It is often characterized in plants by a reduction in turgor potential (P), stomatal closure and wilting (Osakabe et al., 2014). Severe water deficit (SWD) can lead to the arrest of photosynthesis, metabolic disturbances, dysfunction in sap movements, and eventually death. Given the profound impact of water deficit on agricultural and ecological systems, understanding its perception and unraveling plants responses holds immense importance.

2. Water status and water signal in plant cells

The plant cell can be viewed as an aqueous cytoplasm enclosed by a plasma membrane (PM) and a cell wall (CW). The PM permits the movement of small, uncharged molecules like water, but restricts the movement of many dissolved solutes (Kramer and Boyer, 1995). Consequently, when solute concentration increases on one side of the membrane, water moves through osmosis from the less concentrated compartment to the more concentrated one until the osmotic gradient is dissipated (**Fig 1**). The flow of water between compartments is determined by their water potential (Ψ), representing the potential energy of water per unit area compared to pure water (Kramer and Boyer, 1995). Water movement is driven by the Ψ gradient between those compartments, with water flowing from zones of high potential to low potential. This process continues until the cell and its surrounding space reach Ψ equilibrium. However, the presence of a rigid CW prevents excessive cell increase in volume (swelling) caused by water flow, as the wall resists deformation and maintains intracellular hydrostatic pressure (turgor) at several atmospheres, supporting the plant's upright shape (**Fig 1**) (Kramer and Boyer, 1995). Hence, the total Ψ of a cell comprises both osmotic potential (Π), influenced by the concentration of solutes

within the cell, and pressure potential, resulting from the pressure of the cytoplasm against the PM and then against the CW.

Decrease in soil Ψ reduces the osmotic gradient between the cell's apoplast and interior, thereby weakening or even reversing water uptake in plants. As a result, reduced water availability will not suffice to meet the plant's water demand, leading to plants experiencing a water deficit. Water deficit can be simulated in a controlled environment where plants grow by adding osmotically active compounds such as PEG, NaCl, or sorbitol. All of these treatments cause osmotic stress by reducing the external Ψ, but they have specific impacts on plants because of different property. PEG 8000 is a large hygroscopic molecule that has the ability to adhere to water molecules. In other words, it reduces Ψ primarily by inducing matric forces rather than osmotic forces (Juenger and Verslues, 2023). Besides, high concentration of PEG 8000 treatment cause cytorrhysis which is characterized by a cell collapse and "shrivel" caused by non-osmotic drought treatments, rather than plasmolysis, because it is not able to penetrate the pores of plant CW (Oertli, 1985). NaCl dissolves in water, forming Na^+ and Cl^+ ions, which can be absorbed by plants. NaCl treatment introduces additional ionic stress due to Na^+ accumulation in plants (Zhu, 2002). Sorbitol, as a major sugar in sorbitol-rich species, such as Pyrus, Malus and Prunus genera, can be absorbed and forming the boron-sorbitol complexes that are mobile in phloem of these species (Brown and Hu, 1996). Another "uncommon" osmoticum is EG, which is a small organic molecule that can easily cross the lipid bilayer and thus will induce little osmotic gradient across the membrane (Yamazaki et al., 1992).

In plants, osmotic stress translates into a variety of initial cellular events, such as CWI (cell wall integrity) perturbation, P reduction, or cell damage (Chen et al., 2020a; Zhang et al., 2022). SWD can result in plasmolysis and cell volume shrinkage (Lang et al., 2014; Wang et al., 2022). Then, these events are multi-fold amplified to trigger signaling cascades, such as "classic" ones involving Ca^{2+}, ABA, and/or protein phosphorylation. These signalings regulate gene expression, physiological responses, and biochemical reactions at the cellular and organ levels, thus allowing plant stress tolerance (Zhu, 2016).

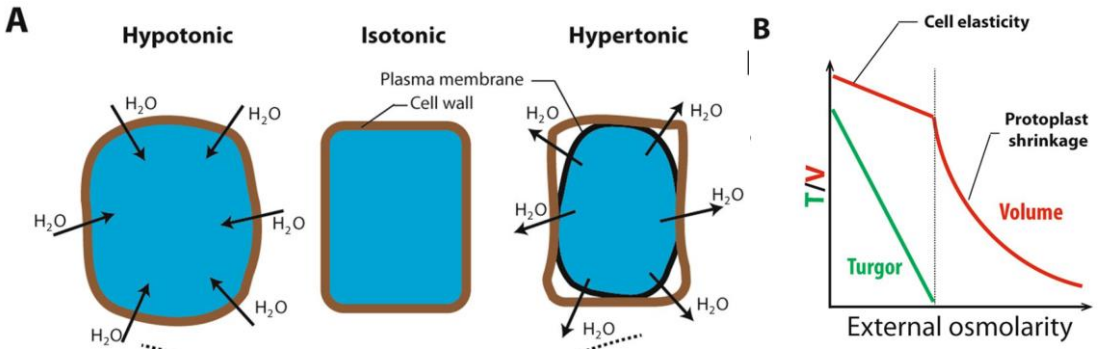

Figure 1. Nature of the osmotic signal and suspected sensing mechanisms.

(Figure and legend reproduced from (Gorgues et al., 2022)). A Drawing of the relation between osmotic, water fluxes and cellular volume regulation. A reduced (hypotonic) or increased (hypertonic) external osmolarity results in an influx or efflux of water, respectively. Depending on CW elasticity, these fluxes lead to changes in cellular volume. B Relative variations of cell turgor and volume in response to an increase of external osmolarity. In the absence of cellular osmoregulation, the turgor tends to decrease linearly with increasing osmolarity. In contrast, the cellular volume is expected to decrease in a two-phase mode, a quasi-linear mode as long as turgor is maintained in the cell, followed by a hyperbolic decay when turgor is absent.

3. Perception of osmotic stress in plants

Three essential stages—perception, signaling, and response—constitute the stress-responsive machinery in plants. Among them, stress perception is the first key stage in the responsive machinery of osmotic stress (Nongpiur et al., 2020). However, it remains unclear whether plants can directly feel osmotic stress or indirectly feel the initial cellular events triggered by it through mechanosensitive channels and protein kinases.

3.1 CWI monitoring in osmosensing

Plant CWs are elaborate, dynamic and extensible structures surrounding all plant cells. They provide structural support, protect cells against environmental changes as well as ensure containment of turgor (Colin et al., 2022). The integrity of CW is monitored by plant cells, and its impairment results in responses mediated by the CWI maintenance mechanism (Somerville et al., 2004; Vaahtera et al., 2019; Rui and Dinneny, 2020). CWI impairment is caused by cell wall damage (CWD) that occurs during plant cell growth and development, as well as under environmental stress. Studies have proposed that receptor-like kinases and ion channels are typically involved in sensing CWI impairment and activating responses such as hormone accumulation, such as JA, SA and ethylene, as well as ROS production and calcium signaling activation (Baez et al., 2022).

Several CW-sensors involved in CWI monitoring have been identified, although many issues remain to be addressed in this process (Wolf, 2017). For example, dysfunction of FERONIA (FER) lead to cells bursting during growth recovery under high-salinity treatments, a phenotype linked to defects in CW monitoring and repair (Feng et al., 2018). Meanwhile, FER can bind to pectin fragments in vitro, to rapid alkalinization factor (RALF) peptides and also interact with leucine-rich repeat extensins (LRXs). These features strongly suggest that FER could work as a CWI sensor and core component of CWI maintenance (Shih et al., 2014; Feng et al., 2018; Zhao et al., 2020). A recent study has suggested that the CWI sensor THESEUS1 modulates the mechanical properties of walls, turgor loss point and ABA biosynthesis and signaling (Bacete et al., 2022). Most of these identified sensors belong to the subfamily of Catharanthus roseus receptor like kinase 1-like (CrRLK1L), which

are CW-associated and PM-localized proteins, and counts 17 members in Arabidopsis (Lindner et al., 2012). These sensors harbor a transmembrane domain, and typically display a highly conserved cytoplasmic serine/threonine kinase domain, as well as an extracellular domain of 400 amino acids with varying length and sequence (Wolf, 2017). This extracellular domain is thought to bind to CW components and is thereby ideally suited to transduce CWI signals to the cell by mediating interactions between the CW and the interior of cell (Decreux et al., 2006; Feng et al., 2018). Besides CrRLK1L proteins, several other proteins belonging to the leucine rich repeat (LRR) and wall-associated kinase (WAK) receptor kinase families are proposed to bind CW components and trigger intracellular responses when the CWI is affected (Herger et al., 2019).

Ion channels may be involved in CWI monitoring too. The CW can act as a rigid anchor to which the PM is attached at the Hechtian reticulum (Yoneda et al. Plants 2020). CWI perturbations during hyperosmotic stress may alter cellular turgor pressure, resulting in membrane stretching because of these attachments, thereby opening the mechanosensitive Ca^{2+} channels (Hamann, 2012; Bacete and Hamann, 2020; Nongpiur et al., 2020). Furthermore, plasmolysis generates tensions on the CW at the PM–CW attachment sites, resulting in alterations of CW, such as mechanical bending and CWD (Feng et al., 2016). These alterations could be monitored by CW-monitoring proteins. Nongpiur et al proposed a model of CWI monitoring (**Fig. 2**) (Zhang et al., 2018; Nongpiur et al., 2020).

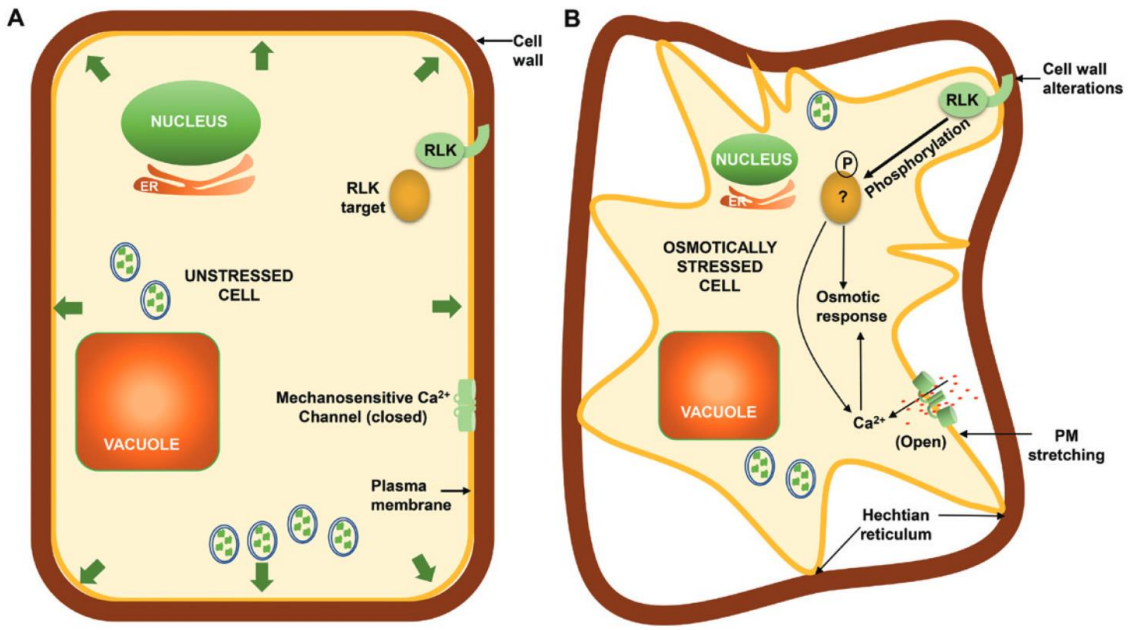

Figure 2: The role of the cell wall (CW) and associated proteins in osmosensing.

(Figure and legend reproduced from (Nongpiur et al., 2020)). (A) Under normal osmotic conditions, cell turgor pushes the PM towards the CW, where cellular homeostasis and cell shape are maintained. The CW is intact and CW-monitoring receptor-like kinases (RLK)

are inactive, while the stretch-activated mechanosensitive channels are also closed. (B) Osmotic stress induces changes in the CW and plasmolysis, which can also cause CW alterations through mechanical stress at the PM–CW adhesion sites. This could result in the activation of the CW-monitoring RLKs, which phosphorylate cytosolic target proteins and mediate signaling for osmotic stress responses such as CW repair, similar to the mechanism that operates during cell expansion. Additionally, plasmolysis would result in membrane stretching due to the attachment of the PM to the CW at the Hechtian reticulum. This results in the opening of mechanosensitive channels and an influx of Ca^{2+}, which stimulates the appropriate cell signaling for the osmotic stress response (Hayashi and Takagi, 2003; Hayashi et al., 2006; Feng et al., 2018).

3.2 Cell volume monitoring in osmosensing

Researches from animal cells have clearly clarified the importance of macromolecular crowding on intracellular biological processes and cell physiology (Mourão et al., 2014). Cell volume decreases because water molecules move out from plant cells upon hyperosmotic stress. Meanwhile, the presence of abundant macromolecules, such as lipids, nucleic acids and proteins, and the synthesis of compatible osmolytes lead to an increase in molecular crowding (Hoffmann et al., 2009). However, little is known about the mechanism by which plant cells sense the increase of molecular crowding during hyperosmotic stress. Cuevas-Velazquez et al. developed a FRET biosensor, SED1, by utilizing the Arabidopsis intrinsically disordered AtLEA4-5 protein to monitor rapid intracellular changes upon hyperosmotic stress. SED1 is highly sensitive to macromolecular crowding and displays large and near-linear osmolarity-dependent changes in FRET inside living bacteria, yeast, plant, and human cells (Cuevas-Velazquez et al., 2021). This indicates that disordered proteins have the potential to function as sensors of cell volume changes in response to hyperosmotic stress. Indeed, Wang et al. recently reported that SEUSS (SEU), a transcriptional factor, plays a key positive transcriptional regulator role in response to hyperosmotic stress in Arabidopsis (Wang et al., 2022). SEU quickly responds to hyperosmotic stress by rapidly coalescing into liquid-like nuclear condensates, and its intrinsically disordered region 1 (IDR1) is responsible for this condensation by undergoing conformational changes to adopt more compact states. SEU condensation confers plants with the ability to resist to osmotic stress, and its dysfunction remarkably impairs the expression of stress tolerance genes. The unique mechanism of bimolecular condensates in osmosensing by plants is depicted in **Fig. 3** (Sharma et al., 2023).

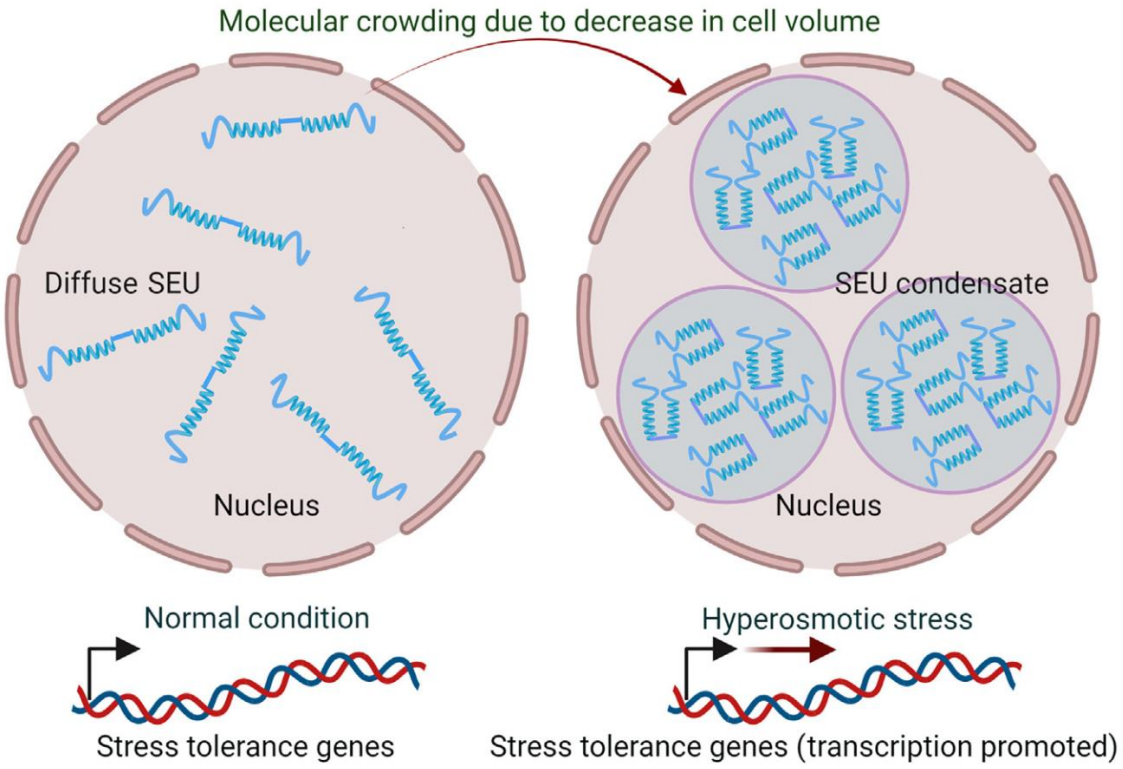

Figure 3: Mechanism of action of the SEUSS transcriptional coregulator (SEU).

(Figure and legend reproduced from (Sharma et al., 2023)). SEU is diffusely present in the nucleus under normal growth conditions. Hyperosmotic stress leads to cell shrinkage which in turn results in increased molecular crowding. This leads to the formation of SEU condensates, and phase-separated SEU then induces the transcription of stress-tolerance genes. Figure created with BioRender.com.

3.3 Ca^{2+} elevation in osmosensing

Transient elevations of cytosolic Ca^{2+} concentration have been detected and play a vital role in response to salinity and drought (Knight et al., 1997). More importantly, they're one of the earliest known detectable events which occur in response to osmotic stress (within seconds) (Yuan et al., 2014). Ion channels that link osmosensing to elevation of cytosolic Ca^{2+} are the best known, but only a few of them have been identified or proposed so far. Reduced hyperosmolality-induced $[Ca^{2+}]_i$ increase 1(OSCA1) is responsible of the hyperosmolality-induced transient elevations of Ca^{2+}. OSCA1 is a calcium channel located at the PM, and its dysfunction results in decreased Ca^{2+} influx in root cells and guard cells, reduced root growth and defective leaf transpiration in plants under hyperosmotic stress (Yuan et al., 2014). There are 15 OSCA1 homologs in Arabidopsis, similar to OSCA1, CSC1 (Calcium-permeable Stress-gated cation Channel 1, also named OSCA1.2) is responsible of transient changes in Ca^{2+} in response to osmotic stress (Hou et al., 2014). Meanwhile, OSCA1 and its paralog OSCA3 are mechanosensitive channels that respond to membrane tension trigered by osmotic stress (Zhang et al., 2018). A putative mechanism for their function as sensors has been proposed by analyzing

the structure of OSCA1 family proteins in Arabidopsis thaliana and Oryza sativa (rice)—that is, the decreased turgor pressure under hyperosmotic stress reduces the lateral tension on the membrane lipid bilayer, causing the OSCA ion channels to open and enabling Ca^{2+} transport into the cell (Jojoa-Cruz et al., 2018; Liu et al., 2018; Maity et al., 2019). Nongpiur et al. proposed a simplified version of the (osmo) mechanosensing mediated by OSCA1 according to Zhang's description (**Fig. 4**) (Zhang et al., 2018; Nongpiur et al., 2020). In addition, Jiang et.al identified MOCA1, a glucuronosyltransferase for glycosyl inositol phosphorylceramide (GIPC) sphingolipids in the PM. MOCA1 is crucial for Ca^{2+} spikes and waves under salt stress by a specific binding of Na^{+} that will enable gating Ca^{2+} influx channels (Jiang et al., 2019). .

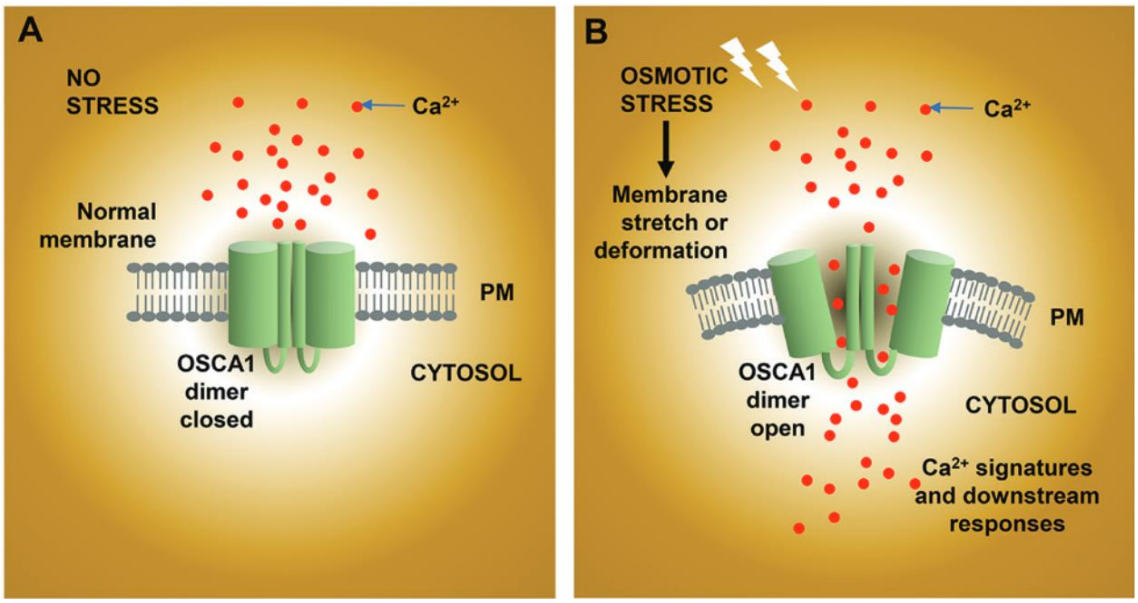

Figure 4: Mechanosensitive calcium channels in osmosensing.

(Figure and legend reproduced from (Nongpiur et al., 2020)). (A) Under non-stress conditions, the PM is not stretched and the mechanosensitive channels (such as OSCA1, OSCA3, or CSC1, which function as dimers) remain closed, keeping extracellular Ca^{2+} from entering the cytosol. (B) Under osmotic stress, the PM is bent and stretched, most probably due to plasmolysis, leading to a mechanically induced change in channel conformation. This opens the pores of the dimeric mechanosensitive calcium channels, leading to an influx of Ca^{2+} into the cytosol. (Based on (Zhang et al., 2018)).

3.4 ABA accumulation in osmosensing

ABA accumulation in plants is tightly controlled by synthesis, degradation, metabolism, (de)conjugation and transport because of its essential function in growth and development, as well as in response to abiotic stresses (Chen et al., 2020b). Although several putative osmosensors have been identified in plants, the mechanisms that link osmosensing to ABA accumulation is unclear. AHK1 can functionally complement SLN1 (a yeast osmosensing HK) in yeast and enhance osmotic stress resistance in Arabidopsis (Urao et al., 1999; Tran et al.,

2007). Under osmotic stress, *ahk1* mutants showed a lower ABA content and the expression of *NCED3*, which encodes 9-cis-epoxycarotenoid dioxygenase, a key enzyme in the biosynthesis of abscisic acid, while its overexpression lines showed opposite results (Wohlbach et al., 2008). This suggested that *AHK1* works upstream of *NCED3* induction, which occurs within minutes of the onset of osmotic stress. However, Sussmilch reported that leaf turgor loss triggers *de novo* ABA biosynthesis and induces *NCED3* expression within 5 min, but AHK1 does not play an indispensable role as a turgor-sensor within this pathway (Sussmilch et al., 2017). Therefore, there are contradictory studies regarding the function of AHK1 as an osmosensor. It is possible that there are proteins with redundant functions or which work under specific conditions or in specific tissues. Nevertheless, Nongpiur et al. proposed a possible model for an osmosensing mechanism mediated by AHK1 in Arabidopsis according to the osmosensing pathway mediated by the TCS in yeast (**Fig. 5**) (Nongpiur et al., 2020).

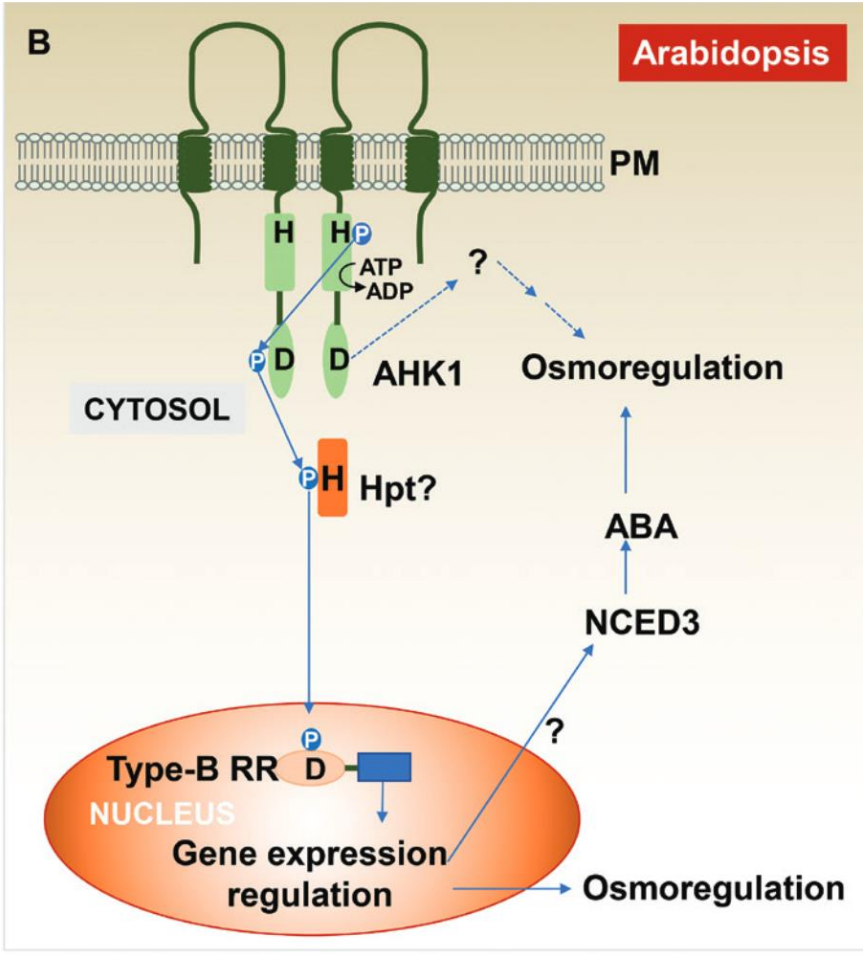

Figure 5: The proposed two-component histidine–aspartate phosphorelay operational in the osmotic stress response in Arabidopsis.

(Figure and legend reproduced from (Nongpiur et al., 2020)). Osmotic stress leads to the autophosphorylation of AHK1, which transfers

the phosphoryl group to a HPT (most likely AHP2) which then transfers the phosphoryl group to Type B response regulators (RRs). Type B RRs have a myb-DNA binding domain and could potentially function as transcription factors to regulate the expression of many stress-responsive genes, such as NCED3, which is the rate-limiting enzyme in ABA synthesis. ABA signaling results in the regulation of a large number of transcription factors, which further regulate the expression of genes involved in osmoregulation through the synthesis and accumulation of osmolytes such as proline (Urao et al., 2000; Hwang et al., 2002; Wohlbach et al., 2008; Fujita et al., 2011; Kumar et al., 2013).

4. Signaling of plants responses to osmotic stress

Stress perception triggers multiple signal transductions, including various combination of secondary messengers such as Ca^{2+}, ROS, ABA, phospholipids and nitric oxide, and post-translational modifications of proteins such as dephosphorylation, phosphorylation, ubiquitylation and oxidation, as well as systemic signal such as ROS-Ca^{2+} waves, hydraulic signal and electrical signals (Zhu, 2016; Zhang et al., 2022). In this section, we focus on Ca^{2+} signaling, ROS signaling, systemic signaling and protein phosphorylation, which are major and well-known features of signal transduction in plants in response to osmotic stress.

4.1 Ca^{2+} signaling

When the plant senses stress, Ca^{2+} influx occurs through both the PM and organellar membranes, leading to Ca^{2+} spikes in the cytosol. These spikes exhibit cell type-specific and stress-specific patterns in terms of timing, intensity, and frequency (Zhang et al., 2022). Under salt stress conditions, Arabidopsis thaliana perceives a distinct cytosolic Ca^{2+} signal through the Salt Overly Sensitive (SOS) pathway. Consequently, this signal triggers the export of Na^{+} from root epidermal cells into the soil environment and from xylem parenchyma cells into the xylem vessels for long-distance transport to the leaves (Zhu, 2016). In the SOS pathway, SCaBP8 or SOS3 (an EF-hand Ca^{2+} binding protein) interacts with and activates SOS2, which is a member of the SnRK3 family of kinases, also known as the CIPKs (Zhu, 2016). Various SCaBP/CBL-CIPK complexes can be found in plants, further highlighting their significance in stress response pathways (Zhang et al., 2022). Apart from their involvement in regulatory proteins, Ca^{2+} signals can also be transduced to the calmodulin-binding transcriptional activators CAMTA1/2/3. These activators then bind to the promoters of CBF genes and activate their expression, facilitating cold stress responses (Kim et al., 2013). Zhu proposed that the elevation of Ca^{2+} caused by OSCA1 may activate CPKs and CBLs-CIPKs, while until now in Arabidopsis, only AtCBL1 has been clearly reported to be induced by drought and involved in drought tolerance (Cheong et al., 2003; Zhu, 2016).

4.2 ROS signaling

An essential characteristic in plant response to environmental challenges is the generation of reactive oxygen species (ROS), including H_2O_2, superoxide anion, hydroxyl radical, and singlet oxygen (Zhang et al., 2022). While ROS can become harmful to biomolecules when their abundances exceed the cellular detoxification capacity, they also play significant roles in ABA signaling (Klingler et al., 2010). ROS accumulation during osmotic stress does not depend on ABA accumulation induced by stress, but the production of H_2O_2 is clearly regulated by ABA signaling through SnRK2-mediated activation of NADPH oxidases RbohD/F (Zhang et al., 2022). Extracellular H_2O_2 is likely detected by GHR1 (specifically in guard cells) and leucine-rich repeat receptor kinases HPCA1 (found throughout the whole plant) in Arabidopsis, leading to the generation of Ca^{2+} signals through the activation of Ca^{2+} channels (Zhang et al., 2022). In guard cells, this Ca^{2+} signal is further transduced to downstream components such as Ca^{2+}-dependent protein kinases (CPKs/CDPKs), which can phosphorylate ABA-response effectors (Zhu, 2016). Consequently, osmotic stress-induced regulation of stomatal closure can be mediated by not only the ABA-PYL-PP2C-SnRK2 module, but also through an H_2O_2-HPCA1/GHR1-Ca^{2+}-CPK module. Furthermore, both signaling modules are interconnected: ABA triggers the generation of H_2O_2, which then inactivates ABI1 and ABI2, hence relieving inhibition of GHR1 mediated by ABI2 (Zhang et al., 2022).

4.3 Protein phosphorylation

Protein phosphorylation is a common and essential event in signal transduction during plant responses to environmental stimuli, as the protein phosphatase 2C (PP2C) family and SnRK2 protein kinase subfamily are key components in various stress signaling pathways (Zhang et al., 2022). SnRK2s are categorized into three subclasses: I, II, and III, and they play crucial roles not only in ABA-responsive regulation but also in ABA-independent regulation under drought stress responses (Soma et al., 2021). SnRK2s are divided into three subclasses: I, II, and III. Subclass III plays a pivotal role in ABA-dependent signaling pathways, while subclass II is also involved in ABA-dependent pathways (Mizoguchi et al., 2010). In contrast, subclass I SnRK2s are not activated by ABA (Soma et al., 2021). Here, we will focus on well-known subclass III and subclass I SnRK2s.

ABA-dependent phosphorylation signaling via subclass III SnRK2s

When plants experience water deficit, a significant accumulation of ABA occurs in plant cells. Subsequently, ABA receptors PYR/PYL/RCAR bind to ABA, forming ABA-PYR/PYL/RCAR complexes. These complexes release SnRK2s by competitively interacting with PP2C, which acts as an inhibitor of the kinase activity of subclass III SnRK2s in the absence of ABA (Zhu, 2016). The released SnRK2s are then activated either by autophosphorylation or by phosphorylation from other protein kinases (Soma et al., 2021). These three

components - PYR/PYL/RCAR, PP2C, and subclass III SnRK2 - are now well-established as core components involved in ABA sensing and signaling (Soma et al., 2021) (**Figure 6**). The ABA-dependent drought stress signaling pathway primarily involves three subclass III SnRK2s: SRK2D/SnRK2.2, SRK2E/SnRK2.6/OST1, and SRK2I/SnRK2.3. The srk2dei (snrk2.2/snrk2.6/snrk2.3) triple mutant exhibits severe ABA-insensitive viviparity, ABA-insensitive germination, and increased sensitivity to drought (Soma et al., 2021). One key target of phosphorylation by subclass III SnRK2s is the group A bZIP transcription factor (TF) ABA-RESPONSIVE ELEMENT BINDING PROTEIN/ABA-RESPONSIVE ELEMENT BINDING FACTOR (AREB/ABF). SnRK2s mediate the activation of AREB/ABF through multisite phosphorylation of conserved domains (Furihata et al., 2006). AREB/ABF TFs are responsible for regulating the expression of ABA-inducible genes in response to drought stress or ABA (Soma et al., 2021).

SnRK2s demonstrate activation in ABA-deficient and ABA-insensitive mutants, indicating that under drought stress, they can be activated by upstream kinases independently of ABA (Soma et al., 2021). Direct regulation of SnRK2 activity during osmotic stress has been attributed to B-type MPK KINASE KINASE (MAPKKK) Raf-like kinases (Soma et al., 2021). Among the B3 Raf-like kinases, three ARK/ANR homologs, namely M3Kδ1/RAF3, M3Kδ6/RAF5/SIS8, and M3Kδ7/RAF4, were identified as activators of subclass III SnRK2s in Arabidopsis (Takahashi et al., 2020). Moreover, RAF10, one of the B2 Raf-like kinases closely related to the B3 kinases, has the ability to phosphorylate and activate subclass III SnRK2s by releasing them from PP2Cs (Soma et al., 2021). These findings suggest that both B2 and B3 Raf-like kinases play roles in the activation of subclass III SnRK2s.

ABA-independent phosphorylation signaling via Subclass I SnRK2s

In Arabidopsis, five SnRK2s—SRK2A/SnRK2.4, SRK2B/SnRK2.10, SRK2G/SnRK2.1, SRK2H/SnRK2.5 and SRK2J/SnRK2.9—are categorized as subclass I SnRK2s (Hrabak et al., 2003). Interestingly, these SnRK2s display strong activation in response to osmotic stress but not to ABA (McLoughlin et al., 2012). Their kinase activities are augmented by dehydration stress, both prior to ABA accumulation and in ABA-deficient plants (McLoughlin et al., 2012). While subclass I SnRK2s play a role in the osmotic stress and cadmium response, the specific substrates of these kinases remain elusive (Kulik et al., 2012; McLoughlin et al., 2012). Recent interactome analyses revealed the interaction between subclass I SnRK2s and VARICOSE (VCS), a scaffold protein associated with mRNA-decapping complexes (Soma et al., 2017). Furthermore, under osmotic stress, mRNA decay of genes associated with subclass I SnRK2s was impaired in these plants. Conversely, the expression of several stress-induced genes decreased in both *srk2abgh* and VCS-knockdown plants compared to

wild-type plants under osmotic stress. These findings suggest that the subclass I SnRK2-VCS signaling module positively regulates the expression of drought stress-responsive genes through posttranslational regulation (Soma et al., 2017) (**Figure 6**).

During the early stage of osmotic stress, all functional subclass I SnRK2s undergo phosphorylation at the Ser-154 residue by unknown kinases (Soma et al., 2021). Recent findings identified three B4 Raf-like kinases, namely RAF18, RAF20, and RAF24, as the protein kinases responsible for phosphorylating Ser-154 of subclass I SnRK2s and activating them under osmotic stress. In a *raf18/20/24* triple mutant, the activities of subclass I SnRK2s under osmotic stress were significantly reduced (Soma et al., 2020). Interestingly, while the RAF18/20/24-subclass I SnRK2-VCS signaling module is well-conserved in seed plants, it is absent in moss (Soma et al., 2017; Soma et al., 2020), suggesting its evolutionary significance in enhancing adaptability to stress conditions in seed plants. Notably, subclass I SnRK2s contain a phosphatidic acid (PA)-binding domain (Alerasool et al., 2022), which implies that PA may regulate the kinase activity of these kinases.

In brief, subclass III SnRK2s activated by ABA, play a crucial role in regulating the expression of numerous stress-responsive genes at the transcriptional level and physiological responses during dehydration stress. On the other hand, subclass I SnRK2s are activated independently of ABA and in response to dehydration, precisely controlling the expression of stress-induced genes by governing the mRNA population. However, the osmosensors responsible for receiving the osmotic signal and triggering ABA accumulation or directly activating RAF-SnRK2 in an ABA-independent manner remain largely unidentified (Soma et al., 2021) (**Figure6**).

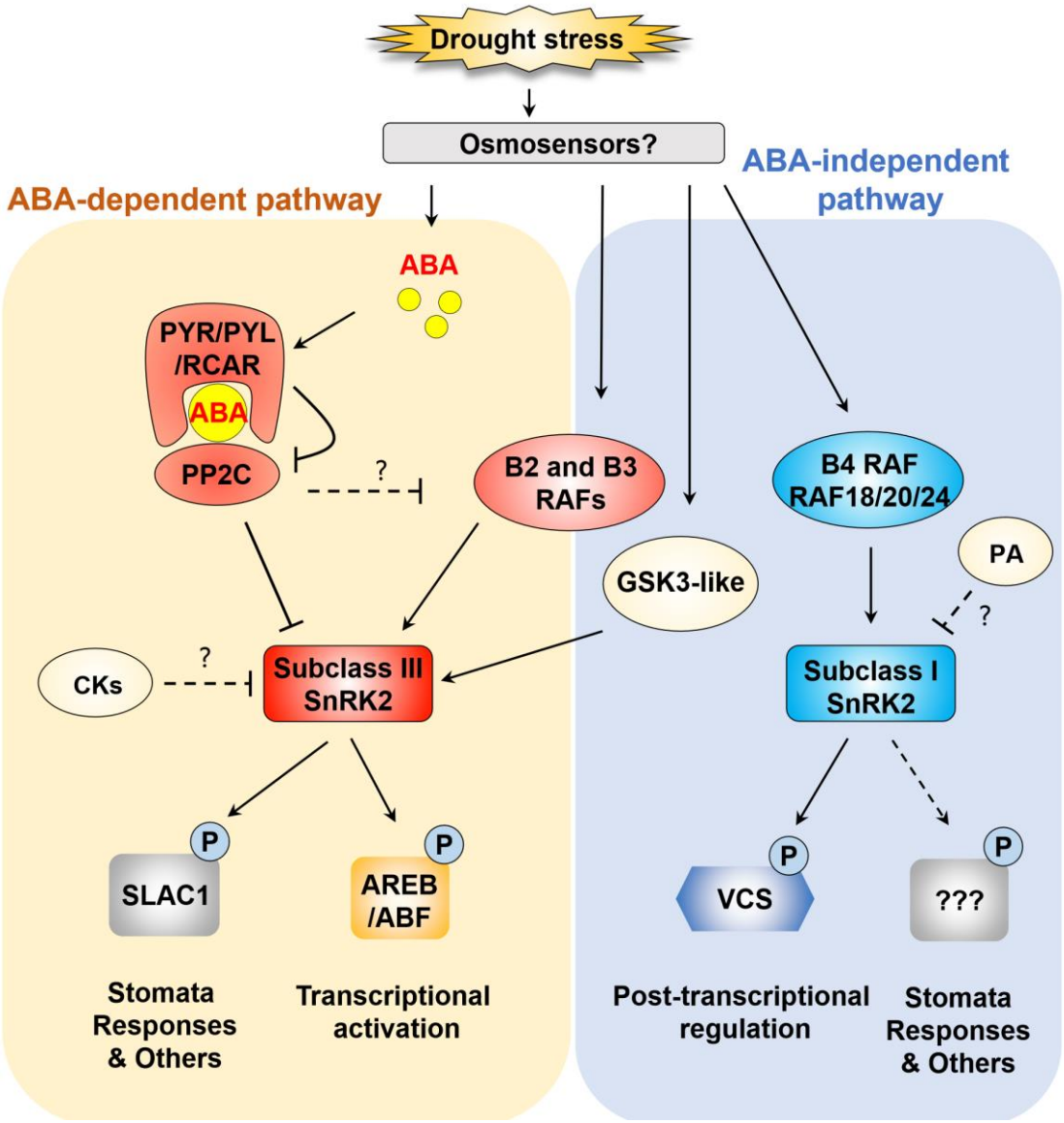

Figure 6: SnRK2-mediated drought stress signaling and gene expression.

(Figure and legend reproduced from (Soma et al., 2021)). Subclass III SNF1-related protein kinases 2 (SnRK2s) play key roles in abscisic acid (ABA) signaling under osmotic stress. Negative regulation of subclass III SnRK2s is released via inhibition of protein phosphatases 2C (PP2C) by ABA-pyrabactin resistance1/pyr1-like/regulatory components of ABA receptor (ABA-PYR/PYL/RCAR) complexes under osmotic stress. Subclass III SnRK2s are phosphorylated and activated by B-type Raf-like kinases and GSK3-like kinases in an ABA-independent manner. Activated subclass III SnRK2s phosphorylate a variety of substrates, including ABA-responsive element binding proteins/ABA-responsive element binding factor (AREB/ABF), to induce the expression of stress-responsive genes. ABA-unresponsive subclass I SnRK2s are quickly activated in response to osmotic stress in an ABA-independent manner. Osmotic stress-activated subclass I SnRK2s regulate mRNA decay by phosphorylating the mRNA-decapping activator VCS. The B4 Raf-like kinases RAF18, RAF20 and RAF24 are responsible for the activation of subclass I SnRK2s. Dashed lines indicate possible but unconfirmed routes.

4.4 Systemic signaling

Osmotic stress is also known to trigger systemic signaling in plants, which results in stress responses in unexposed tissues, leading to systemic acquired acclimation (Zhu, 2016). For instance, water stress applied to the root system resulted in the generation of ABA pools in the shoot (Christmann et al., 2005). Plant vascular systems are thought as the essential pathways of long-distance communication that allow plants to adapt to changes in internal and external environments at the whole plant level (Notaguchi and Okamoto, 2015). Here, we focus on the systemic signals involved in response to osmotic stress, including chemical signals (ABA, peptides, Ca^{2+} and ROS) and hydraulic signaling.

Early studies proposed the hypothesis that ABA generated in the roots undergoing rhizospheric stresses moves to the shoots to mediate stomatal closure as well as more general adaptive shoot responses (Jackson, 1993; Wilkinson and Davies, 2002). Subsequent studies reported a contradictory perspective that root-inflicted water deficit elicits directly shoot ABA generation and response which is sufficient and necessary for stomatal closure (Christmann et al., 2005; Christmann et al., 2007). Therefore, ABA does not appear to act as the long-distance signal when roots are suffering from water deficit. Later on, Takahashi et al. demonstrated that dehydration induces the production of a small peptide, CLE25, which moves through the vasculature from root to shoot where it activates ABA biosynthesis through its association with BAM RLKs in leaves, ultimately resulting in stomatal closure (Takahashi et al., 2018). Malone summarized that basipetal mass flows associated with certain signals can sweep elicitors from wound sites to the remainder of the plant at rates of about 7 mm/s (in maize) to 9 mm/s (in tomato) (Boari and Malone, 1993; Malone et al., 1993). CLE25 is a mobile molecule in the vascular tissues of Arabidopsis, its propagation speed is estimated to be about 10 mm/s which is consistent with other circulating molecules.

Ca^{2+} and ROS waves triggered by stress have been observed in transgenic plants by expressing calcium-sensitive fluorescent protein and luciferase reporter driven by a ROS responsive promoter, respectively (Miller et al., 2009; Choi et al., 2014). The formation of Ca^{2+} waves requires the vacuolar Ca^{2+} channel TPC1 while the formation of ROS waves depends on RbohD in vascular bundles (Miller et al., 2009; Choi et al., 2014; Zandalinas et al., 2020). Ca^{2+} and ROS waves can move at speeds exceeding 1 mm/s, tens of cells per second, and both of them have been demonstrated to trigger transcriptional responses in distal tissues (Miller et al., 2009; Choi et al., 2014). Zhu proposed a Ca^{2+}-ROS wave model in which ROS generated by NADPH oxidases triggers a cytosolic calcium signal to activate more NADPH oxidases via calcium responsive kinases, hence generating a self-propagating mutual activation circuit between Ca^{2+} and ROS signals (Zhu, 2016) (**Fig. 7**).

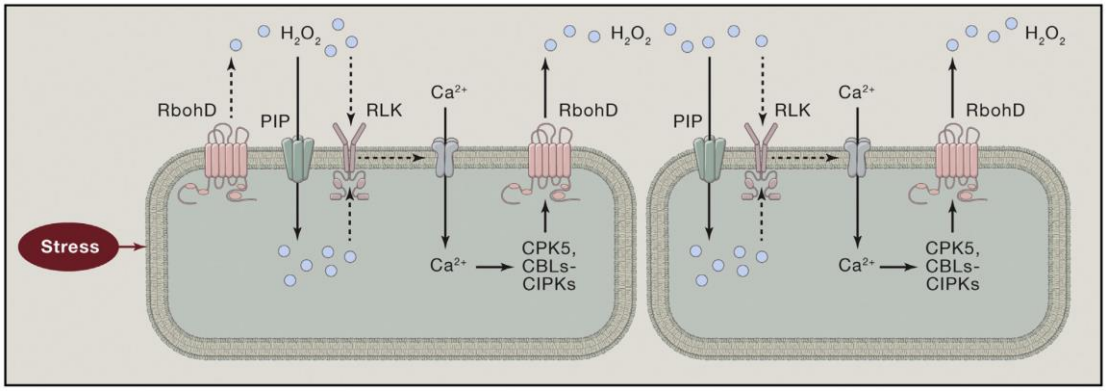

Figure 7: Model of Systemic Stress Signaling Local exposure to stress generates H_2O_2 and Ca^{2+} signals.

(Figure and legend reproduced from (Zhu, 2016)).The Ca^{2+} signal can activate CPKs and CBLs-CIPKs, which phosphorylate and activate RbohD. Activated RbohD generates H_2O_2 that diffuses through the CW to neighboring cells, where it induces a Ca^{2+} signal through RLKs like GHR1. H_2O_2 may activate Ca^{2+} signaling at the cell surface and may also enter the cell through PIP water channels and then activate Ca^{2+} signaling intracellularly. The mutual activation between the Ca^{2+} and H_2O_2 signals generates self-propagating calcium and ROS waves that can travel to distant tissues to cause systemic acquired acclimation responses. Dashed lines indicate postulated regulation.

Hydraulic signals are self-propagating changes in water (fluid) pressure, including changes in turgor pressure, pressure waves and mass flow (Huber and Bauerle, 2016). By this broad definition they are ubiquitous in plants, occurring throughout the continuous water phase in the apoplast between neighboring cells, across cell membranes, and within all hydrated cells (Malone et al., 1993). The front of pressure waves in xylem will propagate at up to the speed of sound (1500 m/s in water) (Malone et al., 1993), even between leaves, the front of the hydraulic signal induced by wound was shown to travel through the plant at rates of at least 10 cm/s (Malone, 1992). These finding suggest that hydraulic signals can be transmitted from the roots to the shoots immediately. A current model of hydraulic signaling of water deficit is the following: soil water deficit turns into a reduced Ψ in the roots, and especially in the stele, which elicits a hydraulic response moving up to the shoots, which precedes ABA synthesis and signaling, and a subsequent stomatal closure (Christmann et al., 2007). Moreover, it has been reported that finite control can be achieved via the hydraulic feedback loop alone, but for tighter control, other elements may be needed to link transpiration rate and guard cell osmotic pressure (Franks, 2004). Stahlberg proposed that electrical signal APs (action potentials) can be induced by increasing xylem pressure or turgor (Brenner et al., 2006). Long-distance turgor pressure changes caused by mechanical stresses, such as hypo-osmotic stress in root cells, induce the local activation of AtGLR3.3, a plant glutamate receptor-like channel that is required for systemic cytosolic Ca^{2+} elevation (Grenzi et al., 2023). Christmann et al. have

shown that ABA acts downstream of the hydraulic signal in communicating water deficit between shoot and root, but it is unknown how the biophysical signal is sensed to activate ABA signaling for stomatal closure (Christmann et al., 2007). Hydraulic forces generated in the vascular system of plants might stimulate stretch-activated sensors that elicit subsequent ABA signaling (Sukharev and Corey, 2004; Kung, 2005; MacRobbie, 2006). Moreover, these results have been confirmed by current studies where cytoplasmic Ca^{2+} transients occurred in response to mechanical perturbations and make it likely that such an increase is an early event in hydraulic signaling (Monshausen et al., 2009). Meanwhile, Ca^{2+} transients are also involved in early ABA responses therefore it is hard to discern Ca^{2+}-action downstream or upstream of ABA, or both (Miller et al., 2009; Kim et al., 2010). Ca^{2+} transients may then activate NADPH oxidase RBOH D thereby generating a ROS signal (Miller et al., 2009; Devireddy et al., 2018). Interestingly, ROS signals as well are also part of the ABA signaling pathway and include stimulation of NADPH oxidase by the ABA-activated SnRK protein kinase OST1 (Sirichandra et al., 2009; Joshi-Saha et al., 2011).

Altogether, these results suggest that hydraulic signals, an immediate long-distance signal during roots water deficit, have the ability to trigger various signaling, thereby integrative control physiological response in plants. A simplify model of long-distance signaling in plant stress response is depicted in **Fig. 8** (Takahashi and Shinozaki, 2019).

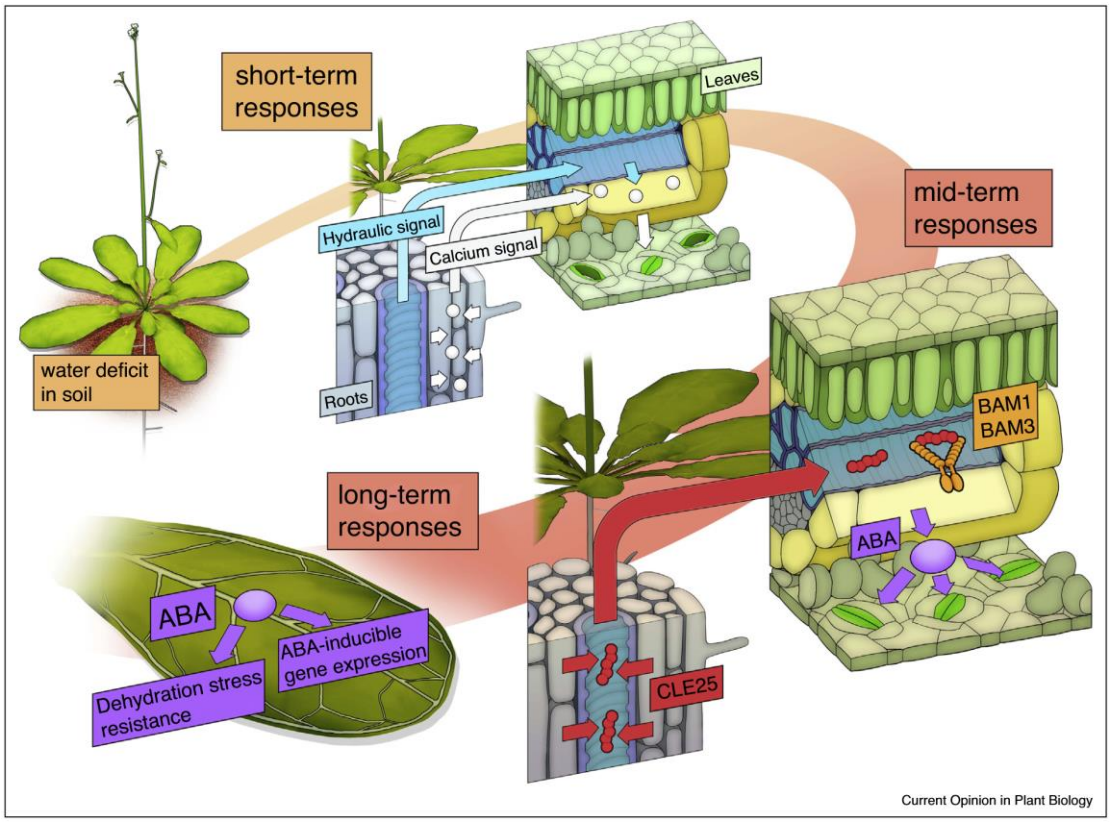

Figure 8: Spatiotemporal and stepwise responses at cellular, organ, and whole plant levels under abiotic stress.

(Figure and legend reproduced from (Takahashi and Shinozaki, 2019)).Stress responses and resistance among various organs are robustly regulated through several mobile signals at different times for adaptation to prolonged stress and/or varying environmental conditions. For example, hydraulic changes and calcium currents are thought to function rapidly, whereas the movement of peptides and phytohormones constitutes rather slow signals to amplify the expression of stress-inducible genes. Accumulated ABA plays important roles in stomatal response and the production of various types of osmolytes and cellular proteins that protect cells from dehydration. Plants integrate stress signals among distant organs through long-distance and/or cell-to-cell communications, which are crucial to respond to and tolerate abiotic stress at the whole plant level.

5. Transcriptional regulations of plant responses to osmotic stress

Stress-transduced signals induce genome-wide transcriptional reprogramming that result in changes in gene expressions and diverse protective mechanisms (Zhang et al., 2022). In plants, regulation of gene expression in response to osmotic stress by ABA-dependent pathway is the most well-known mechanism (Vishwakarma et al., 2017; Chen et al., 2020b). In addition, ABA-independent transcriptional regulatory mechanisms also play essential roles in dehydration stress responses (Soma et al., 2021). Various transcription factors (TFs) are involved in both processes and constitute an elaborate regulatory network which is indispensable for the correct expression of stress-responsive gene (**Fig. 9)** (Shinozaki and Yamaguchi-Shinozaki, 2007; Hrmova and Hussain, 2021).

5.1 ABA-dependent pathway

Transcriptional activation mediated by the 'abscisic acid (ABA)-activated SnRK2 protein kinases–ABA-responsive element (ABRE)-AREB/ABFs' signalling module is a crucial step in the expression of stress-inducible genes under osmotic stress conditions in Arabidopsis, known as ABA-dependent pathway (Furihata et al., 2006; Fujii et al., 2009; Fujii and Zhu, 2009; Fujita et al., 2009). Thousands of genes are transcriptionally regulated by salinity, drought and cold stress via ABA signaling, although many stress-responsive genes are also induced by an ABA-independent pathway (Zhu, 2016). The ABA-responsive cis-element (ABRE) ACGTGG/TC is present in the promoter regions of many ABA-regulated genes and is mainly recognized by bZIP-type transcription factors, AREBs/ABFs (Maruyama et al., 2012; Soma et al., 2021). Arabidopsis AREB1/ABF2, AREB2/ABF4 and ABF3 have conserved amino acid sequences that are phosphorylated by subclass III SnRK2s (SnRK2.2, SnRK2.3 and SnRK2.6) and regulating the expression of ABA- and drought-responsive genes through binding to the ABRE motif directly (Soma et al., 2021). However, some ABA-inducible genes do not harbor the ABRE motif in their promoter regions. For example, *MYC2* does not have an ABRE motif in its promoter, yet it can be strongly induced by ABA under various abiotic stresses (Abe et al., 2003). Moreover,

other TFs are also transcriptionally regulated through the ABA-dependent pathway, including MYB, HD-Zip and WRKY TFs (Hrmova and Hussain, 2021).

5.2 ABA-independent pathway

The expression of dehydration-responsive element-binding protein 2A gene (*DREB2A*) is induced by dehydration and osmotic stress treatments (Liu et al., 1998). DREB TFs belong to ABA-independent dehydration-responsive TFs and regulate a series of stress-responsive gene expressions in response to various abiotic stresses (salt, drought, heat and cold) by binding the dehydration-responsive cis-element (DRE) TACCGACAT in their promoter region (Soma et al., 2021). Moreover, sequence analysis of DREB2A uncovered that a negative regulatory domain (NRD), located in its central region, is crucial for the regulation of its transcriptional activity (Sakuma et al., 2006). Overexpressing *DREB2A* without the NRD fragment enhances plants' resistance to dehydration stress and stress-responsive gene expression (Soma et al., 2021).

The expression of many more genes changes later in the stress response, usually driven by TFs that display rapid early responses to stress. For instance, the expression of *CBFs* peaks at 1–3 h after cold treatment, while the downstream *COR* genes culminate at approximately 1 day (Medina et al., 2011). Under abiotic stress, the majority of late-responsive genes in Arabidopsis encode proteins with protective activities, such as detoxification enzymes and osmoprotectant biosynthesis enzymes (Zhang et al., 2022). Besides strengthening stress responses, negative feedback regulation also occurs at transcriptional regulation level. For instance, ABA weakens ABA signalling by inhibiting the transcription of some of its receptor genes during drought stress (Zhang et al., 2022). Combination of responsive-genes and their transcription level are strongly dependent on stress severity (Claeys et al., 2014).

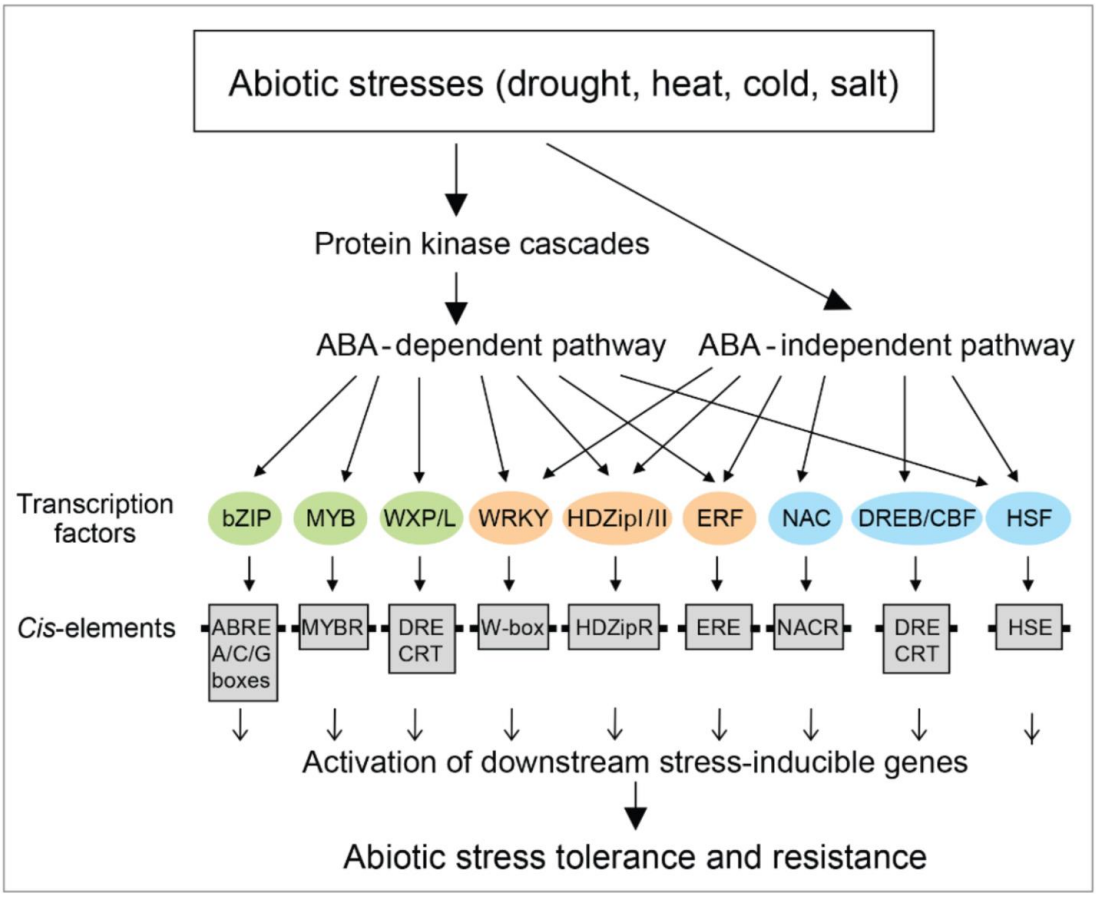

Figure 9: Biotic and biotic stresses are perceived by plants through ABA-dependent and ABA independent pathways or between cross-talks of these pathways (based on (Bi et al., 2016; Sornaraj et al., 2016; Bi et al., 2017)).

(Figure and legend reproduced from (Hrmova and Hussain, 2021)).Color coding differentiates between TFs that are controlled by ABA-dependent (green), ABA-independent (cyan) and ABA-dependent/independent (orange) pathways.

6 Transcripts degradation regulation

Besides transcriptional regulation, mRNA abundance is also controlled by transcripts degradation, which play an essential role in plant stress tolerance (Kawa and Testerink, 2017; Zhang et al., 2022). The expression of many stress-responsive genes is misregulated in *VCS*-knockdown plants which are defective mutants in mRNA degradation (Kawaguchi et al., 2004; Soma et al., 2017). This indicates that post-transcriptional regulations are involved in response to osmotic and salinity stresses. Indeed, many genes involved in response to stress, including osmotic stress, have been proven to be regulated by their mRNA stability (Romero-Santacreu et al., 2009; Maldonado-Bonilla, 2014; Steffens et al., 2015; Perea-Resa et al., 2016). In this section we will highlight pivotal steps controlling most mRNAs stability in cytoplasm, including deadenylation, mRNA decay and their regulations, which may serve as potential mechanisms for modulation under osmotic stress.

6.1 Deadenylation

Poly(A) tails are added co-transcriptionally in the nucleus and are necessary for the export of mature mRNAs into the cytoplasm, for their translational status and for their stability (Passmore and Coller, 2022) (**Fig. 10**). In all eukaryotes, the shortening of the 3' poly(A) tail, known as deadenylation, is the first critical and rate-limited step of mRNA decay machinery, and is mediated by deadenylases (Parker and Song, 2004; Doma and Parker, 2007; Garneau et al., 2007; Chen and Shyu, 2011). Three mRNA deadenylases have been identified in eukaryotic cells, including the poly(A)-specific ribonuclease (PARN), the two-subunit poly(A) nuclease 2 (PAN2)–PAN3 deadenylase, and the multi-subunit C–C chemokine receptor 4-negative on TATA (CCR4–NOT) complex (Yan, 2014).

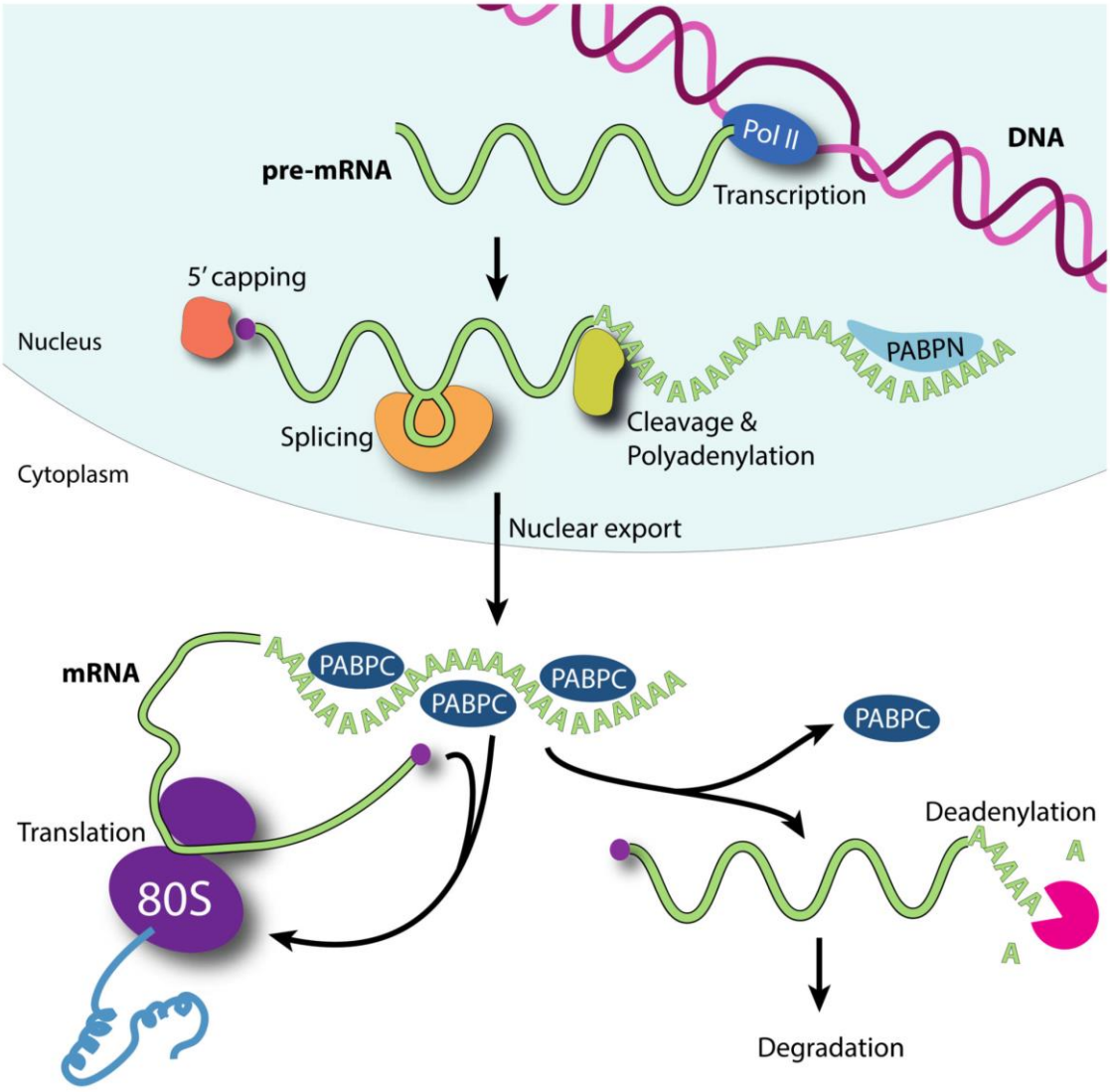

Figure 10: mRNA Poly(A) tails function as master regulators of gene expression in the cytoplasm.

(Figure and legend reproduced from (Passmore and Coller, 2022)). In the nucleus, pre-mRNAs are transcribed by RNA polymerase II (Pol II) and processed, including 5'-capping, splicing and 3'-cleavage and polyadenylation. Nuclear poly(A) binding proteins (PABPN)

function in the nucleus to control poly(A) tail addition. Mature, polyadenylated mRNAs are exported into the cytoplasm. Cytoplasmic poly(A)- binding protein (PABPC) binds poly(A) and promotes translation by the 80S ribosome. Poly(A) tails and PABPC also influence mRNA stability: removal or shortening of the poly(A) tail (deadenylation) releases PABPC and leads to mRNA degradation.

AtPARN performs deadenylation of a subset of embryonic transcripts in Arabidopsis and its dysfunction leads to embryo lethality (Chiba et al., 2004; Reverdatto et al., 2004). The expression of *AtPARN* is also induced by ABA, salt and osmotic stress (Nishimura et al., 2005). In addition, Ccr4-Not is a 0.5 MDa complex consisting of seven core subunits, including two exonucleases: an EEP-type exonuclease named Ccr4 (as known as CNOT6, CNOT6L) and a DEDD-type exonuclease named Caf1 (CCR4-ASSOCIATED FACTOR1, as known as Pop2, CNOT7 or CNOT8) (Tucker et al., 2001; Thore et al., 2003; Finoux and Séraphin, 2006). Dysfunction of either Caf1 or Ccr4 in yeast leads to impaired deadenylation (Daugeron et al., 2001; Tucker et al., 2001). In Arabidopsis, all the genes encoding the core subunits of CCR4-NOT are present and eleven *CAF1* genes have been found (Liang et al., 2009). AtCAF1a and AtCAF1b are involved in response to various environmental stimuli, typically by non-redundantly targeting different subsets of transcripts (Walley et al., 2010). The deadenylation activity of some CAF1 homologs in rice and Arabidopsis has been demonstrated in vitro (Liang et al., 2009; Chou et al., 2014). Meanwhile, overexpression of AtCAF1a and AtCAF1b from Arabidopsis or CaCAF1 from pepper has been shown to alter biotic stress responses in transgenic plants (Sarowar et al., 2007; Liang et al., 2009). Furthermore, PAN2-PAN3 was first found through fractionation of yeast extracts and it contains a DEDD/RNaseD-type exonuclease in its Pan2 subunit (Sachs and Deardorff, 1992; Boeck et al., 1996; Brown et al., 1996). Notably, The PAN2–PAN3 complex has not yet been identified in plants so far (Abbasi et al., 2013). Based on the above discoveries, Passmore and Coller proposed a model of deadenylation mediated by PAN2-PAN3 and Ccr4-Not (Passmore and Coller, 2022) (**Fig. 11**).

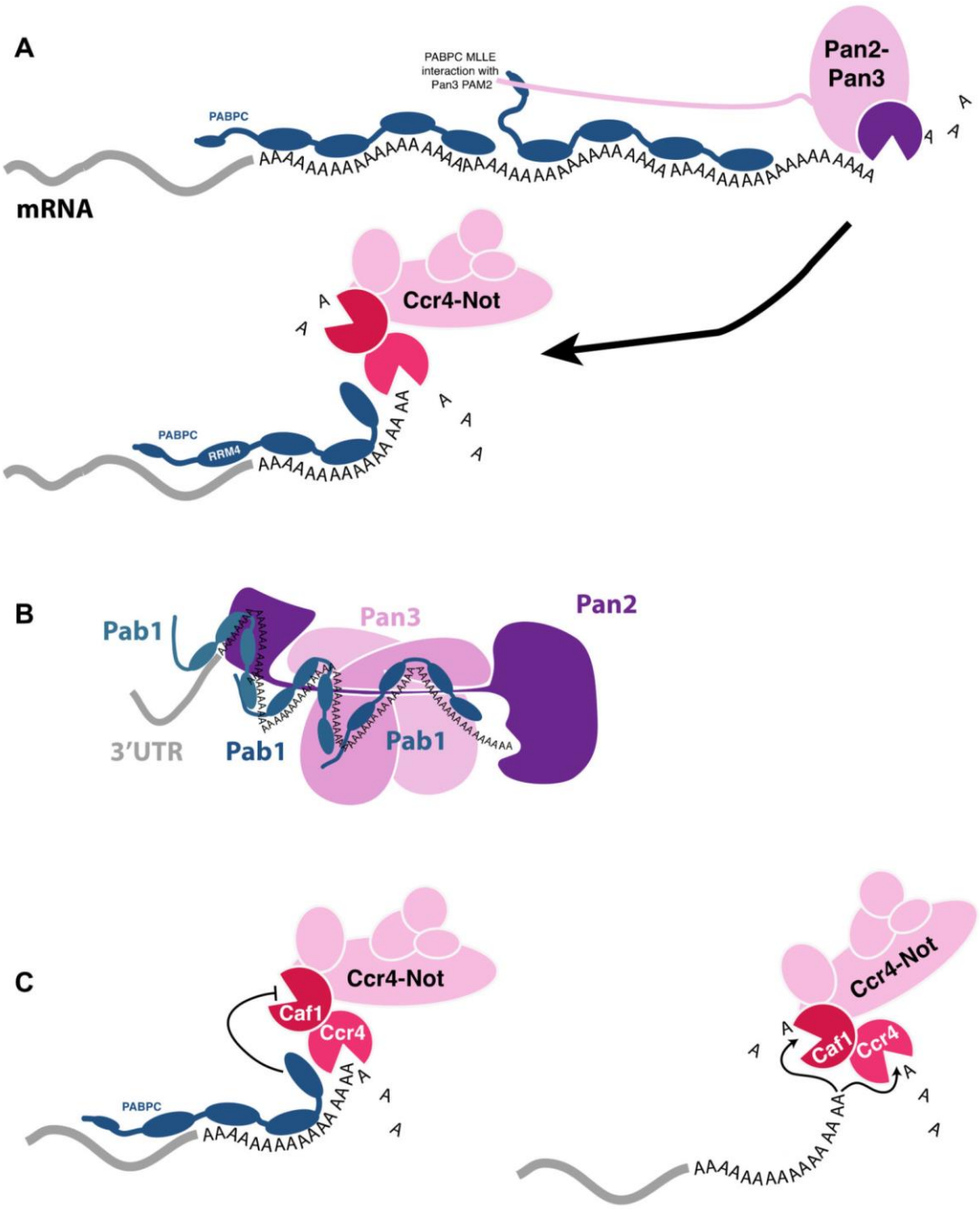

Figure 11: Deadenylation by Pan2-Pan3 and Ccr4-Not.

(Figure and legend reproduced from (Passmore and Coller, 2022)). A Sequential (or biphasic) model of deadenylation. In this model, PAN2-PAN3 preferentially removes the distal part of the poly(A) tail. A PABPC-interacting motif 2 (PAM2) within an intrinsically-disordered segment of Pan3 interacts with the C-terminal mademoiselle (MLLE) domain in PABPC. Ccr4-Not removes the poly(A) tail that is more proximal to the 3'-UTR. The most 5' PABPC protein may be positioned on the poly(A) tail such that its RRM4 is located on the 3'-UTR of the mRNA. B Model of the Pan2-Pan3-Pab1-poly(A) complex. A cryoEM structure (PDB 6R5K) (Schäfer et al., 2019) shows that PAN2-PAN3 contacts the interface between adjacent Pab1 molecules, providing an explanation for why it preferentially

functions on longer poly(A) tails. In the structure, three Pab1 molecules are bound to a 90 nt poly(A) tail. C Ccr4 is a general deadenylase that degrades poly(A), even when it is bound by PABPC. Caf1 is a specialized deadenylase that degrades naked poly(A) and is blocked by PABPC (Webster et al., 2018).

6.2 mRNA decay

In a textbook model of RNA decay from plants and metazoans, the poly(A) tail of cytoplasmic RNAs is first shortened to 10-12 nt before transcripts can undergo either 3'-5' mRNA decay (via the RNA exosome or the exoribonuclease SUPPRESSOR OF VCS (SOV)/DIS3L2), or 5'-3' mRNA decay which removes the 7-methyl guanosine cap followed by exoribonucleolytic decay by EXORIBONUCLEASE (XRN1 or XRN4) (Schoenberg and Maquat, 2012; Zhang and Guo, 2017; Sorenson et al., 2018) **(Fig. 12)**.

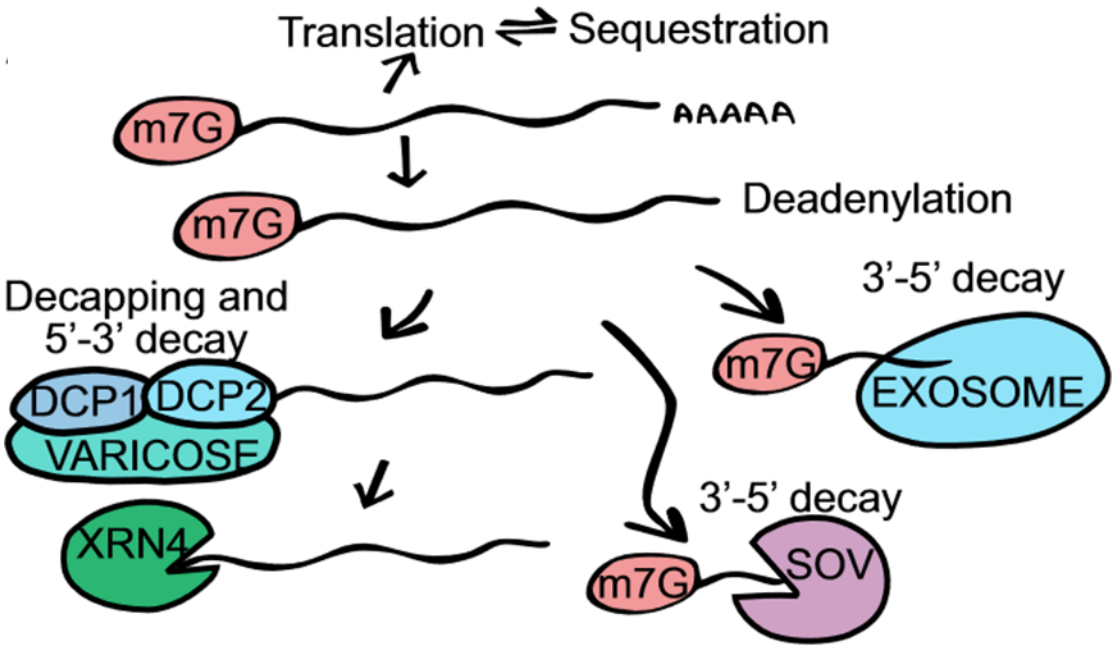

Figure 12: Schematic of cytoplasmic RNA decay pathways in Arabidopsis

(Figure from (Sorenson et al., 2018)).

3'-5' mRNA decay

The RNA exosome, a ubiquitous endo- and 3'-5' exoribonuclease in eukaryotic cells, is responsible for processing, degradation and quality control of essentially all classes of RNA by collaborating with several co-factors (Januszyk and Lima, 2014). The RNA exosome in eukaryote consists in an exosome core (Exo9), a distributive 3'-5 exoribonuclease (Rrp6), an endoribonuclease and 3'-5' exoribonuclease (Rrp44), and co-factors (Januszyk and Lima, 2014). The architecture of Exo9 is similar to phosphorolytic exoribonucleases (PNPase) but it lacks phosphorolytic activity in most of eukaryotes (Symmons et al., 2000; Liu et al., 2006). In fact, it has evolved to form two complexes: a nuclear RNA exosome called Exo11$^{44/6}$ (Exo9, Rrp44 and Rrp6) and a

cytoplasmic RNA exosome called Exo10[44] (Exo9 and Rrp44,), through recruiting Rrp44 and/or Rrp6 and regulating their RNase activities (Symmons et al., 2000; Chen et al., 2001; Liu et al., 2006; Dziembowski et al., 2007; Tomecki et al., 2010; Malecki et al., 2013). Here, we focus specifically on the subunits of the cytoplasmic Exo10[44].

In Arabidopsis, the subunits of the exosome complex were identified by using tandem affinity purification (TAP)-tagged RRP4 and RRP41 (Chekanova et al., 2007). The *rrp41l* mutant is enriched in mRNA transcripts encoding seed storage proteins, ABA biosynthesis, and ABA signaling pathway-related proteins, which has been most probably attributed to a delay in mRNA decay (Yang et al., 2013). Only one Rrp44 has been observed in budding yeast, while three Rrp44 have been identified in humans, called DIS3, DIS3L, and DIS3L2 (Tomecki et al., 2010; Chang et al., 2013; Malecki et al., 2013). Notably, DIS3L2 specific targets to RNA substrates harboring 3' polyU tails and has also been proved to degrade mRNAs and noncoding RNAs (Chang et al., 2013; Pirouz et al., 2016; Towler et al., 2016). In Arabidopsis, SOV, a homolog of DIS3L2, is a conserved 3'-5' exoribonuclease that inhibits the phenotype of *vcs* mutants and is dedicated to degradation of decapping transcripts (Zhang et al., 2010). The Arabidopsis *sov* mutant, also known as Col_0, has been widely used as a wild-type strain. However, the contribution of SOV in RNA homeostasis is still poorly understood, although a few RNAs have been identified as its substrates, exhibiting slower decay rates in *sov* mutants (Sorenson et al., 2018).

5'-3' mRNA decay starts with decapping

Deadenylated transcripts can also be directed to 5'-3' decay, where decapping is the first step of their degradation (Belostotsky and Sieburth, 2009). During the initial phases of transcription in eukaryotes, all RNA polymerase II-derived transcripts are modified at their 5' terminal by the addition of a cap structure, called m^7G-cap structures, which consist in a N7-methylguanosine (m^7G) linked by a 5'-5'-triphosphate bridge to the first transcribed nucleotide (N) of the nascent RNA (Cho et al., 1997; Fabrega et al., 2003). The interactions between this 5' cap and numerous dedicated cap-binding proteins dictate the fate of both nuclear and cytoplasmic mRNAs, and affects many vital cellular processes such as pre-mRNA processing, nuclear export, translation initiation, miRNA silencing and bulk mRNA decay (Ramanathan et al., 2016; Galloway and Cowling, 2019). The most fundamental role of the 5' cap is to avoid cytoplasmic mRNAs from unrestrained degradation, as incompletely capped or uncapped transcripts are rapidly degraded by the XRN family of 5'-3' exoribonucleases (Nagarajan et al., 2013).

mRNA decapping is executed in distinct cytoplasmic foci named processing bodies (P-bodies) through

the action of the decapping complex, which consists of the core decapping complex (the decapping enzyme DCP2, the essential activator DCP1, and the metazoan-specific scaffolding protein Edc4/Hedls/VCS) and other activators (DCP5, DHH1, PAT1, and the LSM1-7 complex) in higher eukaryotes (Xu and Chua, 2009). In the last decade, an increasing number of studies have indicated that decapping complex is also involved in response to environmental changes (Perea-Resa et al., 2016; Soma et al., 2017; Kawa et al., 2020). First, the stability of salt- and osmotic-responsive transcripts seems to be controlled through DCP1 and its interaction with other proteins. MAP kinase 6 (MPK6) is activated and phosphorylates DCP1 within 15 min upon dehydration, which triggers DCP1 dimerization and binding to DCP2 and DCP5. Increased assembly and activity of the decapping complex induces decay of transcripts involved in nutrient balance and lipid metabolism (Xu and Chua, 2012). Second, LSM1 has been involved in the response to drought and salt stress. The abundance of transcripts involved in both hormonal signaling and stress defense is altered in the *lsm1a lsm1b* double mutant (Golisz et al., 2013). Transcriptome analysis of *lsm1a lsm1b* exposed to osmotic stress uncovered that transcripts encoding negative factors for salinity tolerance were stabilized, while drought stress resulted in stabilization of mRNAs of positive regulators of drought tolerance. Especially, mRNAs of *NCED3*, an ABA biosynthesis gene, are specifically stabilized in response to salt stress (Perea-Resa et al., 2016). Finally, under salt and osmotic stress conditions, LSM1 guides target mRNAs to P bodies and activates their decapping, thus exposing them to degradation, which indicates that it is also crucial for formation of P bodies (Perea-Resa et al., 2016).

5'-3' cleavage

In eukaryotes, the degradation of decapped mRNAs depends on the XRN family of exoribonucleases. XRN2 and XRN1 are the primary 5'-3' exonucleases in the fungal and metazoan nucleus and cytoplasm, respectively (Nagarajan et al., 2013). Although the orthologs of XRN1 do not exist in plants, the orthologs of the yeast XRN2 are present in Arabidopsis with the nuclear AtXRN2 and AtXRN3, as well as the cytoplasmic AtXRN4 (Kastenmayer and Green, 2000; Nagarajan et al., 2013). XRN2/Rat1 is responsible for rRNA and snoRNA processing in yeasts, whereas XRN1 catalyzes 5' to 3' mRNA degradation (Garneau et al., 2007; Houseley and Tollervey, 2009). Similarly, AtXRN2 and AtXRN3, with partial functional redundancy, are involved in pre-rRNA processing while AtXRN4 is responsible for the degradation of uncapped mRNAs in the cytoplasm (Kastenmayer and Green, 2000; Gy et al., 2007; Nagarajan et al., 2013).

Transcriptome analysis of the *xrn4* mutant revealed that XRN4 impacts a set of target mRNA species in function-dependent or a sequence-specific manner. Specifically, 27 hexamer motifs were found to be overrepresented in transcripts or miRNA-cleavage products accumulating in *xrn4*, and transcripts encoding

nucleic acid–binding proteins and chloroplast-targeted proteins were over-represented, while transcripts for stamen-associated proteins and hydrolases were under-represented (Rymarquis et al., 2011). Moreover, abundance of many transcripts is reduced in the *xrn4* mutant indicating that XRN4 can regulate transcripts levels not only through its exoribonucleic activity, but also indirectly (Rymarquis et al., 2011). The abundance of EBF1 and EBF2 mRNA in *xrn4*, encoding F-box proteins involved in the degradation of the primary transcriptional regulator of ethylene signaling EIN3, is reduced too (Olmedo et al., 2006; Potuschak et al., 2006). Moreover, XRN4 is involved in the inhibition of heat stress response after return to normal temperature via directly degrading transcripts of the heat shock factor A2 (HSFA2) (Nguyen et al., 2015). Interestingly, XRN4 contributes to the destabilization of mRNA of AtRAP which encodes a RAP-domain protein involved in disease resistance, by long siRNAs (AtlsiRNA-1) and thus confers resistance against pathogen invasion (Katiyar-Agarwal et al., 2007). Recently, AtXRN4 has been found to be involved in regulating root growth under normal conditions as well as modulating root system architecture in response to salinity stress (Kawa et al., 2020).

6.3 Regulation of mRNA degradation pathways upon stress exposure

Increasing evidences indicate that components involved in mRNA degradation pathways are phosphorylated in response to environment stimulations. Phosphoproteomics studies have revealed an upregulation of the phosphorylated forms of MAP3K, MAP4Ka1, SnRK2.1/4/5/6/10, and DCP2 within 5 min upon osmotic stress treatment (Umezawa et al., 2013; Stecker et al., 2014). Nine out of ten SnRK2 protein kinases in Arabidopsis are activated rapidly after osmotic stress treatments for 10 min, while the activity of SnRK2.2, SnRK2.3 and SnRK2.6 is also regulated by ABA (Boudsocq et al., 2004). Arabidopsis MAP kinase 4 (AtMPK4) and AtMPK3/AtMPK6 phosphorylates PAT1, an activator of decapping, and DCP1, upon flagellin treatment, respectively (Roux et al., 2015; Yu et al., 2019). AtMPK6 also participates in the phosphorylation of DCP1 in response to drought stress (Xu and Chua, 2012). The MPK phosphorylation motif was also found in LSM1, which could explain its stress-dependent substrate specificity (Perea-Resa et al., 2016). Moreover, a phosphoproteomic approach revealed that the phosphorylation of DCP2 increases, via an unknown mechanism, in response to osmotic stress (Stecker et al., 2014). Another component, VCS, was also differentially phosphorylated under drought and osmotic stress (but not under ABA treatment) (Umezawa et al., 2013; Stecker et al., 2014). It is unknown whether the activity of plant DCP2 depends on its phosphorylation status, or is possibly triggered by phosphorylation of DCP1 or VCS (Kawa and Testerink, 2017). Although a study has shown that the phosphorylation of DCP1 mediated by immune-activated MAPKs contributes to P-body disassembly, it's still unclear whether phosphorylation of DCP1, DCP2 and VCS affects their re-localization to P bodies or

assembly of the decapping complex (Yu et al., 2019).

A recent study has shown that VCS and VARICOSE RELATED (VCR) are phosphorylated by SnRK2.5, SnRK2.6, and SnRK2.10 (Kawa et al., 2020). The "subclass I SnRK2s-VARICOSE" signaling module has been proposed as a post-transcriptional regulation mechanism of gene expression. This mechanism involves the ABA-unresponsive osmotic stress-activated subclass I SnRK2s phosphorylating VCS upon osmotic stress, thereby regulating mRNA decay (Soma et al., 2017). Altogether, these results suggest that environmental stimulations lead to the differential phosphorylation of components of the decapping complex, which could enable them to control gene expressions by targeting only a specific subset of transcripts (Kawa and Testerink, 2017) (**Fig. 13**).

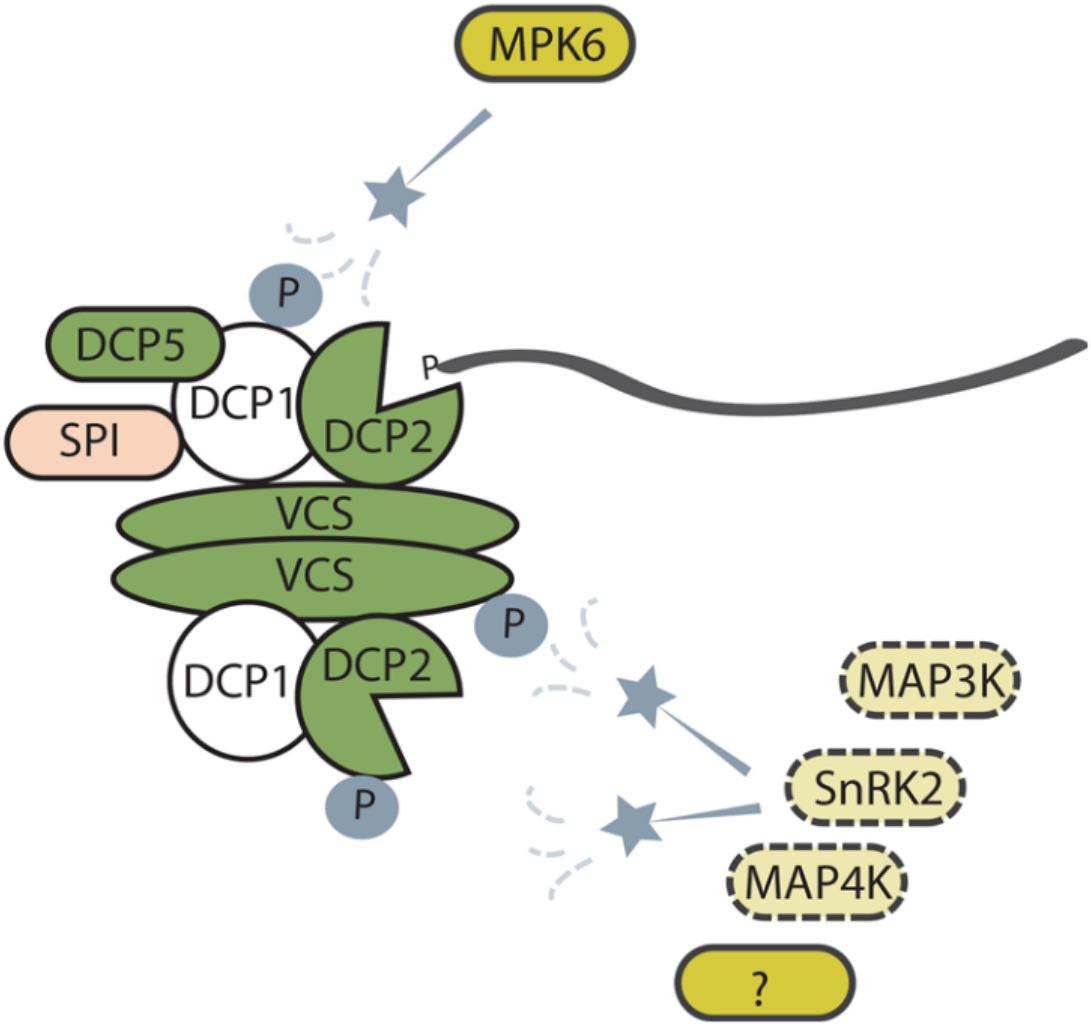

Figure 13: Involvement of protein kinases in regulation of mRNA decapping processes.

(Figure and legend reproduced from (Kawa and Testerink, 2017)). In Arabidopsis MPK6 is activated by drought and phosphorylates DCP1, thus inducing DCP1 interactions with DCP2 and DCP5. Upon salt stress, SPI protein binds to DCP1 and facilitates its recruitment to P bodies. Phosphorylation of DCP2 and VCS is triggered by osmotic stress, but kinases functioning upstream remain

still unknown. Phosphoproteomic profiling studies may suggest involvement of SnRK2 or MAP kinases in this process.

Other regulators are also involved in mRNA degradation, through binding to transcripts or interacting with components of mRNA decay. One of the most well-known regulators are the tandem CCCH zinc finger proteins (TZFs), which have been proposed to regulate transcript abundance at the post-transcriptional level in response to salt and osmotic stress (Guo et al., 2009; Bogamuwa and Jang, 2014). Mammalian TZFs are able to bind to ARE elements, AU-rich sequences at mRNA 3' terminal, and this interaction recruits enzymes participating in deadenylation, decapping and exonucleolitic cleavage (Lykke-Andersen and Wagner, 2005; Fabian et al., 2013). In plants, only AtTZF1 has been proven to have the ability to induce degradation of transcripts containing the ARE element so far (Qu et al., 2014). Expression of AtTZF2, AtTZF3, AtTZF10 and AtTZF11 are induced by ABA, salinity and osmotic stress, while AtTZF1 is triggered by salt only (Sun et al., 2007; Lee et al., 2012). Similar to mammalians, TZFs can shuttle between nucleus and cytoplasm, and localize to P bodies and stress granules in plants (Franks and Lykke-Andersen, 2007; Pomeranz et al., 2010; Bogamuwa and Jang, 2016). Most importantly, alteration in TZFs expression usually affects a subset of transcripts (Sun et al., 2007; Huang et al., 2012; Lee et al., 2012). Furthermore, the LSM1 protein was also co-purified with some stress-responsive proteins without RNA-binding properties (Golisz et al., 2013). Arabidopsis SPI, participating to the maintenance of membrane integrity, is recruited to P bodies upon interaction with DCP1 and regulates the uptake of mRNA into P bodies and RNP formation through an unknown mechanism (Saedler et al., 2009; Steffens et al., 2015).

Based on these informations, Kawa and Testerink proposed a model of plant mRNA metabolism in response to salinity and osmotic stress (Kawa and Testerink, 2017) **(Fig. 14)**.

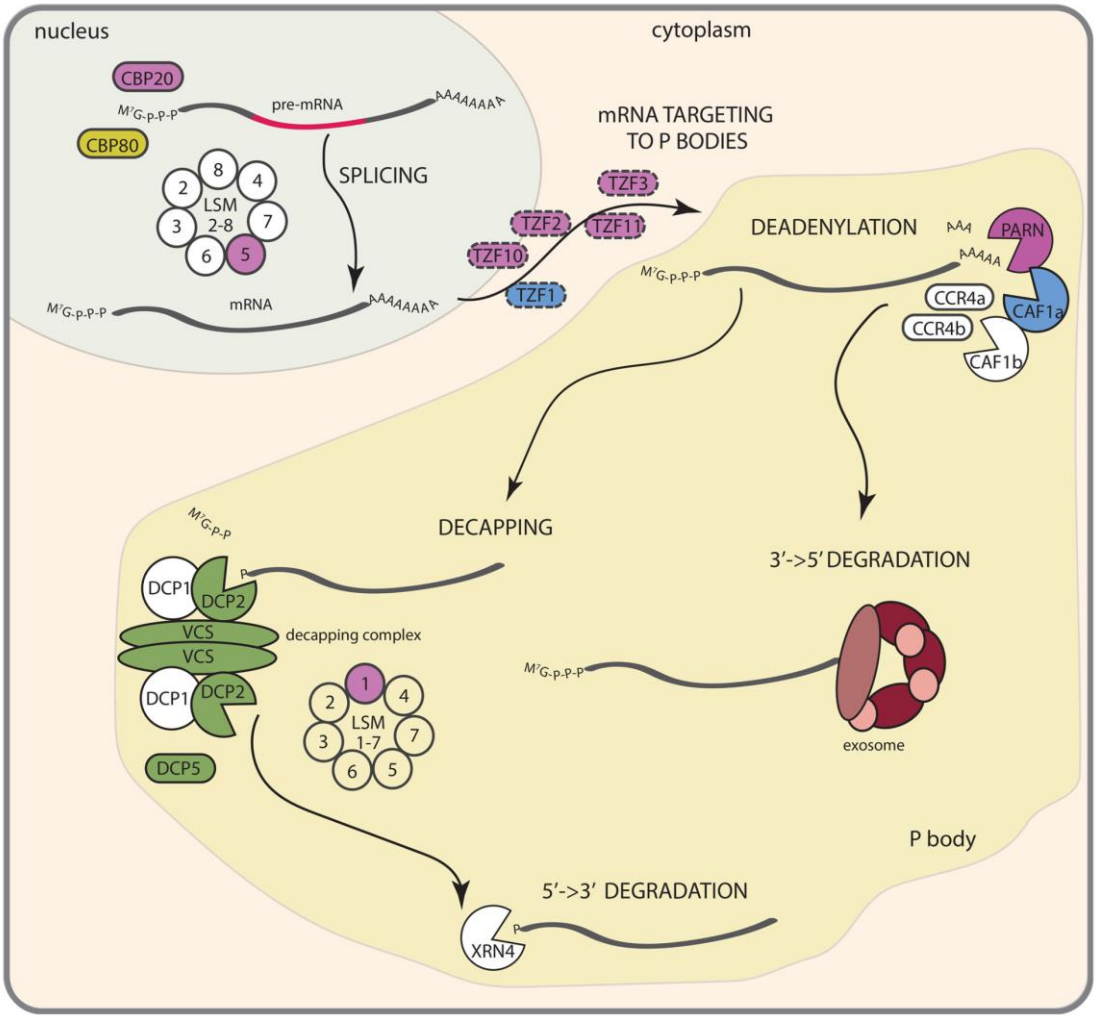

Figure 14: Contribution of mRNA metabolism processes to plant responses to salinity and osmotic stress.

(Figure and legend reproduced from (Kawa and Testerink, 2017)). Control of splicing occurs in the nucleus and is controlled by CBP20, CBP80 and the LSM2-8 complex. Targeting of specific transcript subsets to P bodies is hypothesized to be guided by TZF proteins. Cytoplasmic mRNA decay starts with deadenylation. After shortening the poly (A) tail, transcripts can be degraded from their 3' end via the exosome complex or undergo 5' cap removal in a process of decapping followed by 5' → 3' decay catalyzed by XRN4. Proteins marked in blue and green are involved in responses to salt and osmotic stress, respectively, purple color denotes factors involved in salt, osmotic and ABA signaling, while yellow indicates proteins responding to osmotic stress and ABA. Proteins for which function is only hypothetical are marked with dashed circles. XRN4 is involved in response to salt stress by modulating root system architecture (Kawa et al., 2020).

Context and objectives

Water is a fundamental component of life, and water deficit dramatically limits plant growth and development as well as crop yield worldwide. Currently, the exceptional pace of global climate changes intensifies the amplitude and frequency of extreme weather events, including salt and drought events that reduce water availability in plants. Therefore, deciphering how plants perceive and respond to water deficit has become essential.

Water deficit is a stress that is experienced by plants as soon as the water demand exceeds the water uptake capacity. Researchers frequently simulate it with osmotic stress through the introduction of osmotically active compounds into the plant root's growth environment. However, many studies concerning Arabidopsis response to osmotic stress have been conducted under SWD conditions that might not reflect the reality of the plant's natural environment or its physiological state. Two typical treatment conditions involve using 150 mM NaCl and 300 mM sorbitol, with some studies even performed under hyperosmotic stress condition through treatment with 600 mM sorbitol (Claeys et al., 2014; Yuan et al., 2014). These conditions lead to drastic changes in plant cells, in particular a partial detachment of the cell membrane from the cell wall—plasmolysis. Meanwhile, decline in external Π caused by mild water deficit (MWD) usually reduces P in plants in a quantitative manner and both parameters could be perceived by plants. Osmotic stress does not only reduce Π and P but also has other harmful impacts on plant, which depend on the specific osmotically active compounds being used (see introduction). Therefore, it is a huge challenge to distinguish between the specific and common response mechanisms to Π and P variations (Zhu, 2016). This topic also integrates into the more general question of how physical parameters of the environment, or of the cell, translate into biological signals. Transcriptomics researches are a conventional approach for revealing potential target transcripts and signaling pathways for a given stress factor. However, most transcriptomics researches concerning plants responses to osmotic stress have used only one or two osmotically active compounds with one or two concentrations, which is not sufficient to overcome this challenge. Furthermore, although one well-known early study was conducted after subjecting 5-day-old Arabidopsis plants to 140 mM NaCl treatment for 30 minutes (Dinneny et al., 2008), .most research has primarily focused on transcriptomes hours or days after treatments (Kreps et al., 2002; Kilian et al., 2007; Zeller et al., 2009; Kang et al., 2020).

Consequently, the question of which transcripts can be specifically influenced by changes in Π and/or P during the initial phases (15 min) of MWD conditions—where primary root cortical cells maintain turgidity—

remains unanswered. The first main objective of the thesis was to provide an answer to that.

Little is known about plant molecular responses to osmotic stress, particularly with respect to the early stages of the perception of the physical signal. So far only an osmosensor, OSCA1, has been identified clearly, while most known signaling pathways have not been connected to it (Yuan et al., 2014). Since OSCA1 is widely expressed in plants, including leaves, flowers, roots, and guard cells, the timing and location at which plants sense osmotic stress in a manner that triggers signaling and genome-wide transcriptional reprogramming do not rely on this protein alone. Hydrotropism is an emerging approach to explore the perception site in plants response to water deficit. Although the mechanism is still unclear, AtSnRK2.2 and the hydrotropism-specific AtMIZ1 function specifically in the cortical cells of the elongation zone and are essential for hydrotropism (Dietrich et al., 2017). Subsequently, Chang et al. reported that asymmetric distribution of cytokinins in the meristem zone is key for uneven cell division and subsequent root hydrotropism in Arabidopsis (Chang et al., 2019). Recently, Mielke et al. uncovered that increased JA production caused by turgor-driven mechanical compression facilitates *kor1* mutant response to root hydrotropism (Mielke et al., 2021). These findings suggest that hydrotropism is controlled by a comprehensive mechanism involving multiple hormones and signaling. Besides, the method employed to study hydrotropism might not accurately represent how plant roots respond to water deficit, as it used 7-day-old plants that haven't yet developed a complete root architecture. Recently, Steinhorst et al. discovered that Na^+ stress rapidly triggers primary calcium signals specifically in a cell group within the root differentiation zone by using the Ca^{2+} reporter (Steinhorst et al., 2022). Thus, reporters could help answer the question of when and where plants sense changes in Π and/or P.

In plants, two biophysical signals, P and Π, constitute a crucial thermodynamic parameter Ψ, which determine water movement between the different compartments of the soil/plant/atmosphere continuum. A study reported that P drops caused by MWD can be restored after about 40 min to many hours of onset, depending on the intensity of the water stress and the resistance of the plants (Shabala and Lew, 2002). Therefore, it is essential to test whether the Π- and/or P- correlated genes originating from objective 1 respond to dynamic changes in P caused by MWD. Additionally, a key difference between MWD and SWD with respect to the physical parameters P and Π is that under SWD, P will reach 0, while Π (approximately equals to Ψ in hydroponics) can still increase as the concentration of solutes is rising. Thus, it is also important to test whether these Π- and/or P- correlated genes quantitatively respond to changes in Π caused by SWD during the early stages of treatments. This question has been addressed in the section 2 of the manuscript.

Measuring Ψ in plants is technically difficult: it is so far obtained by a combination of challenging and

indirect techniques such as pressure chambers, cell pressure probes or pico-osmometers (Shabala and Lew, 2002; Boursiac et al., 2022). There is a real need for improved tools since Ψ in plants is constantly fluctuating (within minutes) due to growth, soil and air humidity, light variation. Reporters are helpful tools to monitor plant fitness, their nutrient status, or the activation of signalization pathways at the origin of their adaptation to a challenging environment. Among them, genetically encoded markers, and especially promoter-reporter gene fusions, allow very sharp spatial and temporal analysis of the parameter. Such reporters have been isolated for the accumulation of ABA and the redox status of the cell, as well as visualization of boric acid transport in plant (Christmann et al., 2005; Miller et al., 2009; Fukuda et al., 2018). Notably, given that *HSP70* expression is quantitatively induced by elevated ambient temperature, Kumar and Wigge developed a temperature biosensor by using ProHSP70::luciferase construct and used it to isolate a temperature sensor, the alternative histone H2A.Z in Arabidopsis (Kumar and Wigge, 2010). Therefore, to develop competent Π- and P- reporters, the main difficulty is to obtain regulatory elements of gene expression that quantitatively respond to their change. It has been proposed that gene expression is tightly controlled at both the transcriptional (promoter activity) and post-transcriptional levels (mRNA degradation) under drought and salinity stress (Kawa and Testerink, 2017). To obtain the reliable regulatory elements of Π- and P- correlated candidates, it is indispensable to investigate at which levels their expressions are regulated by water deficit. We evaluated these aspects in section 2 of the manuscript.

Another crucial objective is to employ the regulatory elements of genes originating from above investigations to drive the expression of reporters, hence allowing for the visualization of how changes in Π or P are perceived during water deficit conditions. We also addressed whether these reporters effectively report changes in Π or/and P and whether they are regulated through putative CWI and ABA signaling pathway upon water deficit. This is addressed in section 2 of the manuscript.

In section 3, we tried to better understand the sensitivity and limits of our reporter system from section 2. We attempted to explore in detail the expression regulation mechanism of one of my candidate genes under water deficit treatments, as we have not yet obtained its reliable expression regulation elements. Furthermore, given that stress responsive genes can be involved in plant stress adaptation, we also tried to explore whether the unknown function gene also plays a role in the plant stress response. The main manuscript is written in 3 sections. The first section includes a manuscript that has been accepted by JXB. Section 2 contains a draft of a manuscript to be submitted soon, and section 3 present with aspects of my work that are not conclusive yet, or that were not integrated in the first two articles.

Chapter 1: Distinct early transcriptional regulations by turgor and osmotic potential in the roots of Arabidopsis

Journal of Experimental Botany
https://doi.org/10.1093/jxb/erad307 Advance Access Publication 21 August 2023

RESEARCH PAPER

Distinct early transcriptional regulations by turgor and osmotic potential in the roots of Arabidopsis

Amandine Crabos[1,†], Yunji Huang[1,†], Thomas Boursat[1,2], Christophe Maurel[1], Sandrine Ruffel[1], Gabriel Krouk[1] and Yann Boursiac[1,*]

[1] Institute for Plant Sciences of Montpellier (IPSiM), Univ Montpellier, CNRS, INRAE, Institut Agro, Montpellier, France
[2] Laboratoire de Mécanique et Génie Civil (LMGC), Univ Montpellier, CNRS, Montpellier, France

[†] These authors contributed equally to this work.
[*] Correspondence: yann.boursiac@inrae.fr

Received 11 June 2023; Editorial decision 26 July 2023; Accepted 28 July 2023

Editor: Bjorn Usadel, Forschungszentrum Jülich, Germany

Abstract

In a context of climate change, deciphering signaling pathways driving plant adaptation to drought, changes in water availability, and salt is key. A crossing point of these plant stresses is their impact on plant water potential (Ψ), a composite physico-chemical variable reflecting the availability of water for biological processes such as plant growth and stomatal aperture. The Ψ of plant cells is mainly driven by their turgor and osmotic pressures. Here we investigated the effect of a variety of osmotic treatments on the roots of Arabidopsis plants grown in hydroponics. We used, among others, a permeating solute as a way to differentiate variations on turgor from variations in osmotic pressure. Measurement of cortical cell turgor pressure with a cell pressure probe allowed us to monitor the intensity of the treatments and thereby preserve the cortex from plasmolysis. Transcriptome analyses at an early time point (15 min) showed specific and quantitative transcriptomic responses to both osmotic and turgor pressure variations. Our results highlight how water-related biophysical parameters can shape the transcriptome of roots under stress and provide putative candidates to explore further the early perception of water stress in plants.

Keywords: Ethylene glycol, NaCl, osmotic pressure, PEG, sorbitol, transcriptional response, turgor pressure, water potential.

Introduction

How the environment is perceived by plants is of major importance for their life cycle. This is particularly true for water deficit (Maurel and Nacry, 2020; Verslues *et al.*, 2023) which can be summarized as an imbalance between the plant's requirement and loss of water and its uptake capacity. Water deficit directly impacts the plant water status. One of the ways in which plant water status is assessed is via plant water potential (Ψ), a composite variable which, in plant cells, integrates the turgor potential (or turgor pressure, P) and the osmotic potential (Π) (Haswell and Verslues, 2015). When considering the soil/plant/atmosphere continuum, Ψ can also be influenced by gravity and matric potentials. Ψ gradients allow evaluation of the motive forces that generate net flows of water between different compartments of this continuum. Together with the

Abbreviations: DEG, differentially expressed gene; DEP, differentially expressed probe; EG, ethylene glycol; P, turgor pressure (MPa); PEG, polyethylene glycol; Π, osmotic pressure (MPa); Ψ, water potential (MPa).

viscoelastic properties of the cell wall, P is responsible for the elongation of cells and organs, and for the rigidity of stems and leaves, allowing them to act against gravity and optimize light interception, among others. Π is related to the concentration of solutes in a compartment. The presence of a Π gradient across a semi-permeable barrier causes osmosis: a net directional flow of water, even in the absence of any hydrostatic pressure difference (Bowler, 2017). Π influences biochemical reactions, and can be directly regulated by the cell through osmoticum accumulation, synthesis, and transport (Beauzamy *et al.*, 2014).

A critical issue in plant biology is to understand which physico-chemical parameters are perceived by plants. Terms such as osmosensing and mechanosensing are employed to describe phenomena related to perceiving the plant water status (Beauzamy *et al.*, 2014; Haswell and Verslues, 2015; Hamant and Haswell, 2017; Scharwies and Dinneny, 2019). Many molecular players, such as mechanosensitive channels and protein kinases from multiple families (detailed in the reviews cited above), are thought to be involved in this perception or are contributing to associated phenomena. However, we lack a clear picture of the early perception of water deficit. One difficulty is that water deficit translates into multiple variations in the cell status. It is still discussed, for example, whether Π or P changes are directly sensed by plants or whether it is rather their impact on cell processes, cell wall status, or cell volume (Sack *et al.*, 2018;Verslues *et al.*, 2023).

Another difficulty is that the links between the intensity of the stress causing the water deficit and cell parameters is hard to establish. Measuring plant physico-chemical parameters under physiological conditions is indeed difficult at cell-scale resolution. Π or P can be measured using a combination of challenging, low-throughput, and/or indirect techniques such as pressure chambers and pico-osmometers, cell pressure probes, picogauges, or indenters (Beauzamy *et al.*, 2014; Knoblauch *et al.*, 2014; Boursiac *et al.*, 2022). Thus, there is a real need for improved tools and non-destructive techniques using, for example, chemical probes, protein reporters, or marker genes.

Here, we addressed the early stages of water deficit perception by considering that the drop in external Ψ would primarily provoke a change in either Π or P. Using hydroponically grown Arabidopsis plants that were osmotically challenged with permeating and non-permeating solutes, we first evaluated the impact of a drop in external Ψ on the P of root cortical cells. We then investigated root transcriptional regulations as a readout, to test whether Π or P can trigger specific and quantitative responses, a first step into the question of whether Π or P can be genuinely perceived by plant cells.

Materials and methods

Plant material and culture conditions

All experiments were performed using *Arabidopsis thaliana* ecotype Col-0. Seeds were surface-sterilized and kept at 4 °C in the dark until sowing on 1/2 Murashige and Skoog (MS) basal salt medium agar plates [2.2 g l^{-1} MS (Sigma), 1% sucrose (Euromedex), 0.05% MES (Euromedex), and 0.7% agar (Sigma), pH 5.7 adjusted using KOH]. For pre-germination, plates were incubated vertically in growth chamber under long-day conditions (16 h/8 h, 21 °C, 60% humidity). After 10 d, seedlings were transferred to a hydroponic medium [1.25 mM KNO_3, 0.75 mM $MgSO_4$, 1.5 mM $Ca(NO_3)_2$, 0.5 mM KH_2PO_4, 50 µM Fe-EDTA, 50 µM H_3BO_3, 12 µM $MnSO_4$, 0.70 µM $CuSO_4$, 1 µM $ZnSO_4$, 0.24 µM MoO_4Na_2, 100 µM Na_2SiO_3] and further grown under the same culture conditions. Cell pressure probe measurements, transcriptomic analyses, and treatments for quantitative PCR (qPCR) analysis were performed at 4–8, 6, or 6–11 d after transfer, respectively.

Osmotic treatments

Osmotic stress treatments were performed using a hydroponic solution containing either 25, 50, 75, or 100 mM NaCl (Sigma); 50, 100, or 150 mM sorbitol (Sigma); 75, 100, 125, or 150 gl^{-1} polyethylene glycol (PEG) 8000 (Sigma); or 50, 100, 550, and 200 mM ethylene glycol (EG; Sigma). Table 1 recapitulates the solutions and their respective osmotic potential.

Cell pressure probe measurements

Cell pressure probe measurements were performed as described previously (Javot *et al.*, 2003). Our device uses a pulled and beveled glass microcapillary (tip external diameter: 4–8 µm), filled with mineral oil and mounted onto a pressure probe. Primary root tip segments of ~2–3 cm were excised from Arabidopsis seedlings and laid on a filter paper perfused with hydroponic or treatment solution. Measurements were performed within a distance of 1 cm from the elongation of the first root hairs. Data were recorded using a specially designed software (Pfloek; Department of Plant Ecology, University of Bayreuth, Germany). Due to the dead volume of the system and the maximal speed of the peristaltic pump, it took ~2 min to fully change the perfusion solution around the root.

Transcriptomic analyses

Osmotic treatments were performed by transferring plants for 15 min into a hydroponic or treatment solution. The whole roots were harvested after 15 min of treatment and immediately frozen in liquid nitrogen. Each sample was a pool of three plants, and two sets of plants were treated independently. Frozen samples were ground using an MM 400 mixer mill (Retsch). Total RNA was extracted using TRI Reagent (Molecular Research Center, Inc.), DNA contamination was removed by digestion with DNase I (Promega), and further purification of the RNAs was performed using the MinElute Cleanup Kit (Qiagen), all according to the manufacturers' instructions. Concentration and purity of the RNAs were assessed by spectrophotometry, and integrity was confirmed using RNA 6000 Nanochips with a 2100 Bioanalyzer (Agilent). Gene expression measurements were performed using Arabidopsis Affymetrix Gene1.1 ST array strips (Affymetrix). For each sample, 100 ng of total RNA was processed using the GeneChip WT PLUS Reagent Kit (Affymetrix) following the manufacturer's instructions. Hybridization on array strips was performed for 16 h at 48 °C. The arrays were washed, and stained, using GeneAtlas Hybridization, Wash and Stain Kit for WT Array Strips following the manufacturer's instructions. Array strips were scanned on the GeneAtlas system.

Microarray raw data were processed with GCRMA available in the Expression Console Software package developed by Affymetrix. The Affymetrix Microarrays data have been deposited in the National Center for Biotechnology Information's Gene Expression Omnibus in

Table 1. Summary of the osmotic treatments applied to the roots, and the factors of the ANOVA model

Solute	Concentration (mM, g l^{-1} for PEG)	Π	P_{cort}	$NaCl_{factor}$	$Sorbitol_{factor}$	PEG_{factor}	EG_{factor}
None	0	0.021	0.41	0	0	0	0
NaCl	25	0.117	0.32	25	0	0	0
	50	0.238	0.25	50	0	0	0
	75	0.355	0.14	75	0	0	0
	100	0.425	0.05	100	0	0	0
Sorbitol	50	0.134	0.32	0	50	0	0
	100	0.255	0.18	0	100	0	0
	150	0.370	0.1	0	150	0	0
PEG 8000	75	0.073	0.31	0	0	75	0
	100	0.131	0.26	0	0	100	0
	125	0.209	0.2	0	0	125	0
	150	0.280	0.14	0	0	150	0
EG	50	0.151	0.3	0	0	0	50
	100	0.268	0.29	0	0	0	100
	150	0.394	0.29	0	0	0	150
	200	0.516	0.26	0	0	0	200

Solutes were dissolved in the hydroponic solution. The osmotic potential of the solution was measured at 20 °C with an osmometer (Wescor); three digits after the decimal point are shown. The osmotic potential is the opposite of the osmotic pressure.

compliance with Minimum Information about Microarray Experiment standards (https://www.ncbi.nlm.nih.gov/geo/) and are accessible through Gene Expression Omnibus Series accession no. GSE223207.

Transcriptomic data analyses

The multi-way type II ANOVA model and one-way ANOVA analyses for gene expression correlation to Π and P were run in R (v.4.2.0). Thresholds for the selection of differentially expressed probes (DEPs) were adjusted by comparison of the *P*-values versus false discovery rate (FDR)-corrected *P*-values and their frequency. A general cut-off of FDR <0.2 was ruled out, which yielded non-adjusted *P*-value thresholds of 0.001 for the solutes (NaCl, sorbitol, PG, and EG), and 0.0004 and 0.0012 for Π and P, respectively. A few genes were removed from the Π- and P-specific lists since they were associated with at least two probes and gave inconsistent ANOVA test results. Those removed from 'Π-specific genes' were At1g72850, At1g78270, At2g24540, At2g33810, At4g13920, At4g24410, At4g25880, and At4g26490; and those removed from 'P-specific genes' were At1g07130, At1g07725, At1g08590, At1g51640, At1g56240, At1g72850, At2g11851, At2g22960, At3g22070, At3g54630, At3g56770, At4g24410, At4g28650, At4g36030, At4g38210, At4g38550, and At5g59730.

Treatment clustering was obtained in RStudio (RStudio 2022.07.1 + 554) by calculating the Euclidean distance between treatments using the function dist(), then the clusters obtained by hclust() were plotted using plot(), with default values. Venn diagrams were elaborated with the nVennR package (Pérez-Silva *et al.*, 2018).

Semantic analysis of the clusters was performed using Genecloud (Krouk *et al.*, 2015) from the m2sb.org webpage with an FDR threshold set to 1%. Gene Ontology (GO) enrichment was performed in R using ClusterProfiler v.4.4.2 (Wu *et al.*, 2021) and org.At.tair.db (v3.15.1) for the Arabidopsis genome-wide annotation database (Carlson, 2017). Overlaps scores of lists were obtained using the Genesect algorithm from the Virtual Plant platform (Katari *et al.*, 2010).

Quantitative reverse transcription–PCR (RT–qPCR)

RNA extraction was performed by using the Direct-zol RNA Miniprep Plus Kits from Zymo Research (No. 2072). cDNA solution was synthesized from 1 µg of RNA and oligo-DT_{15}, dNTPs, and M-MLV (Promega) according to the manufacturer's protocol. At1g13320 (PDF2) and At4g34270 (TIP41-like) were selected as internal normalizing genes, because of their stability in roots under abiotic stresses (Czechowski *et al.*, 2005). RT–qPCR primers were designed by using the primer3 online website (version 4.1.0, Supplementary Table S1). RT–qPCRs were performed according to the procedure recommended by the manufacturer (Takara) [0.5 µl of H_2O, 0.25 µl of forward/reverse primers, 4 µl of cDNA, and 5 µl of TAKARA SYBR premix Ex Taq at 95 °C for 30 s; 95 °C for 5 s, 60 °C for 30 s (40 cycles)]. RStudio software was used to calculate gene expression according to Vandesompele's method (Vandesompele *et al.*, 2002).

mRNA decay analysis

The half-life time of mRNAs ($T_{1/2}$) was calculated from data available in Sorenson *et al.* 2018. It is based on the decay rate (α) modeled from RNA-seq data upon cordycepin treatment on *sov* mutant seedlings (i.e. Col 0), and is calculated as $T_{1/2}=\ln(2)/\alpha$ (Sorenson *et al.*, 2018). The $T_{1/2}$ values of each mRNA from genes in the clusters are presented individually and as boxplots. The values above the boxplots correspond to a non-parametric estimation of the *P*-value of the $T_{1/2}$ of a given cluster being smaller than that of the whole genome. In this boostrap-based approach, the median $T_{1/2}$ of the cluster is compared with the median $T_{1/2}$ of a sample (of the same size) from the whole-genome data. The number of occurrences where the genome sample median $T_{1/2}$ is smaller than the cluster median $T_{1/2}$ divided by the number of tests realized (10^4 tests), namely the frequency, is reported.

Results

Turgor response of root cortical cells to osmotic challenges

We determined the P of root cortical cells with a cell pressure probe (Boursiac *et al.*, 2022) upon root perfusion with

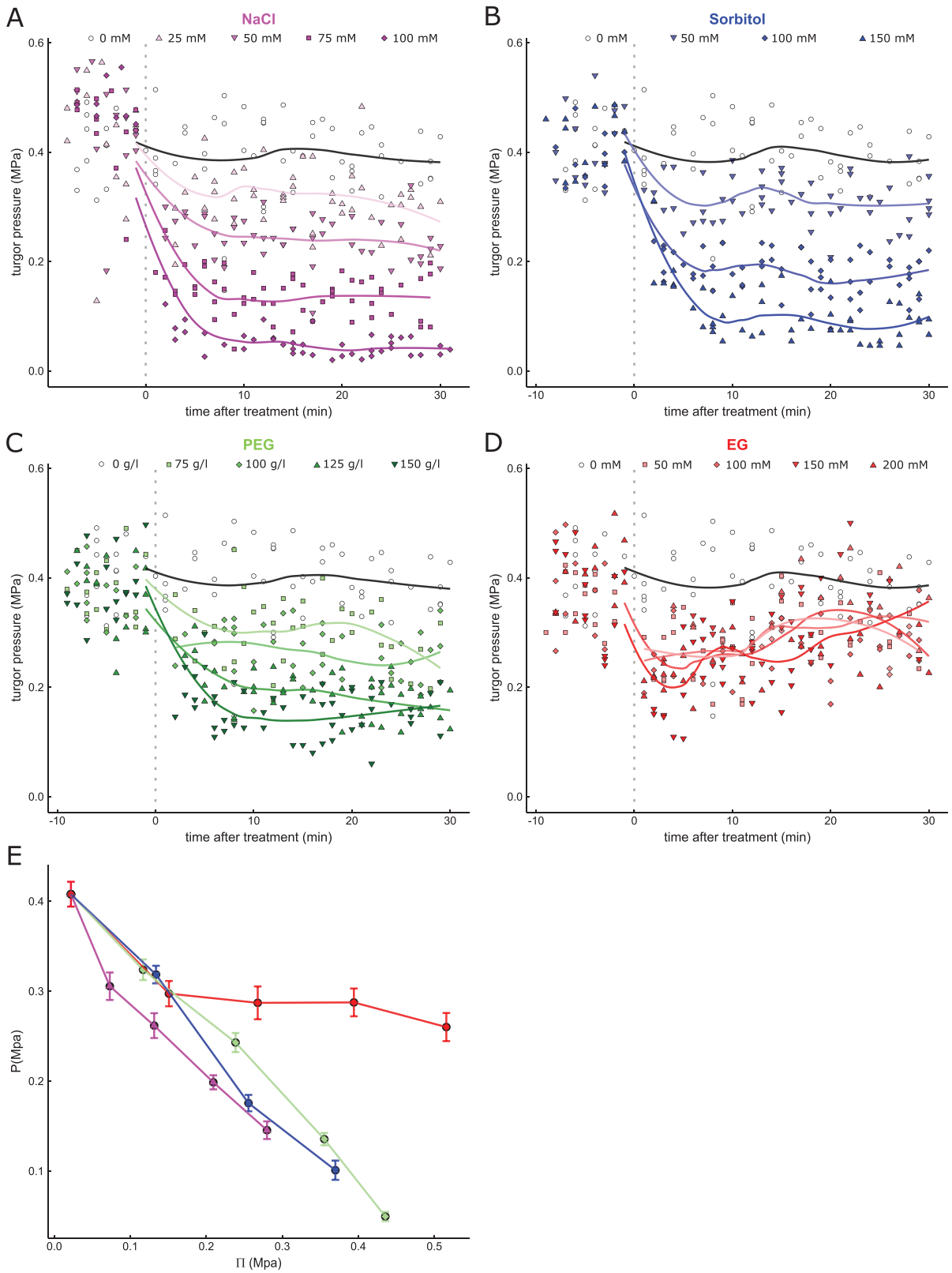

Fig. 1. Osmotic treatments reduce the P of root cortical cells in Arabidopsis. A portion of ~3 cm of root of 21-day-old plants, laid on a perfused Whatman paper, was treated with various solutes at different concentrations. Cortical cell P was measured with a cell pressure probe. (A–D) Measurement kinetics performed on plants treated with NaCl at concentrations of 0, 25, 50, 75, and 100 mM (the darker the color, the more concentrated; $n>2$ for each treatment), sorbitol at 50, 100, and 150 mM, PEG 8000 at 75, 100, 125, and 150 g l^{-1}, and EG at 50, 100, 150, and

200 mM, respectively. Zero on the time axis indicates the change in perfusion from hydroponic solution to the same solution complemented with treatments. A lowess smoothing was added in order to highlight the general behavior of P after each treatment. (E) Plot recapitulating the measurements of P within the 10–20 min time frame as a function of the osmotic pressure of the solution (average value ±SEM, $n \geq 2$, blue, sorbitol; pink, NaCl; green, PEG; red, EG).

a standard hydroponic solution, or the same solution supplemented with various concentrations of distinct solutes: NaCl, sorbitol, PEG 8000, or EG (Table 1). In contrast to others, the latter solute can significantly diffuse through cell membranes. Thus, EG is expected to concomitantly reduce the Ψ of the solution and cells, without significantly changing the Ψ gradients between compartments (Creelman and Zeevaart, 1985). Figure 1A–D shows cortical cell pressure measurements over the course of ~30 min of a perfusion with various concentrations of NaCl, sorbitol, PEG, and EG. For all treatments, we observed a progressive reduction in P, which reached a minimal value within 10 min. P remained stable for at least an additional 10 min for most conditions except EG treatments, where a partial restoration of P was eventually observed. We averaged P within 10–20 min of treatment and represented it as a function of $\prod$ of the bathing solution (Fig. 1E). For all solutes except EG, we observed a linear and relatively similar relationship between $\prod$ of the solution and cortical cell P. In the 10–20 min time range, EG provoked a reduction in P of ~0.1 MPa, independently of its concentration, and thereby of $\prod$. Note that treatments were designed so that P remained positive in cortical cells, and hence cortical cells were not plasmolysed. These results suggest that root cortical cells behave as osmometers with the solutes except EG, and show no major osmotic regulation within the time frame of the experiment. The 15 min time point, which corresponds to a mostly stable P, seems to be well adapted to studying the early molecular events triggered by osmotic challenges.

Transcriptional response of roots osmotically challenged for 15 min

We treated Arabidopsis plants for 15 min using the various conditions tested above, and performed transcriptomic analyses on RNA extracted from their roots. This genome-wide investigation of gene expression in response to 15 distinct osmotic challenges (plus a control condition in which plants were transferred into an identical hydroponic solution, Table 1) was recorded using Affymetrix *A. thaliana* genome arrays (Gene1.1 ST array strip, two independent biological experiments). We used the probe data from the genome array to perform a hierarchical classification of the osmotic challenges, and explore their convergence in transcriptional control (Fig. 2A). A general feature is that most of the challenges were grouped by the nature of the solute (NaCl, sorbitol, PEG, or EG), suggesting that it represents a main determinant of whole-genome transcriptional status. EG treatments were clustered next to the hydroponic condition, which echoes the limited effect of this solute on P. Treatments with the two highest PEG concentrations were also separate from the other challenges, which suggests that these conditions trigger responses of yet another type.

The datasets were then modeled through ANOVA with the following linear model:

$$Y_i = \alpha.\mathrm{NaCl}_{\mathrm{factor}} + \beta.\mathrm{sorbitol}_{\mathrm{factor}} + \gamma.\mathrm{PEG}_{\mathrm{factor}} + \delta.\mathrm{EG}_{\mathrm{factor}}$$

where Y_i is the signal intensity of an ATH1 probe, α, β, γ, and δ are coefficients representing the effect of each of the factors, respectively, and $\mathrm{NaCl}_{\mathrm{factor}}$, $\mathrm{sorbitol}_{\mathrm{factor}}$, $\mathrm{PEG}_{\mathrm{factor}}$, and $\mathrm{EG}_{\mathrm{factor}}$ are factors indicating the concentration of each treatment (Table 1; full results are provided in Supplementary Dataset S1) (Ristova *et al.*, 2016). Note that this model uses partial regressions against factors that are derived from the concentration of the solutes. Importantly, the factors are set to 0 when another solute is used as a treatment and, as a consequence, are negatively impacting the score of genes which could be regulated by common underlying processes (such regulations are addressed in the next section). Note also that all solutes are included in the model, despite the fact that no co-treatment was performed and thus no interaction is investigated, in a bid to increase the statistical power. We then considered a probe as differentially expressed if its ANOVA *P*-value was significantly different at $P<0.001$ (FDR <0.2) for any of the four factors. A total of 526 DEPs, corresponding to 436 differentially expressed genes (DEGs), were retrieved with this analysis. In order to estimate the amplitude of the transcriptomic regulation, we first separated and sorted the DEPs according to the conditions in which they were regulated (Fig. 2B). Probes regulated specifically by one solute only were the most represented. PEG was the solute with the most specific impact, with 182 DEPs (159 DEGs). NaCl, sorbitol, and EG treatments resulted in 127 (92), 68 (60), and 14 (12) specific DEPs (DEGs), respectively. The remaining 135 DEPs were regulated significantly in ≥2 solute treatments (Fig. 2B). Because DEGs could be either up- or down-regulated by the treatments, we separated the genes regulated by each specific solute in two clusters based on their averaged, centered, expression signal. Figure 2C visually confirms that the DEGs identified by this approach indeed exhibit a quantitative transcriptional regulation mostly for a particular solute.

Do $\prod$ or P trigger specific gene regulations?

Because all treatments share a common osmotic component (Table 1), the transcriptional response can also be observed

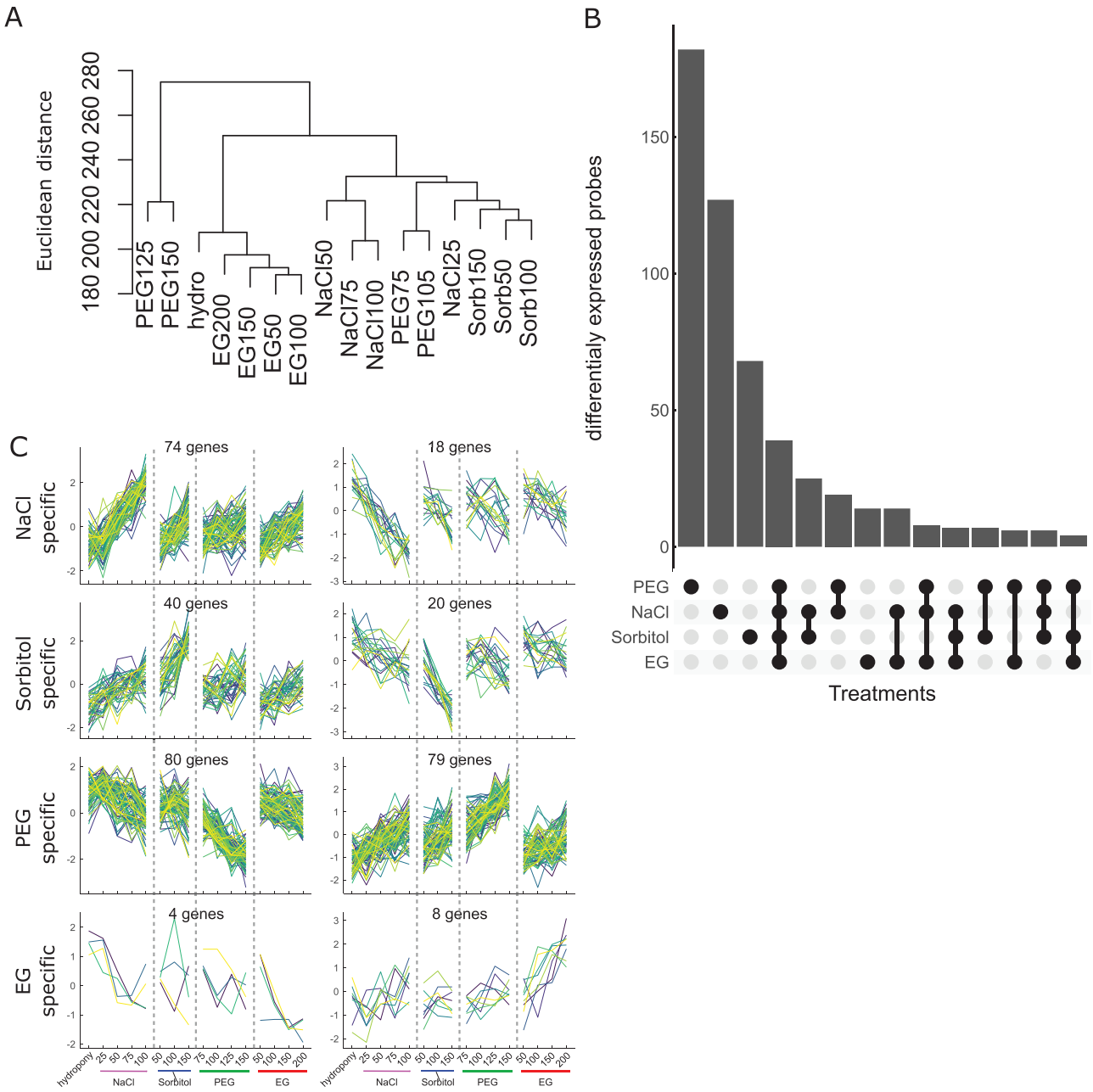

Fig. 2. Features of the early transcriptomic response to osmotic treatments. (A) Dendrogram illustrating the effects of the solute nature and concentration on the regulation of gene expression. (B) Number of DEPs classified according to the solute used for the treatment. The matrix below indicates if those DEPs were found for a single or for various solute(s). (C) Gene expression signals in the different treatments. Genes regulated by one solute only were selected from (B) and split into two clusters. The average, centered, expression value for each gene is plotted against the combination of solutes and concentrations used in the transcriptomic approach.

with the prism of a dose-dependent response to osmotic pressure. We therefore performed a one-way ANOVA on our transcriptomic data, using Π as the explanatory, continuous, variable (Supplementary Dataset S1). This analysis retrieved 72 DEGs. EG was also used for its capacity to reduce the Ψ of the solution; however, at variance with the other treatments, it provoked only a limited reduction in P (Fig. 1D, E). With the aim of differentiating the effect of an osmotic treatment on the transcriptome through either the osmotic potential or its impact on P, we performed a similar one-way ANOVA of the 15 min transcriptomic response to the treatments, but with P as the explanatory variable (Supplementary Dataset S1). This analysis resulted in 179 DEGs. While 53 DEGs were identified in both Π and P response (see the Discussion), 19 and 126 DEGs were specific for Π and P, respectively (Fig. 3A). Each group of Π

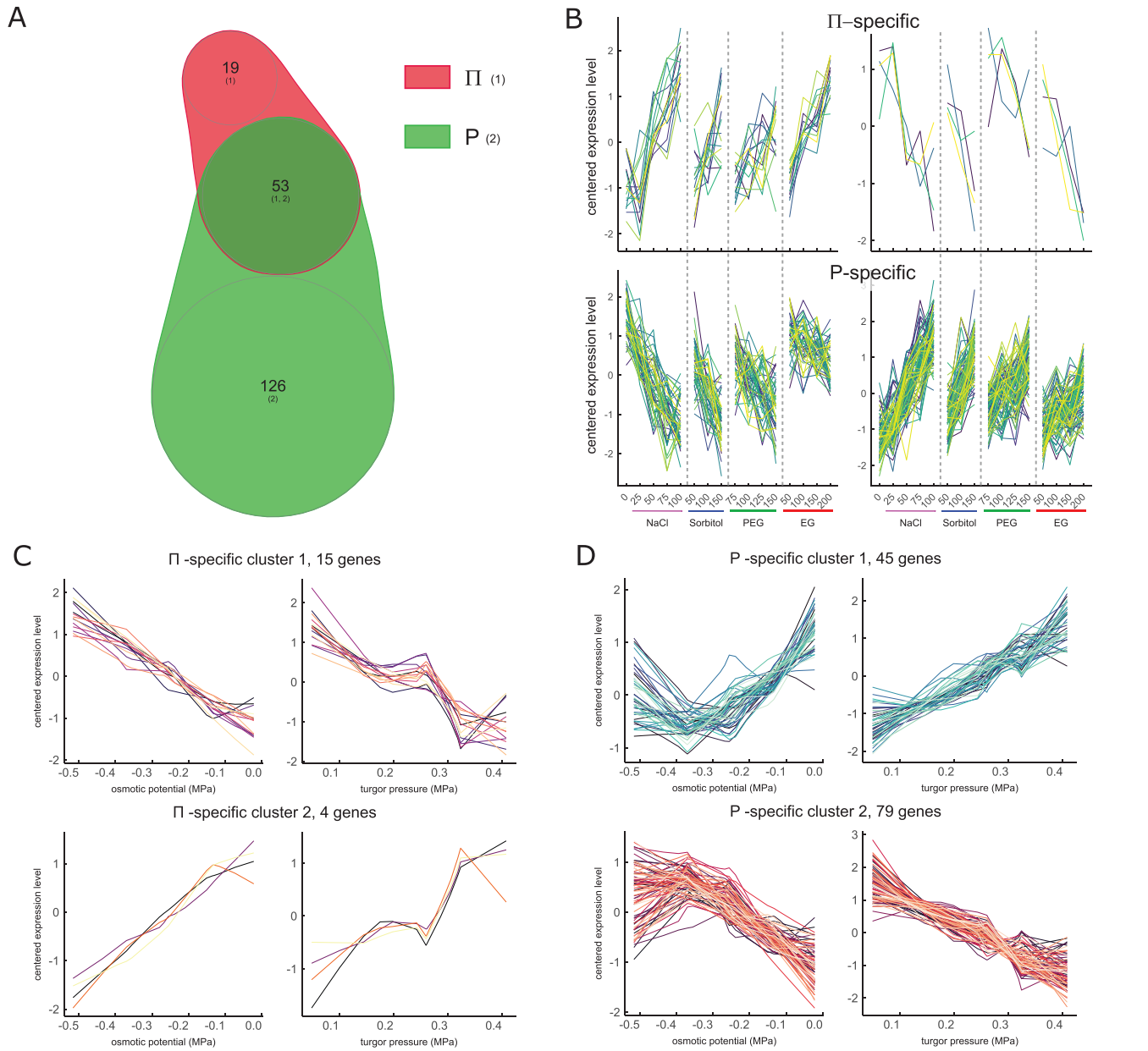

Fig. 3. Correlations between gene expression and osmotic or turgor pressure. (A) Venn diagram showing the number of genes, in the same transcriptomic approach as in Fig. 2, whose expression is significantly correlated to Π, P, or both. (B) The 19 'Π-specific' genes and 126 'P-specific' genes were split into two clusters each, and their average centered expression is expressed as a function of the solute/treatment combination corresponding to the biological assays of the transcriptome approach. (C) The 19 'Π-specific' genes were separated into two clusters and their average centered expression is expressed as a function of the osmotic potential of the solution of treatment, or the cortical cell turgor pressure. (D) The same representation as in (C) but for the 126 'P-specific' genes.

or P DEGs was split into two clusters, in order to account for potential up- and down-regulation. For the Π-specific genes, the mRNA abundance of the DEGs appeared to be regulated quantitatively for all solutes employed (Fig. 3B, upper panels), while a similar regulation for NaCl, sorbitol, and PEG, but not EG, was observed for the P-specific genes (Fig. 3B, lower panels). Most importantly, a clear quantitative correlation to Π or P was confirmed for the Π-specific (Fig. 3C) and P-specific (Fig. 3D) DEGs, respectively. Altogether, our transcriptomic approach suggests that while cells remain turgid, at least two components of the osmotic treatment, P and the Π of the bathing solution, are able to provoke specific quantitative responses of the transcriptome, resulting in both up- and down-regulations.

Are promoter activity and mRNA decay pathways involved in the ∏ or P transcriptional regulation?

The 1 kb promoter regions of the DEGs were analyzed using the MEME suite (Bailey *et al.*, 2015; Grant and Bailey, 2021, Preprint). Both new and already known (O'Malley *et al.*, 2016) enriched motifs were considered for ∏-cluster 1 or the P-specific clusters (with only four genes, ∏-cluster 2 was not analyzed, Supplementary Datasets S2, S3A–C). All clusters showed an enrichment in motifs (or similar motifs) known to bind ABI3VP1 transcription factors (TFs). All other motifs were found enriched in one cluster only: REM, C2C2dof, and BBRBPC-binding elements for P-cluster 2; C2H2 and ZFHD-binding motifs for P-cluster 1; and an ARID-binding motif for ∏-cluster 1.

We also considered whether the regulation of the mRNA abundance of the DEGs could be post-transcriptional, and in particular due to their degradation. Using the transcription inhibitor cordycepin and a model-assisted RNAseq approach, Sorenson *et al.* (2018) performed a global evaluation of mRNA decay rates in Arabidopsis and evaluated the implication of the three main decay pathways. As a first hint of this type of regulation for the DEGs identified herein, we used the mRNA decay rates obtained in the above-mentioned study, for the *sov* Col genotype, to calculate the mRNA half-life of our genes of interest in their growth conditions ($T_{1/2}$). The median $T_{1/2}$ of all mRNAs detected in this study was ~101 min. The median $T_{1/2}$ calculated for genes of the ∏-specific clusters and P-specific cluster 2 were significantly lower, with values of 56, 23, and 69 min, respectively (Fig. 4), and was not different for genes of P-specific cluster 1.

A short list of ∏- or P-correlated genes

In a bid to confirm the robustness of the microarray approach, and select potentially good candidates that could serve as markers of P or ∏, we ranked genes of the four categories (∏- or P-specific, up- or down-regulated) according to three parameters: the adjusted R^2 of a linear fit of their averaged centered expression as a function of ∏ or P; the slope of the linear fit; and the average expression level in control conditions (Supplementary Dataset S4). We randomly selected a few genes, among the best ranked of each list, to confirm their regulation by RT–qPCR, upon 15 min NaCl, sorbitol, and EG treatments, and in three new, independent, biological replicates. Figure 5 shows plots of the comparison between the means of the microarray signals and of the signals obtained by RT–qPCR. Ten genes out of 12 displayed a significant correlation between both signals, thus globally confirming the results obtained by the microarray approach. The ∏-specific cluster 2 showed poor reliability, with only one gene out of three having a similar behavior upon confirmation by RT–qPCR and in new biological replicates. The P-specific cluster 1 exhibited the highest rate of confirmation, in both the *P*-value of the correlation and the R^2 of the relationship. Among them, At1g64640 stood out, with a correlation *P*-value <1e-3 and an R^2 >0.9. The expression of this gene is therefore robustly and quantitatively correlated to P, at 15 min after an osmotic challenge.

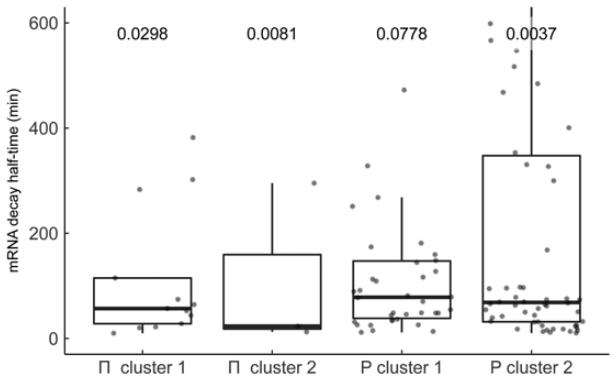

Fig. 4. mRNA half-life time is reduced in three clusters in control conditions. The half-life time of mRNAs ($T_{1/2}$) was calculated from Sorenson *et al.* (2018) based on the decay rate (α) modeled upon cordycepin treatment on *sov* mutant seedlings [i.e. Col 0, $T_{1/2}$=ln(2)/α]. $T_{1/2}$ values of each mRNA from genes in the clusters are presented individually and as boxplots. The numbers above the boxplots correspond to the *P*-value of a bootstrap-based test of $T_{1/2}$ of the cluster being smaller than the whole-genome median $T_{1/2}$ (see the Materials and methods).

What are the gene functions altered by ∏ or P?

A semantic analysis of the gene annotation present in the four clusters (∏- or P-specific, up- or down-regulated) using Genecloud (Krouk *et al.*, 2015) revealed that the ∏-specific clusters do not show any particular semantic enrichment. Arabinogalactan, Cys/His-rich proteins, 'protein kinase C', and TF-related terms were detected in cluster 1 of P-specific genes (Fig. 6A, left). Cluster 2 of P-specific genes showed enrichments in terms related to ethylene-dependent and other types of transcriptional regulation, as well as defense responses (Fig. 6A, right).

A GO enrichment analysis was also performed. The ∏-specific cluster 1 was found to be specifically enriched in genes associated with defense responses and the cell wall (Fig. 6B, left). Results for P-specific clusters were quite consistent with the semantic analysis. P-specific cluster 1 was enriched in 'anchored components' which echoes the arabinogalactan term above. P-specific cluster 2 was enriched in terms associated with ethylene and defense responses. In a bid to sharpen the above-mentioned GO analysis, we also evaluated the overlap between our gene lists and the GO list 'response to NaCl' (GO:0009651) as well as two of the upstream terms: 'response to abiotic stress' (GO:0009628) and 'response to stimulus' (GO:0050896) (Fig. 6C). The two up-regulated clusters, ∏-specific cluster 1 and P-specific cluster 2, showed a significant overlap with the genes in the categories 'response to stimulus' and 'response to abiotic stress', but not with 'response to salt stress', indicating the convergence of our approach with existing knowledge. Because the specificity of the response might not prevail under short-term treatment, and a general stress response (GSR) may rather

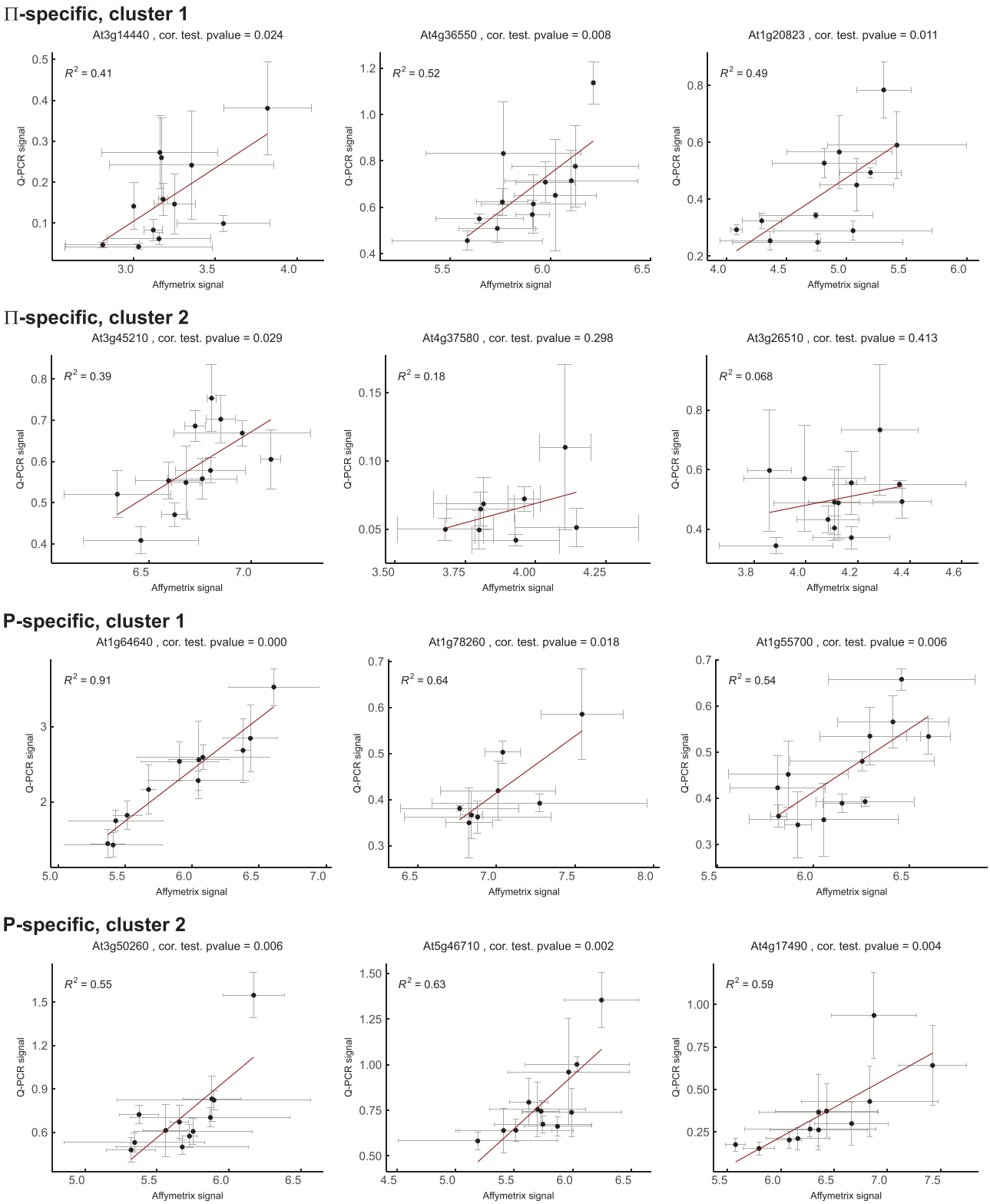

Fig. 5. RT–qPCR validation of osmotic or turgor pressure clusters. The expression of three candidates per list: Π or P, clusters 1 and 2 were investigated by RT–qPCR in three independent biological replicates. The plants were harvested 15 min after transfer into a hydroponic solution, or the solution complemented with 25, 50, 75, or 100 mM NaCl, 50, 100, or 150 mM sorbitol, or 50, 100, 150, or 200 mM EG. For each gene, the normalized RT–qPCR signal (±SEM) is expressed as a function of the averaged signal (±SEM) obtained from the transcriptome analysis. The *P*-value of a correlation test (Pearson) as well as the linear fit (with its R^2 value) between the average values are indicated for each gene.

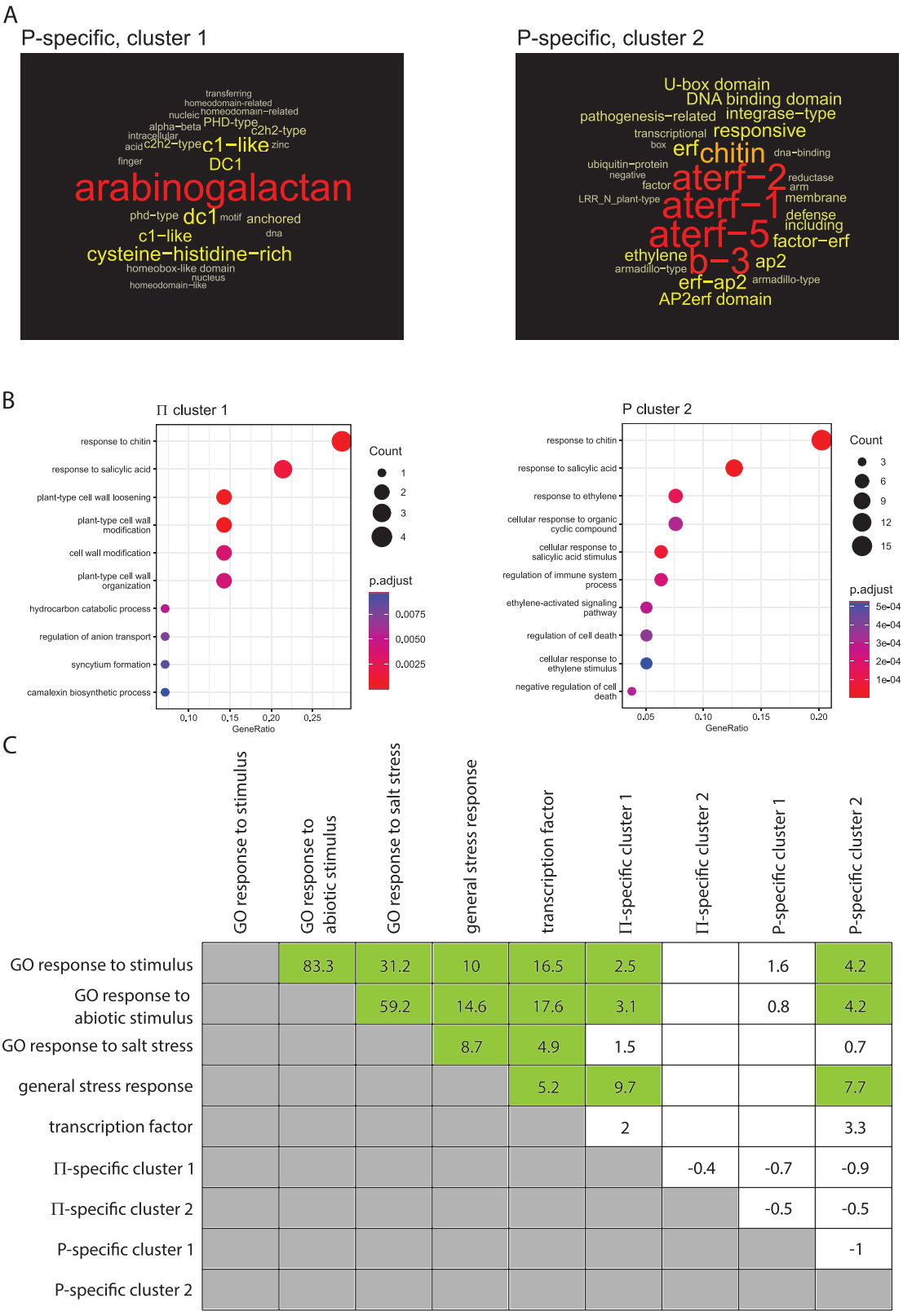

Fig. 6. Classification of the Π- and P-correlated genes. (A) Output of the Genecloud semantic analysis for the two clusters showing a significant enrichment. (B) Output of a Gene Ontology analysis for the two clusters showing significant enrichments in GO terms. The GO terms, gene counts for each GO term, and adjusted *P*-value of the enrichment are presented. (C) Degree of overlap (Z-score) between our gene lists and public gene lists related to osmotic stress, the general stress response, and a list of transcription factors, using the Genesect algorithm.

be activated (Bjornson *et al.*, 2021), we also compared our lists with the genes identified as GSR from the work of Ma and Bohnert (2007). In this study, the authors analyzed a collection of transcriptome profiles of plants under various treatments, and highlighted a stress-dependent cluster that could represent cell-level stress responses (Ma and Bohnert, 2007). ∏-Specific cluster 1 and P-specific cluster 2 showed a significant overlap with the GSR genes, with a greater Z-score than for the previous comparisons (Fig. 6C). This analysis suggests that some of the up-regulated genes that are quantitatively (and inversely) correlated to ∏ or P belong to a common and early response to stresses.

Finally, our candidates were also compared with a list of genes encoding TFs (Pruneda-Paz *et al.*, 2014), and this showed no significant enrichment in this category of genes (Fig. 6C).

Discussion

This study was designed to improve our comprehension of which component of a water deficit can be perceived by plant roots. For this, we considered both the ∏ of the bathing solution and the P of root cells as possible input signals (Fig. 1) and used whole-genome transcriptional responses as a readout. The approach was meant to unravel any quantitative relationship between the input signals and responses.

Parameters at the origin of the transcriptional responses

In addition to solute-specific transcriptional responses (Fig. 2D), our study revealed 72 genes whose expression correlated to ∏, independently of the solute used (∏-specific clusters, Fig. 3A, C). These results suggest that plant cells have the capacity to sense and transduce the external osmotic potential. Measurement with a cell pressure probe allowed us to also look for correlations between gene expression and the P of root cortical cells. In this approach, the use of EG as a permeating osmoticum was critical to make a distinction between the effects of the solutes on P and ∏ (Fig. 1E). A total of 179 genes were found to be correlated to P (P clusters 1 and 2; Fig. 3A, D) and suggest that plant cells also have the capacity to specifically sense and respond to the internal pressure. Due to the experimental design and variability, 53 genes could not be assigned to a ∏- or P-specific response (Fig. 3A) and would deserve more investigation, in particular with the use of other permeating solutes. Nevertheless, the identification of genes whose expression is quantitatively correlated to all possible combinations (∏ or P, up- or down-regulation) highlights the multiplicity of water deficit responses in plant cells. Since we uncovered potentially distinct regulatory mechanisms, our results will help in clarifying studies on mechano- and osmosensing as well as our understanding of plant response to water deficit. For example, turgor recovery upon plant adaptation to low external water potential by solute synthesis/accumulation necessarily implies an uncoupling between P and ∏.

∏ or P may not be the exact physico-chemical parameters that are genuinely perceived by plants. It has been suggested that, in leaves, accumulation of abscisic acid (ABA) is triggered by a drop in relative water content (RWC) rather than variations in P or ∏ (Jia *et al.*, 2001; Sack *et al.*, 2018). This distinction was made possible by experiments of leaf dehydration beyond the turgor point loss. In our experiments, turgor was preserved because we anticipated that plasmolysis could trigger distinct responses and, on a crude assumption, the relative change in cell volume ($\Delta V/V$) is linearly correlated to the variation in P (ΔP) according to $\Delta P=\varepsilon\cdot\Delta V/V$ where ε stands for the cell wall elastic modulus (Hüsken *et al.*, 1978). Thus, we cannot differentiate P or RWC and may use them interchangeably in our interpretations. It would also be interesting to establish whether the internal (intracellular) osmotic potential (Π_{int}) can be sensed and trigger specific transcriptional responses. Because cells behave as osmometers in the presence of NaCl, sorbitol, and PEG, Π_{int} can be expressed, at equilibrium as $\Pi_{int}=\Pi+P$. Since the effects on ∏ and P were close (Fig. 1E), those solutes do not allow us to distinguish Π_{int} from ∏. EG flux was not completely equilibrated after a 15 min treatment (Fig. 1D), and Π_{int} could be calculated based on equations that describe P variations in cells perfused with a permeating solute (Steudle, 1989). However, experimental variations did not allow us to achieve a sufficient resolution of the hydraulic and solute relaxation phases in cells under EG treatment. Thus, our current study cannot conclude on the ability of root cells to respond to changes in Π_{int}.

Finally, we would like to point out other avenues for interpreting our data. Firstly, ∏ changes are isotropic in the hydroponic solution, so that all root parts were somewhat homogeneously challenged. In contrast, P, which was only measured in resting cortical cells, close to the root tip, may be different in other cell types. For example, epidermal cells of Arabidopsis roots usually show a P that is ~0.1 MPa lower than that of cortical cells (Javot *et al.*, 2003). This difference translates into a shift in the response curve of P to ∏ and could eventually lead to plasmolysis, in a limited number of cell types, and under the most severe osmotic challenges. Secondly, gene expression data were obtained from a whole-root mRNA extraction, and could mask cell type-specific regulations which are known to exist (Ma and Bohnert, 2007; Dinneny *et al.*, 2008). Finally, the transcriptome status at 15 min is the consequence of regulatory mechanisms that were activated within the first 10 min, where turgor pressure was in a transient status. A more detailed kinetic analysis of the early events would shed light on the gene regulatory networks (Krouk *et al.*, 2010) activated very early by ∏ or P variations. All these aspects deserve more investigations at the cell, gene, and genome levels, for which our current work provide a well-defined framework.

Mechanisms of mRNA abundance regulation by ∏ or P

In this study, mRNA abundance, as monitored by microarrays or RT–qPCR, was employed as a readout of water deficit signaling. We realize that changes in abundance of an mRNA

can be due to many molecular aspects acting on their synthesis or decay. We gathered information for two of them: the corresponding promoter activity and its RNA degradation.

We first analyzed the promoters of genes in the ∏- or P-specific clusters for the presence of binding sites for putative TFs that could regulate their expression at the transcriptional level (Supplementary Datasets S3, S4). We mostly identified binding sites for TFs belonging to the C2C2dof, ABI3VP1, BBR/BPC, C2H2, ZFHD, and REM families. Members of these families have been involved in a broad range of processes but are not specific for water deficit (Yamaguchi-Shinozaki and Shinozaki, 2006; Coutand *et al.*, 2009; Noguero *et al.*, 2013; Mantegazza *et al.*, 2014; Taylor-Teeples *et al.*, 2015; Perrella *et al.*, 2018; Lai *et al.*, 2021; Yan *et al.*, 2021; Wang *et al.*, 2022). This result corroborates the idea that a multiplicity of TFs can regulate each gene. It also indicates that the short-term responses to both ∏ and P probably occur through transcriptional regulation, for which we could not identify representative motifs or the critical role of specific TFs.

To address a possible role for mRNA degradation, we referred to a previous work that studied mRNA decay, but under control conditions (Sorenson *et al.*, 2018). With a median $T_{1/2}$ of >100 min at the whole-genome level, we hypothesized that a short $T_{1/2}$ in resting conditions might be a prerequisite for genes we identified as down-regulated within 15 min by the osmotic treatments (∏ cluster 2 and P cluster 1; Figs 3, 4). Indeed, the relatively short $T_{1/2}$ calculated for genes of ∏-specific cluster 2, together with a promoter activity arrest, is compatible with the regulation we observed. Conversely, this may not be the case for genes of P cluster 1 which showed a median $T_{1/2}$ similar to that of the whole genome. Here, we speculate that on top of a down-regulation of their promoter activity, a reduction in their $T_{1/2}$ should be induced by the osmotic challenges, thereby leading to their rapid down-regulation. Indeed, phosphorylation of proteins of the mRNA decapping complex is regulated by osmotic stresses (Sieburth and Vincent, 2018). The multiplicity of ∏ or P responses that we identified therefore seems to translate into a similar complexity of mRNA regulation mechanisms, and provides an interesting avenue for further investigation.

Functions regulated by ∏ or P

Our approach could possibly identify genes which function in ∏ or P signaling. Semantic and GO enrichments were performed on the gene lists and identified complementary terms. Generic terms retrieved by this approach were mainly associated with transcriptional regulation, responses to abiotic or biotic stimuli, and the cell wall (Fig. 6A, B). It is difficult to extract any precise signaling pathway here since many annotations of these genes are inferred, and some of the terms define diverse functions. For example, arabinogalactan proteins are involved in many processes in roots, including biotic and abiotic responses (Hromadová *et al.*, 2021), and genes of the C1-like domain superfamily have been associated with various biological/developmental processes, including root epidermal cell differentiation (Bruex *et al.*, 2012). It is also somehow surprising to extract terms related to biotic stresses and defense responses. However, this may result from genes whose annotation originates from, but is not necessarily restricted to, 'biotic' conditions, or whose function was only indirectly inferred. Indeed, our approach uncovers genes associated with the 'short-term', less specific, general stress response (Fig. 6C) (Bjornson *et al.*, 2021). Importantly, we introduce here the notion that there is a quantitative relationship between the mRNA abundance of these genes and physico-chemical parameters (Fig. 3C).

Quantitative responses to physico-chemical parameters

Our study integrates into earlier works focused on the perception of the physico-chemical conditions of cells. We investigated here the dose-dependent effects of physico-chemical parameters on the root transcriptome. Such an approach has been successfully applied in poplar, where it was shown that the abundance of ZFP2 mRNA is correlated to the sum of strains upon stem bending (Coutand *et al.*, 2009), and which initiated great advances on the understanding of thigmomorphogenesis. With respect to water, a study was performed in sunflower where a generalized linear model fed by the expression level of three genes was developed in order to compute integrated parameters such as the pre-dawn water potential or the soil water content (Marchand *et al.*, 2013). There is a gap between obtaining correlations between physico-chemical parameters and gene expression—such as what we present here—and creating biomarkers or biosensors (Jones, 2014). Nevertheless, the genes identified in the four clusters could serve as molecular reporters to investigate the perception and signaling of ∏ or P. Indeed, this has been successfully achieved for temperature sensing, where the promoter of HSP70 was used as a quantitative reporter of ambient temperature, and allowed discovery of the role of H2A.Z proteins in the temperature-dependent modulation of transcription (Kumar and Wigge, 2010).

Conclusion

Thanks to a combination of physiological techniques and a transcriptome approach, we showed the existence of rapid, specific transcriptional responses to water-related physico-chemical parameters. We propose herein a list of early responsive genes whose mRNA abundance in quantitatively correlated to external ∏ or to cell P. This list provides potential reporter genes that could serve to elaborate biomarkers of the plant cell water status. This study also paves the way for future dissection of the molecular perception of water deficit in plants, through the identification of how their mRNA abundance is regulated.

Supplementary data

The following supplementary data are available at *JXB* online.

Table S1. Primer sequences for the RT–qPCR analysis.

Dataset S1. *P*-values of the ANOVAs and probe/AGI correspondence for the Gene1.1 ST array.

Dataset S2. Summary of TF-binding site enrichment in the ∏ and P clusters.

Dataset S3. Output of the promoter analysis for each cluster.

Dataset S4. Gene list of each cluster, highlighting the genes that were tested further by RT–qPCR.

Acknowledgements

We thank Alexandre Martinière, François Parcy, and François Tardieu for helpful discussions, and Cécile Fizames for help in the promoter analysis. We thank two anonymous reviewers for helping us improve this manuscript.

Authors contributions

YB and GK: conceptualization; AC and YH: performing the research with contributions from TB for physiological measurements; YH, GK, and YB: data analysis with contributions from SR and CM; YB: writing the article with insights from CM. All authors contributed to reviewing the manuscript and agreed to its content.

Conflict of interest

None declared.

Funding

This project was funded through Labex AGRO 2011-LABX-002, project number 1403-012 to YB, in the I-Site Muse framework, coordinated by Agropolis Fondation, and by the CNRS through the MITI interdisciplinary programs ('Turgomap' to YB). YH is supported by the China Scholarship Council. TB is supported by the LabEx NUMEV (ANR-10-LABX-0020) within the I-Site MUSE (ANR-16-IDEX-0006) and by Region Occitanie.

Data availability

The transcriptomic data that support the findings of this study are openly available in Gene Expression Omnibus Series (https://www.ncbi.nlm.nih.gov/geo/) GSE223207.

The code and source files (besides transcriptomic data) used to analyze the data and/or to generate Figs 1–5 can be downloaded from https://github.com/ybinrae/Watermarker_paper1.git.

References

Bailey TL, Johnson J, Grant CE, Noble WS. 2015. The MEME Suite. Nucleic Acids Research **43**, W39–W49.

Beauzamy L, Nakayama N, Boudaoud A. 2014. Flowers under pressure: ins and outs of turgor regulation in development. Annals of Botany **114**, 1517–1533.

Bjornson M, Pimprikar P, Nürnberger T, Zipfel C. 2021. The transcriptional landscape of *Arabidopsis thaliana* pattern-triggered immunity. Nature Plants **7**, 579–586.

Boursiac Y, Protto V, Rishmawi L, Maurel C. 2022. Experimental and conceptual approaches to root water transport. Plant and Soil **478**, 349–370.

Bowler MG. 2017. The physics of osmotic pressure. European Journal of Physics **38**, 055102.

Bruex A, Kainkaryam RM, Wieckowski Y, *et al*. 2012. A gene regulatory network for root epidermis cell differentiation in Arabidopsis. PLoS Genetics **8**, e1002446.

Carlson M. 2017. Genome wide annotation for Arabidopsis. R package version 3.8.2. org.At.tair.db.

Coutand C, Martin L, Leblanc-Fournier N, Decourteix M, Julien J-L, Moulia B. 2009. Strain mechanosensing quantitatively controls diameter growth and PtaZFP2 gene expression in poplar. Plant Physiology **151**, 223–232.

Creelman RA, Zeevaart JAD. 1985. Abscisic acid accumulation in spinach leaf slices in the presence of penetrating and nonpenetrating solutes. Plant Physiology **77**, 25–28.

Czechowski T, Stitt M, Altmann T, Udvardi MK, Scheible W-R. 2005. Genome-wide identification and testing of superior reference genes for transcript normalization in Arabidopsis. Plant Physiology **139**, 5–17.

Dinneny JR, Long TA, Wang JY, Jung JW, Mace D, Pointer S, Barron C, Brady SM, Schiefelbein J, Benfey PN. 2008. Cell identity mediates the response of Arabidopsis roots to abiotic stress. Science **320**, 942–945.

Grant CE, Bailey TL. 2021. XSTREME: comprehensive motif analysis of biological sequence datasets. bioRxiv https://doi.org/10.1101/2021.09.02.458722. [Preprint].

Hamant O, Haswell ES. 2017. Life behind the wall: sensing mechanical cues in plants. BMC Biology **15**, 59.

Haswell ES, Verslues PE. 2015. The ongoing search for the molecular basis of plant osmosensing. Journal of General Physiology **145**, 389–394.

Hromadová D, Soukup A, Tylová E. 2021. Arabinogalactan proteins in plant roots—an update on possible functions. Frontiers in Plant Science **12**, 674010.

Hüsken D, Steudle E, Zimmermann U. 1978. Pressure probe technique for measuring water relations of cells in higher plants. Plant Physiology **61**, 158–163.

Javot H, Lauvergeat V, Santoni V, *et al*. 2003. Role of a single aquaporin isoform in root water uptake. The Plant Cell **15**, 509–522.

Jia W, Zhang J, Liang J. 2001. Initiation and regulation of water deficit-induced abscisic acid accumulation in maize leaves and roots: cellular volume and water relations. Journal of Experimental Botany **52**, 295–300.

Jones HG. 2014. The use of indirect or proxy markers in plant physiology. Plant, Cell & Environment **37**, 1270–1272.

Katari MS, Nowicki SD, Aceituno FF, *et al*. 2010. VirtualPlant: a software platform to support systems biology research. Plant Physiology **152**, 500–515.

Knoblauch J, Mullendore DL, Jensen KH, Knoblauch M. 2014. Pico gauges for minimally invasive intracellular hydrostatic pressure measurements. Plant Physiology **166**, 1271–1279.

Krouk G, Carré C, Fizames C, Gojon A, Ruffel S, Lacombe B. 2015. GeneCloud reveals semantic enrichment in lists of gene descriptions. Molecular Plant **8**, 971–973.

Krouk G, Mirowski P, LeCun Y, Shasha DE, Coruzzi GM. 2010. Predictive network modeling of the high-resolution dynamic plant transcriptome in response to nitrate. Genome Biology **11**, R123.

Kumar SV, Wigge PA. 2010. H2A.Z-containing nucleosomes mediate the thermosensory response in Arabidopsis. Cell **140**, 136–147.

Lai W, Zhu C, Hu Z, Liu S, Wu H, Zhou Y. 2021. Identification and transcriptional analysis of Zinc Finger-Homeodomain (ZF-HD) family genes in cucumber. Biochemical Genetics **59**, 884–901.

Ma S, Bohnert HJ. 2007. Integration of *Arabidopsis thaliana* stress-related transcript profiles, promoter structures, and cell-specific expression. Genome Biology **8**, R49.

Mantegazza O, Gregis V, Mendes MA, Morandini P, Alves-Ferreira M, Patreze CM, Nardeli SM, Kater MM, Colombo L. 2014. Analysis of the arabidopsis REM gene family predicts functions during flower development. Annals of Botany **114**, 1507–1515.

Marchand G, Mayjonade B, Varès D, *et al*. 2013. A biomarker based on gene expression indicates plant water status in controlled and natural environments. Plant, Cell & Environment **36**, 2175–2189.

Maurel C, Nacry P. 2020. Root architecture and hydraulics converge for acclimation to changing water availability. Nature Plants **6**, 744–749.

Noguero M, Atif RM, Ochatt S, Thompson RD. 2013. The role of the DNA-binding One Zinc Finger (DOF) transcription factor family in plants. Plant Science **209**, 32–45.

O'Malley RC, Huang SC, Song L, Lewsey MG, Bartlett A, Nery JR, Galli M, Gallavotti A, Ecker JR. 2016. Cistrome and epicistrome features shape the regulatory DNA landscape. Cell **165**, 1280–1292.

Pérez-Silva JG, Araujo-Voces M, Quesada V. 2018. nVenn: generalized, quasi-proportional Venn and Euler diagrams.. Bioinformatics **34**, 2322–2324.

Perrella G, Davidson MLH, O'Donnell L, Nastase A-M, Herzyk P, Breton G, Pruneda-Paz JL, Kay SA, Chory J, Kaiserli E. 2018. ZINC-FINGER interactions mediate transcriptional regulation of hypocotyl growth in Arabidopsis. Proceedings of the National Academy of Sciences, USA **115**, E4503–E4511.

Pruneda-Paz JL, Breton G, Nagel DH, Kang SE, Bonaldi K, Doherty CJ, Ravelo S, Galli M, Ecker JR, Kay SA. 2014. A genome-scale resource for the functional characterization of Arabidopsis transcription factors. Cell Reports **8**, 622–632.

Ristova D, Carré C, Pervent M, *et al*. 2016. Combinatorial interaction network of transcriptomic and phenotypic responses to nitrogen and hormones in the *Arabidopsis thaliana* root. Science Signaling **9**, rs13.

Sack L, John GP, Buckley TN. 2018. ABA accumulation in dehydrating leaves is associated with decline in cell volume, not turgor pressure. Plant Physiology **176**, 489–495.

Scharwies JD, Dinneny JR. 2019. Water transport, perception, and response in plants. Journal of Plant Research **132**, 311–324.

Sieburth LE, Vincent JN. 2018. Beyond transcription factors: roles of mRNA decay in regulating gene expression in plants. F1000Research **7**, F1000 Faculty Rev-1940.

Sorenson RS, Deshotel MJ, Johnson K, Adler FR, Sieburth LE. 2018. *Arabidopsis* mRNA decay landscape arises from specialized RNA decay substrates, decapping-mediated feedback, and redundancy. Proceedings of the National Academy of Sciences, USA **115**, E1485–E1494.

Steudle E. 1989. Water flow in plants and its coupling to other processes: an overview. Methods in Enzymology **174**, 183–225.

Taylor-Teeples M, Lin L, de Lucas M, *et al*. 2015. An Arabidopsis gene regulatory network for secondary cell wall synthesis. Nature **517**, 571–575.

Vandesompele J, De Preter K, Pattyn F, Poppe B, Van Roy N, De Paepe A, Speleman F. 2002. Accurate normalization of real-time quantitative RT–PCR data by geometric averaging of multiple internal control genes. Genome Biology **3**, research0034.1.

Verslues PE, Bailey-Serres J, Brodersen C, *et al*. 2023. Burning questions for a warming and changing world: 15 unknowns in plant abiotic stress. The Plant Cell **35**, 67–108.

Wang Z, Wong DCJ, Chen Z, Bai W, Si H, Jin X. 2022. Emerging roles of plant DNA-binding with one finger transcription factors in various hormone and stress signaling pathways. Frontiers in Plant Science **13**, 844201.

Wu T, Hu E, Xu S, *et al*. 2021. clusterProfiler 4.0: a universal enrichment tool for interpreting omics data. The Innovation **2**, 100141.

Yamaguchi-Shinozaki K, Shinozaki K. 2006. Transcriptional regulatory networks in cellular responses and tolerance to dehydration and cold stresses. Annual Review of Plant Biology **57**, 781–803.

Yan J, Liu Y, Yang L, He H, Huang Y, Fang L, Scheller HV, Jiang M, Zhang A. 2021. Cell wall β-1,4-galactan regulated by the BPC1/BPC2-GALS1 module aggravates salt sensitivity in *Arabidopsis thaliana*. Molecular Plant **14**, 411–425.

Chapter 2: Development of a genetic reporter of hydraulic changes in the root of Arabidopsis requires both mRNA synthesis and decay functions

Development of a genetic reporter of hydraulic changes in the root of Arabidopsis requires both mRNA synthesis and decay functions

Yunji Huang, Christophe Maurel, Gabriel Krouk, Yann Boursiac

Institute for Plant Sciences of Montpellier (IPSiM), Univ Montpellier, CNRS, INRAE, Institut Agro, Montpellier, France

Short title: Development of a genetic osmo-reporter in Arabidopsis

Author for correspondence: Yann Boursiac, yann.boursiac@inrae.fr

Abstract

Water deficit caused by osmotic stresses, including salinity and drought, presents a significant environmental challenge to plant growth and crop yield. In seconds to hours, it results in diverse responses in plants, including the impairment of cell wall integrity (CWI), the decline in turgor potential (P), the generation and signaling of abscisic acid (ABA), as well as reprogramming of gene expression. These processes have been studied extensively but, so far, no clear picture of when and where water deficit is perceived by plants exists. In a previous work, we identified genes whose mRNA abundance in roots was quantitatively correlated to changes in either the osmotic potential (Π) or cortical cells turgor pressure. In this work, we focused on two of those candidates, *ENODL8* and *NCED3*, and unravel that plasmolysis is a turning point in their dynamic of response to osmotic stress. Both promoter activity and mRNA decay pathways are required for their proper regulation. Finally, we created a luciferase-based construct that was able to report hydraulic changes which, although initially designed in roots, was also responsive in shoots.

Keywords: water potential, turgor potential, osmotic potential, hydraulic, water deficit, reporter, ABA, cell wall integrity, perception, root

Introduction

Water deficit is a stress that is experienced by plants as soon as the water demand exceeds the water uptake capacity (Bray, 1993). It may not be related to the water content of a plant tissue, since low water content can be the regular status of some specific developmental stages in higher plants, for instance during seed maturation (Bray, 1993). Currently, the exceptional pace of global climate change intensifies the amplitude and frequency of extreme weather events, including salt and drought events, that reduce water availability in plants (Lobell and Field, 2007; Mukherjee et al., 2018). Given the profound impact of water deficit on agricultural and ecological systems, understanding the molecular mechanisms of plant responses holds immense importance (Wang et al., 2003).

A decrease in osmotic potential (Π) of the soil solution is a common crossing-component of water

deficit treatments - including salinity and drought. It results in a variety of initial cellular events, such as decrease of turgor potential (P), increase of intracellular Ca^{2+}, ABA accumulation and alteration in cell wall (CW)-plasma membrane (PM) connections (Chen et al., 2020; Zhang et al., 2022). Subsequently, these initial signals are integrated and multi-fold amplified to trigger signaling cascades that regulate gene expressions, and physiological and biochemical reactions, hence improving plant resistance (Zhu, 2016; Zhang et al., 2022). Only a few water-deficit associated stress sensors have been clearly identified so far, such as the osmosensor OSCA1 and the Na^+-sensor GIPC (Yuan et al., 2014; Jiang et al., 2019). Many other proteins are regarded as putative sensors as well, such as aquaporins and CSCs (other members of the family of OSCA1), but their biochemical sensing mechanisms and/or physiological functions have yet to be characterized in details (Nongpiur et al., 2020; Zhang et al., 2022). Moreover, the majority of known signaling pathways and transcriptional regulatory networks have not been linked to these sensors (Zhang et al., 2022).

The main difficulties in the identification of osmosensors are genetic redundancy and lethality, as well as the crosstalk between various signaling pathways (Zhu, 2016). Reporters are helpful tools for that purpose (Sadanandom and Napier, 2010). For example, Kumar and Wigge developed a genetic reporter of temperature by using a *pHSP70::Luc* (luciferase) construct, and used it to identify a temperature sensor: the alternative histone H2A.Z in Arabidopsis (Kumar and Wigge, 2010); OSCA1, as an osmosenor, has been identified via genetic screens of transgenic plants expressing aequorin-based Ca^{2+} indicators (Yuan et al., 2014). Therefore, developing an osmo-reporter, i.e. a tool able to report changes in the plants hydraulics parameters or their variations such as P, Π or Ψ, would be beneficial for identifying osmosensors and unraveling osmo-signaling pathways. In addition, although there have been some explorations into osmosensing, such as ABA signaling specifically in the elongation zone of the future cortical cells and asymmetric distribution of cytokinins in the meristem zone for hydrotropism, the timing and location at which plants sense homogeneous osmotic stress in a manner that triggers gene expression alteration remains unknown (Dietrich et al., 2017; Chang et al., 2019). Recently, by performing high-resolution Ca^{2+} imaging, Steinhorst et al. reported that when exposed to Na^+ stress, primary calcium signals are specifically triggered in a cell group located within the root differentiation zone (Steinhorst et al., 2022). Therefore, in situ and live imaging reporters could enable us to elaborate how plants spatially and temporally perceive and respond to water deficit.

In plants, two biophysical signals, Π and P, primarily compose the thermodynamic parameter water potential (Ψ), which allows to understand water movement between the different compartments of the soil/plant/atmosphere continuum (Haswell and Verslues, 2015). Π is closely linked to solute concentration within cellular compartments, influencing biochemical reactions. The cells have the capacity to regulate Π directly through processes like osmoticum synthesis, accumulation and transport. In conjunction with the viscoelastic properties of the CW, P plays a pivotal role in cell and organ elongation, as well as in conferring rigidity to structures such as stems and leaves (Beauzamy et al., 2014). Measuring Ψ in plants is technically difficult: it is so far obtained by a combination of challenging and indirect techniques such as pressure chambers, cell pressure probes or pico-osmometers (Shabala and Lew, 2002; Boursiac et al., 2022). There is a real need for improved tools since Ψ in plants is constantly fluctuating (within minutes) due to growth, soil and

air humidity, light variation, etc...

We recently unraveled a differential impact of Π and P on the gene responses upon water deficit treatments, and presented a short list of Π and P quantitatively and specifically regulated genes. In the current study, we explored in more details the regulations of two of those genes, with the aim of understanding better the plant cells parameters and the transcriptional mechanisms at the origin of their regulation. We used these informations to build a genetic reporter that was able to respond quantitatively to changes in P within minutes, and Π within a 30min-3h time window. With this work, we aim at opening a new field of investigation in water deficit perception, with the ability to report, almost in real-time, variations in plant hydraulic parameters.

Results

Plasmolysis acts as a turning point in the early transcriptional regulation of two P or Π correlated genes.

We reported that, among others, *At1G64640* (*ENODL8)* and *NCED3* mRNA levels respond quantitatively to turgor potential (P) and osmotic potential (Π), respectively, after 15min of mild water deficit (MWD) treatments that preserved the turgidity of root cortical cells (P > 0) (Crabos, Huang et al.). We explored how this quantitative correlation would persist in response to more severe water deficit (SWD). For this, we treated hydroponically grown plants for 15 min with concentrations up to 200mM NaCl, 400mM sorbitol, 400mM EG, or 250g/l PEG, and monitored the expressions of *ENODL8* and *NCED3* in whole roots (**Figure 1A**). *ENODL8* mRNA abundance decreased quantitatively upon treatments with increasing concentrations of NaCl, Sorbitol and PEG of up to 125mM, 250mM and 200g/l, respectively, and not with EG treatments, consistently with our previous results. Surprisingly, this correlation was inverted for higher concentrations, as mRNA levels decreased less (compared to control conditions) with increasing solutes concentrations. *NCED3* expression showed the same, but inverted, bell-shaped regulation dynamic for NaCl, sorbitol and PEG treatments, while it showed a continuous increase in mRNA levels upon EG treatments. As a control, the *COR* gene, which was not found in our initial screen, didn't show any significant expression change (**Fig. 1A**). These results indicate that, 15 min after treatment, these 2 genes do not respond anymore in the same way to extended changes in Π from mild to severe water deficit. This can be visualized through the correlation between gene expression and Π — $R < 0.6$ and $P > 0.05$ for both genes (**Supplementary Figure 1A**). Noticeably, the expression of *ENODL8* remained relatively stable throughout the whole range of EG treatments (**Fig. 1A**), which is consistent with our earlier observation that the mRNA abundance of this gene seems to be correlated better to P than to Π (**Supplementary Figure 1B**). On the contrary, the expression of *NCED3* showed a dose-dependent induction under the same treatments (**Fig. 1A)**, which implied a different quantitative response, somehow related to Π, caused by these treatments (**Supplementary Figure 1A**).

We hypothesized that the turning point of the transcriptional correlation to Π or P of our 2 reporters, *ENODL8* and *NCED3*, under water deficit could be due to the plasmolysis of cortical cells caused by the high concentrations of solutes. To test this, the junction between two consecutive root cortical cells at the end of the meristematic zone of the primary root was observed with the plasma membrane (PM) marker line LTI6b-GFP (Cutler et al., 2000), 15 to 25 min after treatments. In order to determine whether plasmolysis occurred, we defined a "plasmolysis

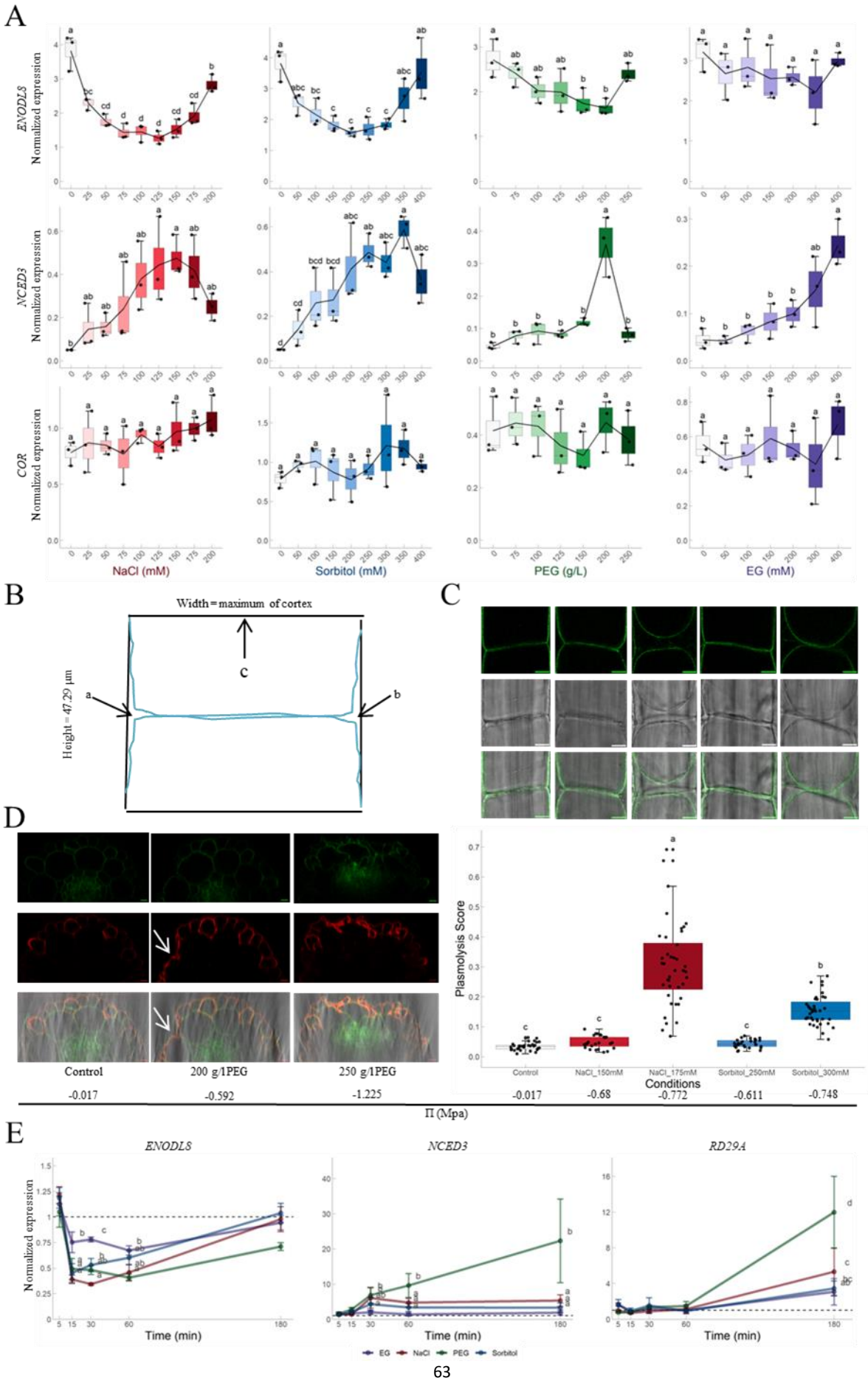
A
ENODL8
Normalized expression
NCED3
Normalized expression
COR
Normalized expression
NaCl (mM)
Sorbitol (mM)
PEG (g/L)
EG (mM)
B
Width = maximum of cortex
c
a
b
Height = 47.29 µm
C
D
Control
200 g/1PEG
250 g/1PEG
-0.017
-0.592
-1.225
Plasmolysis Score
Control
NaCl_150mM
NaCl_175mM
Sorbitol_250mM
Sorbitol_300mM
Conditions
-0.017
-0.68
-0.772
-0.611
-0.748
Π (Mpa)
E
ENODL8
NCED3
RD29A
Normalized expression
Time (min)
Time (min)
Time (min)
EG
NaCl
PEG
Sorbitol

Fig 1. Plasmolysis in cortical cells of the primary root disrupts the quantitative regulation of *ENODL8* and *NCED3* expressions in response to changes in P upon water deficit

(A) Normalized expression of 3 genes in Arabidopsis roots after osmotic treatments for 15min. Normalized expression means that gene expression are presented relatively to the expression of internal control genes (see M&M). (B) "plasmolysis score" was defined as the ratio of the area outside the plasma membrane to the total area (a+b)/c. (C) Plasmolysis of cortical cells in the primary root occurred when Π decreased to less than -0.7 MPa caused by treatments with 175 mM NaCl and 300 mM sorbitol. Each expriment has 2 biological repeats and each repeat has 2 plants. 5-14 junctions of cortex cells from 1 plant were observed and representive images are shown. Corresponding statistical results of plasmolysis score are shown below the confocal images. (D) Reconstructed cross-sections of roots upon PEG8000 treatments under confocal microscope. Up: GFP, middle: PI staining, bottom: overlapped image. (E) Relative expressions in the roots under 50 mM NaCl, 100 mM sorbitol, 150 g/L PEG and 100 mM EG treatments. Relative expression means that the normalized expression of a gene under treatment is compared to the normalized expression of the same gene under control conditions at the same time point. Scale bars : 10 μm. Osmolality (MPa) of each treatment is shown at the bottom. Black lines in A represent mean value of 3 biological repeats and each point means one biological repeat. The error bars represent the standard error (se) (mean ± se) and different letters mean a significant difference among conditions at a given time point after anANOVA followed by Tukey's HSD test ($P < 0.05$).

score" as the ratio of the area outside the PM to the total observed area ((a+b)/c, **Fig. 1B**). This plasmolysis score was not different from control condition for concentrations up to 150mm NaCl (Π = -0.662 MPa) or 250mM sorbitol (Π = -0.616 MPa). A clear increase in this score was then observed under only slightly more severe treatments, with 175mM NaCl (Π = -0.79 MPa) or 300mM sorbitol (Π = -0.741MPa) (**Fig. 1C**). In contrast to NaCl and sorbitol, PEG800 does not cross the apoplast, and elevated concentrations will result in cytorrhesis rather than plasmolysis (Carpita et al., 1979). Indeed, epidermal cells, but not cortical cells, showed signs of cytorrhesis after a treatment with 200 g/L PEG8000 (Π = -0.692 MPa) while cortical cells were in cytorrhesis too in a treatment of 250 g/L (**Fig. 1D**). Note that neither plasmolysis nor cytorrhesis could be observed for high concentrations of EG as turgor always remained positive within 15 min after treatment with 300 or 400 mM. Thus, in our conditions, the concentrations at which plasmolysis in cortical cells begins, around -0.7 MPa, clearly coincide with the turning point in the accumulation of *ENODL8* and *NCED3* mRNA. These results suggest that cortical cells plasmolysis introduce yet another dynamic of transcriptional regulation in response to water deficit. A feature that should be bore in mind when interpreting data from water deficit treatments.

NCED3 and *ENODL8* expression quantitatively respond to changes in P, rather than Π, over the course of 3 h of MWD.

Turgor drop, as a consequence of water deficit treatment, will be restored after about 40 min to many hours of onset, depending on the intensity of the water stress and the resistance of the plants (Shabala and Lew, 2002). The findings depicted in **Fig. 1A** as well as our earlier work (Crabos, Huang et al. 2023) showed that *ENODL8* and *NCED3* quantitatively responded to changes in P or Π after MWD treatments for 15 min, but it is unknown whether this quantitative response persists over time during water deficit treatments. To test this, gene expression was monitored in the roots over 3 hours of water deficit, consisting in treatments with 50 mM NaCl, 100 mM sorbitol, 150 g/L PEG and 100 or 250 mM EG. *ENODL8* mRNA levels were not different at 5 min after treatment, but were significantly reduced at 15 min and up to 1 h for all treatments (**Fig. 1E**).

Recovery of the initial abundance was observed in the roots after 3 h for NaCl, sorbitol and EG, while PEG treatment persisted in a trend for lower abundance without reaching statistical significance. Importantly, the decrease in *ENODL8* expression caused by EG treatment was significantly weaker compared to the other treatments at 15 min and 30 min (**Fig. 1E**). Meanwhile, *NCED3* was induced by all treatments, displaying a significant increase of over 2-folds after NaCl, sorbitol and PEG treatments for 30 min, while no such effect was observed upon EG treatment. No recovery of its mRNA abundance was observed in the roots under PEG, NaCl and sorbitol treatments. PEG treatment had the most impact, as *NCED3* levels continued to rise over the kinetic. These results suggest that *ENODL8* expression exhibit a quantitative response to changes in P over time, both in reduction and recovery under MWD treatments, while *NCED3* shows a quantitative response within 1h only for the induction phase, and seems not to be correlated to P anymore after that period. When looking at more severe treatments (**Supplementary Figure 2**), 250 mM sorbitol and 250 mM EG showed a similar kinetic of response, but 400 mM resulted in a continuous reduction in the expression of *ENODL8* with no recovery. This last response may be attributed to an alternate regulation after plasmolysis, as discussed above, and/ or to a delay in turgor recovery. As a control, the abiotic-responsive gene *RD29A* (Yamaguchi-Shinozaki and Shinozaki, 1994) expression rose, as expected, after 1h of treatment and showed a dose- and time- dependent response, confirming the impact of our water deficit treatments on the plants (**Fig. 1E** and **Supplementary Figure 2**). Altogether, the expression level of *ENODL8* within 3h is consistent with changes in P over time during MWD treatments, which makes it a good candidate able to report P in roots. The expression level of *NCED3* is consistent with changes in P only during the first 30 mins of treatment, and then might be related better to Π for MWD treatments.

Promoter activity and mRNA decay pathway are both involved in the regulation of *ENODL8* and *NCED3* mRNA abundance under osmotic challenge

We previously showed that many genes whose expression correlated to P or Π exhibited reduced mRNA half-life time ($T_{1/2}$) under standard conditions (Crabos, Huang et al.). We used the transcriptional inhibitor cordycepin (Holbein et al., 2009; Sorenson et al., 2018) in order to test to which extent mRNA decay could be responsible of the regulation of *ENODL8* and *NCED3* under an osmotic challenge (**Fig. 2A**). Under 50mM NaCl treatment, the expression of *ENODL8* showed a continuous decrease during the first 30 min, then recovered up to the initial level at 3 h, compared to the mock treatment. Under cordycepin treatment, its expression showed a continuous decrease and reached within 60min a plateau that lasted at least 3h, consistent with the mRNA abundance observed for many genes in previous reports using this drug (Sorenson et al., 2018; Chantarachot et al., 2020). Importantly, the double treatment cordycepin + NaCl resulted in a stronger and faster reduction of *ENODL8* mRNA abundance in the first 30min compared to a treatment by cordycepin alone, very similar to the NaCl treatment alone. This result indicates that the mRNA decay pathway responsible for the degradation of *ENODL8* mRNA has probably been upregulated by osmotic stress, hence reducing $T_{1/2}$. On the contrary to NaCl treatment alone after 30 min, the mRNA abundance of *ENODL8* was not restored in the double treatment which suggests that, under MWD, activation of its promoter at later stages is overriding its mRNA decay.

We created two reporter lines where the promoter of *ENODL8* controlled the expression of either a GFP-GUS fusion (*pENODL8::eGFP-GUS*) or a short-lived version of the luciferase (*pENODL8::Sluc*) (Luc-hCL1-PEST, luciferase sequence fused with destabilization sequences hCL1 and PEST) which had been used to perform rapid high-throughput screening in HeLa cells (Younis et al., 2010). We monitored the expression of the native *ENODL8* and of the reporters in those lines under 200 or 250mM sorbitol treatments (**Fig. 2B**). In all transgenic lines, the native *ENODL8* showed a decrease in the first 30 min of treatments and then at least a partial recovery, consistent with our results above (**Supplementary Figure 2**). However, the expressions of *GFP* and *Sluc* did not exhibit any significant reduction. These results indicate that the promoter of *ENODL8* does not recapitulate the regulation of its mRNA abundance, and confirm the importance of a mRNA degradation pathway for this gene during the early phase of a water deficit – a feature that is lost in the reporter lines. Notably, a slight induction of the mRNA abundance of the reporters could be observed after 15 min, which may contribute to the recovery of the native *ENODL8* expression and is consistent with the hypothesis that the promoter activity of *ENODL8* is being activated after the initial phase under MWD.

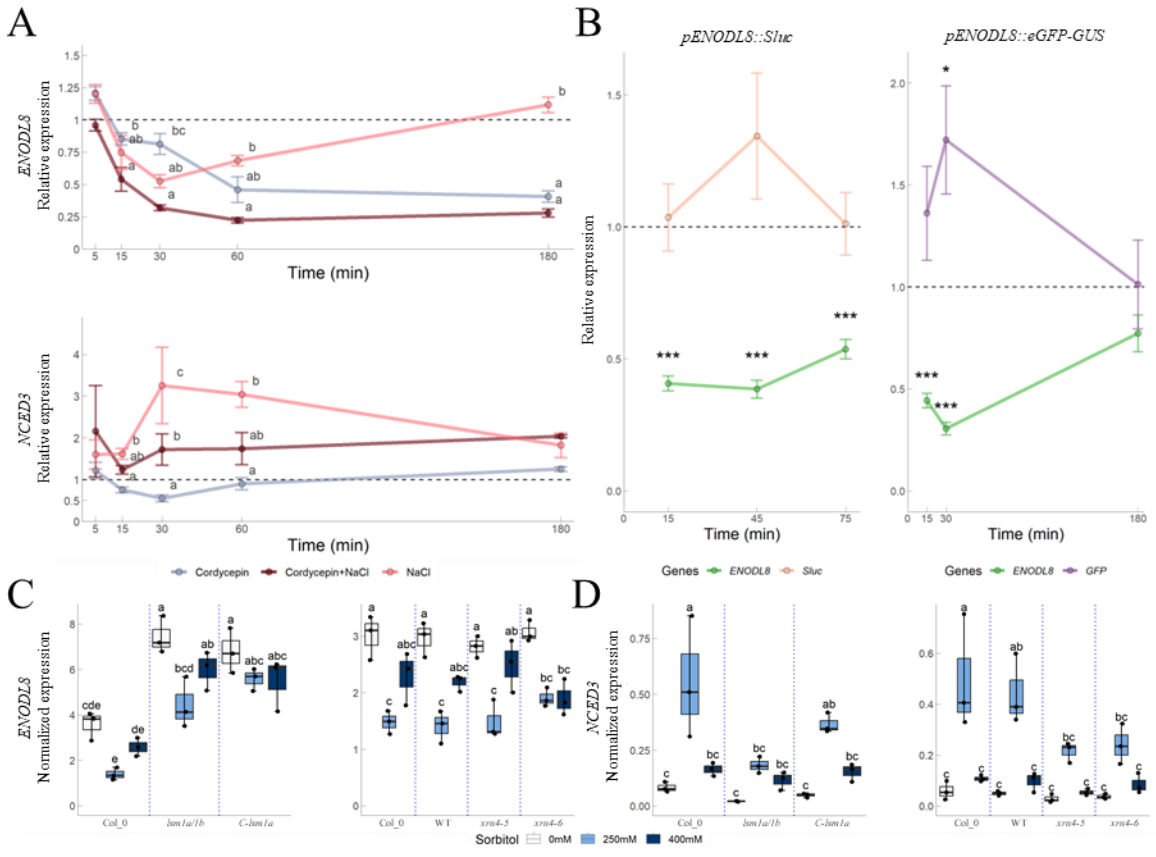

Fig 2. The expression of *ENODL8* and *NCED3* is controlled both at the transcriptional and mRNA decay levels, which are modulated by changes in P during water deficit treatments.

(A) Relative expression in the roots under 50mM NaCl, 100 µg/ml cordycepin and NaCl + cordycepin treatments. Relative expression means that the normalized expression of a gene under treatment is compared to the normalized expression of the same gene under control conditions at the same time point. 3 biological repeats per treatment. Different letters mean a significant difference among conditions for the same time point (mean ± se, ANOVA and Tukey's HSD test (P< 0.05)). (B) Relative mRNA abundance of *ENODL8*

and of the reporters *Sluc* or *GFP* in roots after sorbitol treatment. Constructs are depicted in the upside of the graph, *pENODL8*::*Sluc* and *pENODL8*::*eGFP-GUS* expressing plants were treated with 200mM and 250mM sorbitol, respectively. Each point is the average of the relative expression in 3 biological repeats of 3 lines (*pENODL8*::*Sluc*) or 2 lines (*pENODL8*::*eGFP-GUS*) under the same conditions. Asterisks highlight a significant difference between control and treatments at a given time point (mean ± se, ANOVA and Tukey's HSD test (P< 0.05)). (C-D) Normalized expressions of *ENODL8* and *NCED3* in the roots of mRNA decay mutants after 250 and 400 mM sorbitol treatments for 15 min. Normalized expression means that gene expression is referenced to the expression of internal control genes. 3 biological repeats for each treatment. (ANOVA and Tukey's HSD test ($P < 0.05$)).

The expression of *NCED3* under NaCl, relative to mock treatment, showed a significant increase from 15 to 60 min (**Fig. 2A**), consistent with our results above (**Fig. 1E**). The first 30 min of cordycepin treatment saw a decrease in *NCED3* mRNA abundance as expected but, to our surprise, were followed by a continuous increase in the next 2.5 hours. Note that we can rule out any issue in the drug effectiveness since these results were obtained from the same samples than those used to monitor *ENODL8* expression. We hypothesize that the mRNA abundance of this gene is tightly controlled/buffered by yet other monitoring mechanisms that may be activated after 30 min. The double treatment cordycepin + NaCl showed an intermediate dynamic between NaCl and cordycepin treatments alone. In particular, at 30 min, its mRNA level was significantly higher under double treatment compared to cordycepin treatment, yet significantly lower compared to NaCl treatment. This suggests that the NaCl treatment is capable of increasing the mRNA abundance of *NCED3* by decreasing its mRNA degradation, and/or increasing its mRNA abundance through cordycepin-insensitive mechanisms.

mRNA abundance is governed by the opposing forces of synthesis and decay. Most transcripts don't have dedicated decay pathways and instead primarily undergo cytoplasmic mRNA degradation, including 5'-3' mRNA decay and 3'-5' mRNA decay (Perea-Resa et al., 2012; Sorenson et al., 2018). To test whether the mRNAs of *ENODL8* and *NCED3* are degraded through these pathways during water deficit, we monitored their expressions in mutants defective in the 5'-3' mRNA decay pathway (*lsm1a/1b* double mutant and *xrn4*) (Perea-Resa et al., 2012; Kawa et al., 2020) and a 3'-5' decay pathway gain-of-function line (WT [Col_SOV^{Ler}]) (Sorenson et al., 2018) after 250 and 400 mM sorbitol treatments for 15 min. In Col_0 and all mutants, the expression of *ENODL8* showed a consistent "bell-shaped response" characterized by a decrease upon 250 mM sorbitol treatment and not upon 400 mM sorbitol treatment. *ENODL8* mRNA abundance exhibited a ~2-fold higher expression in the *lsm1a/1b* double mutant over all conditions, while complementation (*C-lsm1a*) of the *lsm1a/1b* mutant with one of the alleles, *lsm1a,* was not sufficient to restore its expression level back to Col_0 plants (**Fig. 2C**). These results suggest that *LSM1A* and/or *LSM1B* are involved in regulating the absolute expression of *ENODL8*, but not its response to MWD. Moreover, no significant difference was observed between Col_0 and *WT*/*xrn4* mutant after treatments, although it showed a slightly lower reduction only in *xrn4-6* after 250 mM sorbitol treatment. We confirmed that *xrn4-5* may not be a knock-out mutant and that *xrn4* was significantly induced in the *xrn4-5* mutant after 250 mM sorbitol treatment, which could explain the different response between the two lines (**Supplementary Figure 3**), but does not allow us to positively conclude on the role of XRN4 in regulating the expression of *ENODL8*.

In Col_0 and all the other genotypes, the expression of *NCED3* also showed a consistent "bell-

shaped response": it was induced almost always significantly by 250 mM sorbitol treatment and not induced by 400 mM sorbitol treatment (**Fig. 2D**). Importantly, the induction of *NCED3* in *lsm1a/1b* was significantly lower than in Col_0 after 250 mM sorbitol treatment, and this was, at least partially, rescued in the complementary line *C-lsm1a*. This suggests that *LSM1a* is required for the induction of *NCED3* in response to osmotic stress, aligning with the finding that the LSM1-7 complex regulates *NCED3* mRNA turnover in Arabidopsis when exposed to high salt or cold (Perea-Resa et al., 2016). No significant difference was observed between Col_0 and WT after treatments. Unlike *ENODL8*, the induction of *NCED3* was significantly lower in both *xrn4-5* and *xrn4-6* mutants compared to Col_0. This indicates that regular levels of XRN4 are required for *NCED3* regulation in response to osmotic stress. However, because LSM1 and XRN4 acts in the degradation of mRNAs, which should act the opposite way to the mRNA accumulation we observe, we suspect that they might be acting indirectly.

Altogether, our results suggest that P and Π quantitatively shape the expression of *ENODL8* and *NCED3* by integrating both transcriptional regulation and mRNA decay during water deficit. For *ENODL8*, mRNA levels would be controlled by LSM1 and, upon stress, a degradation pathway would be activated first, followed by a secondary promoter activation. *NCED3* expression would be under tight control by a probable mRNA buffering/monitoring system and, upon stress, would be indirectly regulated by XRN4.

pNCED3::Sluc-3'UTR construct is able to reproduce the expression of *NCED3* in response to water deficit treatments, while *pENODL8::Sluc-3'UTR* is not.

Since *ENODL8* and *NCED3* mRNA levels appear to quantitatively report components of Ψ, or at least their variations, we next attempted to use them to develop hydraulic reporters. As an example of such reporter, a construct *uNIP5;1-Luc* had been generated by fusing a short-lived version of the luciferase *sLuc* (*Luc-PEST*) with the *NIP5;1 5'-UTR,* which promotes mRNA degradation in response to increased abundance of boric acid in the cytosol. Such a construction allowed to visualize the spatial and temporal changes in boron in Arabidopsis (Younis et al., 2010). Considering that mRNA decay is an essential part of the expression of our candidates under water deficit, we used a similar approach in which both the promoters and 3'UTR of *ENODL8* and *NCED3* were used to control the expression of *Sluc*. Transgenic plants carrying *pENODL8::Sluc-3'UTR* construct or carrying *pNCED3::Sluc-3'UTR* were generated, and the mRNA abundance of *Sluc* and *ENODL8* or *NCED3* were monitored after treatments with 50/100 mM NaCl, 100/200 mM sorbitol, 100/150 g/L PEG, or 100 mM EG for 15 min (**Supplementary Figure 4A-D**). After 15 min of treatments, the expression of both native *ENODL8* and *NCED3* showed the expected quantitative response in the *pENODL8::Sluc-3'UTR* and *pNCED3::Sluc-3'UTR* transgenic plants, respectively, consistent with our results in untransformed plants. The *Sluc* mRNA was induced slightly by the treatments in two independent lines (L7 and L16) plants carrying the *pNCED3::Sluc-3'UTR* construct, but no clear response of *Sluc* was observed in two independent lines (L13 and L15) plants carrying *pENODL8::Sluc-3'UTR*. Analyzing in more details the correlations between the native and the Sluc mRNAs (**Fig. 3A**), we confirmed that such construction was not able to recapitulate the behavior of *ENODL8* expression. However, *Sluc* mRNA from the *pNCED3::Sluc-3'UTR* construct correlated

significantly to the endogenous *NCED3* mRNA. This correlation was even stronger at 30 min (**Fig. 3B** and **supplementary Figure 4G**). In summary, plants carrying a *pNCED3::Sluc-3'UTR* construct appear to be capable of reporting with confidence the expression of *NCED3* in water deficit conditions.

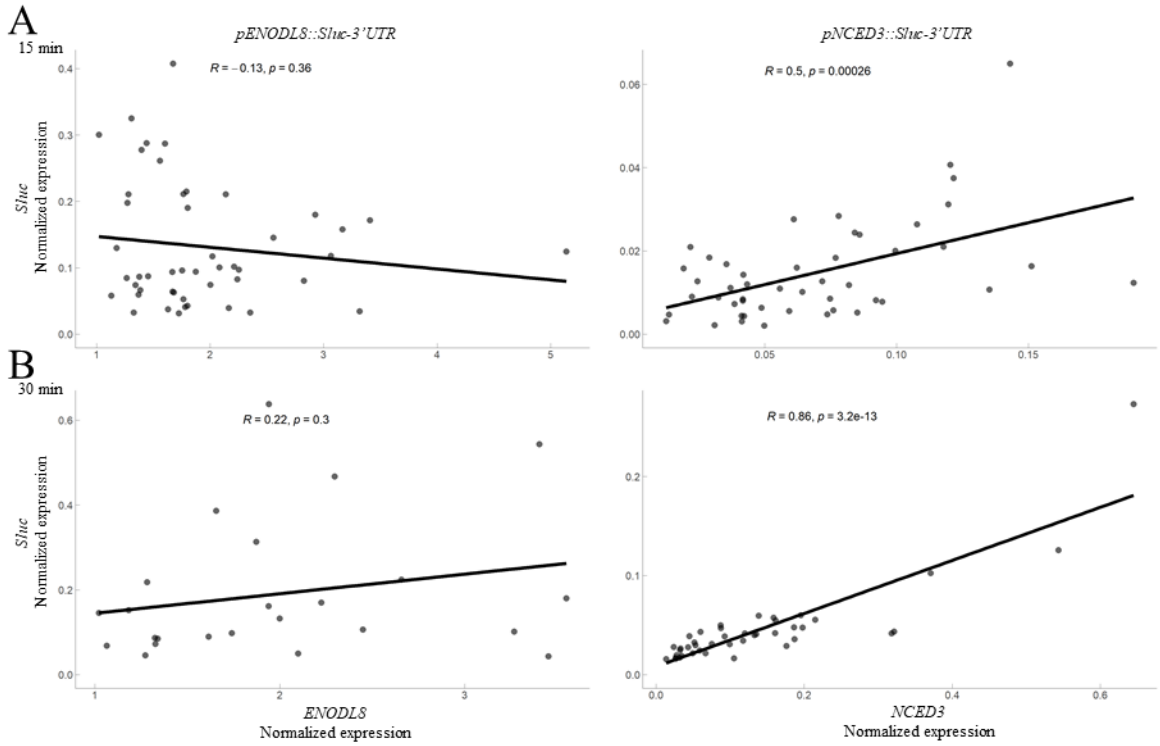

Fig 3. Only in *pNCED3::Sluc-3'UTR* expressing lines is the mRNA abundance of the reporter able to report that of its native gene in response to water deficit.

(A) Pearson correlation analysis between the abundance of *Sluc* and *ENODL8* or *NCED3* transcripts after treatments with 50/100 mM NaCl, 100/200 mM sorbitol, 100/150 g/L PEG and 100 mM EG for 15 min. Gene expressions were monitored in 2 lines for both *pNCED3::Sluc-3'UTR* (L7 and L16) and *pENODL8::Sluc-3'UTR* (L13 and L15) constructs. (B) Pearson correlation analysis between the expression of *Sluc* and *ENODL8* after treatments with 100/150/200 mM sorbitol for 30 min or the expression of *Sluc* and *NCED3* after treatments with 50/75/100 mM NaCl, 100/150/200 mM sorbitol, 100/125/150 g/L PEG, and 100/150/200 mM EG for 30 min. Expressions were monitored in 2 lines for *pNCED3::Sluc-3'UTR* construct and 1 line (L7) for *pNCED3::Sluc-3'UTR*. Normalized expression means that gene expression is referenced to the expression of internal control genes. 3 biological repeats for each treatment and each point stands for one repeat of one treatment. Pearson coefficient (R) and p-values are showed in the graph for the black, solid, regression lines.

The luminescence signal from *pNCED3::SLuc-3'UTR* expressing plants can report hydraulic changes

To test the ability of Sluc in plants carrying the *pNCED3::Sluc-3'UTR* construct to report for plant hydraulic changes in luciferase imaging assays, we measured the Sluc luminescence signals in whole roots and shoots (**Fig. 4A**) of two transgenic lines (L7 and L16) during treatments with a series of concentrations of NaCl, sorbitol, PEG8000 and EG. Under control conditions, Sluc signal in the roots and shoots of L7 and L16 plants did not differ from the signal in of WT, whereas it was extremely elevated in roots of a reference line (*p35S::Sluc*) and relatively high in shoots (**Fig. 4B**). It has been reported that wild-type GFP and firefly luciferase proteins have a ~26 h and 3-4 h half-life in mammalian cells,

respectively (Corish and Tyler-Smith, 1999; Leclerc et al., 2000). By using cordycepin on this reference line, we calculated that the luciferase signal had a half-life of about 1 h (**Fig. 4 C**), which makes this construct a relatively "fast" genetic reporter.

In control conditions, Sluc signal in roots from the *pNCED3::Sluc-3'UTR* expressing line L7 remained relatively stable for 2 h (**Fig. 4 D**). The most visible feature of the Sluc kinetics upon treatments was a dose-dependent response to 50-175 mM NaCl, 100-350 mM sorbitol, 100-175 g/l PEG and all the EG treatments within ~120 to ~180 min (**Fig. 4D**). During this period, the Sluc signal showed a quantitative response to changes in Π (**Fig. 4 E**). This was further corroborated by correlation analyses between Sluc signals in roots (of L7) and Π-All (Π under all conditions) (**Fig. 4 F, upper row**). Π-All consistently maintained a significant correlation ($R > 0.6$ and $P < 0.01$) with the Sluc signals for the treatments after 29.4 min. Similar results were also acquired in roots of L16 (**Supplementary Figure 5 A-C**), which suggest that the *pNCED3::Sluc-3'UTR* construct could be used as a Π-reporter during the 30min-3.5h period of water deficit treatments.

Sluc signals in L7 roots were, however, not significantly induced in the first 15 min and hence not well correlated to Π-All nor to the initial regulations of NCED3 mRNA that we unraveled. Because treatments with concentrations that induce plasmolysis in the cortical cells might change the dynamics of response, as we have shown for the native mRNA earlier, we evaluated the correlation of Sluc signals with Π-Turgid, Π values under treatments that maintained cortical cells turgid only, but found not much differences from correlations with Π-All (**Fig. 4F, second row**). Given that the first increase in Sluc signal appeared after 15 to 30 min, we looked into more details at this initial phase. Treatments with the lowest concentrations of solutes (25 mM NaCl, 50 mM sorbitol, 75 and 100 g/l PEG and 50 mM EG; in which P dropped by about 0.1MPa) resulted in transient, yet significant, increases in Sluc signals at ~25 min. Importantly, the bell-shaped response to increasing concentrations in solutes (cf **Fig. 1A**) was found back but mainly for a 25 to ~50 min period after treatment (**Fig. 4G**). We therefore hypothesized that a delay would be necessary between the mRNA regulation and the Sluc signal, due to the post-transcriptional steps required to reach a fully functional luciferase. In order to test this, we correlated the kinetic of Sluc with the kinetic of P (conditions when P > 0 MPa, 25-100 mM NaCl, 50-150 mM sorbitol, 75- 150 g/l PEG and 50-200/300/400 mM EG treatments) measured with a cell pressure probe, but with no constraint about the initial starting time (**Fig. 4G**, lower part). The best correlations were observed when the kinetic of P (starting 6 min after treatment) was correlated to the kinetic of Sluc signals starting from 25.2 to 37.8 min, and lasting up to the 42 to 54.6 min time points. In other words, the Sluc signals in L7 roots showed strong correlations to P during the early phase of treatments, but with a 19 to 31 min delay (**Fig. 4C**). Similar results, although with lower significances, were observed in the roots of L16 (**Supplementary Figure 5A**). Overall, results from the 2 independent lines suggest that the *pNCED3::Sluc-3'UTR* construct can report early changes in P, as it is able to feel small changes down to 0.1 MPa of P in the PR, suggesting that the *pNCED3::Sluc-3'UTR* construct is also a robust P-reporter during the first 25-60 min of MWD treatments.

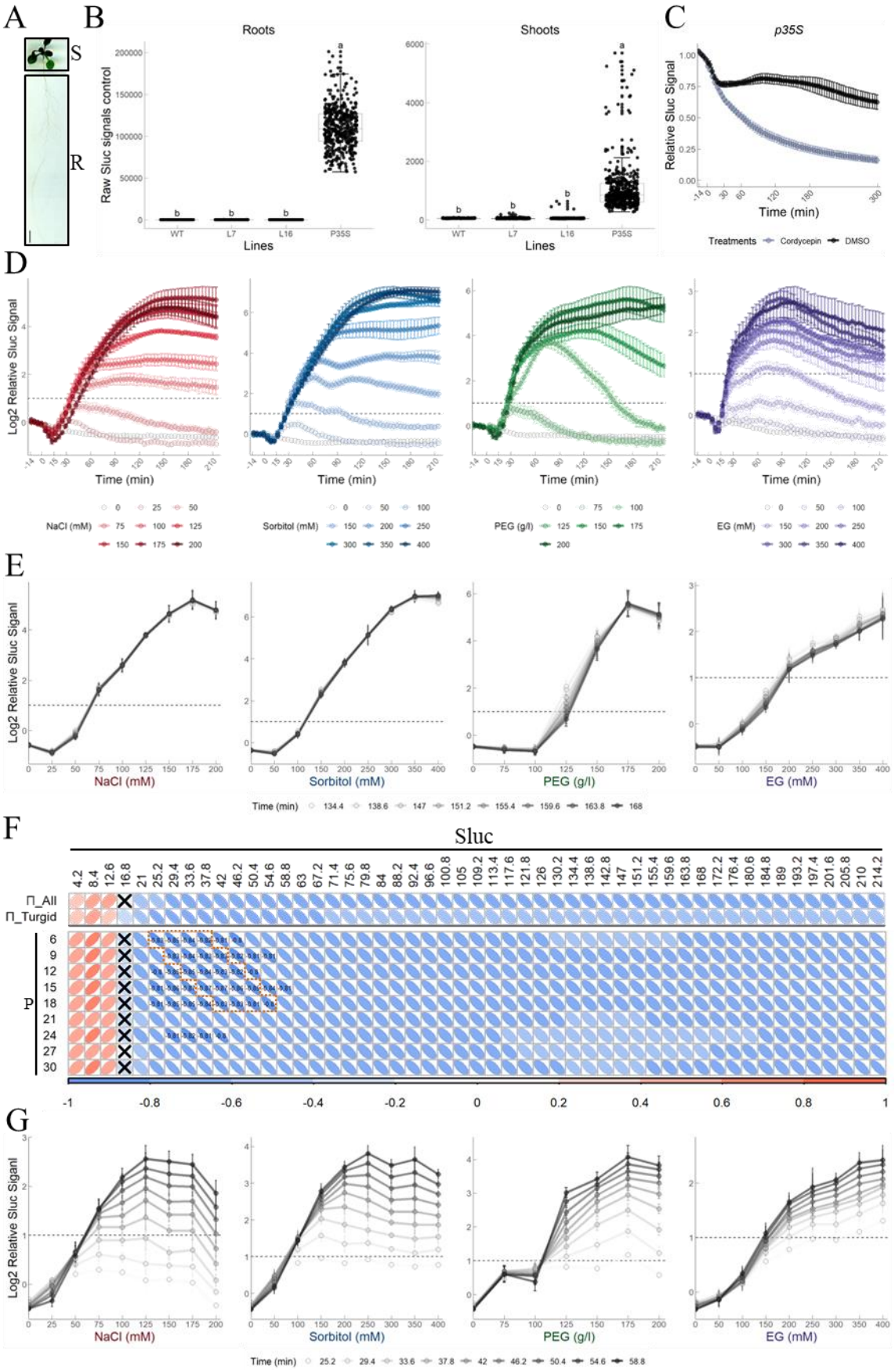

Fig 4. The luminescence signal of Sluc from *pNCED3::Sluc-3'UTR* expressing lines can report P and Π changes

(A) Picture of a 10-days old Arabidopsis seedling showing where Sluc signals were measured. The gap between S (shoots) and R

(roots) is about 5 mm. Scale bar 5mm. (B) Raw Sluc signals in WT, L7, L16 and P35S (*p35S::Sluc*) plants before treatments. Each repeat has 4 time point readings. (C) Sluc signals in the roots of P35S plants under cordycepin or DMSO (in which the cordycepin was dissolved) treatments. 3 biological repeats are shown, and each repeat has 2-3 plants (n=8). Exposure time of 10 s and about 4 min between measurements. (D) log2 (relative Sluc signal) in L7 roots over 3.5h during water deficit treatments. Relative Sluc signals were calculated by dividing the Sluc raw readouts at each time point by the average of Sluc raw readouts taken from four time points before treatments. The log2 (relative Sluc signal) was obtained by applying the log2 function to the relative Sluc signals. The dotted lines mean 2-fold changes (log2). Each condition has 3-4 biological repeats and each repeat has 1-2 plants (n=6-8). (E) The log2 (relative Sluc signal) in the roots of L7 at the late stage of treatments (mean ± se). (F) Pearson correlations heatmap between the relative Sluc signal and Π or P over time during treatments. Π_All and Π_Turgid represent the correlation between the relative Sluc signal and measured Π in all treatments, or measured Π in treatments that do not lead to plasmolysis, respectively. P represents the correlations between the relative Sluc signal and measured P under treatments, including 25-100 mM NaCl, 50-150 mM sorbitol, 75-150 g/l PEG8000, and 50-200, 300 and 400 mM EG. Each row represents the correlations calculated by using the relative Sluc signal over time against P measurements with a cell pressure probe at the indicated time points. P measurements were averaged in 3-minute intervals from 5 to 31 minutes. Cells with a cross represent p-values > 0.01 and cells displaying a correlation coefficient greater than 0.8 show their actual values. (G) log2 (relative Sluc signal) in the roots of L7 at the early stage of treatments (mean ± se).

Altogether, the *pNCED3::SLuc-3'UTR* construct appears to efficiently tracks early declines in P in roots during the initial phase of MWD treatments, and then is able report external Π.

pNCED3::Sluc-3'UTR construct can also report hydraulic changes in shoots under SWD treatments

It has been reported that osmotic stress applied to roots induces stress responses almost immediately in shoots through an hydraulic signaling mechanism (Christmann et al., 2013). We therefore observed Sluc signals in the shoots for the *pNCED3::SLuc-3'UTR* expressing lines under various osmotic treatments applied to the roots (**Fig. 5**). Indeed, increases in Sluc signal were observed for almost all treatments besides EG. These increases resembled more to the late phase of the Sluc signals in the roots, which was confirmed by significant correlations with Π-All and Π-turgid after more than 30min and for more than 2 additional hours (**Fig. 5B**). Additionally, the amplitude of the response was much reduced overall for the PEG treatments compared to NaCl or sorbitol treatments. These results indicate that our construct can report hydraulic changes (of roots) in shoots, but also that the systemic signal provoking this response is dependent on mechanisms that are occurring when the solutes can diffuse through the CW.

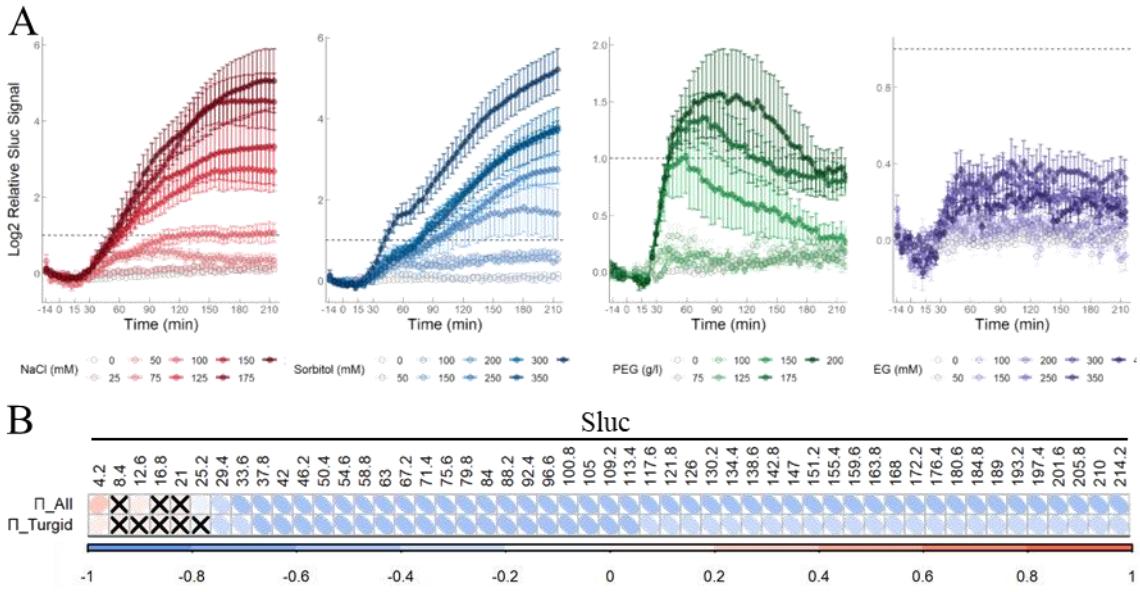

Fig 5. The *pNCED3::Sluc-3'UTR* construct in shoots is also able to report root SWD treatments

(A) log2 (relative Sluc signal) in L7 shoots over 3.5h during water deficit treatments. Relative Sluc signals (mean ± se) were calculated by dividing the Sluc raw readouts at each time point by the average of Sluc raw readouts taken from four time points before the treatments. The log2 (relative Sluc signal) was obtained by applying the log2 function to the relative Sluc signals. The dotted lines mean 2-fold changes (log2). Each condition has 3-4 biological repeats and each repeat has 1-2 plants (n=6-8). 10-days old plants, 10 s exposure time and 4.2 min interval time (B) Pearson correlations heatmap between the relative Sluc signal and Π_All and Π_Turgid, respectively (same convention as Fig. 4). Crossed cells have a p-value > 0.01.

Where do plant sense changes in P and Π?

Throughout the current work we studied the regulation of the mRNA abundance of two candidates by the P and Π components of the water potential. Although not adapted to the development of a reporter, the downregulation of *ENODL8* mRNA still indicates that part of, if not all, a mechanism involving the perception of P and events down to its transcriptional regulation are occurring in the cells where it is expressed. We used the *pENODL8::GFP-GUS* construct as way to locate such a "perception zone". The acute transcriptional regulation of *ENODL8* is lost in such construct, we nevertheless hypothesized that the promoter is driving the tissue specificity for this gene, which would be preserved (Zid and O'Shea, 2014). As shown in **Fig. 6A**, a strong GUS staining started at the transition domain (Zluhan-Martínez et al., 2021) of both primary (PR) and lateral roots (LR), and progressively faded away towards the base. A faint GUS staining was also visible in the proliferation domain of the PR (Zluhan-Martínez et al., 2021). In addition, we observed a GUS activity in the fully differentiated columella root cap cells (DCC) in LR only (De Smet et al., 2015; Hong et al., 2015). These results were confirmed by GFP observations **(Fig. 6B)**. Additionally, reconstitution of cross-sections after z-stacks imaging along the root of 9-days-old seedlings showed a GFP signal in both cortical and epidermal cells. Moreover, the GFP

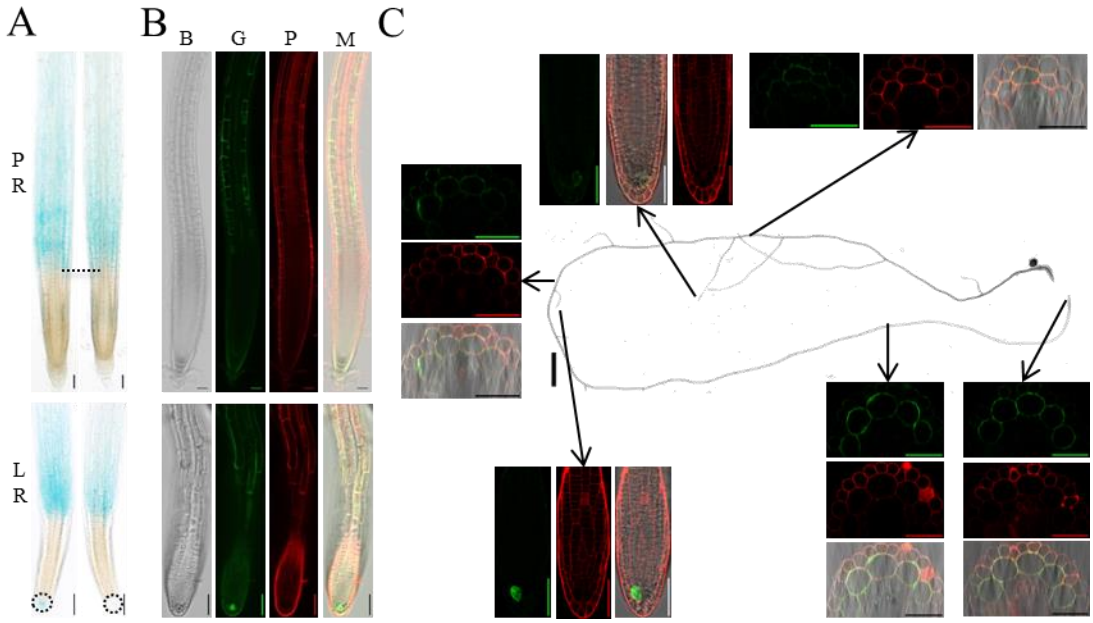

Fig. 6 *pENODL8* promoter localizes GFP and GUS proteins in cortical cells and epidermis of young part of both PR and LR

(A) GUS activity in roots of two independent *pENODL8::eGFP-GUS* expressing lines after staining for 40 min, left is line L1 and right is L13. (B) GFP observation from L13 with an Apotome microscope. Roots were stained with propidium iodide (PI). B, G, P and M are channels for bright field, GFP, PI staining and merged, respectively. (C) GFP observations and reconstructed cross-sections of various zones of the root of L13 imaged with a confocal microscope. First cross-section is around where the first root hair emerges, second is around where the primordium emerges, and others are indicated in the graph. Scale bars equal to 50 µm in GUS and GFP graphs and scale bar equals to 2000 µm in the whole root.

signal in the 2nd DCC was observed again, but eventually decreased as the LR grew older **(Fig. 6C)**. The young parts of the root therefore seem to bear at least part of the molecular mechanisms that allow a quantitative response to P.

It has been shown that the activity of the *NCED3* promoter is located in the vascular tissues of cotyledons, stems and roots (Yang and Tan, 2014). We observed the Sluc signals in our *pNCED3::SLuc-3'UTR* expressing lines under the same treatments than above. No visible signals were observed in L7 below 75 mM NaCl, 150 mM sorbitol, 100 g/l PEG, or 200 mM EG treatments over 3.5 h. Under MWD treatments, including 100 and 125 mM NaCl, 200 and 250 mM sorbitol, 125 g/l PEG and 300 - 400 mM EG, signals became visible after 35 min, first in the mature part of the PR with many LRs (**Fig. 7A)**. Under SWD treatments, including 150 – 200 mM NaCl, 300 - 400 mM sorbitol and 200 g/l PEG, bright signals were visible in the hypocotyl first. This was also supplemented by a signal coming from the mature part of the PR in the case of high concentrations of sorbitol (and one PEG treatment) (**Fig. 7A)**. A similar response was observed in L16, but with signals of lower magnitude and a higher response threshold (**Supplementary Figure 7A**). These sites correspond to sites of ABA accumulation in response to water deficit treatments (Christmann et al., 2005; Rowe et al., 2023).

Over time and up to 3h, the signals increased, extended to the rosette and spanned more PR length, as well as surrounding LRs, but did not propagate to the really young part of PR (**Fig. 7B - C**). Ultimately, visible signals were observed in the hypocotyl and cotyledons under 100 - 200 mM NaCl, 250 – 400 mM sorbitol, 175 - 225 g/l PEG and 350 – 400 mM EG

treatments. Notably, signals in both roots and shoots under EG treatments were always faint while signals in the roots under sorbitol treatments were the strongest, consistent with the quantification depicted in **Fig .4A**. A similar response was observed in L16, although again less intense (**Supplementary Figure 7B-C**). Signal activation of the reporter suggests that the whole root and the hypocotyl may be able to perceive changes in Π, but it has to be noted that the timeframe is also compatible with earlier signalings that would lead to the synthesis of ABA and the subsequent local activation of *pNCED3* in those zones.

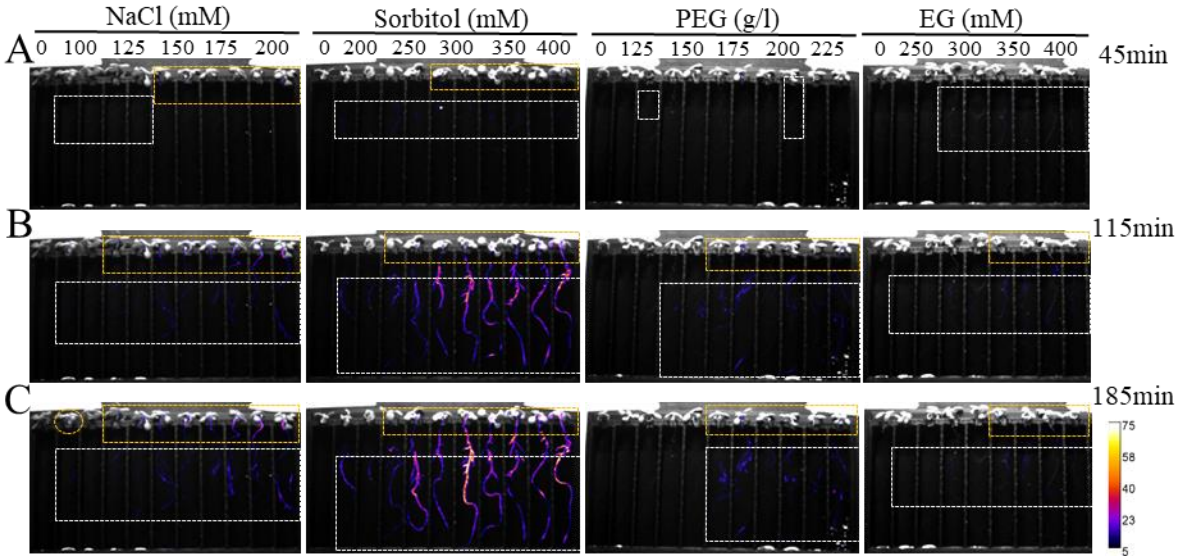

Fig 7. Emergence of Suc signals from the *pNCED3*::Sluc-3'UTR expressing plants (L7), is observed in the mature middle part of the PR and in the hypocotyl in response to water deficit treatments

(A-C) Overlapped pictures of Sluc signals and a bright field image after 45, 115 and 185 min. Images were obtained from 5 min after the beginning of the treatments and continued for 3.5 h. Exposure time was 10 min. Orange boxes and white boxes delineate the portions of shoots and roots, respectively, where a significant Sluc signal could be observed. The distance between each plant is ~8.6 mm.

The capacity of *pNCED3::Sluc-3'UTR* to report hydraulic changes under water deficit is initially independent from, but then become partially dependent on, ABA synthesis and signaling

Studies have demonstrated that *AtNCED3* is responsible for ABA synthesis in Arabidopsis and is induced by ABA treatments (Kalladan et al., 2019). We also confirmed that the expression of *NCED3* is induced significantly after 1 and 50 µM ABA treatments for 15min (**Fig. 8A, left**, while that of *ENODL8* is not, **supplementary Figure 8**). These results lead us to test whether the *pNCED3::Sluc-3'UTR* construct also responds to ABA treatments in roots. Sluc signals in L7 roots increased in response to exogenous ABA application (**Fig. 8B left**) and showed a dose-dependent response within ~135 to 168 min (**Fig. 8C**). Only slight increases were observed in the shoots under those conditions, except for the highest concentration tested of 1 µM ABA, when a clear peak of more than 2-fold changes was detected after 2 h of treatment (**Fig. 8B, right**). Similar results were observed in the roots of L16 (**Supplementary Figure 9A-B**).

The ability of the *pNCED3::Sluc-3'UTR*

construct to report both P/Π on a short-/mid- term and ABA prompted us to test whether its response to water deficit would be dependent on ABA signaling. The 15min induction of *NCED3* caused by 250mM sorbitol was significantly reduced in the *aba2* mutant lacking ABA, but not in *snrk2.2,2.3* double mutant (**Fig. 8A, right**), suggesting that a basal ABA level is required for its induction, but that ABA signaling through these SNRKs are not. To mimic ABA deficiency only during the water deficit treatment, we pretreated plant roots for 24h of 10 µM fluridone, an inhibitor of the synthesis of carotenoids that will prevent ABA *de novo* synthesis (Zeevaart and Creelman, 1988). In order to determine the efficiency of fluridone pre-treatment, we used a *ProAtBH6::Luc* expressing line (*pHB6*), which has been characterized as an ABA-dependent water-stress reporter (Christmann et al., 2005). We measured Sluc signals in *pNCED3::Sluc-3'UTR* (L7) and *pHB6* under 300 mM sorbitol treatment after a 24h pretreatment with fluridone. As shown in **Supplementary Figure 10**, fluridone treatment for 34.5 h (24 h + 10.5 h) did not alter the Sluc signal observed in all the lines compared to the mock treatment (with DMSO). Sluc signal in the *pHB6* roots slowly but continuously increased after sorbitol treatment displaying a significant difference to DMSO after ~4h (**Fig. 8D**). The induction by sorbitol was almost completely abolished by fluridone pretreatment. These results confirm that pretreating plant roots with fluridone inhibits the water-deficit induced ABA synthesis in our conditions. Unlike the *pHB6* plant, sorbitol and fluridone + sorbitol treatments were both increasing Sluc signals in the *pNCED3::Sluc-3'UTR* roots after about 30 min, reaching significant differences to DMSO condition after ~70min. Only slight significant differences between sorbitol and fluridone + sorbitol treatments were observed around 2 and 5h after sorbitol treatment. Those results indicate that, while ABA synthesis might be required for the long term regulation of *NCED3* expression, the early phase during which the *pNCED3::Sluc-3'UTR* can report hydraulic parameters is independent of *de novo* ABA synthesis.

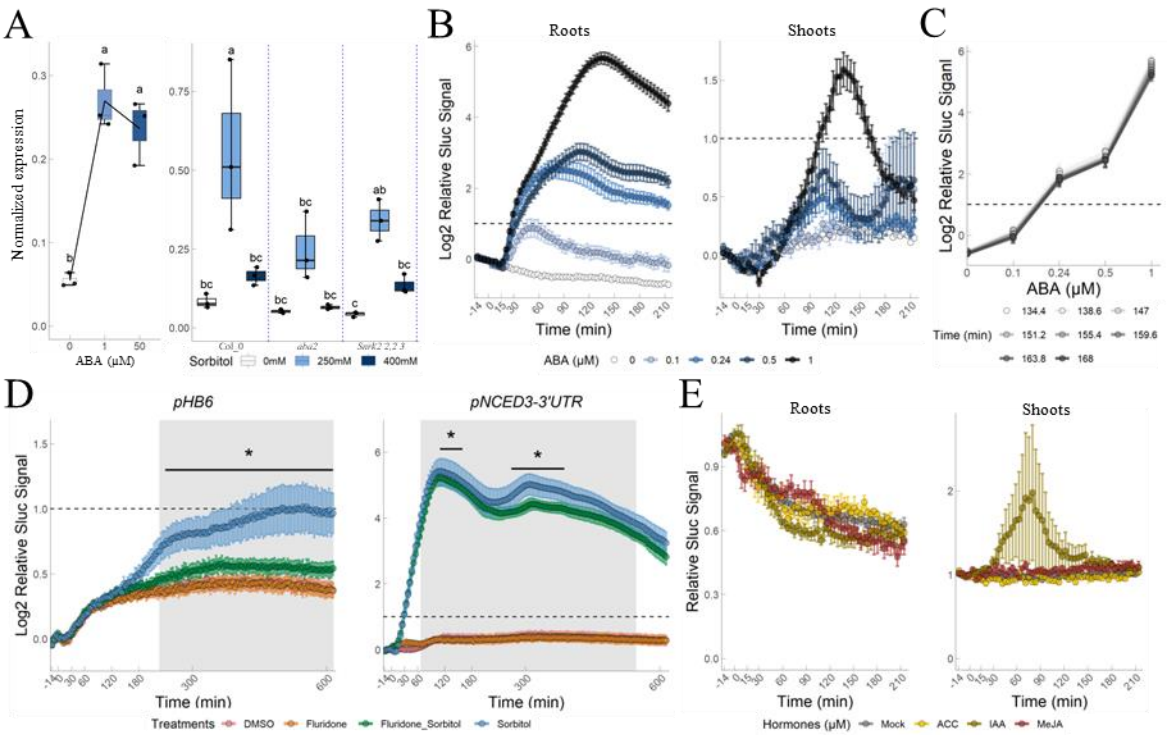

Fig 8. ABA signaling is not involved in the first phase, but is for the second phase, of *pNCED3::Sluc-3'UTR* plant (L7) regulation in response to water deficit

(A) Normalized *NCED3* gene expression in the roots of Col_0 plants after 1 and 50 µM ABA treatments for 15min (left), or in the roots of two ABA related genotypes after 250 and 400 mM sorbitol treatments for 15min (right). Normalized expression means that gene expression is referenced to the expression of internal control genes. 3 biological repeats for each treatment. (B) log2 (relative Sluc signal) in the roots and shoots of L7 under ABA treatments. 3 biological repeats and each repeat has 2 plants (n=6). (C) log2 (relative Sluc signal) in the roots of L7 at the late stage (134.4-168 min) of ABA treatments. (D) The log2 (relative Sluc signal) in the roots of *pHB6* and *pNCED3::Sluc-3'UTR* under mock (DMSO), 10 µM fluridone, 300 mM sorbitol or 10 µM fluridone + 300 mM sorbitol treatments. 10-days old plants, 10 s exposure time and 4.2 min interval time. 6 biological replicates with 1 plant per repeat (n=6). Shaded regions highlight a significant difference between sorbitol and DMSO treatments, and horizontal lines with an asterisk highlight significant differencse betweeen sorbitol and fluridone + sorbitol treatments. (E) Relative Sluc signal in the roots and shoots of L7 under 1 µM IAA, 1 µM MeJA and 1 µM ACC treatments. 2 biological repeats with 2 plants per replicate (n=4). (mean ± se, ANOVA and Tukey's HSD test ($P < 0.05$)).

Other phytohormones are also involved in plant responses to osmotic stress, such as ethylene, auxin and jasmonic acid (Waadt et al., 2022). To test if the *pNCED3::Sluc-3'UTR* reporter is dependent on those signaling pathways, we measured the Sluc signals under ACC (1-Aminocyclopropane-1-carboxylic acid, an ethylene precursor), IAA (Indole-3-acetic acid) and MeJA (Methyl jasmonate) treatments. As shown in **Fig. 8E,** Sluc signals did not show any significant response to ACC, IAA and MeJA treatment in both roots and shoots. Similar results were obtained in L16 (**Supplementary Figure 8C**), suggesting that the *pNCED3::Sluc-3'UTR* construct is specifically regulated by ABA after the initial phase.

The capacity of *pNCED3::Sluc-3'UTR* to report changes in Ψ under water deficit is initially independent on the cell wall integrity in roots, but is on the long term, as well as for its systemic signaling in shoots

Cell wall integrity (CWI) is indispensable for the phytohormone-modulating turgor pressure and ABA production (Bacete et al., 2022). To test whether CWI is involved in the regulation of Sluc signals in *pNCED3::Sluc-3'UTR* expressing lines (L7) in response to water deficit treatments, we treated *pNCED3::Sluc-3'UTR* and *pHB6* with 300 mM sorbitol with or without 100 nM isoxaben (ISX), a cellulose biosynthesis inhibitor that causes CW damage and impairs CWI (Heim et al., 1990). As shown in **Fig. 9A** and **B**, Sluc signals in the roots and shoots of *pHB6* and *pNCED3::Sluc-3'UTR* were relative stable under mock and ISX treatments, and no significant differences between those treatments were observed for over 10h. This is consistent with a similar study showing that ISX treatment did not trigger obvious GFP accumulation in *pRAB18::GUS-GFP,* an ABA reporter (Bacete et al., 2022). In the *pHB6* line, Luc signals were induced slowly but continuously after both sorbitol and ISX + sorbitol treatments. A difference between both treatments was observed only after more than 6h. In the roots of *pNCED3::Sluc-3'UTR*, the induction of Sluc signals by sorbitol and ISX + sorbitol treatments was indistinguishable during the first 80 min, and only then a ~2-fold reduction was observed with the addition of ISX (1 unit in log2 scale, **Fig. 9A**, **right**). These findings suggest that CWI plays a key role in the late activation of *pNCED3::Sluc-3'UTR* in the roots in response to water deficit treatments, when it seems to report changes in Π. In the early stage

though, while the construct is reporting P, it is a bit paradoxical that CWI seems not to be necessary for the proper regulation of *NCED3*. In shoots, the sorbitol-induced Sluc signal appeared to be both delayed and 2-fold reduced by ISX co-treatment (**Fig. 9B, right**) although a difference between sorbitol and ISX + sorbitol treatments became significant only in the 3-6h window after treatment. These results indicate that CWI also plays an essential role in the activation of *pNCED3::Sluc-3'UTR* in the shoots in response to water deficit treatments.

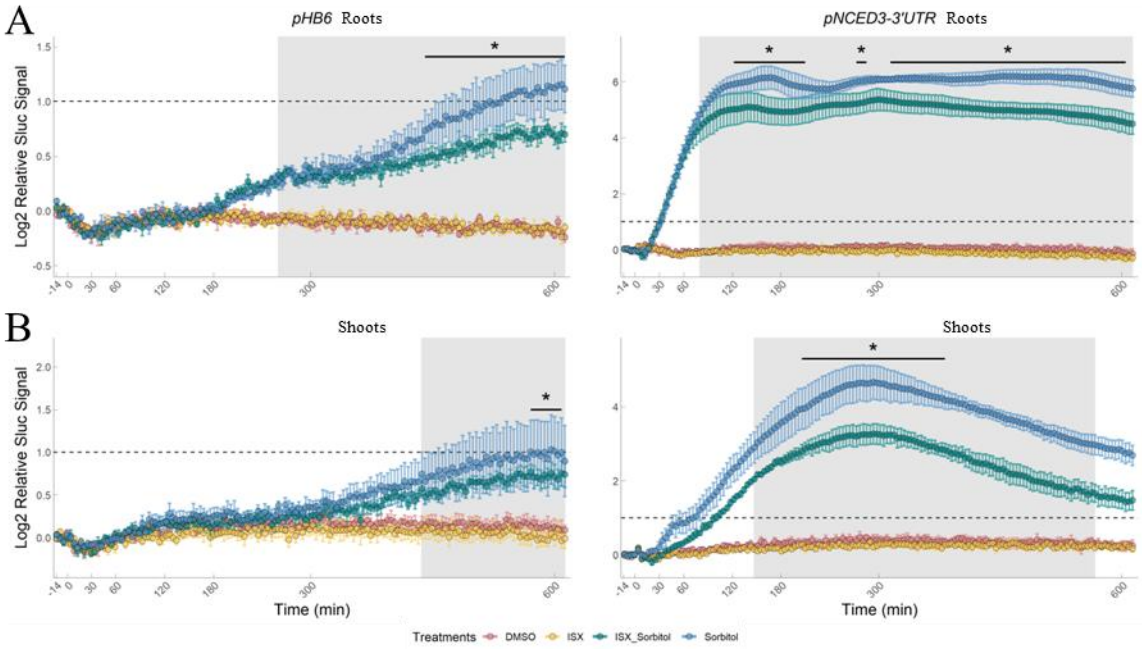

Figure 9. Cell wall integrity is not required for the initial regulation of the Sluc signals from the osmo-reporter in response to water deficit, but plays a role in the late phase as well as in the systemic signaling

(A-B) The log2 (relative Sluc signal) in the roots and shoots of L7 and *pHB6* under 300 mM sorbitol treatment with or without co-treatment with the cellulose synthase inhibitor isoxaben (ISX), respectively. 10-days old plants, and 10 s of exposure time and 4.2 min of interval time. 4 biological repeats and each repeat has 1 plant (n=4). Horizontal lines with an asterisk highlight significant differences between sorbitol and ISX + sorbitol treatments, and shaded region highlight significant differences between sorbitol and DMSO treatments. (mean ± se, ANOVA and Tukey's HSD test (*$P < 0.05$)).

Discussion

Plants need to rapidly perceive fluctuations in soil water availability to adapt their growth and development, thereby improving their chances of survival and fitness. Although researches related to hydrotropism suggest that cortical cells in the elongation zone of the PR could be a privileged site for root responses to local water scarcity (Dietrich et al., 2017), determining when and where plant roots sense the homogeneous water deficit in a manner that reprograms gene expression still remains unclear. We reported here that the *pNCED3::Sluc-3'UTR* construct exhibits quantitative responses to acute changes in P (as low as 25 mM NaCl, which drops P by about 0.1MPa) in the cortical cells of the root elongation zones, within first 25 to 55 min of MWD treatments. Over the course of a water deficit treatment, it also exhibits quantitative responses to the external Π intensity, as well as to exogenous ABA.

To our knowledge, we provide a new, almost real-time and highly sensitive, genetic osmo-reporter in Arabidopsis, which will be beneficial for deciphering when, where, and how plants sense variations in Ψ within their habitat.

The mRNA abundances of ENODL8 and NCED3 are regulated by water deficit at transcriptional level

Under MWD treatments, cell morphology remains relatively unimpaired, allowing plants to optimize water utilization efficiency by accumulating solutes to enhance water uptake and closing stomata to limit water loss. This mechanism for achieving a balance between water uptake and loss is referred to as stress avoidance (Claeys and Inzé, 2013). Changes in gene expression are a significant component of these processes and are reversible, enabling cells to rapidly adjust transcripts abundance after both onset and removal of stress (de Nadal et al., 2011). *ENODL8* exhibits a quantitative response to dynamic changes in P, encompassing both reduction and recovery, caused by MWD treatments. This suggests that its expression is tightly and specifically controlled by P (**Fig. 1A** and **E**). *NCED3* exhibits a quantitative response to reductions in P caused by MWD treatments. However, it maintains a high expression level during P recovery, suggesting a role in adjusting plant living with reduced P. Indeed, *NCED3* encodes a key rate-limiting enzyme for *de novo* ABA synthesis in Arabidopsis (Tan et al., 2003), which echoes to both avoidance and tolerance (see below) responses being primarily coordinated by ABA (Claeys et al., 2014).

Gene expression can be tightly controlled at both the transcriptional and post-transcriptional levels under drought and salinity stress (Kawa and Testerink, 2017). ENODL8 protein function and the molecular mechanisms of its expression are poorly understood so far (Mashiguchi et al., 2009). *ENODL8* expression is not affected by ABA treatments and does not show different pattern in *aba2* and *snrk2.2,2.3* mutants under treatments (**Supplementary Figure 8**), while *NCED3* expression is rapidly induced by ABA treatments. In response to osmotic stress, the expression of many stress-inducible genes is governed by the "ABA-activated SnRK2-ABA-responsive element (ABRE)-binding proteins/ABRE-binding factors (AREB/ABFs)" (Soma et al., 2021). A study reported that a distal ABRE element (GGCACGTG, -2372 to -2364 bp) in the promoter of *NCED3* is essential for its ABA induction, although a known ABRE binding factor, ABF3, does not regulate its expression (Yang and Tan, 2014). NGATHA family and ATAF1 transcriptional factors (TFs) also regulate the expression of *NCED3* by directly binding to its promoter region (Jensen et al., 2013; Sato et al., 2018). It was also shown that a decrease in leaf P induces its expression within 5 min, but from an unknown mechanism (Sussmilch et al., 2017). It is possible that the decrease in plant Ψ with our osmotic treatments regulates the abundance of *NCED3* mRNA through these TFs.

The mRNA abundances of ENODL8 and NCED3 are regulated by water deficit at post-transcriptional level

Our study shows that reduction in P caused by MWD accelerates the mRNA decay of *ENODL8*, while LSM1a/1b elevates its absolute expression without participating in its regulation under water deficit (**Fig. 2A** and **C**). Two previous studies using transcriptomic analyses showed that under normal conditions, the mutation of *vcs* in the WT (Col_SOV^{Ler}) background results in a 27% reduction in the expression of *ENODL8*, while dysfunction of *sov* (Col_0) has no significant impact on its expression (**Supplementary Figure 11A)**. Meanwhile, the mutation of *vcs*

(*vcs_sov* mutant) in the Col_0 background leads to a 49% reduction in the expression of *ENODL8*. However, no differences in its mRNA half-life was observed among these 4 genotypes (**Supplementary Figure 11B**) (Sorenson et al., 2018). These findings suggest that dysfunction of the decapping factor VCS in 5'-3' mRNA decay pathway positively regulates the absolute expression of *ENODL8* rather than affecting its mRNA half-life. This paradox could be attributed to RNA buffering, a feedback regulatory mechanism for mRNA decay defects in yeast, where mutants with impaired mRNA decay rates exhibit decreased transcription rates, while deficient RNA polymerase II lead to slower mRNA decay rates (Sun et al., 2012). This feedback regulation aims to maintain RNA levels close to WT and is believed to involve the cytoplasmic 5'-to-3' exoribonuclease enzyme XRN1 which also serves as a broad transcriptional repressor (Sorenson et al., 2018). However, another transcriptomic research revealed that under normal condition, not only the expression of *ENODL8* in the *rh6812* mutant was reduced to 0.31 compared to Col_0 (sov mutant) but its mRNA half-life was also enhanced from 68 min in Col_0 to 153 min in the triple mutant *rh6812* (**Supplementary Figure 11C-D**) (Chantarachot et al., 2020). Unlike VCS, a scaffold protein of the decapping complex, the RH6/8/12 (DHH1/DDX6-like RNA helicases) and LSM1-7 complex participate in the 5'-3' mRNA decay as decapping activators. These findings suggest that manipulating different components of the decapping complex may have drastically different effects on gene expression, and that water deficit may play a role in regulating their activity. It should be noted that the *rh6812* and *lsm1a/1b* mutants exhibit sick phenotypes, while the *vcs* and *vcs_sov* mutants display even more severe symptoms (homozygous mutant are almost nonviable). Therefore, further work would be needed in mutants with less impact on plant growth.

Our results show that LSM1a/1b and XRN4 is indirectly involved in regulating the expression of *NCED3* under MWD treatments, but not under control condition. Notably, Perea-Resa et al. demonstrated that while the capped mRNA level of *NCED3* was significantly higher in the *lsm1/a/1b* mutant under normal condition compared to Col_0, its capped mRNA level was significantly induced by exposure to 4°C for 10 hours, rather than by PEG or NaCl treatment (Perea-Resa et al., 2016). Sorenson et al. transcriptome also revealed that, under normal conditions, the mutation of vcs in the WT (Col_SOV^{Ler}) background results in 4 folds induction in the expression of *NCED3*, while dysfunction of *sov* (Col_0) has no significant impact on its expression (**Supplementary Figure 11A**). Meanwhile, the mutation of *vcs* (*vcs_sov* mutant) in the Col_0 background leads to 16 folds induction in the expression of *NCED3* (**Supplementary Figure 12A**) (Sorenson et al., 2018). These findings strongly suggest the 5'-3' mRNA decay is also crucial for regulating *NCED3* expression and that stresses may regulate different components of this pathway. Notably, Sorenson et.al also revealed that the mRNA abundance of *NCED3* declined synchronously in the first 30 min of cordycepin treatment and then remained relative stable in *vcs* and *vcs_sov* mutants, but progressively recovered in WT and Col_0 (**Supplementary Figure 12B**) (Sorenson et al., 2018). Coincidentally, Chantarachot et al. also found that the recovery sign of *NCED3* expression was found in Col_0 after cordycepin treatment for 2 h (**Supplementary Figure 12C**) (Chantarachot et al., 2020). Similar recovery of *NCED3* expression is also found in our cordycepin assays (**Fig. 2A**). Transcriptome from Arabidopsis seeds under cordycepin treatment also showed many genes can be induced by cordycepin (Bai et al., 2018). These

somehow puzzling results could be interpreted by either considering that the transcription is not completely blocked by cordycepin or would suggest that the regulatory pathways of genes such as *NCED3*, which are induced by water deficit, are insensitive to a cordycepin treatment. Indeed, it has been proposed that mutation of poly(A) polymerase in yeast (*pap1-1*) neutralized the effects of the cordycepin on gene expression (Holbein et al., 2009). Overall, this complex pattern of regulation for *NCED3* makes it a strong candidate to pursue further the exploration of transcriptional and post-transcriptional regulations under stress.

It has been reported that, under osmotic stress, ABA-unresponsive subclass I SnRK2 protein kinases are phosphorylated and activated by three B4 Raf-like MAP kinase kinase kinases (MAPKKKs), RAF18, RAF20 and RAF24 (Soma et al., 2020). In response to osmotic stress, subclass I SnRK2, such as SnRK2.5, SnRK2.6, and SnRK2.10, interact with and phosphorylate VCS, potentially affecting the decapping complex's functionality and resulting in either enhancement or inhibition of mRNA decay (Soma et al., 2017; Kawa et al., 2020). It is probable that other components of the decapping complex are phosphorylated by SnRK2s or MAP kinases (Kawa and Testerink, 2017). Therefore, it is highly possible that the expression of *ENODL8* and *NCED3* under water deficit are regulated at the post-transcriptional level through the "subclass I SnRK2s-vcs" signaling module.

Plasmolysis alters regulation of gene expression in response to water deficit

When stress avoidance is no longer sufficient to deal with stress severity, the mechanisms of stress tolerance come into play, involving the accumulation of protective proteins and detoxification of reactive oxygen species (ROS) (Claeys and Inzé, 2013). Correspondingly, the expressions of *ENODL8* and *NCED3* in response to SWD were altered compared to MWD, suggesting that regulation of their expression is either delayed or disrupted by SWD. This is consistent with a previous study showing that stress severity strongly determines combinations of stress-responsive genes and their expression level (Claeys et al., 2014). Plasmolysis must be considered in experiments involving plants subjected to salt shocks (plants are subjected suddenly to solution containing high concentration of NaCl), as the overall gene expression profiles and the expression alterations in specific target genes will diverge from when treated progressively with the same NaCl concentration for inducing salt stress (Shavrukov, 2013). We proved that plasmolysis of cortical cells in the elongation zone could potentially serve as a switch for regulating these two genes expression (**Fig. 1**). Moreover, the expression of Sluc in *pENODL8::Sluc-3'UTR* expressing plants did not respond to MWD (**Supplementary Figure 4**), while it was reduced significantly after SWD treatment for 3h (**Supplementary Figure 13**). This suggests that although the open reading frame (ORF) of *ENODL8* is essential for regulating its expression under MWD, it may not be essential for its regulation under SWD. Further studies are needed to explore the mechanism for regulating *ENODL8* expression, and probably many other genes, by what appears to be different pathways switching depending on the severity of stress.

Perception sites of water deficit in Arabidopsis

Osmosensing, as an essential step in plant response to osmotic stress, is poorly understood so far (Nongpiur et al., 2020). Under SWD treatments (above 150 mM NaCl and 300 mM sorbitol treatments), we observed a rapid and strong initiation of Sluc signals in the *pNCED3::Sluc-3'UTR* shoots. Studies reported that

primary sites of ABA synthesis are in the shoots vascular tissues, not in the roots, when roots experience water stress (Christmann et al., 2005; Endo et al., 2008; Ikegami et al., 2009; Kuromori et al., 2014; McAdam et al., 2016). This is due to hydraulic signals rapidly propagating through the vascular bundles from the roots to the shoots (Christmann et al., 2013). *NCED3* encodes a key enzyme for ABA synthesis and its promoter activity localizes in the vascular tissues (Yang and Tan, 2014; Kalladan et al., 2019). Therefore, both rapid accumulation of ABA and strong initiation of Sluc signals in shoots appear to be dependent on the hydraulic changes caused by SWD treatments.

Under MWD treatments with 100/125 mM NaCl, 200/250 mM sorbitol, 200 g/l PEG or above 250 mM EG, bright Sluc signals initiated first in the mature part of PR (bearing many LRs), suggesting that this zone could be a perception site under MWD. To be noticed is that we were unable to visualize the response of Sluc signals under MWD treatments with relative low concentrations, such as 50 mM NaCl and 100 mM sorbitol treatments. Therefore, the perception site for plant responses to MWD could be in other positions. Inhibition of ABA synthesis abolished the luc induction in the *pHB6* roots under water stress. These results suggest that stress-induced ABA synthesis indeed occurs in the roots too. The paradox of ABA synthesis sites could be explained by the possibility that previous results were obtained after SWD treatments such as dehydration, by transferring plants to filter paper to absorb excess water or by using high concentrations of osmolytes, resulting in decrease in Ψ down to -0.8 or -1 MPa (Christmann et al., 2005; Endo et al., 2008; Ikegami et al., 2009). Therefore, in future research, greater emphasis should be placed on investigating ABA biosynthesis under MWD, with the use of ABA reporters such as ABACUS2s.

It has been reported that ABA accumulation in dehydrating leaves is associated with reduction in cell volume rather than changes in P (Sack et al., 2018). Turgor loss or significant reduction in cell volume results in detachment of cell PM from CW — plasmolysis (Lang et al., 2014; Gorgues et al., 2022). In fact, our study confirmed that plasmolysis of cortical cells in the end meristem zone of PR disrupted the regulation of gene expression (**Fig. 1**). Vaahtera et al. proposed the hypothesis that SWD treatments result in plasmolysis, triggering remarkable accumulation of ABA (Vaahtera et al., 2019). It has been reported that older cells exhibit greater sensitivity to water stress treatments compared to young cells, and that plasmolysis occurs in the older root cells before the younger ones. This is attributed to the smaller turgor pressure of the older root cells in wheat (PRITCHARD et al., 1991). We also found that bright signals appeared first at the mature zone of the PR with many LRs under SWD treatments. These findings suggest that significant ABA accumulation, and the initiation of visible signals in the *pNCED3::Sluc-3'UTR* construct may attributed to plasmolysis. Additional investigations are required to determine whether plasmolysis coincides with the visible signal in the mature part of the PR in Arabidopsis under the 200 and 250 mM sorbitol, 100 and 125 mM NaCl, and 250 - 400 mM EG treatments.

Although the *pENODL8::eGFP-GUS* construct does not contain all the regulatory elements of P-reporter gene *ENODL8*, GFP localization present in the young part of the PR and LR, including the elongation zone and end of meristem zone (transition domain). Study showed that ABA signaling in the cortical cell of elongation zone and asymmetric distribution of cytokinins in the meristem zone are essential for hydrotropism (Dietrich et al., 2017; Chang et al., 2019). The xerobranching response, in

which lateral root formation is suppressed when a root loses contact with water, is supposed to require a radial movement of phloem-derived ABA in the meristem and elongation zones (Mehra et al., 2022). These findings suggest that elongation zone and meristem zone could also represent perception sites of the water deficit, and the natural regulation of *ENODL8* expression should be further investigated.

ABA content and CWI are not required for the initiation of Sluc signals induction in plants carrying the pNCED3::Sluc-3'UTR

Our results showed that Sluc signals in the roots of *pNCED3::Sluc-3'UTR* and in the roots of *pHB6::Luc* (an ABA marker) were induced 30 min and 3 h after water deficit treatments for, respectively (**Fig. 8**). This is consistent with the idea that endogenous ABA concentration is thought to become elevated after a few hours of water stress (Waadt et al., 2022). Exogenous ABA treatments induced Sluc signals, but pretreatment with fluridone did not impair the induction of Sluc signals from *pNCED3::Sluc-3'UTR* at the early stage of water deficit treatments. These results suggest that both ABA -dependent and –independent pathways are involved in the increase in Sluc signal in the roots. However, the chronology of the experiments with fluridone suggests that ABA is not needed for the initial Sluc signal induction by osmotic stress. A study revealed that group B2 and B3 Raf-like kinases are essential for activating SnRK2.2/3/6 under ABA or osmotic stress. In addition to ABA-mediated phosphosites, such as Ser171 and Ser175 of SnRK2.6, additional RAF phosphosites of SnRK2.6 were found under osmotic stress. Those additional RAF phosphosites of SnRK2.6 may circumvent the PP2C-mediated inhibition under osmotic stress (Lin et al., 2020). This ABA-independent activation of SnRK2s subsequently phosphorylates multiple substrates, thereby inducing the expression of stress-responsive genes (Soma et al., 2021). This could also explain why no impairment of Sluc induction was observed under long-term sorbitol treatment after fluridone pretreatment.

It was shown that CWI is required for ABA production (Bacete et al., 2022), and we consistently observed in our conditions that the induction of Luc signals in *pHB6* plants was impaired under water deficit + Isoxaben treatments. The initiation of Sluc signals in the roots of plant carrying the *pNCED3::Sluc-3'UTR* construct was not affected by CWI, but its long-term induction was compromised. Impaired CWI also had a stronger impact on the initiation and long-term induction of Sluc signals in the shoots compared to the roots (**Fig. 9**). Hydraulic signals triggered by water deficit first consist in a decline in P, followed by a moderate elevation in solutes concentrations due to water expulsion from cells, and ultimately exerting mechanical forces at CW and CW-PM interface (Christmann et al., 2013). Christmann et al. also proposed two general modes for decoding hydraulic signals, which are sensing the osmotic environment or sensing the altered mechanical forces exerted by changes in Ψ. Therefore, in response to hydraulic changes caused by water deficit in roots, the induction of Sluc signals in the shoots may partially depends on altered mechanical forces mediated by CWI, while Sluc signals in roots may be induced by sensing the osmotic environment. In addition, radial scans with a Brillouin microscope showed that ISX or 300 mM sorbitol treatments significantly reduce the stiffness in the stele of Col_0 plant roots, while ISX + sorbitol treatments exhibited the same stiffness compared to mock condition (Bacete et al., 2022). These results suggest that the impairment of Sluc signal induction under a long-term ISX + sorbitol treatment could be attributed to a relatively unimpaired CW stiffness that helps cells

maintain their shape and resist external forces.

Reporter of variation in Ψ in plants

The Sluc signals in the roots of plants carrying the *pNCED3::Sluc-3'UTR* construct is quantitatively and rapidly induced by changes in P caused by MWD at early stage (25-60 min), suggesting the *pNCED3::Sluc-3'UTR* construct is a P-reporter. At a later stage (30 min – 3.5h), the Sluc signals in the roots of plants carrying the *pNCED3::Sluc-3'UTR* construct quantitatively responds to external Π under both MWD and SWD, suggesting the *pNCED3::Sluc-3'UTR* construct is a Π-reporter too. To our knowledge, the only existing reporter for tracking the physico-chemical effects of osmotic stress on plant cells is SED1, which worked well in tobacco cells but not after stable expression in Arabidopsis (Cuevas-Velazquez et al., 2021). Moreover, it showed a response mostly to SWD treatments (> 200 mM NaCl). In our hands, the *pNCED3::Sluc-3'UTR* construct was able to report small variations in P (P drops of ~0.1 MPa caused by 25 mM NaCl or 50 mM sorbitol) and exhibited a quantitative response to changes in Π ranging from -0.12 (50 mM sorbitol) to -0.9 (350 mM sorbitol) MPa. Another available hydrogel nanoreporter for measuring Ψ in leaf of maize, called AquaDust, has been developped (Jain et al., 2021). AquaDust's responsive gel matrix reacts to alterations in local Ψ by expanding or contracting, resulting in shifts in the emission spectrum through Förster Resonance Energy Transfer (FRET). This reporter, however, has limitations such as the need for pre-infiltration and reliance on in local situ imaging, which can be inconvenient and restrict its applicability primarily to leaves. As a genetic reporter, *pNCED3::Sluc-3'UTR* can be used easily to study variations of Ψ in both roots and shoots and further explore osmosensing and osmo-signaling. In addition, it also provides a useful way to identify the water availability changes in soil without the need to access the root. Given that the *pNCED3::Sluc-3'UTR* construct can real-time and quantitatively report variations in plant hydraulic parameters, including P, Π, and hydraulic signals, we refer to it as an osmo-reporter. The initial generation of genetically encoded biosensors is typically associated with several limitations (Greenwald et al., 2018). To confirm the perception site under MWD treatments, the subsequent optimization of this reporter should focuses on enhancing brightness to achieve improved performance.

Conclusion

We have demonstrated that the *pNCED3::Sluc-3'UTR* construct serves as a genetically encoded osmo-reporter capable of dynamically monitoring Arabidopsis responses to water deficit in a quantitative fashion. These responses include complex transcriptional and post-transcriptional regulations, among others. This reporter also represents a tool for deciphering the perception site of water stress and screening potential osmosensors.

Material and methods

Plant material, water deficit treatments

Sterilized Arabidopsis seeds were sowed onto 1/2 MS medium containing 1% sucrose and subsequently placed at 4°C in darkness for 48 h for vernalization. Plates were positioned vertically in Aralab incubator (16h/8h, 60% humidity). After a span of 10 days, plants were transferred to hydroponic solution. Osmotic pressure and turgor pressure measurements were performed as described in previous section (Amandine). **Supplementary Table 1** summarizes the osmoticums, concentrations and osmotic potential of each treatment solution and the turgor pressure in cortical cells under the corresponding treatment.

Constructs and transgenic plants

2897 bp of the 5'-upstream sequence of *ENODL8* (potential promoter) was cloned into PGWB207 entry vector (P4'), and then recombined into pKGWFS7 to construct the *pENODL8:eGFP-GU*S. This promoter fragment, and 2665bp of the 5'-upstream sequence of *NCED3* (potential promoter), and *p35S* fragment from pH7WG2 were cloned into pDONR^{TM} P4-P1R entry vector (P5'), to construct the P5'-*pENODL8*, P5'-*pNCED3*, P5'-*p35S* vectors, respectively. 1830 bp sequence of short-lived luciferase (*Sluc*) was cloned into PGWB207 entry vector to construct the P4'-*Sluc* (Younis et al., 2010). 1kb of the 3'-downstream sequence of *ENODL8* (including 197bp 3'-UTR and 803bp 3'-downstream sequence) and 1kb of the 3'-downstream sequence of *NCED3* (including 392bp 3'-UTR and 608bp 3'-downstream sequence) were cloned into pDONR^{TM} P2R-P3 entry vector (P3'), to construct the P3'-*3'UTR$_{ENODL8}$*, P3'-*3'UTR$_{NCED3}$,* respectively. The P5'-*pENODL8,* P4'-*Sluc* and P3'-*mock* were ligated into the pK7m34GW destination vector, to drive the *Sluc* expression under the *pENODL8* promoter alone (Pkana-*pENODL8:Sluc*). The P5'-*pENODL8,* P4'-*Sluc* and P3'-*3' UTR$_{ENODL8}$* were ligated into the pK7m34GW destination vector, to drive the *Sluc* expression under the *pENODL8* promoter (Pkana-*pENODL8:Sluc-3'UTR*). The P5'-*pNCED3,* P4'-*Sluc* and P3'-*3' UTR$_{NCED3}$* were ligated into the pK7m34GW destination vector, to drive the *Sluc* expression under the *pNCED3* promoter (Pkana-*pNCED3:Sluc-3'UTR*). The P5'-*p35S,* P4'-*Sluc* and P3'-*mock* were ligated into the pK7m34GW destination vector, to drive the *Sluc* expression under the *p35S* promoter (Pkana-*p35S:Sluc*). All the oligos (**Supplementary Table 2**) synthesis and sequencing were serviced by Eurofins Genomics. All the BP reactions and LR reactions were performed using the Gateway™ BP Clonase™ II Enzyme mix (Thermo Fisher) and the Gateway™ LR Clonase™ II Enzyme mix (Thermo Fisher), respectively. Transgenic Arabidopsis plants were generated through Agrobacterium-mediated floral dip transformation and T3 homozygotes were used in this paper.

Cordycepin kinetic assays

Cordycepin treatments were performed as previously described (Han et al., 2004). In brief, 3 weeks-old plants were transferred to a beaker containing 200 ml of hydroponic solution complemented with 100 µg/ml cordycepin (3'-deoxyadenosine, Sigma), or 50 mM NaCl, or both. Subsequently, the whole roots were collected after treatments for 5, 15, 30, 60 and 180 min. All the samples were frozen in liquid nitrogen until RNA extraction.

Q-RT-PCR

RNA extraction, cDNA synthesis, qPCR and subsequent analysis were performed as described in previous section (Amandine). *At1G13320* (*PDF2*) and *At4G34270* (*TIP41-like*) were selected as internal control genes for water deficit treatments of Col 0 plants (Czechowski et al., 2005). Given the expression of *PDF2*, *At3G18780* (*Actin2*) and *At5G60390* (*EF-1α*) were relative stable in the cordycepin kinetic assays, they were selected as internal control genes (Czechowski et al., 2005; Zhang et al., 2010; Sorenson et al., 2018). *PDF2*, *TIP41-like* and *18S rRNA* were selected as internal control genes in the water deficit treatments of mutants (Czechowski et al., 2005; Soma et al., 2017). All primer sequences are shown in the **Supplementary Table. 2.**

Gus staining and microscopy

Gus staining was performed as follows. Nine days seedlings from hydroponic were incubated in glutaraldehyde paraformaldehyde fixation solution and vacuum infiltrated for half an hour. Subsequently, seedlings were rinsed 3 times with GUS assay buffer (Phosphate buffer [pH-7], 0.1% Triton X-100, 0.5 mM $K_4[Fe(CN)_6].3H_2O$, 0.5 mM $K_3[Fe(CN)_6]$). Seedlings were transferred into fresh GUS assay buffer containing 1mM X-gluc and placed in the dark at 37°C. After about 40min, seedlings were rinsed and bleached with a series in gradient of ethanol solutions. Propidium iodide (PI) staining was conducted following the established procedure on plants aged 9 days, with an incubation period of 10 minutes, and on

plants aged 20 days, with an extended incubation period of 40 minutes (Alassimone et al., 2010).

Luciferase assays

Sterilized Arabidopsis seeds were sowed onto 1/2 MS medium containing 1% sucrose and subsequently placed at 4°C in darkness for 48 h for vernalization. Plates were positioned vertically in an Aralab incubator (16h/8h, 60% humidity). After a span of 6 days, plants were transferred onto an hydroponic solution. After 3 days, a pre-feeding step was performed, involving the application of 100 µM Luciferin-EF™ (Promega) to the plants roots for 24 h. 10-days-old seedlings were translocated into a 24-wells plate. The roots were positioned in a well containing 800 µL of hydroponic solution, while the shoots were placed in another separate well interconnected with the roots well through a 3D-printed bridge. Treatments to the root were administered by introducing 100 µL of treatment solution with a nine-fold concentration into the root wells. Signals were detected in BMG labtech clariostar® plus microplate reader (BMG Labtech, Ortenberg, Germany) under a series of water deficit treatments, or ABA treatments, or cordycepin treatment. Treatments were performed by introducing 200 µL of treatment solution with a nine-fold concentration into 1600 µL of hydroponic in the root modules, after about 3 min pictures of seedlings signals were captured using a CCD luciferase camera.

Statistical analyses

All the statistical analyses were performed with the R software (R Core Team, 2022, version 4.1.3) by engaging the packages dplyr (Wickham, et al., 2022), ggplot2 (Wickham, 2016), emmeans (Russell, 2023) and multcomp (Hothorn et al., 2008). Differences were tested by using a one-way ANOVA (fdr) followed by a Tukey HSD test. Correlation analyses used the Pearson correlation test.

Acknowledgements

We thank Alexander Christmann (TUM, Munich) for the *pHB6* line, Christa Testerink (Wageningen University) for the *xrn4-5* (SAIL_681_E01) and *xrn4-6* (SALK_014209) lines, Julio Salinas (CSIC - Consejo Superior de Investigaciones Científicas) for the *lsm1a/b* and *C-lsm1a* lines, Leslie E. Sieburth (University of Utah) for the WT (Col_0 [$SOV^{L.er}$]) line and helpful discussions, as well as Tou Cheu Xiong, Carine Alcon and the MRI imaging facility, member of the national infrastructure France-BioImaging supported by the French National Research Agency (ANR-10-INBS-04, «Investments for the future»).

Authors contributions

YB and YH conceptualized the research with insights from GK, YH performed the experiments and analyses with the help of YB. YH and YB wrote the paper with contributions from CM.

Conflict of interest

Non declared

Funding

YH is supported by the China Scholarship Council.

References

Alassimone J, Naseer S, Geldner N (2010) A developmental framework for endodermal differentiation and polarity. Proc Natl Acad Sci **107**: 5214–5219

Bacete L, Schulz J, Engelsdorf T, Bartosova Z, Vaahtera L, Yan G, Gerhold JM, Tichá T, Øvstebø C, Gigli-Bisceglia N, et al (2022) THESEUS1 modulates cell wall stiffness and abscisic acid production in Arabidopsis thaliana. Proc Natl Acad Sci **119**: e2119258119

Bai B, Novák O, Ljung K, Hanson J, Bentsink L (2018) Combined transcriptome and translatome analyses reveal a role for tryptophan-dependent auxin biosynthesis in the control of DOG1-dependent seed dormancy. New Phytol **217**: 1077–1085

Beauzamy L, Nakayama N, Boudaoud A (2014) Flowers under pressure: ins and outs of turgor regulation in development. Ann Bot **114**: 1517–1533

Boursiac Y, Protto V, Rishmawi L, Maurel C (2022) Experimental and conceptual approaches to root water transport. Plant Soil **478**: 349–370

Bray EA (1993) Molecular Responses to Water Deficit. Plant Physiol **103**: 1035–1040

Carpita N, Sabularse D, Montezinos D, Delmer DP (1979) Determination of the Pore Size of Cell Walls of Living Plant Cells. Science **205**: 1144–1147

Chang J, Li X, Fu W, Wang J, Yong Y, Shi H, Ding Z, Kui H, Gou X, He K, et al (2019) Asymmetric distribution of cytokinins determines root hydrotropism in Arabidopsis thaliana. Cell Res **29**: 984–993

Chantarachot T, Sorenson RS, Hummel M, Ke H, Kettenburg AT, Chen D, Aiyetiwa K, Dehesh K, Eulgem T, Sieburth LE, et al (2020) DHH1/DDX6-like RNA helicases maintain ephemeral half-lives of stress-response mRNAs. Nat Plants **6**: 675–685

Chen K, Gao J, Sun S, Zhang Z, Yu B, Li J, Xie C, Li G, Wang P, Song C-P, et al (2020) BONZAI Proteins Control Global Osmotic Stress Responses in Plants. Curr Biol. doi: 10.1016/j.cub.2020.09.016

Christmann A, Grill E, Huang J (2013) Hydraulic signals in long-distance signaling. Curr Opin Plant Biol **16**: 293–300

Christmann A, Hoffmann T, Teplova I, Grill E, Müller A (2005) Generation of Active Pools of Abscisic Acid Revealed by In Vivo Imaging of Water-Stressed Arabidopsis. Plant Physiol **137**: 209–219

Claeys H, Inzé D (2013) The Agony of Choice: How Plants Balance Growth and Survival under Water-Limiting Conditions. Plant Physiol **162**: 1768–1779

Claeys H, Van Landeghem S, Dubois M, Maleux K, Inzé D (2014) What Is Stress? Dose-Response Effects in Commonly Used in Vitro Stress Assays. Plant Physiol **165**: 519–527

Corish P, Tyler-Smith C (1999) Attenuation of green fluorescent protein half-life in mammalian cells. Protein Eng **12**: 1035–1040

Cuevas-Velazquez CL, Vellosillo T, Guadalupe K, Schmidt HB, Yu F, Moses D, Brophy JA, Cosio-Acosta D, Das A, Wang L, et al (2021) Intrinsically disordered protein biosensor tracks the physical-chemical effects of osmotic stress on cells. bioRxiv 2021.02.17.431712

Cutler SR, Ehrhardt DW, Griffitts JS, Somerville CR (2000) Random GFP::cDNA fusions enable visualization of subcellular structures in cells of Arabidopsis at a high frequency. Proc Natl Acad Sci **97**: 3718–3723

Czechowski T, Stitt M, Altmann T, Udvardi MK, Scheible W-R (2005) Genome-Wide Identification and Testing of Superior Reference Genes for Transcript Normalization in Arabidopsis. Plant Physiol **139**: 5–17

De Smet S, Cuypers A, Vangronsveld J, Remans T (2015) Gene Networks Involved in Hormonal Control of Root Development in Arabidopsis thaliana: A Framework for Studying Its Disturbance by Metal Stress. Int J Mol Sci **16**: 19195–19224

Dietrich D, Pang L, Kobayashi A, Fozard JA, Boudolf V, Bhosale R, Antoni R, Nguyen T, Hiratsuka S, Fujii N, et al (2017) Root hydrotropism is controlled via a cortex-specific growth mechanism. Nat Plants **3**: 17057

Endo A, Sawada Y, Takahashi H, Okamoto M, Ikegami K, Koiwai H, Seo M, Toyomasu T, Mitsuhashi W, Shinozaki K, et al (2008) Drought Induction of Arabidopsis 9-cis-Epoxycarotenoid Dioxygenase Occurs in Vascular Parenchyma Cells. Plant Physiol **147**: 1984–1993

Gorgues L, Li X, Maurel C, Martinière A, Nacry P (2022) Root osmotic sensing from local perception to systemic responses. Stress Biol **2**: 36

Greenwald EC, Mehta S, Zhang J (2018) Genetically Encoded Fluorescent Biosensors Illuminate the Spatiotemporal Regulation of Signaling Networks. Chem Rev **118**: 11707–11794

Han M-H, Goud S, Song L, Fedoroff N (2004) The Arabidopsis double-stranded RNA-binding protein HYL1 plays a role in microRNA-mediated gene regulation. Proc

Natl Acad Sci **101**: 1093–1098

Haswell ES, Verslues PE (2015) The ongoing search for the molecular basis of plant osmosensing. J Gen Physiol **145**: 389–394

Heim DR, Skomp JR, Tschabold EE, Larrinua IM (1990) Isoxaben Inhibits the Synthesis of Acid Insoluble Cell Wall Materials In *Arabidopsis thaliana*. Plant Physiol **93**: 695–700

Holbein S, Wengi A, Decourty L, Freimoser FM, Jacquier A, Dichtl B (2009) Cordycepin interferes with 3' end formation in yeast independently of its potential to terminate RNA chain elongation. RNA N Y N **15**: 837–849

Hong JH, Chu H, Zhang C, Ghosh D, Gong X, Xu J (2015) A quantitative analysis of stem cell homeostasis in the Arabidopsis columella root cap. Front. Plant Sci. 6:

Hothorn T, Bretz F, Westfall P (2008) Simultaneous inference in general parametric models. Biom J Biom Z **50**: 346–363

Ikegami K, Okamoto M, Seo M, Koshiba T (2009) Activation of abscisic acid biosynthesis in the leaves of Arabidopsis thaliana in response to water deficit. J Plant Res **122**: 235–243

Jain P, Liu W, Zhu S, Chang CY-Y, Melkonian J, Rockwell FE, Pauli D, Sun Y, Zipfel WR, Holbrook NM, et al (2021) A minimally disruptive method for measuring water potential in planta using hydrogel nanoreporters. Proc Natl Acad Sci. doi: 10.1073/pnas.2008276118

Jensen MK, Lindemose S, de Masi F, Reimer JJ, Nielsen M, Perera V, Workman CT, Turck F, Grant MR, Mundy J, et al (2013) ATAF1 transcription factor directly regulates abscisic acid biosynthetic gene NCED3 in Arabidopsis thaliana. FEBS Open Bio **3**: 321–327

Jiang Z, Zhou X, Tao M, Yuan F, Liu L, Wu F, Wu X, Xiang Y, Niu Y, Liu F, et al (2019) Plant cell-surface GIPC sphingolipids sense salt to trigger Ca 2+ influx. Nature **572**: 341–346

Kalladan R, Lasky JR, Sharma S, Kumar MN, Juenger TE, Des Marais DL, Verslues PE (2019) Natural Variation in 9-Cis-Epoxycartenoid Dioxygenase 3 and ABA Accumulation. Plant Physiol **179**: 1620–1631

Kawa D, Meyer AJ, Dekker HL, Abd-El-Haliem AM, Gevaert K, Van De Slijke E, Maszkowska J, Bucholc M, Dobrowolska G, De Jaeger G, et al (2020) SnRK2 Protein Kinases and mRNA Decapping Machinery Control Root Development and Response to Salt1 [OPEN]. Plant Physiol **182**: 361–377

Kawa D, Testerink C (2017) Regulation of mRNA decay in plant responses to salt and osmotic stress. Cell Mol Life Sci **74**: 1165–1176

Kumar SV, Wigge PA (2010) H2A.Z-Containing Nucleosomes Mediate the Thermosensory Response in Arabidopsis. Cell **140**: 136–147

Kuromori T, Sugimoto E, Shinozaki K (2014) Intertissue signal transfer of abscisic acid from vascular cells to guard cells. Plant Physiol **164**: 1587–1592

Lang I, Sassmann S, Schmidt B, Komis G (2014) Plasmolysis: Loss of Turgor and Beyond. Plants **3**: 583–593

Leclerc GM, Boockfor FR, Faught WJ, Frawley LS (2000) Development of a Destabilized Firefly Luciferase Enzyme for Measurement of Gene Expression. BioTechniques **29**: 590–601

Lin Z, Li Y, Zhang Z, Liu X, Hsu C-C, Du Y, Sang T, Zhu C, Wang Y, Satheesh V, et al (2020) A RAF-SnRK2 kinase cascade mediates early osmotic stress signaling in higher plants. Nat Commun **11**: 613

Lobell DB, Field CB (2007) Global scale climate–crop yield relationships and the impacts of recent warming. Environ Res Lett **2**: 014002

Mashiguchi K, Asami T, Suzuki Y (2009) Genome-wide identification, structure and expression studies, and mutant collection of 22 early nodulin-like protein genes in Arabidopsis. Biosci Biotechnol Biochem **11**: 2452～2459

McAdam SAM, Brodribb TJ, Ross JJ (2016) Shoot-derived abscisic acid promotes root growth. Plant Cell Environ **39**: 652–659

Mehra P, Pandey BK, Melebari D, Banda J, Leftley N, Couvreur V, Rowe J, Anfang M, Gernier HD, Morris E, et al (2022) Hydraulic flux–responsive hormone redistribution determines root branching. Science. doi: 10.1126/science.add3771

Mukherjee S, Mishra A, Trenberth KE (2018) Climate Change and Drought: a Perspective on Drought Indices. Curr Clim Change Rep **4**: 145–163

de Nadal E, Ammerer G, Posas F (2011) Controlling gene expression in response to stress. G E N E Ti C S

Nongpiur RC, Singla-Pareek SL, Pareek A (2020) The quest for osmosensors in plants. J Exp Bot **71**: 595–607

Perea-Resa C, Carrasco-López C, Catalá R, Turečková V, Novak O, Zhang W, Sieburth L, Jiménez-Gómez JM, Salinas J (2016) The LSM1-7 Complex Differentially Regulates Arabidopsis Tolerance to Abiotic Stress Conditions by Promoting Selective mRNA Decapping. Plant Cell **28**: 505–520

Perea-Resa C, Hernández-Verdeja T, López-Cobollo R, del Mar Castellano M, Salinas J (2012) LSM proteins provide accurate splicing and decay of selected transcripts to ensure normal Arabidopsis development. Plant Cell **24**: 4930–4947

PRITCHARD J, JONES RGW, TOMOS AD (1991) Turgor, Growth and Rheological Gradients of Wheat Roots Following Osmotic Stress. J Exp Bot **42**: 1043–1049

Rowe J, Grangé-Guermente M, Exposito-Rodriguez M, Wimalasekera R, Lenz MO, Shetty KN, Cutler SR, Jones AM (2023) Next-generation ABACUS biosensors reveal cellular ABA dynamics driving root growth at low aerial humidity. Nat Plants 1–13

Sack L, John GP, Buckley TN (2018) ABA Accumulation in Dehydrating Leaves Is Associated with Decline in Cell Volume, Not Turgor Pressure1[OPEN]. Plant Physiol **176**: 489–495

Sadanandom A, Napier RM (2010) Biosensors in plants. Curr Opin Plant Biol **13**: 736–743

Sato H, Takasaki H, Takahashi F, Suzuki T, Iuchi S, Mitsuda N, Ohme-Takagi M, Ikeda M, Seo M, Yamaguchi-Shinozaki K, et al (2018) Arabidopsis thaliana NGATHA1 transcription factor induces ABA biosynthesis by activating NCED3 gene during dehydration stress. Proc Natl Acad Sci U S A **115**: E11178–E11187

Shabala SN, Lew RR (2002) Turgor Regulation in Osmotically Stressed Arabidopsis Epidermal Root Cells. Direct Support for the Role of Inorganic Ion Uptake as Revealed by Concurrent Flux and Cell Turgor Measurements. Plant Physiol **129**: 290–299

Shavrukov Y (2013) Salt stress or salt shock: which genes are we studying? J Exp Bot **64**: 119–127

Soma F, Mogami J, Yoshida T, Abekura M, Takahashi F, Kidokoro S, Mizoi J, Shinozaki K, Yamaguchi-Shinozaki K (2017) ABA-unresponsive SnRK2 protein kinases regulate mRNA decay under osmotic stress in plants. Nat Plants **3**: 16204

Soma F, Takahashi F, Suzuki T, Shinozaki K, Yamaguchi-Shinozaki K (2020) Plant Raf-like kinases regulate the mRNA population upstream of ABA-unresponsive SnRK2 kinases under drought stress. Nat Commun **11**: 1373

Soma F, Takahashi F, Yamaguchi-Shinozaki K, Shinozaki K (2021) Cellular Phosphorylation Signaling and Gene Expression in Drought Stress Responses: ABA-Dependent and ABA-Independent Regulatory Systems. Plants **10**: 756

Sorenson RS, Deshotel MJ, Johnson K, Adler FR, Sieburth LE (2018) Arabidopsis mRNA decay landscape arises from specialized RNA decay substrates, decapping-mediated feedback, and redundancy. Proc Natl Acad Sci **115**: E1485–E1494

Steinhorst L, He G, Moore LK, Schültke S, Schmitz-Thom I, Cao Y, Hashimoto K, Andrés Z, Piepenburg K,

Ragel P, et al (2022) A Ca2+-sensor switch for tolerance to elevated salt stress in Arabidopsis. Dev Cell **57**: 2081-2094.e7

Sun M, Schwalb B, Schulz D, Pirkl N, Etzold S, Larivière L, Maier KC, Seizl M, Tresch A, Cramer P (2012) Comparative dynamic transcriptome analysis (cDTA) reveals mutual feedback between mRNA synthesis and degradation. Genome Res **22**: 1350–1359

Sussmilch FC, Brodribb TJ, McAdam SAM (2017) Up-regulation of NCED3 and ABA biosynthesis occur within minutes of a decrease in leaf turgor but AHK1 is not required. J Exp Bot **68**: 2913–2918

Tan B-C, Joseph LM, Deng W-T, Liu L, Li Q-B, Cline K, McCarty DR (2003) Molecular characterization of the Arabidopsis 9-cis epoxycarotenoid dioxygenase gene family. Plant J **35**: 44–56

Vaahtera L, Schulz J, Hamann T (2019) Cell wall integrity maintenance during plant development and interaction with the environment. Nat Plants **5**: 924–932

Waadt R, Seller CA, Hsu P-K, Takahashi Y, Munemasa S, Schroeder JI (2022) Plant hormone regulation of abiotic stress responses. Nat Rev Mol Cell Biol **23**: 680–694

Wang W, Vinocur B, Altman A (2003) Plant responses to drought, salinity and extreme temperatures: towards genetic engineering for stress tolerance. Planta **218**: 1–14

Yamaguchi-Shinozaki K, Shinozaki K (1994) A novel cis-acting element in an Arabidopsis gene is involved in responsiveness to drought, low-temperature, or high-salt stress. Plant Cell **6**: 251–264

Yang Y-Z, Tan B-C (2014) A Distal ABA Responsive Element in AtNCED3 Promoter Is Required for Positive Feedback Regulation of ABA Biosynthesis in Arabidopsis. PLOS ONE **9**: e87283

Younis I, Berg M, Kaida D, Dittmar K, Wang C, Dreyfuss G (2010) Rapid-Response Splicing Reporter Screens Identify Differential Regulators of Constitutive and Alternative Splicing. Mol Cell Biol **30**: 1718–1728

Yuan F, Yang H, Xue Y, Kong D, Ye R, Li C, Zhang J, Theprungsirikul L, Shrift T, Krichilsky B, et al (2014) OSCA1 mediates osmotic-stress-evoked Ca 2+ increases vital for osmosensing in Arabidopsis. Nature **514**: 367–371

Zeevaart JAD, Creelman RA (1988) Metabolism and Physiology of Abscisic Acid. Annu Rev Plant Physiol Plant Mol Biol **39**: 439–473

Zhang H, Zhu J, Gong Z, Zhu J-K (2022) Abiotic stress responses in plants. Nat Rev Genet **23**: 104–119

Zhang W, Murphy C, Sieburth LE (2010) Conserved RNaseII domain protein functions in cytoplasmic mRNA decay and suppresses Arabidopsis decapping mutant phenotypes. Proc Natl Acad Sci **107**: 15981–15985

Zhu J-K (2016) Abiotic Stress Signaling and Responses in Plants. Cell **167**: 313–324

Zid BM, O'Shea EK (2014) Promoter sequences direct cytoplasmic localization and translation of mRNAs during starvation in yeast. Nature **514**: 117–121

Zluhan-Martínez E, López-Ruíz BA, García-Gómez ML, García-Ponce B, de la Paz Sánchez M, Álvarez-Buylla ER, Garay-Arroyo A (2021) Integrative Roles of Phytohormones on Cell Proliferation, Elongation and Differentiation in the Arabidopsis thaliana Primary Root. Front. Plant Sci. 12:

Hadley Wickham, Romain François, Lionel Henry and Kirill Müller (2022). dplyr: A Grammar of Data Manipulation. R package version 1.0.8. https://CRAN.R-project.org/package=dplyr

H. Wickham. ggplot2: Elegant Graphics for Data Analysis. Springer-Verlag New York, 2016.

Russell V. Lenth (2023). emmeans: Estimated Marginal Means, aka Least-Squares Means. R package version 1.8.7. https://CRAN.R-project.org/package=emmeans

Supplementary Figures

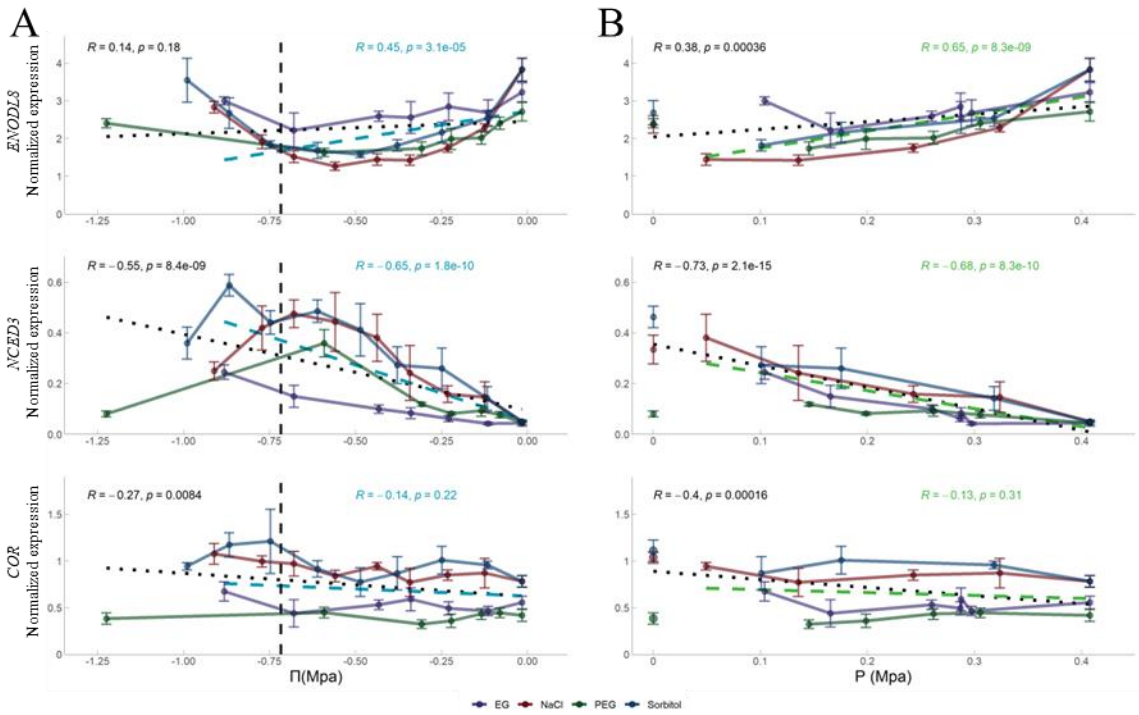

Supplementary Fig 1. Two genes respond quantitatively to changes in osmotic potential (Π) or turgor potential (P) upon mild water deficit treatments for 15min

(A) Correlation analysis between the expression of 3 genes and Π under all conditions, or under mild water deficit treatments (right side of the vertical dashed lines) that preserve cortical cells turgidity only. Black dotted regression lines and blue dashed regression lines represent the fit under all conditions or mild water deficit treatments, respectively. Pearson coefficient (R) and p-value are depicted in the upside of graph. Each point is the average (± se) of 3 biological repeats of the same treatment. (B) Correlation analysis between the expression of 3 gene and the average P around 15 min under mild treatments similar treatment as in (A). Normalized expression means that gene expression is referenced to the expression of internal control genes.

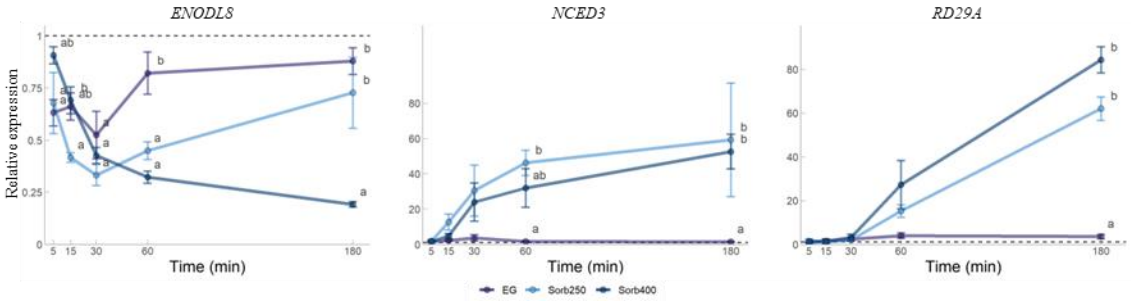

Supplementary Fig 2. Kinetic of *ENODL8*, *NCED3* and *RD29A* expression under mild and severe water deficit treatments

Relative expression of 3 genes in the roots under 250 mM EG, 250 mM and 400 mM sorbitol treatments. 3 biological repeats per treatment. Letters indicate a significant difference among conditions at a given time point. (mean ± se, ANOVA and Tukey's HSD test ($P < 0.05$)).

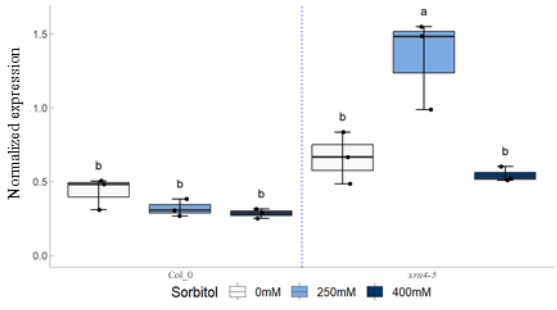

Supplementary Fig. 3 *xrn4-5* is not a knockout mutant

Normalized expression means that gene expression is referenced to the expression of internal control genes. 3 biological repeats for each treatment. ANOVA and Tukey's HSD test ($P < 0.05$).

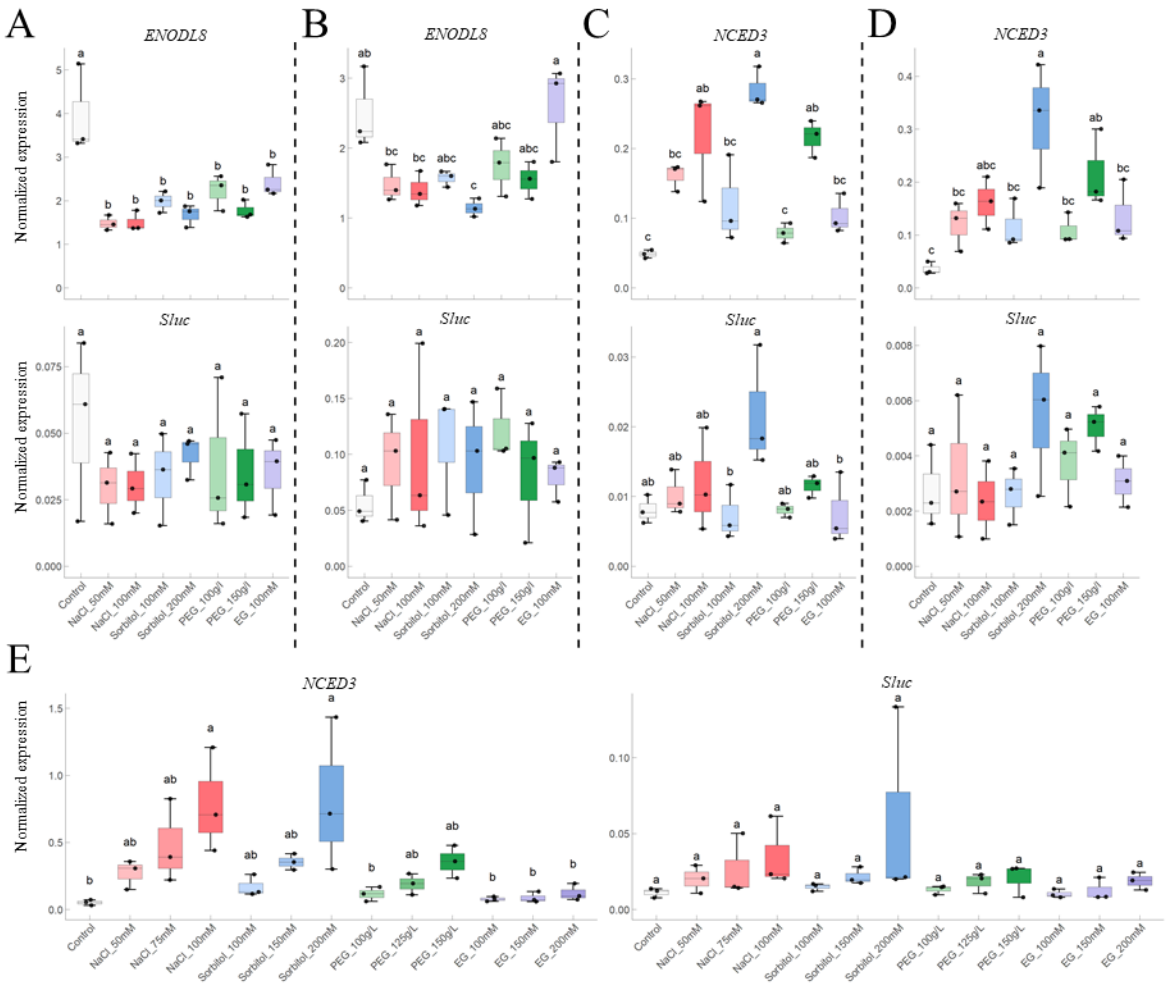

Supplementary Fig. 4 Gene expressions after treatments for 15 and 30min

This supplementary figure shows in more details the results that are being used for the main figure 3. (A-B) gene expressions in roots of two transgenic *pENODL8::Sluc-3'UTR* lines L13 and L15 after treatments for 15 min, respectively. (C-D) gene expressions in roots of two transgenic *pNCED3::Sluc-3'UTR* lines L7 and L16 after treatments for 15 min, respectively. (E) gene expressions in roots of transgenic *pNCED3::Sluc-3'UTR* lines L7 after treatments for 30 min. Normalized expression means that gene expression is referenced to the expression of internal control genes. Each point means one biological repeat. (ANOVA and Tukey's HSD test ($P < 0.05$)).

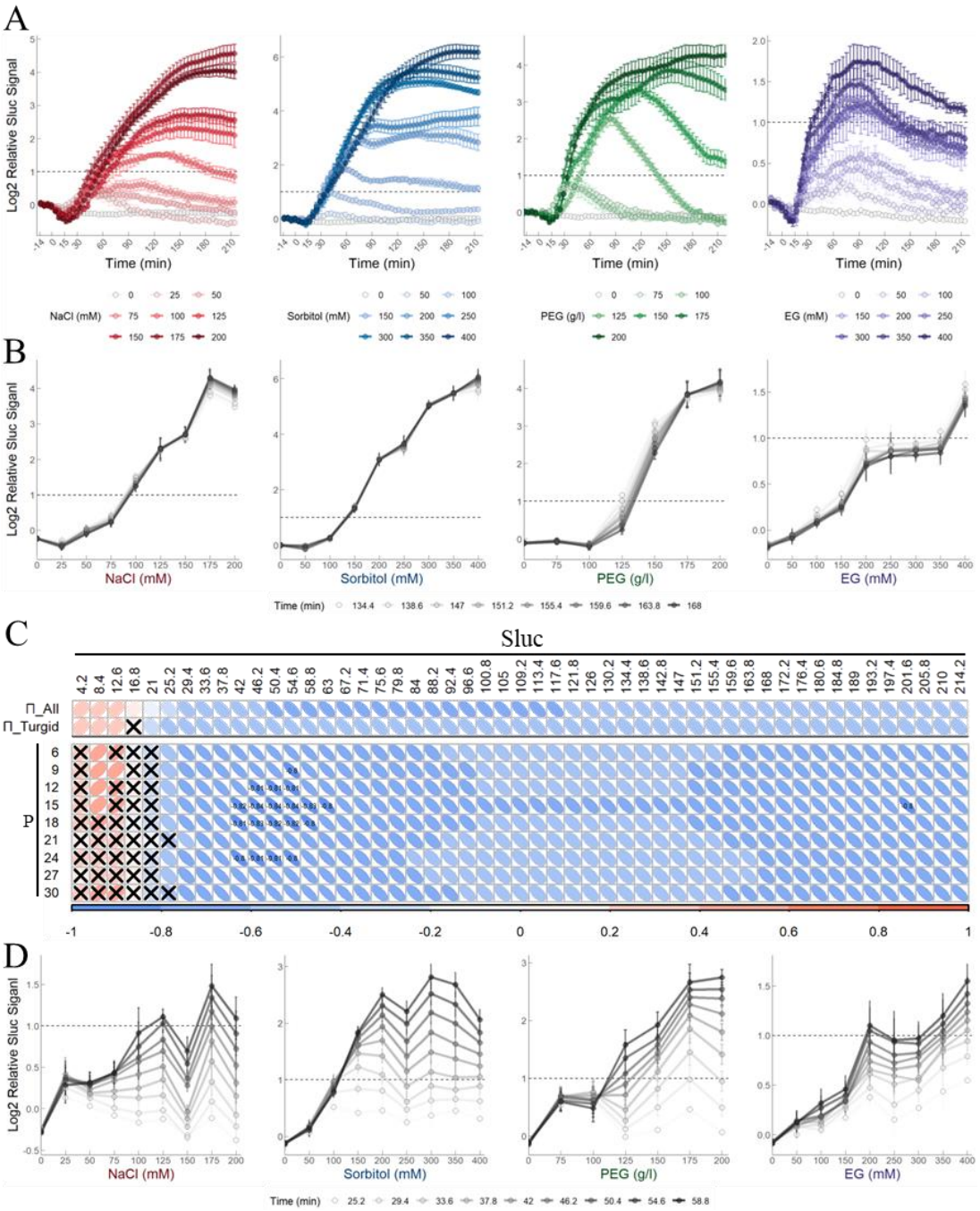

Supplementary Fig 5. The luminescence signal of Sluc from *pNCED3::Sluc-3'UTR* expressing lines can report P and Π changes

(A) log2 (relative Sluc signal) in L16 roots over 3.5h during water deficit treatments. Relative Sluc signals were calculated by dividing the Sluc raw readouts at each time point by the average of Sluc raw readouts taken from four time points before the treatments. The log2 (relative Sluc signal) was obtained by applying the log2 function to the relative Sluc signals. The dotted lines mean 2-fold changes (log2). Each condition has 3-4 biological repeats and each repeat has 1-2 plants (n=6-8). (B) The log2 (relative Sluc signal) in the roots of L16 at the late stage of treatments (mean ± se). (C) Pearson correlations heatmap between the relative Sluc signal and Π or P over time during treatments (same convention as Fig. 4). Cells with a cross represent p-values > 0.01 and cells displaying a correlation coefficient greater than 0.8 show their actual values. (D) log2 (relative Sluc signal) in the roots of L16 at the early stage of treatments. (mean ± se).

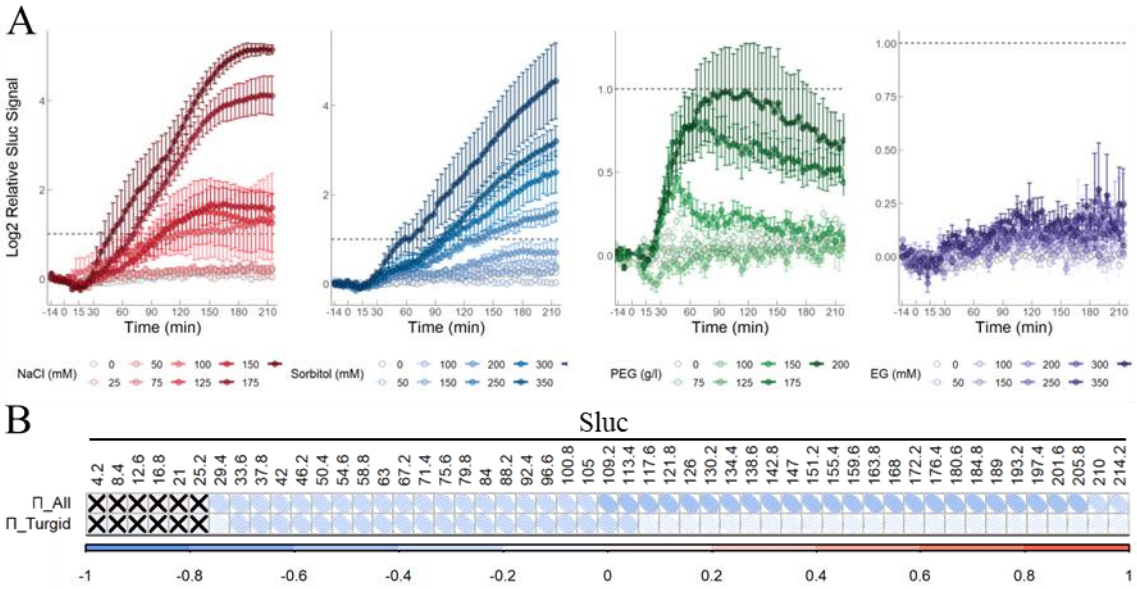

Supplementary Fig 6. The *pNCED3::Sluc-3'UTR* construct in shoots is also able to report root SWD treatments

(A) log2 (relative Sluc signal) in L16 shoots over 3.5h during water deficit treatments. Relative Sluc signals (mean ± se) were calculated by dividing the Sluc raw readouts at each time point by the average of Sluc raw readouts taken from four time points before the treatments. The log2 (relative Sluc signal) was obtained by applying the log2 function to the relative Sluc signals. The dotted lines mean 2-fold changes (log2). Each condition has 3-4 biological repeats and each repeat has 1-2 plants (n=6-8). 10-days old plants, 10 s exposure time and 4.2 min interval time (B) Pearson correlations heatmap between the relative Sluc signal and Π_All and Π_Turgid, respectively (same convention as Fig. 4). Crossed cells have a p-value > 0.01.

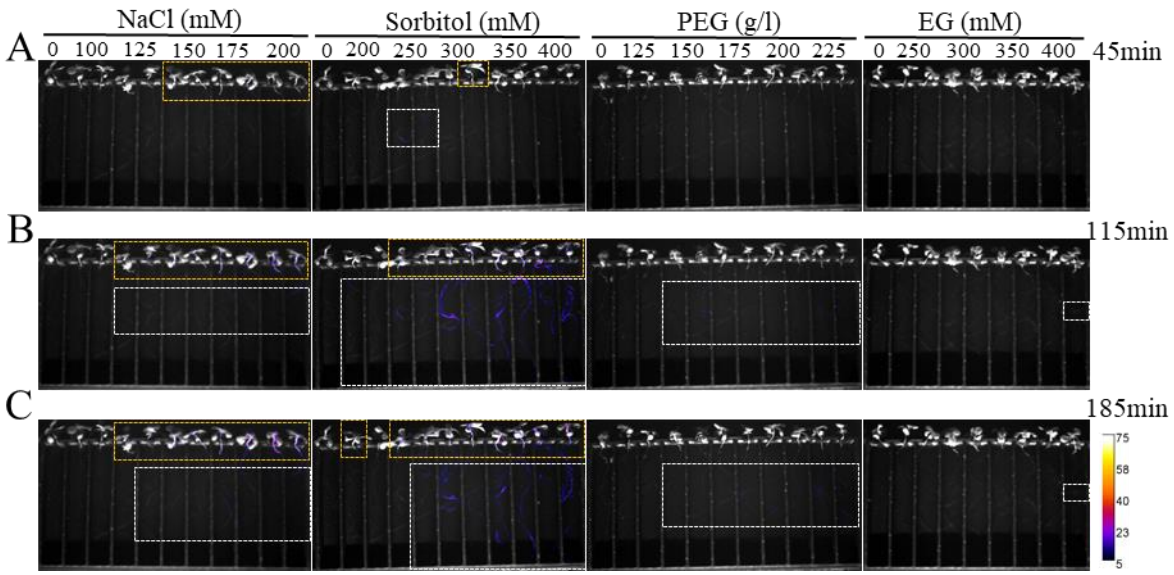

Supplementary Fig 7. Emergence of Suc signals from the *pNCED3*::Sluc-3'UTR expressing plants (L16), is observed in the mature middle part of the PR and in the hypocotyl in response to water deficit treatments

(A-C) Overlapped pictures of Sluc signals and a bright field image after 45, 115 and 185 min. Images were obtained from 5 min after the beginning of the treatments and continued for 3.5 h. Exposure time was 10 min. Orange boxes and white boxes delineate the portions of shoots and roots, respectively, where a significant Sluc signal could be observed. The distance between each plant is ~8.6 mm.

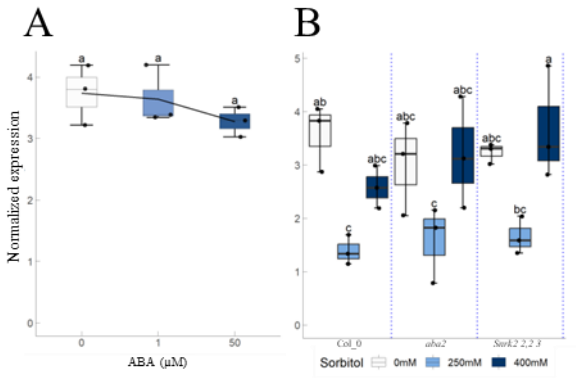

Supplementary Fig 8. The regulation of *ENODL8* expression appears to be ABA independent

(A) Normalized gene expression in the roots after 1 and 50 μM ABA treatments for 15min (left) and normalized gene expression in the roots of ABA-related mutants after 250 and 400 mM sorbitol treatments for 15min (right). Normalized expression means that gene expression is referenced to the expression of internal control genes. 3 biological repeats for each treatment (ANOVA and Tukey's HSD test ($P < 0.05$)).

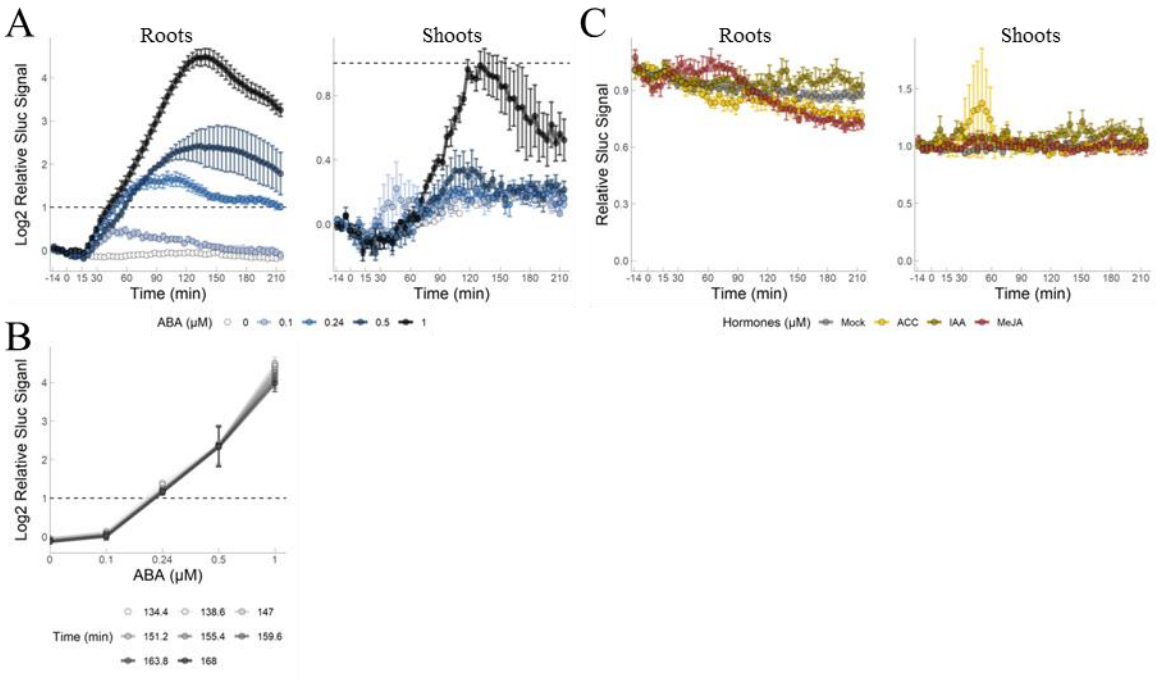

Supplementary Fig 9. The luminescence signal of Sluc from *pNCED3::Sluc-3'UTR* expressing lines (L16) specifically responds to exogenous ABA

(A) log2 (relative Sluc signal) in the roots and shoots of L16 under ABA treatments. 3 biological repeats and each repeat has 2 plants (n=6). (B) log2 (relative Sluc signal) in the roots of L16 at the late stage (134.4-168 min) of ABA treatments. (C) Relative Sluc signal in the roots and shoots of L16 under 1 μM IAA, 1 μM MeJA and 1 μM ACC treatments. 2 biological repeats with 2 plants per replicate (n=4). (mean ± se).

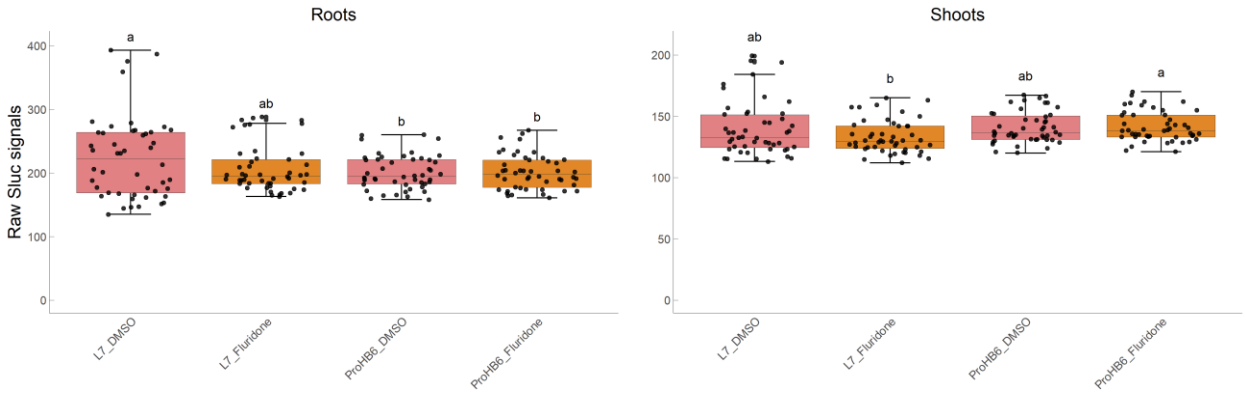

Supplementary Fig 10. Pretreating plants with fluridone did not impact Sluc signals in L7 and *pHB6* plants. Raw readout of Sluc signals after DMSO and fluridone pre-treatments for 24 h. 10-days old plants, and 10 s of exposure time and 4.2 min of interval time. 6 biological repeats and each repeat has 2 plants (n=12), and each replicate has four time point readings. (mean ± se).

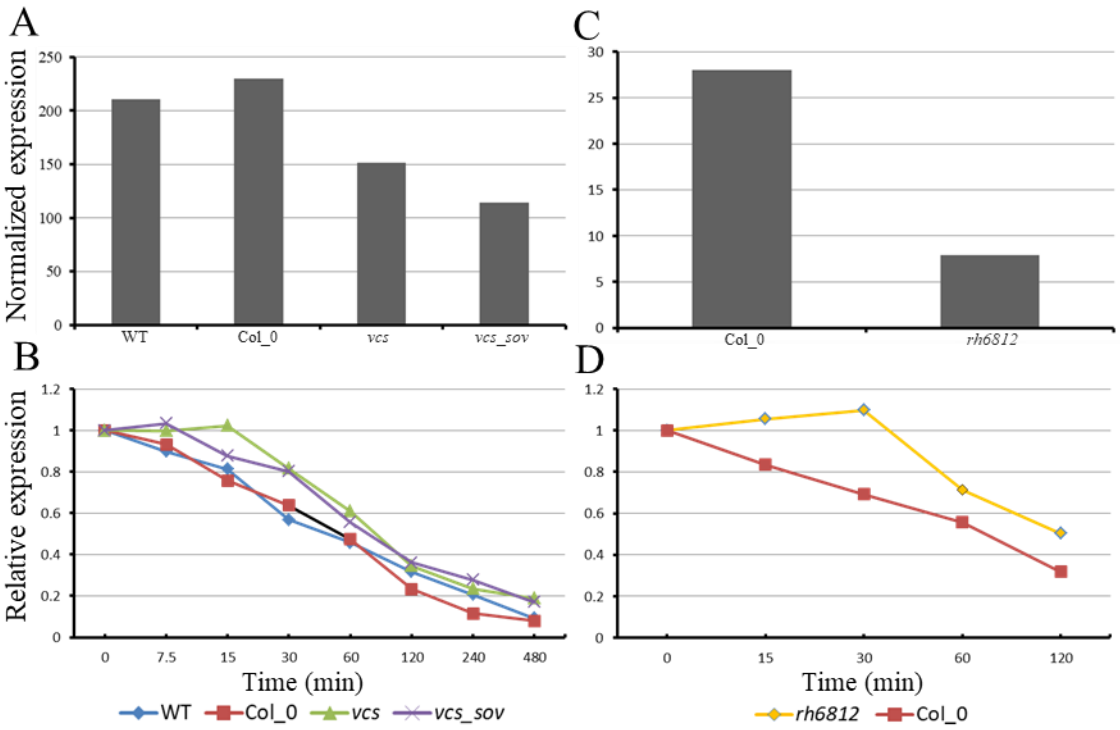

Supplementary Fig 11. In the litterature, *ENODL8* mRNA abundance is controlled by the mRNA decapping complex

(A and C) Normalized expression under control condition in various genotypes with altered functionalities in the mRNA decay pathways. (B and D) Relative expression under cordycepin treatment. 5 days old seedlings were used in these two papers. 3 repeats and presented data are their mean value. WT: Col_*SOV*^{Ler}. Col_0: *sov* mutant. Data were extracted from the supplemental transcriptomic data of the two following papers: (Sorenson et al., 2018; Chantarachot et al., 2020).

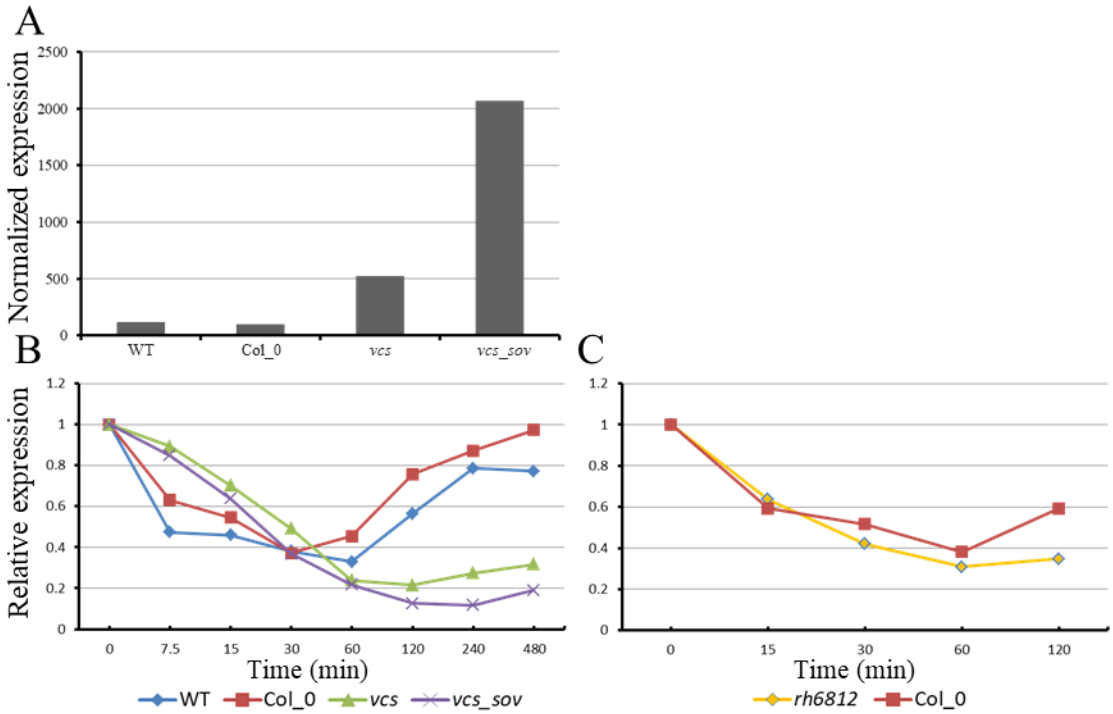

Supplementary Fig 12. In the litterature, *NCED3* mRNA abundance is controlled by the mRNA decapping complex

(A) Normalized expression under control condition in various genotypes with altered functionalities in the mRNA decay pathways. (B and C) Relative expression under cordycepin treatment. 5 days old seedlings were used in these two papers. 3 repeats and presented data are their mean value. WT: Col_*SOV*^{Ler}. Col_0: *sov* mutant. Data were extracted from the supplemental transcriptomic data of the two following papers: (Sorenson et al., 2018; Chantarachot et al., 2020).

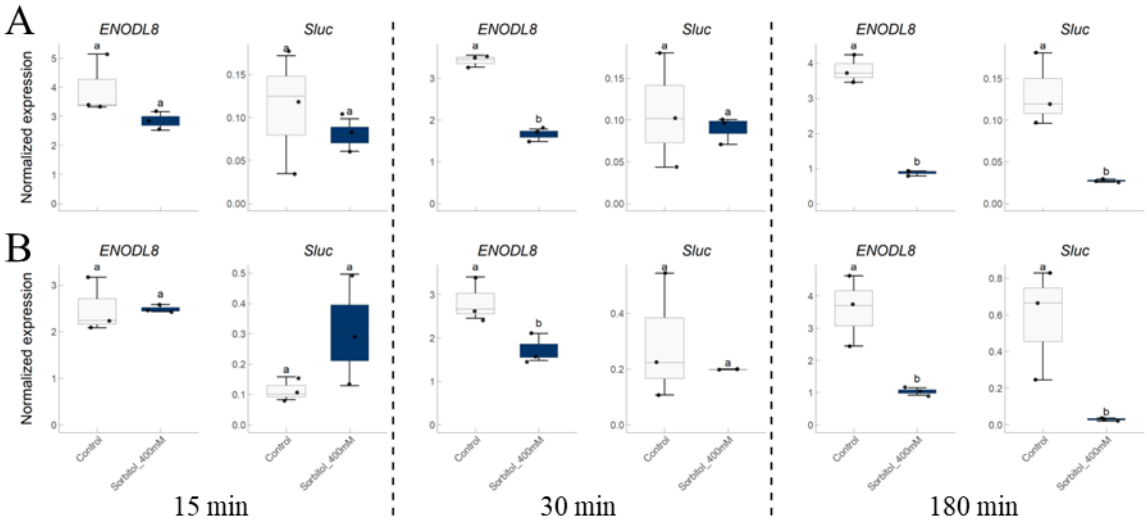

Supplementary Fig 13. *pENODL8+3'UTR* is able to regulate the expression of *ENODL8* under SWD

A and B are gene expressions in roots of two transgenic *pENODL8::Sluc-3'UTR* lines L13 (above) and L15 (below), respectively. Corresponding treatment time points are shown at the botton. Normalized expression means that gene expression is referenced to the expression of internal control genes. Each point means one biological repeat. (ANOVA and Tukey's HSD test ($P < 0.05$)).

Supplementary Tables

Supplementary Table 1. Summary of the osmotic treatments applied to the roots

Solute	Concentration (mM, g l^{-1} for PEG)	Π	P_{cort}	P_{6min}	P_{9min}	P_{12min}	P_{15min}	P_{18min}	P_{21min}	P_{24min}	P_{27min}	P_{30min}
None	0	-0.016	0.41	0.41	0.37	0.39	0.40	0.43	0.38	0.39	0.39	0.38
NaCl	25	-0.125	0.32	0.34	0.33	0.33	0.34	0.30	0.34	0.27	0.30	0.26
	50	-0.232	0.25	0.25	0.25	0.25	0.25	0.23	0.24	0.22	0.24	0.22
	75	-0.342	0.14	0.15	0.12	0.13	0.14	0.13	0.15	0.13	0.12	0.15
	100	-0.438	0.05	0.05	0.05	0.07	0.04	0.05	0.03	0.05	0.05	0.04
	125	-0.560										
	150	-0.680										
	175	-0.772										
	200	-0.912										
Sorbitol	50	-0.117	0.32	0.29	0.32	0.32	0.34	0.30	0.31	0.31	0.29	0.31

	100	-0.249	0.18	0.19	0.20	0.19	0.18	0.18	0.15	0.17	0.17	0.19
	150	-0.379	0.1	0.12	0.09	0.10	0.10	0.09	0.09	0.05	0.09	0.10
	200	-0.486										
	250	-0.611										
	300	-0.748										
	350	-0.868										
	400	-0.990										
PEG 8000	75	-0.081	0.31	2.89	3.40	2.76	3.25	3.22	3.24	2.81	2.24	3.17
	100	-0.134	0.26	2.98	2.61	3.11	2.57	2.61	2.00	2.47	2.41	2.75
	125	-0.222	0.2	2.02	1.83	1.98	2.01	1.92	1.64	1.73	1.70	1.53
	150	-0.308	0.14	1.73	1.65	1.56	1.13	1.47	1.50	1.89	1.57	1.60
	175	-0.438										
	200	-0.592										
	225	-0.944										
	250	-1.225										
EG	50	-0.115	0.3	0.28	0.28	0.25	0.33	0.31	0.33	0.34	0.29	0.24
	100	-0.230	0.29	0.26	0.26	0.26	0.31	0.32	0.31	0.31	0.34	0.32
	150	-0.340	0.29	0.25	0.28	0.23	0.32	0.32	0.41	0.29	0.35	0.27
	200	-0.433	0.26	0.24	0.27	0.24	0.24	0.29	0.31	0.29	0.33	0.35
	250	-0.565										
	300	-0.680	0.17	0.13	0.15	0.19	0.18	0.21	0.23	0.26	0.25	0.26
	350	-0.768										
	400	-0.882	0.10	0.06	0.11	0.06	0.09	0.06	0.21	0.15	0.22	0.07

Solutes were dissolved in the hydroponic solution. The osmotic potential of the solution was measured at 20 °C with an osmometer (Wescor); three digits after the decimal point are shown. The osmotic pressure is the opposite of the osmotic potential. The average of P was calculated in 3-minutes intervals from 5 to 31 minutes.

Supplementary Table 2. All the oligo sequences

Names	Forward oligo	Reverse oligo	Purpose

qENODL8	AGCAAGACGATGGTGGTGGT	TGAGTCTTCGCTTGGTGGGT	qPCR
qNCED3	TGATTGCCCACCCGAAAGTC	CTCCGGCAGCTTGAAAACGA	qPCR
qRD29A	CCGGAATCTGACGGCCGTTTA	CCGTCGGCACATTCTGTCGAT	qPCR
qAt1G13320	TAACGTGGCCAAAATGATGC	GTTCTCCACAACCGCTTGGT	qPCR
qAt4G34270	GTGAAAACTGTTGGAGAGAAGCAA	TCAACTGGATACCCTTTCGCA	qPCR
qCOR	TCAACCGTCTCTTGCTCCAC	CCATTAGTCCTTGCGGTGGT	qPCR
q18SrRNA	AAACGGCTACCACATCCAAG	CCTCCAATGGATCCTCGTTA	qPCR
qAt5G60390	TGAGCACGCTCTTCTTGCTTTCA	GGTGGTGGCATCCATCTTGTTACA	qPCR
qXRN4	TGGCATGAAGACAATAGCAAC	AGAGAAGGCCCTGCTATAGC	qPCR
qActin2	GGTAACATTGTGCTCAGTGGTGG	AACGACCTTAATCTTCATGGCTGC	qPCR
qGFP	TCATGGCCGACAAGCAGAAG	ACCATGTGATCGCGCTTCTC	qPCR
qSluc	CGCCTTTACCGACGCACATA	CACAGCCACACCGATGAACA	qPCR
pENODL8	GGGGACAAGTTTGTACAAAAAAGCAGGCTAT CCTAAAATCCAACAATGA	GGGGACCACTTTGTACAAGAAAGCTGGGTTG CTTCTCAGATCTCCTGA	Constructing pDNOR207_pENODL8 for pKGWFS7_pENODL8::Egfp-GUS
p35S	GGGGACAACTTTGTATAGAAAAGTTGCTGAGA CTTTTCAACAAAGGGT	GGGGACTGCTTTTTTGTACAAACTTGCTGTTC TCTCCAAATGAAATG	Constructing pDONRTM P4 P1R_p35S for pH7m34GW_p35S::Sluc
pENODL8	GGGGACAACTTTGTATAGAAAAGTTGCATCCT AAAATCCAACAATGA	GGGGACTGCTTTTTTGTACAAACTTGCCTTGA TTGGTCTACTTTGCT	Constructing pDONRTM P4 P1R_pENODL8 for pK7m34GW_pENODL8::Sluc and pK7m34GW_pENODL8::Sluc-3'UTR
pNCED3	GGGGACAACTTTGTATAGAAAAGTTGCAACGT GTGTTACCATTTAGAT	GGGGACTGCTTTTTTGTACAAACTTGCTTTTC AAGTGTGTTCAATCA	Constructing pDONRTM P4 P1R_pNCED3 for pK7m34GW_pNCED3::Sluc-3'UTR
Sluc	GGGGACAAGTTTGTACAAAAAAGCAGGCTTC ATGGAAGATGCCAAAAACAT	GGGGACCACTTTGTACAAGAAAGCTGGGTATT AGACGTTGATCCTGGCGC	Constructing pDNOR207_Sluc for pK7m34GW_pENODL8::Sluc and pK7m34GW_pENODL8::Sluc-3'UTR
3'UTR of ENODL8	GGGGACAGCTTTCTTGTACAAAGTGGCTTGGA ATTTTTGAATATCTTTA	GGGGACAACTTTGTATAATAAAGTTGCTGAGT GGAGAGAGGAGAGA	Constructing pDONRTM P2R-P3_3'UTR of ENODL8 for pK7m34GW_pENODL8::Sluc-3'UTR
3'UTR of NCED3	GGGGACAGCTTTCTTGTACAAAGTGGCTGTTC TTATGTGTAAATACGC	GGGGACAACTTTGTATAATAAAGTTGTGCGAA ATATATTTTATAAAA	Constructing pDONRTM P2R-P3_3'UTR of NCED3 for pK7m34GW_pENODL8::Sluc-3'UTR

Chapter 3: Additional results

Context

We introduced *p35S* plants *(p35S::Sluc*) as a reference line in the Sluc assays in the previous section. We monitored Sluc response in *pNCED3::Sluc-3'UTR* and *p35S* at the same time in order to understand better the sensitivity and limits of our system. Moreover, we demonstrated that the expression of *ENODL8* in response to water deficit was not simply controlled by its promoter and 3'UTR. Here, we analyzed in more details the Sluc response in *p35S* under water deficit treatments. In addition, complemented lines were obtained by transferring the *pENODL8:sp-eGFP-ENODL8-3'UTR* construct into *enodl8* mutants, and the regulatory mechanisms of *ENODL8* expression were further investigated in those lines. We also tried to explore whether ENODL8 is not of interest only for its regulation, but also plays a role in the plant stress response.

Results

Is the P35S::Sluc construct able to report P or Π?

In order to test our Sluc system, we measured the Sluc signals in the roots and shoots of a reference line *p35S*, during treatments with a series of concentrations of NaCl, sorbitol, PEG8000 and EG (**Fig. 1A**). Starting from a very high level compared to the background, or to the signal of *pNCED3::Sluc* under MWD (before treatments, the absolute values of Sluc signals were: p35S>11000, L7≈96, L16≈80), Sluc signal from *p35S* decreased within minutes upon stress application in the roots. It then remained relatively stable for 1 h in the NaCl treatments, while it gradually recovered for the other treatments. Quite surprisingly, some Π-related correlations appeared during the kinetic (**Fig. 1B** shows an example at about 2h of treatment), however they are unlikely to be consistent in a broad context because of this stability issue. This was confirmed by the correlation analysis between Sluc signals and Π-All (Π under all the conditions) or Π-Turgid (Π under conditions where cortical cells maintained turgid) or P (P under condition where cortical cells P was measured with a cell pressure probe) ($R < 0.6$ and/or $P > 0.01$) (**Fig. 1C**), which exists but are less robust than for the *pNCED3::Sluc-3'UTR* results. These results suggest that the *p35S::Sluc* construct is not a Π-reporter on a long-term for water deficit treatments. Nevertheless, a consistent dose-dependent response is present during the early stage of treatments (**Fig. 1D**). Correlation

analyses for that period showed that Sluc signals correlated better with P than with Π-All or Π-Turgid (**Fig. 1C**). These results indicate that the *p35S::Sluc* construct could be a P-reporter during the early stages of water deficit.

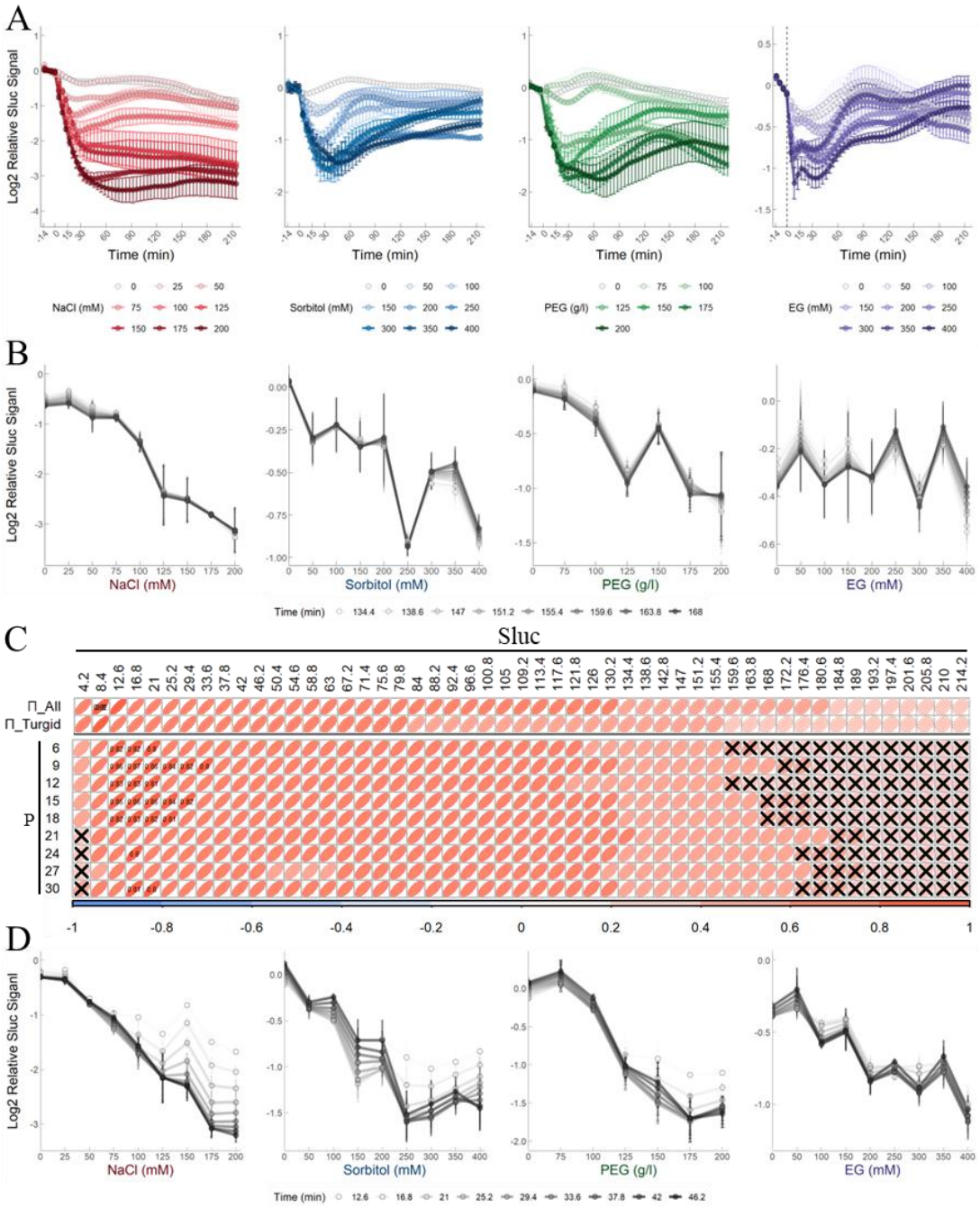

Fig 1. Plant carrying the *p35S::Sluc* construct show signals correlated to P changes in roots under water deficit treatments during the early stage

(A) The log2 (relative Sluc signal) in *p35S* roots over 3.5h during water deficit treatments. Relative Sluc signals were calculated by dividing the Sluc raw readouts at each time point by the average of Sluc raw readouts taken from four time points before the treatments. The log2 (relative Sluc signal) was obtained by applying the log2 function to the relative Sluc signals. Each condition has 3-4 biological repeats and each repeat has 1 plant (n=3-4). Plants were 10-days old, exposure time was 10 s and pictures were taken every 4.2 min. (B) The log2 (relative Sluc signal) in the roots

of *p35S* at the late stage of treatments (134-168 min). (C) Pearson correlaton heatmap between relative Sluc signal and Π or P over times during treatments. All_Π and Π_Turgid represent the correlation between relative Sluc signal and measured Π under all the treatments and treatments who do not provoke the plasmolysis of cortical cells, respectively. "P" represents the correlation between the relative Sluc signals and the turgor pressure P measured under various treatments, including 25/50/75/100 mM NaCl, 50/100/150 mM sorbitol, 75/100/125/150 g/l PEG8000 and 50/100/150/200/300/400 mM EG. Each row represents the correlation calculated by using the relative Sluc signal against the average of P at the corresponding time point. The average of P was calculated in 3-minutes intervals from 5 to 31 minutes. Cells with a cross represent p-values > 0.01 and cells displaying a correlation coefficient greater than 0.8 show their actual values. (D) The log2 (relative Sluc signal) in the roots of *p35S* at the early stage of treatments (12-46 min) (mean ± se).

These surprising results need to be analyzed carefully. First, the treatments were conducted by adding concentrated solutions into hydroponics (adding 100 µl to 800µl, 100 µl/s) in the plate reader. Thus, this quantitative reduction could be attributed to a change in the solution height, which may reduce the amount of photons from the luciferin cleavage reaching the sensor. As expected, such reduction is also observed in L7/L16 during the first 15 min of treatments. It is also possible that other artifacts due to the addition of an osmoticum in the medium could explain these results. For example, through the shrinkage of roots or interference with the luciferase reactions. No clear correlated response was observed in its shoots under all the treatments (**Fig. 2**), which further reinforces the need for additional work in order to confirm if this construct can still be useful for reporting early changes in P, and how. It is important, for the rest of the work presented in section 2, to note that such effect is not interfering much with the ability of *pNCED3::Slug-3'UTR* to report hydraulic changes, since signal from the later is induced by treatments and shows strong correlation with P/Π after 25 min.

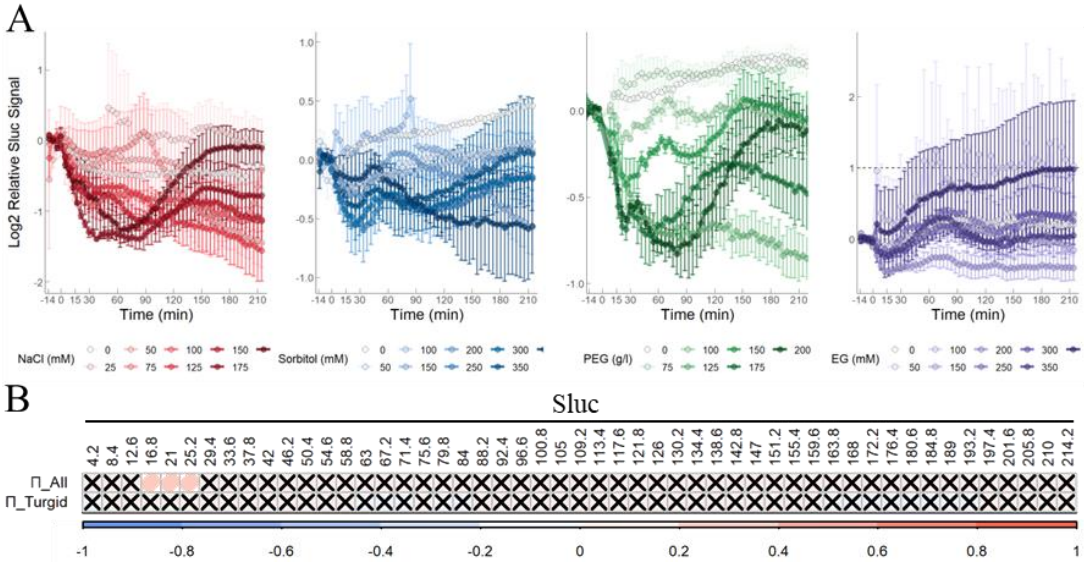

Fig 2. Sluc in shoots of plant carrying the *p35S::Sluc* construct did not show clear response after water deficit treatment

(A) The log2 (relative Sluc signal) in *p35S* shoots over 3.5h during water deficit treatments. Relative Sluc signals were calculated by dividing the Sluc raw readouts at each time point by the average of Sluc raw readouts taken from four time points before the treatments. The log2 (relative Sluc signal) was obtained by applying the log2 function to the relative Sluc signals. Each condition has 3-4 biological repeats and each repeat has 1 plant (n=3-4). Plants were 10-days old, exposure time was 10 s and pictures were taken every 4.2 min. (B) Pearson correlaton heatmap between relative Sluc signal and Π over times during treatments. All_Π and Π_Turgid represent the correlation between relative Sluc signal and measured Π under all the treatments and treatments who do not provoke the plasmolysis of cortical cells, respectively. Cells with a cross represent p-values > 0.01 and cells displaying a correlation coefficient greater than 0.8 show their actual values (mean ± se)

The coding sequence of ENODL8 is essential for its rapid degradation in response to changes in P

Our results presented in section 2 show that the expression of *ENODL8* in response to water deficit is not solely controlled by its promoter and its 3'UTR, which prompted us to investigate the regulation of its mRNA abundance by using its whole genomic sequence (*pENODL8::ENODL8-3'UTR*). We obtained 2 T-DNA mutants *SAIL_603_E07* (L5) and *SALK_062907* (L37) from the NASC (https://arabidopsis.info/). After genotyping and sequencing, we revealed that L5 and L37 have a T-DNA insertion at ~69bp and ~123bp before the start codon, respectively (**Fig. 3A and B**). We confirmed that L5 is a knock-out mutant while L37 is a knock-down mutant by checking the expression of *ENODL8* through RT and PCR amplification (**Fig. 3C**).

In order to express *ENODL8* properly, we had to ligate an *eGFP* sequence in between the signal peptide (SP) sequence and the coding sequence, as this gene is an early nodulin-like protein with a SP at the N-terminal and a predicted GPI anchor (glycophosphatidylinositol) at the C-terminal (**Fig. 3D**) (Mashiguchi et al., 2009). We then monitored the abundance of the mRNAs of the *eGFP* and *NCED3* in two complemented lines (C11 and C40, generated from L5) after 50/100/150/400 mM sorbitol and 100/200 mM EG treatments for 15 min. *NCED3*, as an early responsive "P-marker" gene in response to water deficit in Col_0, showed the "regular" dose-dependent response to treatments, as we have shown earlier. In particular, it was induced significantly after 150 and 400 mM sorbitol treatments (**Fig. 4A**). In contrast to the significant reduction of *ENODL8* by ~50% in Col_0 after 150 mM sorbitol treatment (cf **Fig. 1A** in section 2), the expression of *GFP* was only slightly reduced by ~ 30% and ~ 20% in C11 and C40 after sorbitol and EG treatments, respectively.

Notably, almost no quantitative reduction of *GFP* expression in response to changes in P was observed, and a significant decrease was observed only in C11 line after sorbitol treatments (**Fig. 4B**). These results, at variance from the regulation of ENODL8 depicted in section 2 Fig.1, left us with at least two hypotheses: 1) the *GFP* insertion in complementary lines disrupts the native degradation of *ENODL8* in response to changes in P. 2) the construct *pENODL8::sp-eGFP-ENODL8-3'UTR* does not contain all the regulatory elements required for its proper expression.

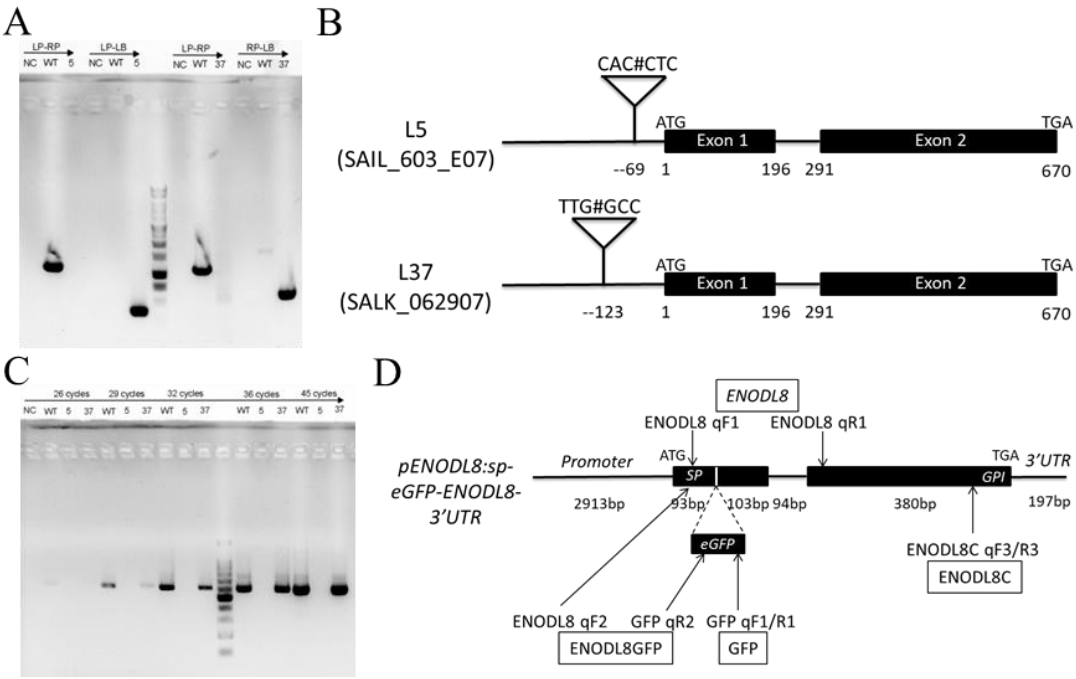

Fig 3. Information for the generation of complemented lines expressing the *pENODL8:sp-eGFP-ENODL8-3'UTR* construct

(A) Genotyping of 2 *enodl8* mutants. LP and RP are oligos in the sequence predicted to be on each side of the T-DNAs insertion site, and LB is a common oligo from the left border of the SALK T-DNA sequence. NC: H_20 as the PCR template. WT: DNA of Col_0 as the PCR template. 5 and 37: genomic DNA of L5 (*SAIL_603_E07*) or L37 (*SALK_062907*) as the PCR template. (B) Illustration of their T-DNA insertion positions. (C) PCR amplification of the whole coding sequence of *ENODL8* in cDNA solution under control condition. Samples were collected after the indicated PCR cycles number and run on the same agar gel. NC represents either no DNA or no cDNA templates. (D) *ENODL8* genomic sequence, and position of the GFP for generating *pENODL8:sp-eGFP-ENODL8-3'UTR* construct as well as positions of the various oligos for qPCR detection of the fragments *ENODL8* and *sp-eGFP-ENODL8* (1347bp).

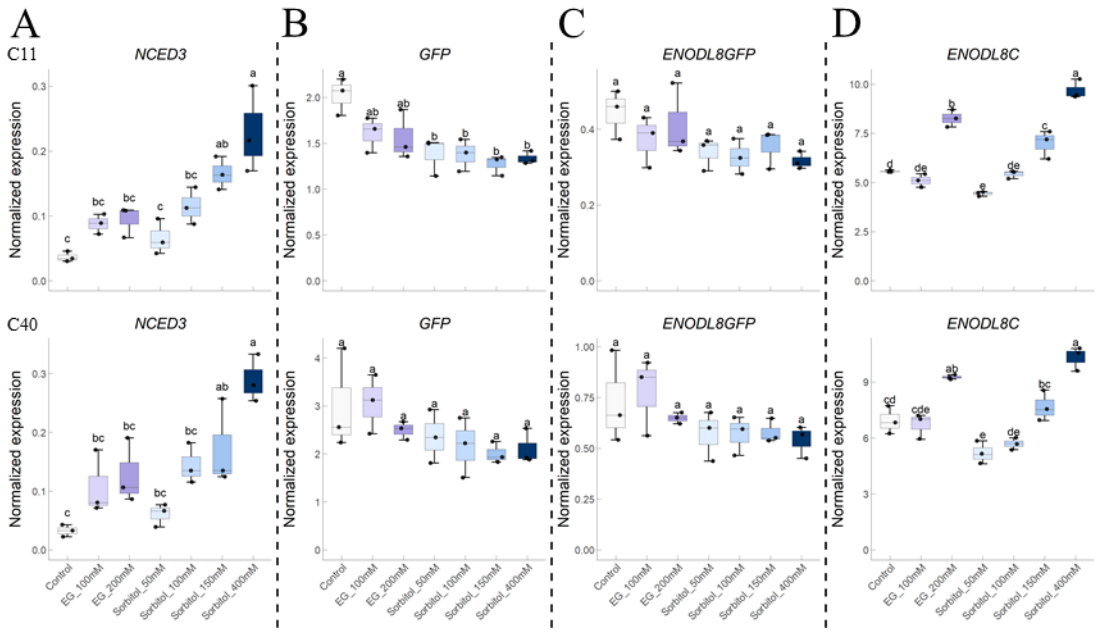

Fig 4. The construct *pENODL8:sp-eGFP-ENODL8-3'UTR* is unable to visualize the perception of changes in P in Arabidopsis.

Normalized expressions of 4 Genes in roots of C11 (above) and C40 (below) after treatments for 15 min. Normalized expression means that gene expression was expressed relatively to the expression of internal control genes (see M&M of this section). Each point represents one biological repeat (ANOVA and Tukey's HSD test, points not sharing the same letter are different at $P < 0.05$).

To gain further insights into this complex regulation, we monitored the expression of other fragments of *sp-eGFP-ENODL8-3'UTR* mRNA. Oligos were designed to detect 2 additional fragments: *ENODL8GFP* (the "forward" oligo being on the GFP while the reverse oligo being on the coding sequence of ENODL8) and *ENODL8C* (forward and reverse oligos is in the middle and near the end of *ENODL8*, respectively, locations are shown in **Fig. 3D**). The *ENODL8GFP* in the complemented lines was supposed to simulate the native version of *ENODL8* mRNA in Col_0, as both of them contain the SP sequence. Although the expression of *ENODL8GFP* showed a nonsignificant reduction in two lines after treatments compared to *GFP*, the abundance of the *ENODL8GFP* mRNA matched that of the *GFP* shown earlier : its expression was slightly reduced by ~ 20% and ~ 10% after sorbitol and EG treatments, respectively (**Fig. 4C**). To our surprise, changes in P caused by both sorbitol and EG treatments quantitatively and significantly induced the expression of the *ENODL8C* sequence in the two lines. In particular, it showed a ~2-fold induction in C11 upon 400mM sorbitol treatment (**Fig. 4D**). We excluded the possibility that other known genes could overlap the *ENODL8C* fragment by checking the surrounding genomic sequence of

ENODL8 (on the NCBI website: https://www.ncbi.nlm.nih.gov/). The contradictory results between the expression of *GFP*/*ENODL8GFP* and *ENODL8C* prompted us to revisit the expression of *ENODL8C* in Col_0 after sorbitol and EG treatments for 15 min. The expression of *ENODL8C* in Col_0 demonstrated the "bell-shaped pattern" and relative stability following sorbitol and EG treatments, respectively, **(Fig. 5)**, almost consistent with the expression of *ENODL8* observed in our previous results (section 2). Given that the T-DNA insertion in the knock-out mutant L5 occurs in the 5'-upstream region of *ENODL8* (**Fig. 3B**), these results lead us to consider the possibility that the expression of the native *ENODL8* would not be completely abolished, and would interfere with our quantification of *ENODL8C* segment, particularly under water deficit treatment.

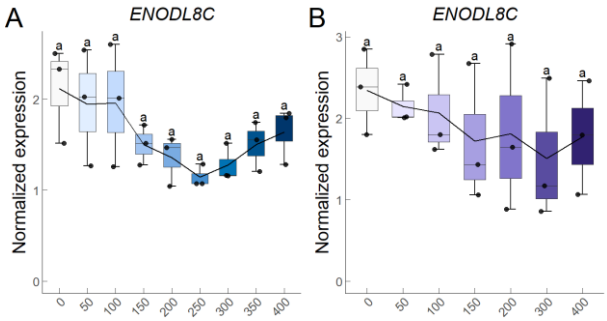

Fig 5. Normalized expression of *ENODL8C* in Col_0 after sorbitol and EG treatments for 15 min

Black lines represent mean value of 3 biological repeats and each point means one biological repeat. Each point represents one biological repeat (ANOVA and Tukey's HSD test, points not sharing the same letter are different at $P < 0.05$).

To confirm this possibility, we monitored the expression of *ENODL8*, *ENODL8C* and *NCED3* in both T-DNA mutants after 150 mM sorbitol and 150 mM EG treatments for 60 min. As a control, we observed that *NCED3* was induced in all plants after sorbitol and EG treatments and no significant difference was observed among the genotypes under the same condition (**Fig. 6A**). The expression of *ENODL8* in Col_0 showed the expected significant decrease after sorbitol treatment (**Fig. 6B**). A decrease, although less important, was also observed under EG treatment. Although the expression of *ENODL8* in L37 was consistently lower than in Col_0, it also showed a decrease in expression after both sorbitol and EG treatments, as in Col_0 (**Fig. 6B**). We did not detect any expression of *ENODL8* in L5 in any of the conditions (**Fig. 6C**). These results clearly indicate that L5 and L37 are a knock-out and knock-down mutants, respectively, which is consistent with the results depicted in **Fig. 3C**. Similar to the expression of *ENODL8*, *ENODL8C* almost showed the

same expression pattern in both Col_0 and L37 under all conditions (**Fig. 6B-C**). Most importantly, we did detect the high expression of *ENODL8C* in L5, which was consistently remarkably higher than in Col_0 under all conditions, except for the lack of significance after EG treatment. EG and sorbitol treatments also significantly reduced its expression in L5 compared to control condition. These results suggest a mechanism in which the knock-out effect, from the T-DNA insertion in L5, on the expression of *ENODL8,* has been compensated or overridden by its surrounding genomic region, guiding the synthesis of new transcript containing *ENODL8C* sequence.

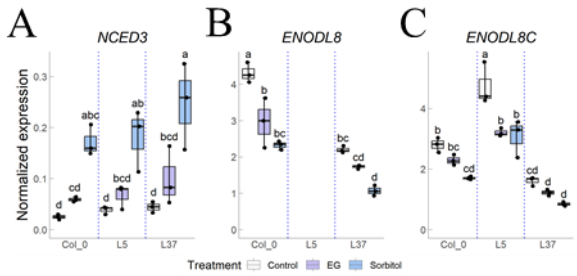

Fig 6. The T-DNA insertion in the *enodl8* mutant resulted in a new transcript containing partial sequence of *ENODL8*

Normalized expression of 3 genes in the roots of *enodl8* mutants after osmotic treatments for 60 min. Each point represents one biological repeat (ANOVA and Tukey's HSD test, points not sharing the same letter are different at $P < 0.05$).

Altogether, since their mRNAs share some identical sequences, we hypothesize that the new transcripts gained from the background of the T-DNA insertion mutant may compete with the *SP-GFP-ENODL8* mRNA in complemented lines for the components of degradation pathway, thereby interfering with each other's degradation. It may even have stronger affinity for the components of mRNA degradation pathway compared to the *SP-GFP-ENODL8* transcript because of the *GFP* insertion in the later. These interferences could explain our results under mild water deficit treatments, in which only a slight reduction in the expression of *GFP* from the *SP-GFP-ENODL8 mRNA* was observed, as well as the contradictory expression between *GFP*/*ENODL8GFP* and *ENODL8C*. At the moment however, we can't exclude other hypotheses, two of them being that the *pENODL8::sp-eGFP-ENODL8-3'UTR* construct does not contain the complete regulatory elements of the native gene, or that the reporter is interfering with the native regulatory mechanism. This second hypothesis could occur, for example, if the mRNA sequence proved to be crucial for its regulation upon stress, by conferring the ability to group into molecular condensates under osmotic

stress by liquid-liquid phase separation such as for the SEUSS proteins (Wang et al., 2022). A property that could be lost because of the addition of the GFP coding sequence.

The membrane associated ENODL8 protein is primarily localized in the epidermal and cortical cells of the transition domain in root

Previous results have shown that the activity of *pEN*ODL8 was predominantly localized in the cortical and epidermal cells of the young section of the root. With the hope that the *pENODL8::sp-eGFP-ENODL8-3'UTR* construct is only altered in the regulation of the mRNA abundance under water deficit conditions, but not in its pattern of expression, we looked at the localization of the ENODL8 protein in the C11 line by GFP imaging under a microscope. As shown in **Fig. 7A**, GFP signals started at the transition domain of the PR (Zluhan-Martínez et al., 2021) and progressively faded toward the base, consistently with the results obtained from the *pENODL8::GFP-GUS* expressing lines (see section 2). When observing all along the PR, GFP signals were predominantly localized in the epidermal and cortical cells, again consistently with the results depicted in section 2. Importantly, the majority of the GFP signals was concentrated around the PI-stained region (**Fig. 7B**), indicating that ENODL8 is in the vicinity or associated to the cell membrane. This observation is consistent with the notion that the family of ENODL proteins, to which ENODL8 belongs, may anchor to the cell membrane through their GPI motif (Mashiguchi et al., 2009; Hou et al., 2016). These results indicate that ENODL8 protein is primarily localized in the young sections of root, including the transition domain and elongation zone, while its promoter activity also localizes in the more mature part of roots in addition to these two regions. This difference potentially results from the post-transcriptional regulation of *ENODL8* transcript and/or protein stability regulation.

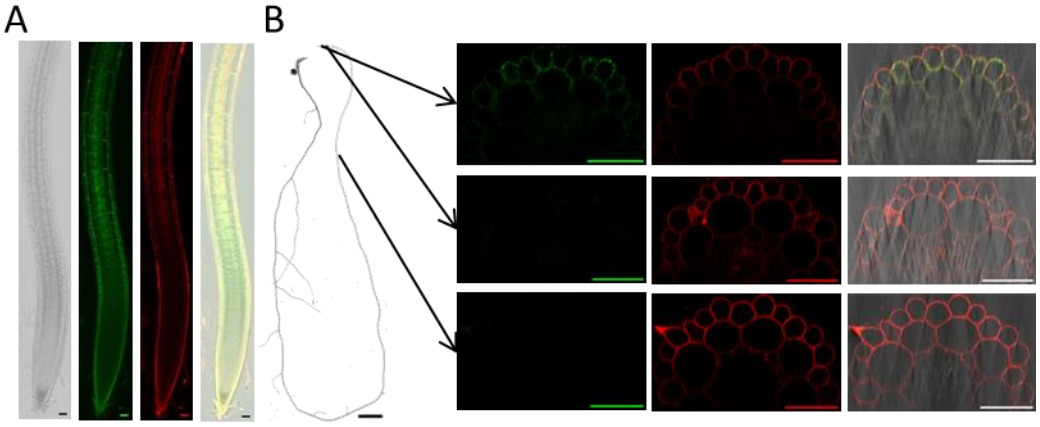

Fig 7. ENODL8 protein is primarily localized in the cortical and epidermal cells of the transition domain in root

In this figure, the green channel corresponds to GFP signal and the red channel shows the pectins of the cell wall after staining with PI (see M&M) (A) observations on the C11 line with an apotome microscope (Zeiss observer 7). (B) cross-section reconstructions from z-stack observations at different zones of the primary root, with a confocal microscope. Upper pictures are from the transition domain, middle ones are from the elongation zone, bottom ones are taken where the lateral root primordium initiates. Scale bars : 50 µm in GFP/PI pictures and 2000 µm in the whole root image.

ENODL8 may be involved in LR root growth and emergence under water deficit treatments

Stress responsive genes can be involved in plant stress adaptation. *NCED3* is a good example since its expression is activated upon water deficit, and is required for plant stress tolerance (Ruggiero et al., 2004). Because ENODL8 is expressed in the growing zone of the root, and although L5 and L37 are not both knock-out mutants, we treated these lines with 150 mM sorbitol and checked their root growth. As shown in **Fig. 8A**, no obvious difference was observed between Col_0 and L5/L37 regarding to length of PR and LR and LR number under control condition. When looking in more details, it appears that the KD line L37 may have a higher total LR length (**Fig. 8D**). Under 150 mM sorbitol treatment, no obvious difference was observed between Col_0 and L5/L37 regarding the length of the PR, while L5/L37 may have shorter LR length and less LR number compared to Col_0 plants (**Fig. 8C-E**). Unfortunately, the growth chambers were experiencing significant biotic stress issues at that time and the growth of Arabidopsis seedlings displayed a lot of heterogeneity on the MS/2 medium without sucrose. To date, this experiment was performed only once with fit plants. Three overexpression lines were also generated by using the *p35S::sp-eGFP-ENODL8* construct, but these lines were not analyzed due to the lack of time. Moreover, given the detection of an unknown transcript introduced by the T-DNA insertion in the L5 mutant, it is crucial to elucidate first its origin before proceeding with further investigations with mutant lines. Additional KO would be valuable as well, and they would probably be better generated by using the CRISPR-Cas9 technique. We tried to generate mutants in Col_0 background by engaging the CRISPR-Cas9 technique. I genotyped more than 80 positives transgenic plants but did not get any *enodl8* mutant. To obtain *enodl8* mutant by using proper approach, we may have to figure out the mechanism of unknown transcript generation in the L5 mutant.

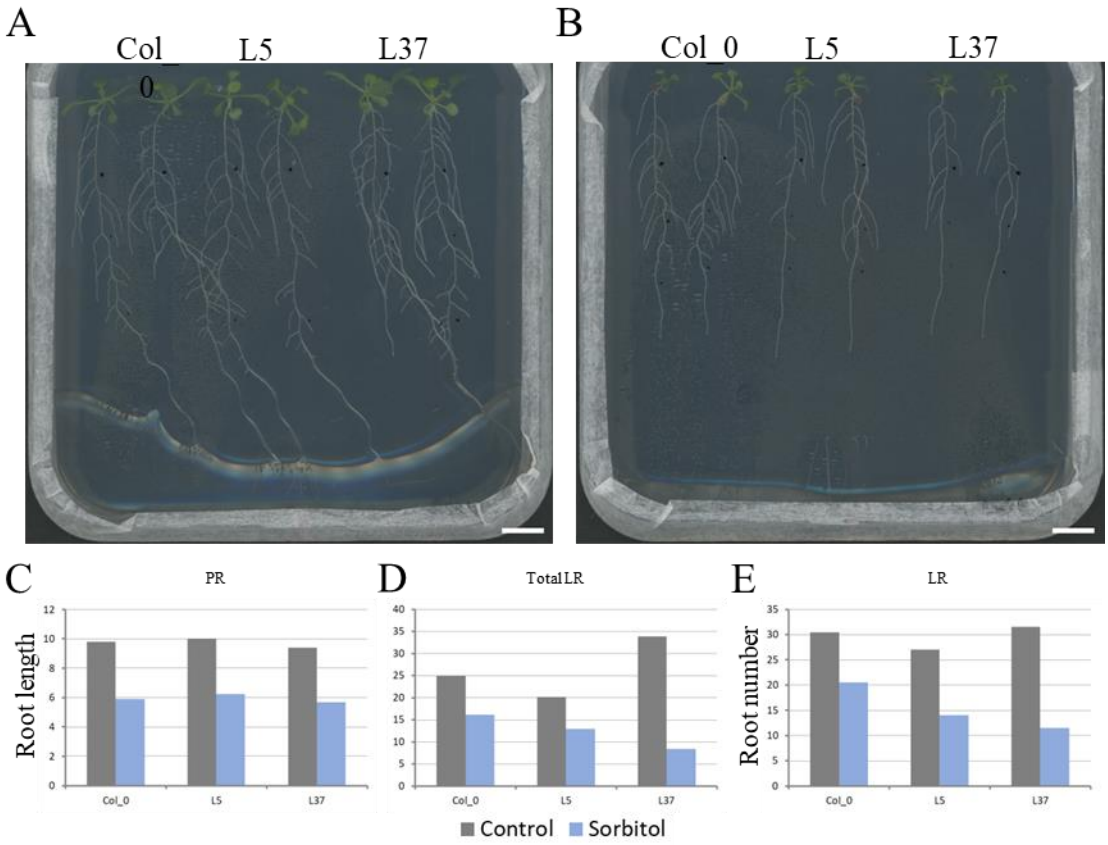

Fig 8. ENODL8 may be involved in LR root growth and emergence under water deficit treatments

(A-B) Plants root growth after being transferred to control condition and undergoing 150 mM sorbitol treatment for 8 days, respectively. Scale bar: 1 cm. (C-D) Average primary root length and total lateral root length after 8 days. (E) Lateral root number after 8 days. One assay only was conducted and included two plants.

Material and methods

Constructs and transgene plants

The CDS of *ENODL8* (TAIR 10 version) was cloned into the PGWB207 entry vector (P4') and recombined into pH7WG2 to construct the *p35S::ENODL8*. The *p35S-sp* sequence from *p35S::ENODL8* construction and another genomic sequence of *ENODL8* (including its promoter and 93 bp sp predicted by SignalP 6.0 Server) were cloned into a pDONR^{TM} P4-P1R entry vector (P5') to construct the P5'-*p35S::sp* and P5'-*pENODL8-sp*, respectively. *eGFP* without the stop codon from pB7FWG2 was cloned into PGWB207 entry vector to construct the P4'-*eGFP*. 483bp of the CDS of *ENODL8* (without the SP sequence) were cloned into a pDONR^{TM} P2R-P3 entry vector (P3') to construct the P3'-*ENODL8-Ncds*.

The P5'-*pENODL8-sp,* P4'-*eGFP* and P3'-*ENODL8-Ngenomic* were ligated into the pH7m34GW destination vector, to construct the complementary vector Phyg-*pENODL8::sp-eGFP-ENODL8-3'UTR*. The P5'-*p35S::sp,* P4'-*eGFP* and P3'-*ENODL8-Ncds* were ligated into the pK7m34GW destination vector, to construct the overexpression

vector Pkana-*p35S::sp-eGFP-ENODL8*. All the oligos (**Table 1**) synthesis and sequencing reactions were delegated to the Eurofins Genomics company. All the BP reactions and LR reactions were performed by using the Gateway™ BP Clonase™ II Enzyme mix (Thermo Fisher) and the Gateway™ LR Clonase™ II Enzyme mix (Thermo Fisher), respectively. Complemented lines were obtained by transforming Phyg-*pENODL8::sp-eGFP-ENODL8-3'UTR* construct to L5 background and overexpression lines were obtained by transforming Pkana-*p35S::sp-eGFP-ENODL8* construct to Col_0 background. Transgenic Arabidopsis plants were generated through Agrobacterium-mediated floral dip transformation and T3 homozygotes were used in this section.

Q-RT-PCR

RNA extraction, cDNA synthesis, qPCR and subsequent analysis were performed as previously described (Crabos, Huang et al. 2023). *At1G13320* (*PDF2*) and *At4G34270* (*TIP41-like*) were selected as internal control genes (Czechowski et al., 2005). All primer sequences are shown in **Table 1**.

Microscopy

Propidium iodide (PI) staining was conducted following the established procedure on plants aged 9 days, with an incubation period of 10 minutes (Alassimone et al., 2010). Images were reconstructed from z-stack by using the ImageJ software.

Phenotype analysis

Sterilized Arabidopsis seeds were sowed onto a 1/2 MS agar medium and subsequently placed at 4°C in darkness for 48 h for vernalization. Plates were then positioned vertically in an Aralab incubator (16h/8h, 60% humidity). After a period of 5 days, the plants were transferred to new plates, with some containing 150 mM sorbitol treatment. Plates were scanned after 8 days.

Table 1. All the oligo sequences

Names	Forward oligo	Reverse oligo	Purpose
ENODL8-L5	AGAAGTGGTGGCCATGTGAAAC	TGGATTGTGTCATTGTGTGTACATATC	Genotyping of SAIL_603_E07
ENODL8-L37	ATTTTGTGCCTTCACCAGATG	GTTTTGGTAAGAGGGAGCGTC	Genotyping of SALK_062907
ENODL8	ATGGGAGTGATGAGTTTGAG	TCACATGATTGCACCGACGA	cds amplification

qENODL8	AGCAAGACGATGGTGGTGGT	TGAGTCTTCGCTTGGTGGGT	qPCR
qNCED3	TGATTGCCCACCCGAAAGTC	CTCCGGCAGCTTGAAAACGA	qPCR
qGFP	TCATGGCCGACAAGCAGAAG	ACCATGTGATCGCGCTTCTC	qPCR
qENODL8GFP	AGACGATGGTGGTGGTGGTAT	GCTGAACTTGTGGCCGTTTAC	qPCR
qENODL8C	ACATGAACGACGGCAACTCTC	AATGAGCGAGGAGGAAGCAGA	qPCR
qAt1G13320	TAACGTGGCCAAAATGATGC	GTTCTCCACAACCGCTTGGT	qPCR
qAt4G34270	GTGAAAACTGTTGGAGAGAAGCAA	TCAACTGGATACCCTTTCGCA	qPCR
ENODL8	GGGGACAAGTTTGTACAAAAAAGCAGGCTATGGGAGTGATGAGTTTGAG	GGGGACCACTTTGTACAAGAAAGCTGGGTCATGATTGCACCGACGACAG	Constructing pDNOR207_ENODL8 for pH7WG2_ENODL8
p35S::spENODL8	GGGGACAACTTTGTATAGAAAAGTTGCTGAGACTTTTCAACAAAGGGT	GGGGACTGCTTTTTTGTACAAACTTGCAGTCGACGACACTTTACCAA	Constructing pDONRTM P4 P1R_p35S::spENODL8 for pK7m34GW_p35S::sp-eGFP-ENODL8
pENODL8::sp	GGGGACAACTTTGTATAGAAAAGTTGCATCCTAAAATCCAACAATGA	GGGGACTGCTTTTTTGTACAAACTTGCAGTCGACGACACTTTACCAA	Constructing pDONRTM P4 P1R_pENODL8::sp for pH7m34GW_pENODL8:;sp-eGFP-ENODL8-3'UTR
eGFP	GGGGACAAGTTTGTACAAAAAAGCAGGCTTCATGGTGAGCAAGGGCGAGGA	GGGGACCACTTTGTACAAGAAAGCTGGGTACTTGTACAGCTCGTCCATGC	Constructing pDNOR207_eGFP for pH7m34GW_pENODL8::sp-eGFP-ENODL8-3'UTR
ENODL8-3'UTR	GGGGACAGCTTTCTTGTACAAAGTGGCTCTATACAAAGTTGGGGACTT	GGGGACAACTTTGTATAATAAAGTTGAATTTAGAACTATATGGATTGT	Constructing pDONRTM P2R-P3_ENODL8-3'UTR for pH7m34GW_pENODL8::sp-eGFP-ENODL8-3'UTR
ENODL8-stop	GGGGACAGCTTTCTTGTACAAAGTGGCTCTATACAAAGTTGGGGACTT	GGGGACAACTTTGTATAATAAAGTTGTCACATGATTGCACCGACGA	Constructing pDONRTM P2R-P3_ENODL8-stop for pK7m34GW_p35S::sp-eGFP-ENODL8

References

Alassimone J, Naseer S, Geldner N (2010) A developmental framework for endodermal differentiation and polarity. Proceedings of the National Academy of Sciences **107**: 5214–5219

Czechowski T, Stitt M, Altmann T, Udvardi MK, Scheible W-R (2005) Genome-Wide Identification and Testing of Superior Reference Genes for Transcript Normalization in Arabidopsis. Plant Physiology **139**: 5–17

Hou Y, Guo X, Cyprys P, Zhang Y, Bleckmann A, Cai L, Huang Q, Luo Y, Gu H, Dresselhaus T, et al (2016) Maternal ENODLs Are Required for Pollen Tube Reception in Arabidopsis. Current Biology **26**: 2343–2350

Mashiguchi K, Asami T, Suzuki Y (2009) Genome-wide identification, structure and expression studies, and mutant collection of 22 early nodulin-like protein genes in Arabidopsis. Bioscience, Biotechnology, and Biochemistry **11**: 2452～2459

Ruggiero B, Koiwa H, Manabe Y, Quist TM, Inan G, Saccardo F, Joly RJ, Hasegawa PM, Bressan RA, Maggio A (2004) Uncoupling the effects of abscisic acid on plant growth and water relations. Analysis of sto1/nced3, an abscisic acid-deficient but salt stress-tolerant mutant in Arabidopsis. Plant Physiol **136**: 3134–3147

Wang B, Zhang H, Huai J, Peng F, Wu J, Lin R, Fang X (2022) Condensation of SEUSS promotes hyperosmotic stress tolerance in Arabidopsis. Nat Chem Biol **18**: 1361–1369

Zluhan-Martínez E, López-Ruíz BA, García-Gómez ML, García-Ponce B, de la Paz Sánchez M, Álvarez-Buylla ER, Garay-Arroyo A (2021) Integrative Roles of Phytohormones on Cell Proliferation, Elongation and Differentiation in the Arabidopsis thaliana Primary Root. Frontiers in Plant Science 12:

General Discussion

Given the ongoing climate change and the increase in the frequency of drought events, understanding the mechanisms through which plants perceive water deficit has become critically significant. In the present work, we investigated how Arabidopsis roots perceive water deficit (WD) and focused on four aspects: alteration of plant hydraulic parameters, transcriptomes, gene expression regulation and osmo-reporter development. The first three aspects acted in concert to unravel which subset of genes were regulated by two biophysical signals: the osmotic potential of the external solution (Π) and the turgor pressure of cortical cells (P), and how. The last aspect developed was to dig into the timing and location at which plants sense hydraulic changes in a manner that triggers a regulation of gene expression.

Water deficit regulates gene expression both at transcriptional and post-transcriptional levels

By analyzing the correlation between early (15 min) transcriptomes and Π or turgor potential (P) after osmotic treatments, we found solute-specific responsive genes, and Π- and P- correlated genes. These results suggest that plant cells have the capacity to specifically sense and respond to the different stress factors. No clear signaling pathway was extracted from this analysis, which is understandable given that major transcriptional reprograming may occur after hours of treatments (Yuan et al., 2014). Altered mRNA half-life of the genes we studied suggests that it is necessary to further study gene expression in response to early water deficit from a transcriptomic perspective, while manipulating mRNA degradation and promoter activity. Indeed, the mRNA turnover in response to early mild water deficit (MWD) is poorly understood.

Gene expression in mRNA decay deficient mutants *lsm1a/1b* and *xrn4* under water deficit treatments showed that our two candidate genes, *ENODL8* and *NCED3*, were regulated tightly at both transcriptional and post-transcriptional levels. The expression of *ENODL8* was enhanced in *lsm1a/1b* under control condition, suggesting that the decapping complex is essential for its absolute expression. Although, we did not find the component of mRNA decay pathways that is involved in regulating its expression under water deficit, the response of the *pENODL8::Sluc-3'UTR* construct suggested that its open reading frame (ORF) is essential for regulating its expression under MWD, not under severe water deficit (SWD). Perhaps some regulatory elements that we have not tested yet are present in its ORF and are essential for its mRNA processing, like polyadenylation and

deadenylation (Zhang et al., 2022). Perhaps also that the presence of a reporter in the coding sequence changes the properties of the mRNA and prevents it from undergoing liquid/liquid phase separation and be relocated in regulatory structures such as p-bodies or stress granules (SEUSS is such an example at the level of the proteins) (Wang et al., 2022). We were unable to unravel the role of its ORF in regulating the expression of *ENODL8*, as currently no clear knock-out T-DNA mutant is available (see section 3, **Fig. 3B** and **Fig. 6**). The next step should focus on generating proper *enodl8* mutants that is also important to explore the biological function of ENODL8. Chantarachot et. al found that its mRNA half-life was enhanced from 68 min in Col_0 to 153 min in the triple mutant *rh6/8/12* under control condition (Chantarachot et al., 2020). Therefore, it's also possible that RH6/8/12 and other decapping activators are involved in regulating its mRNA decay under water deficit treatments. Moreover, the expression of the *ENODL8* and *ENODL8C* fragments in the knock-down T-DNA mutant L37 (T-DNA insertion presents in the 5'-upstream of start codon) also showed a similar reduction to Col-0 after EG and sorbitol treatments for 15 min (see section 3, **Fig. 6**), suggesting that its promoter may not be necessary for regulating its expression during the early stages of water deficit (P drop). However, the promoter *pENODL8* is essential for its absolute expression level and expression recovery under MWD, as lower expression level of *ENODL8* is observed in knock-down T-DNA mutant (see section 3, **Fig. 6**), and *GFP* expression in plants carrying the *pENODL8::eGFP-GUS* construct is induced after sorbitol treatment for 30 min (see section 2, Fig. 2B). Therefore, it is necessary to identify better which elements (promoter, ORF and 3'UTR), or their combination, are responsible for the reduction and/or recovery of *ENODL8* expression under water deficit.

Transcriptome from literature showed that the mutation of *vcs*, a component of the decapping complex, elevated the mRNA abundance of *NCED3* under control conditions (Sorenson et al., 2018). Although mutation of *vcs*, *sov* or *rh6/8/12* did not alter its mRNA degradation rate under control conditions, they may be involved in the regulation of its mRNA degradation under water deficit (see section 2, **Supplementary Fig 12**) (Sorenson et al., 2018; Chantarachot et al., 2020). Our findings revealed that *LSM1a/1b*, a component of the decapping complex, and *XRN4*, a component in the 5'-3' mRNA decay, are indirectly involved in the regulation of *NCED3* expression under MWD treatments, not under control condition. These discoveries suggest that, similar to *ENODL8*, water deficit may regulate *NCED3* expression by modifying the component in the 5'-3' mRNA decay

pathway. Considering that these two genes come from Π- and P- clusters in our transcriptomic analysis, it's highly possible that other genes in these two clusters are also regulated by the 5'-3' mRNA decay pathway. The regulation of *NCED3* expression also involves some transcription factors (TFs), such as the known NGATHA family and ATAF1 TFs, which are required to activate its promoter and induce its expression under water deficit treatments (Jensen et al., 2013; Sato et al., 2018). Recent studies revealed that the "B4 Raf-like MAP kinase kinase kinases (MAPKKKs)-subclass I SnRK2s-VCS" module is essential for the post-transcriptional regulation of gene expression (Soma et al., 2017; Soma et al., 2020). At variance of the classic ABA-dependent activation of subclass III SnRK2s, which are required for regulating stress-inducible gene expression at transcriptional level and involve PYR/PYL/RCAR receptors and PP2C phosphatases, other studies have uncovered an ABA-independent activation mechanism mediated by B2/B3 Raf-like MAP kinase kinase kinases (MAPKKKs) (Katsuta et al., 2020; Soma et al., 2020; Takahashi et al., 2020). Based on these knowledges and our results, we propose a model which summarizes the putative regulatory mechanisms for gene expression under water deficit treatments (**Fig. 1**).

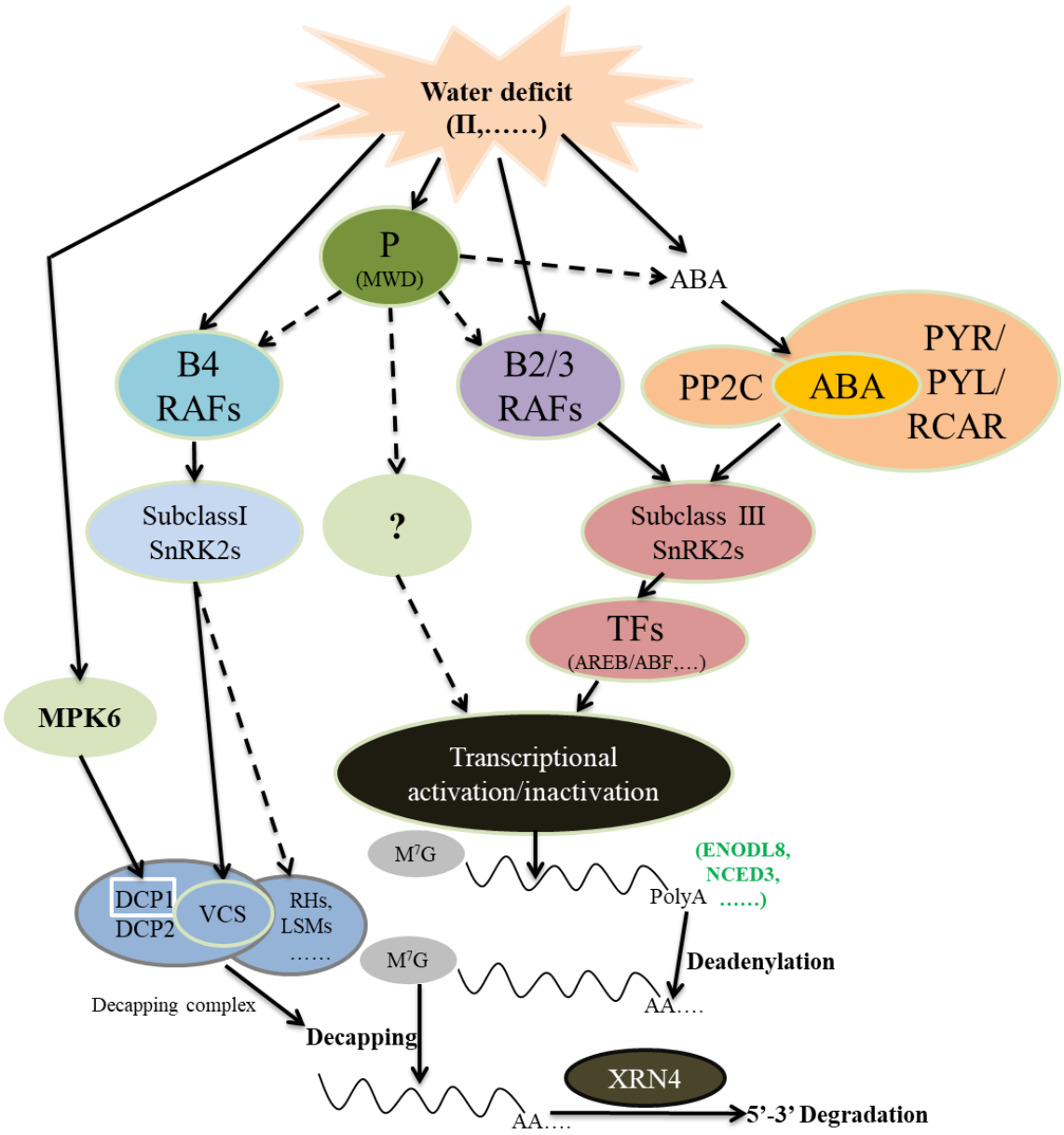

Fig. 1 Water deficit regulate mRNA abundance in Arabidopsis at both transcriptional and post-transcriptional levels, a model.

Subclass III SNF1-related protein kinases 2 (SnRK2s) play key roles in abscisic acid (ABA) signaling under water deficit. Negative regulation of subclass III SnRK2s is released via inhibition of protein phosphatases 2C (PP2C) by ABA-pyrabactin resistance1/pyr1-like/regulatory components of ABA receptor (ABA-PYR/PYL/RCAR) complexes under water deficit. Subclass III SnRK2s are phosphorylated and activated by B2/B3 Raf-like kinases in an ABA-independent manner. Activated subclass III SnRK2s phosphorylate a variety of substrates, including ABA-responsive element binding proteins/ABA-responsive element binding factor (AREB/ABF), to induce the expression of stress-responsive genes. ABA-unresponsive subclass I SnRK2s are quickly activated in response to water deficit in an ABA-independent manner. Water deficit activated subclass I SnRK2s regulate mRNA decay by phosphorylating the mRNA-decapping component VCS. The B4 Raf-like kinases are responsible for the activation of subclass I SnRK2s. MPK6 is activated by drought and phosphorylates DCP1, thus inducing DCP1 interactions with DCP2 and DCP5. Dashed lines indicate possible but unconfirmed routes. MWD: mild water deficit (Kawa and Testerink, 2017; Kawa et al., 2020; Soma et al., 2021).

Plant perception of water deficit and osmo-reporter

Our studies showed that turgor pressure in the young cortical cells of the primary root (PR) rapidly and quantitatively respond to changes in external Π caused by MWD. Decline in Π and P shaped the expression of some specific genes and we used two of them to develop an osmo-reporter. The *pNCED3::Sluc-3'UTR* construct convincingly replicated, with an Sluc signal, the native regulation of *NCED3* expression, while the *pENODL8::Sluc-3'UTR* construct did not. Given that *ENODL8* is a down-regulated gene and is found in the P-specific cluster 1 (see first section), a promising approach would be to develop a P-reporter using other candidates that are up-regulated by P (i.e. in the P-specific cluster 2). At the beginning of my PhD though, *ENODL8* was the most promising candidate because of its extremely good correlation to P.

Bright Sluc signals in plants carrying the *pNCED3::Sluc-3'UTR* construct (osmo-reporter) initiated rapidly in the hypocotyl and cotyledons under SWD (see section 2, **Fig. 7**), suggesting it is a competent reporter of hydraulic changes caused by SWD. Its rapid initiation is probably due to a hydraulic signal caused by SWD in the vascular tissues, as its promoter activity localizes here too (Christmann et al., 2013; Yang and Tan, 2014). This osmo-reporter could also be used as a reporter for judging the water availability in soil without the need to access the root. It was shown that turgor loss in leaves induces the expression of *NCED3* within 5 min, and that reduced foliar humidity leads to ABA accumulation in the elongation zone, which allows maintenance of root growth at low humidity (Sussmilch et al., 2017; Rowe et al., 2023). It would be of interest to investigate whether our osmo-reporter responds to reduction of air humidity as well. Moreover, comparing the spatiotemporal maps of the ABACUS2 ABA reporter (Rowe et al., 2023) and our osmo-reporter in response to MWD and SWD would provide novel insights for deciphering the mechanism between osmo-sensing and ABA signaling.

The osmo-reporter rapidly and quantitatively responded to early changes in P caused by MWD, suggesting that it is a good P-reporter. The site for sensing changes in P caused by MWD in Arabidopsis roots could be the middle portion of PR with many LRs (see section 2, **Fig. 7**). *NCED3* encodes a key rate-limiting enzyme for ABA synthesis, and ABA is essential for inhibiting LR development under water deficit treatments (Waadt et al., 2022). Therefore, it makes sense that the early alteration in *NCED3* transcript abundance occurred here. However, we were unable to visualize the Sluc signals with our current CCD camera setup under treatments with "low"

concentrations of NaCl (<75 mM), sorbitol (<150 mM), PEG (<100g/l mM) or EG (<200 mM) treatments. Studies revealed that plasmolysis is essential for significant ABA accumulation (Vaahtera et al., 2019) and our study confirmed that plasmolysis of cortical cells at the end of the meristematic zone of the PR disrupted the regulation of our candidates genes expression. Because we did not measure the turgor pressure of cortical cells in the old part of the PR yet (results about the localization of the expression of *NCED3* were obtained in the last month of the PhD), it is possible that they were plasmolyzed by MWD treatments with relatively high concentration. Therefore, we cannot exclude that the expression zone we identified may be the perception site for plasmolysis rather than for P changes. As a mid-term objective, confirming whether cortical cells in the older part of the PR are plasmolyzed under such treatments would be necessary.

Studies have shown that ABA signaling in the cortical cell of the elongation zone and an asymmetric distribution of cytokinins in the meristematic zone are essential for hydrotropism (Dietrich et al., 2017; Chang et al., 2019). The xerobranching response, in which lateral root formation is suppressed when a root loses contact with water, is supposed to require a radial movement of phloem-derived ABA in the meristem and elongation zones (Mehra et al., 2022). Coincidentally, the activity of *pENODL8* is localized in the epidermal and cortical cells of young part of the PR and LR, including the elongation zone and end of meristem zone (transition domain). At the moment, we do not exclude the possibility that the response of our osmo-reporter also initiates in these zones under MWD or under similar conditions with heterogeneous water distribution. Indeed, studying the response of our osmo-reporter under conditions with heterogeneous water distribution, such as treating either the PR tip or the middle part of PR with water deficit, would be a valuable approach to determine whether the emergence of visible signals in the middle part of PR originates from the turgor drop in either the PR tip or the middle part of PR. Nevertheless, these findings reinforce the idea that the elongation zone and the meristem zone are perception sites for water deficit. Additionally, in contrast to the localization (transition domain, elongation zone, differentiation zone until the middle part of PR) of GFP drove only by *pENODL8*, the ENODL8 protein primarily localizes to the transition domain and the elongation zone. These results suggest that the ORF plays a role in regulating the localization by governing *ENODL8* mRNA abundance, although this difference also could derive from the different properties of GFP and ENODL8-GFP proteins. The fusion of a protein-independent fluorescent RNA aptamer reporter gene, 3WJ-4 × Bro

(Bai et al., 2020), to the *pENODL8::sp-GFP-ENODL8-3'UTR* structure would be beneficial for investigating the regulation of ENODL8 at both the protein and mRNA levels, and for generating a more specific P-reporter too. Meanwhile, to elaborate a perception map with high resolution at cellular level, it would be highly recommended to generate new constructs, such as *pNCED3::NLS-GFP-3'UTR* (NLS represents a nuclear localization signal for brighter signals) and *pNCED3:: 3WJ-4 × Bro -3'UTR*. Finally, it is important to explore the minimal elements of the osmo-reporter by a deletion approach on the *pNCED3* and *3'-UTR* sequences.

Given that certain cell-specific promoters have been employed to investigate the function of specific genes within particular cell layers (Dietrich et al., 2017; Mielke et al., 2021; Mehra et al., 2022), these P- or Π-specific regulatory elements could also be utilized to examine gene functions under specific water deficit conditions. They may further be employed to regulate the expression of stress-resistant genes, thereby enabling the creation of genetically engineered plants with modified tolerance to water deficit.

Conclusion

The present thesis work contributed to an initial project, named watermarkers, which focused on the development of water potential (Ψ)/water stress markers in Arabidopsis in order to decipher the perception and early signaling of water deficit in plants. The initial phase of my project was dedicated to detection of turgor pressure and transcriptome analysis in Arabidopsis roots under mild water deficit (MWD) treatments. This allowed us to identify genes useful for potential genetic markers of osmotic potential (Π) and turgor potential (P), by analyzing correlations between gene expression and Π or P. The second phase was dedicated to Π- or P- correlation confirmation and to the identification of the regulatory mechanisms acting on our selected candidate genes under both MWD and severe water deficit (SWD). This lead us to determine that both promoter and 3'UTR were required. The last phase was dedicated to the development of a genetic Π- and P- reporter by transferring the promoter::Sluc/eGFP-GUS-3'UTR construct into Arabidopsis. This enabled us to initiate a perception map of water deficit in plants.

Transcriptomic analyses revealed a few genes specifically correlated with Π and/or P. Within 30 minutes of MWD treatments, EG, which reduces Π as any other osmolyte but results in a reduced turgor loss, was employed to distinguishing between Π and P. This distinction effectively delineated

the quantitative correlation between whole-transcriptional responses to Π or P. Specifically, we unraveled *At1G64640* (*ENODL8*), a P-correlated and down-regulated gene with an unknown function, and *At3G14440* (*NCED3*), a Π-correlated and up-regulated gene involved in ABA synthesis.

Comparing the expression of *ENODL8* and *NCED3* after MWD and SWD treatments for 15 min, we found that plasmolysis of cortical cells in the elongation zone of the primary root altered their expression response pattern. By monitoring their expression during a long-term treatment, we discovered that *ENODL8* showed a quantitative response matching well with the dynamic changes in P, while *NCED3* only exhibited a quantitative response to changes in P within 30 min. By studying their expression in Arabidopsis in different genetic backgrounds under water deficits or upon a cordycepin treatment, we found that water deficit regulated their expression both at the transcriptional and post-transcriptional levels. One of the next challenges will be to study how promoters and mRNA degradation pathways coordinately shape the early transcriptome depending on the severity of the stress. For example, by comparing changes in the transcriptome after 15 minutes of treatment with cordycepin + MWD or SWD.

The *pNCED3::Sluc-3'UTR* construct can serve as a reliable reporter not only for detecting early reductions in P caused by MWD but also for monitoring changes in Π and ABA levels over the course of a few hours. We tentatively called it an "osmo-reporter". The initiation of its response is ABA- and cell wall integrity- (CWI) independent. Combined with the promoter activity related to the P-correlated gene *ENODL8*, our findings suggest that the perception site may be located in the elongation and meristem zones, as well as middle part of PR under MWD, and in the hypocotyl and cotyledons under SWD. The next step would be to improve the brightness and resolution of the osmo-reporter imaging, and explore the regulatory mechanism of *ENODL8* expression. Further steps would involve screening the minimal elements of Π- and P-reporters and using them to engineer water relations in plants to improve plant tolerance.

In conclusion, the knowledge gained through my work will provide a useful tool to identify the molecular players involved in the water deficit perception in roots, and link them to known stress signaling networks. These contributions will also support a refined knowledge of plant root stress responses that may be useful for agronomists in designing ideotypes better adapted to rapid environmental changes. Additionally, this project could provide genetic elements regulated by P or

Π. These regulatory elements could be used to develop engineered plants with improved water use efficiency. Finally, another follow up of this project would be to transpose the results emerging from our research to crop plants.

General References

Abbasi N, Park Y-I, Choi S-B (2013) RNA deadenylation and decay in plants. J Plant Biol **56**: 198–207

Abe H, Urao T, Ito T, Seki M, Shinozaki K, Yamaguchi-Shinozaki K (2003) Arabidopsis AtMYC2 (bHLH) and AtMYB2 (MYB) function as transcriptional activators in abscisic acid signaling. Plant Cell **15**: 63–78

Alerasool N, Leng H, Lin Z-Y, Gingras A-C, Taipale M (2022) Identification and functional characterization of transcriptional activators in human cells. Mol Cell **82**: 677-695.e7

Bacete L, Hamann T (2020) The Role of Mechanoperception in Plant Cell Wall Integrity Maintenance. Plants Basel Switz **9**: 574

Bacete L, Schulz J, Engelsdorf T, Bartosova Z, Vaahtera L, Yan G, Gerhold JM, Tichá T, Øvstebø C, Gigli-Bisceglia N, et al (2022) THESEUS1 modulates cell wall stiffness and abscisic acid production in Arabidopsis thaliana. Proc Natl Acad Sci **119**: e2119258119

Baez LA, Tichá T, Hamann T (2022) Cell wall integrity regulation across plant species. Plant Mol Biol **109**: 483–504

Bai J, Luo Y, Wang X, Li S, Luo M, Yin M, Zuo Y, Li G, Yao J, Yang H, et al (2020) A protein-independent fluorescent RNA aptamer reporter system for plant genetic engineering. Nat Commun **11**: 3847

Belostotsky DA, Sieburth LE (2009) Kill the messenger: mRNA decay and plant development. Curr Opin Plant Biol **12**: 96–102

Bi H, Luang S, Li Y, Bazanova N, Borisjuk N, Hrmova M, Lopato S (2017) Wheat drought-responsive WXPL transcription factors regulate cuticle biosynthesis genes. Plant Mol Biol **94**: 15–32

Bi H, Luang S, Li Y, Bazanova N, Morran S, Song Z, Perera MA, Hrmova M, Borisjuk N, Lopato S (2016) Identification and characterization of wheat drought-responsive MYB transcription factors involved in the regulation of cuticle biosynthesis. J Exp Bot **67**: 5363–5380

Boari F, Malone M (1993) Wound-Induced Hydraulic Signals: Survey of Occurrence in a Range of Species. J Exp Bot **44**: 741–746

Boeck R, Tarun S, Rieger M, Deardorff JA, Müller-Auer S, Sachs AB (1996) The yeast Pan2 protein is required for poly(A)-binding protein-stimulated poly(A)-nuclease activity. J Biol Chem **271**: 432–438

Bogamuwa S, Jang J-C (2016) Plant Tandem CCCH Zinc Finger Proteins Interact with ABA, Drought, and Stress Response Regulators in Processing-Bodies and Stress Granules. PLOS ONE **11**: e0151574

Bogamuwa SP, Jang J-C (2014) Tandem CCCH zinc finger proteins in plant growth, development and stress response. Plant Cell Physiol **55**: 1367–1375

Boudsocq M, Barbier-Brygoo H, Laurière C (2004) Identification of nine sucrose nonfermenting 1-related protein kinases 2 activated by hyperosmotic and saline stresses in Arabidopsis thaliana. J Biol Chem **279**: 41758–41766

Boursiac Y, Protto V, Rishmawi L, Maurel C (2022) Experimental and conceptual approaches to root water transport. Plant Soil **478**: 349–370

Brenner ED, Stahlberg R, Mancuso S, Vivanco J, Baluška F, Van Volkenburgh E (2006) Plant neurobiology: an integrated view of plant signaling. Trends Plant Sci **11**: 413–419

Brown CE, Tarun SZ, Boeck R, Sachs AB (1996) PAN3 encodes a subunit of the Pab1p-dependent poly(A) nuclease in Saccharomyces cerevisiae. Mol Cell Biol **16**: 5744–5753

Brown PH, Hu H (1996) Phloem Mobility of Boron is Species Dependent: Evidence for Phloem Mobility in Sorbitol-rich Species. Ann Bot **77**: 497–506

Chang H-M, Triboulet R, Thornton JE, Gregory RI (2013) A role for the Perlman syndrome exonuclease Dis3l2 in the Lin28-let-7 pathway. Nature **497**: 244–248

Chang J, Li X, Fu W, Wang J, Yong Y, Shi H, Ding Z, Kui H, Gou X, He K, et al (2019) Asymmetric distribution of cytokinins determines root hydrotropism in Arabidopsis thaliana. Cell Res **29**: 984–993

Chantarachot T, Sorenson RS, Hummel M, Ke H, Kettenburg AT, Chen D, Aiyetiwa K, Dehesh K, Eulgem T, Sieburth LE, et al (2020) DHH1/DDX6-like RNA helicases maintain ephemeral half-lives of stress-response mRNAs. Nat Plants **6**: 675–685

Chekanova JA, Gregory BD, Reverdatto SV, Chen H, Kumar R, Hooker T, Yazaki J, Li P, Skiba N, Peng Q, et al (2007) Genome-wide high-resolution mapping of exosome substrates reveals hidden features in the Arabidopsis transcriptome. Cell **131**: 1340–1353

Chen C-Y, Gherzi R, Ong S-E, Chan EL, Raijmakers R, Pruijn GJM, Stoecklin G, Moroni C, Mann M, Karin M (2001) AU Binding Proteins Recruit the Exosome to Degrade ARE-Containing mRNAs. Cell **107**: 451–464

Chen C-YA, Shyu A-B (2011) Mechanisms of deadenylation-dependent decay. Wiley Interdiscip Rev RNA **2**: 167–183

Chen K, Gao J, Sun S, Zhang Z, Yu B, Li J, Xie C, Li G, Wang P, Song C-P, et al (2020a) BONZAI Proteins Control Global Osmotic Stress Responses in Plants. Curr Biol. doi: 10.1016/j.cub.2020.09.016

Chen K, Li G-J, Bressan RA, Song C-P, Zhu J-K, Zhao Y (2020b) Abscisic acid dynamics, signaling, and functions in plants. J Integr Plant Biol **62**: 25–54

Cheong YH, Kim K-N, Pandey GK, Gupta R, Grant JJ, Luan S (2003) CBL1, a Calcium Sensor That Differentially Regulates Salt, Drought, and Cold Responses in Arabidopsis. Plant Cell **15**: 1833–1845

Chiba Y, Johnson MA, Lidder P, Vogel JT, van Erp H, Green PJ (2004) AtPARN is an essential poly(A) ribonuclease in Arabidopsis. Gene **328**: 95–102

Cho E-J, Takagi T, Moore CR, Buratowski S (1997) mRNA capping enzyme is recruited to the transcription complex by phosphorylation of the RNA polymerase II carboxy-terminal domain. Genes Dev **11**: 3319–3326

Choi W-G, Toyota M, Kim S-H, Hilleary R, Gilroy S (2014) Salt stress-induced Ca2+ waves are associated with rapid, long-distance root-to-shoot signaling in plants. Proc Natl Acad Sci **111**: 6497–6502

Chou W-L, Huang L-F, Fang J-C, Yeh C-H, Hong C-Y, Wu S-J, Lu C-A (2014) Divergence of the expression and subcellular localization of CCR4-associated factor 1 (CAF1) deadenylase proteins in Oryza sativa. Plant Mol Biol **85**: 443–458

Christmann A, Grill E, Huang J (2013) Hydraulic signals in long-distance signaling. Curr Opin Plant Biol **16**: 293–300

Christmann A, Hoffmann T, Teplova I, Grill E, Müller A (2005) Generation of Active Pools of Abscisic Acid Revealed by In Vivo Imaging of Water-Stressed Arabidopsis. Plant Physiol **137**: 209–219

Christmann A, Weiler EW, Steudle E, Grill E (2007) A hydraulic signal in root-to-shoot signalling of water shortage. Plant J **52**: 167–174

Claeys H, Van Landeghem S, Dubois M, Maleux K, Inzé D (2014) What Is Stress? Dose-Response Effects in Commonly Used in Vitro Stress Assays. Plant Physiol **165**: 519–527

Colin L, Ruhnow F, Zhu J-K, Zhao C, Zhao Y, Persson S (2022) The cell biology of primary cell walls during salt stress. Plant Cell koac292

Cuevas-Velazquez CL, Vellosillo T, Guadalupe K, Schmidt HB, Yu F, Moses D, Brophy JA, Cosio-Acosta D, Das A, Wang L, et al (2021) Intrinsically disordered protein biosensor tracks the physical-chemical effects of osmotic stress on cells. bioRxiv 2021.02.17.431712

Daugeron M-C, Mauxion F, Séraphin B (2001) The yeast POP2 gene encodes a nuclease involved in mRNA deadenylation. Nucleic Acids Res **29**: 2448–2455

Decreux A, Thomas A, Spies B, Brasseur R, Van Cutsem P, Messiaen J (2006) In vitro characterization of the homogalacturonan-binding domain of the wall-associated kinase WAK1 using site-directed mutagenesis. Phytochemistry **67**: 1068–1079

Devireddy AR, Zandalinas SI, Gómez-Cadenas A, Blumwald E, Mittler R (2018) Coordinating the overall stomatal response of plants: Rapid leaf-to-leaf communication during light stress. Sci Signal. doi: 10.1126/scisignal.aam9514

Dietrich D, Pang L, Kobayashi A, Fozard JA, Boudolf V, Bhosale R, Antoni R, Nguyen T, Hiratsuka S, Fujii N, et al (2017) Root hydrotropism is controlled via a cortex-specific growth mechanism. Nat Plants **3**: 17057

Dinneny JR, Long TA, Wang JY, Jung JW, Mace D, Pointer S, Barron C, Brady SM, Schiefelbein J, Benfey PN (2008) Cell Identity Mediates the Response of Arabidopsis Roots to Abiotic Stress. Science **320**: 942–945

Doma MK, Parker R (2007) RNA Quality Control in Eukaryotes. Cell **131**: 660–668

Dziembowski A, Lorentzen E, Conti E, Séraphin B (2007) A single subunit, Dis3, is essentially responsible for yeast exosome core activity. Nat Struct Mol Biol **14**: 15–22

Fabian MR, Frank F, Rouya C, Siddiqui N, Lai WS, Karetnikov A, Blackshear PJ, Nagar B, Sonenberg N (2013) Structural basis for the recruitment of the human CCR4-NOT deadenylase complex by tristetraprolin. Nat Struct Mol Biol **20**: 735–739

Fabrega C, Shen V, Shuman S, Lima CD (2003) Structure of an mRNA Capping Enzyme Bound to the Phosphorylated Carboxy-Terminal Domain of RNA Polymerase II. Mol Cell **11**: 1549–1561

Feng W, Kita D, Peaucelle A, Cartwright HN, Doan V, Duan Q, Liu M-C, Maman J, Steinhorst L, Schmitz-Thom I, et al (2018) The FERONIA Receptor Kinase Maintains Cell-Wall Integrity during Salt Stress through Ca2+ Signaling. Curr Biol **28**: 666-675.e5

Feng W, Lindner H, Robbins NE, Dinneny JR (2016) Growing Out of Stress: The Role of Cell- and Organ-Scale Growth Control in Plant Water-Stress Responses. Plant Cell **28**: 1769–1782

Finoux A-L, Séraphin B (2006) In vivo targeting of the yeast Pop2 deadenylase subunit to reporter transcripts induces their rapid degradation and generates new decay intermediates. J Biol Chem **281**: 25940–25947

Franks PJ (2004) Stomatal control and hydraulic conductance, with special reference to tall trees. Tree Physiol **24**: 865–878

Franks TM, Lykke-Andersen J (2007) TTP and BRF proteins nucleate processing body formation to silence mRNAs with AU-rich elements. Genes Dev **21**: 719–735

Fujii H, Chinnusamy V, Rodrigues A, Rubio S, Antoni R, Park S-Y, Cutler SR, Sheen J, Rodriguez PL, Zhu J-K (2009) In vitro reconstitution of an abscisic acid signalling pathway. Nature **462**: 660–664

Fujii H, Zhu J-K (2009) Arabidopsis mutant deficient in 3 abscisic acid-activated protein kinases reveals critical roles in growth, reproduction, and stress. Proc Natl Acad Sci **106**: 8380–8385

Fujita Y, Fujita M, Shinozaki K, Yamaguchi-Shinozaki K (2011) ABA-mediated transcriptional regulation in response to osmotic stress in plants. J Plant Res **124**: 509–525

Fujita Y, Nakashima K, Yoshida T, Katagiri T, Kidokoro S, Kanamori N, Umezawa T, Fujita M, Maruyama K, Ishiyama K, et al (2009) Three SnRK2 Protein Kinases are the Main Positive Regulators of Abscisic Acid Signaling in Response to Water Stress in Arabidopsis. Plant Cell Physiol **50**: 2123–2132

Fukuda M, Wakuta S, Kamiyo J, Fujiwara T, Takano J (2018) Establishment of genetically encoded biosensors for cytosolic boric acid in plant cells. Plant J **95**: 763–774

Furihata T, Maruyama K, Fujita Y, Umezawa T, Yoshida R, Shinozaki K, Yamaguchi-Shinozaki K (2006) Abscisic acid-dependent multisite phosphorylation regulates the activity of a transcription activator

AREB1. Proc Natl Acad Sci U S A **103**: 1988–1993

Galloway A, Cowling VH (2019) mRNA cap regulation in mammalian cell function and fate. Biochim Biophys Acta Gene Regul Mech **1862**: 270–279

Garneau NL, Wilusz J, Wilusz CJ (2007) The highways and byways of mRNA decay. Nat Rev Mol Cell Biol **8**: 113–126

Golisz A, Sikorski PJ, Kruszka K, Kufel J (2013) Arabidopsis thaliana LSM proteins function in mRNA splicing and degradation. Nucleic Acids Res **41**: 6232–6249

Gorgues L, Li X, Maurel C, Martinière A, Nacry P (2022) Root osmotic sensing from local perception to systemic responses. Stress Biol **2**: 36

Grenzi M, Buratti S, Parmagnani AS, Abdel Aziz I, Bernacka-Wojcik I, Resentini F, Šimura J, Doccula FG, Alfieri A, Luoni L, et al (2023) Long-distance turgor pressure changes induce local activation of plant glutamate receptor-like channels. Curr Biol **33**: 1019-1035.e8

Guo Y-H, Yu Y-P, Wang D, Wu C-A, Yang G-D, Huang J-G, Zheng C-C (2009) GhZFP1, a novel CCCH-type zinc finger protein from cotton, enhances salt stress tolerance and fungal disease resistance in transgenic tobacco by interacting with GZIRD21A and GZIPR5. New Phytol **183**: 62–75

Gy I, Gasciolli V, Lauressergues D, Morel J-B, Gombert J, Proux F, Proux C, Vaucheret H, Mallory AC (2007) Arabidopsis FIERY1, XRN2, and XRN3 are endogenous RNA silencing suppressors. Plant Cell **19**: 3451–3461

Hamann T (2012) Plant cell wall integrity maintenance as an essential component of biotic stress response mechanisms. Front Plant Sci **3**: 77

Hayashi T, Harada A, Sakai T, Takagi S (2006) Ca2+ transient induced by extracellular changes in osmotic pressure in Arabidopsis leaves: differential involvement of cell wall–plasma membrane adhesion. Plant Cell Environ **29**: 661–672

Hayashi T, Takagi S (2003) Ca2+-Dependent Cessation of Cytoplasmic Streaming Induced by Hypertonic Treatment in Vallisneria Mesophyll Cells: Possible Role of Cell Wall–Plasma Membrane Adhesion. Plant Cell Physiol **44**: 1027–1036

Herger A, Dünser K, Kleine-Vehn J, Ringli C (2019) Leucine-Rich Repeat Extensin Proteins and Their Role in Cell Wall Sensing. Curr Biol **29**: R851–R858

Hoffmann EK, Lambert IH, Pedersen SF (2009) Physiology of cell volume regulation in vertebrates. Physiol Rev **89**: 193–277

Hou C, Tian W, Kleist T, He K, Garcia V, Bai F, Hao Y, Luan S, Li L (2014) DUF221 proteins are a family of osmosensitive calcium-permeable cation channels conserved across eukaryotes. Cell Res **24**: 632–635

Houseley J, Tollervey D (2009) The many pathways of RNA degradation. Cell **136**: 763–776

Hrabak EM, Chan CWM, Gribskov M, Harper JF, Choi JH, Halford N, Kudla J, Luan S, Nimmo HG, Sussman MR, et al (2003) The Arabidopsis CDPK-SnRK Superfamily of Protein Kinases. Plant Physiol **132**: 666–680

Hrmova M, Hussain SS (2021) Plant Transcription Factors Involved in Drought and Associated Stresses. Int J Mol Sci **22**: 5662

Huang P, Ju H-W, Min J-H, Zhang X, Chung J-S, Cheong H-S, Kim CS (2012) Molecular and physiological characterization of the Arabidopsis thaliana Oxidation-related Zinc Finger 2, a plasma membrane protein involved in ABA and salt stress response through the ABI2-mediated signaling pathway. Plant Cell Physiol **53**: 193–203

Huber AE, Bauerle TL (2016) Long-distance plant signaling pathways in response to multiple stressors: the gap in knowledge. J Exp Bot **67**: 2063–2079

Hwang I, Chen H-C, Sheen J (2002) Two-component signal transduction pathways in Arabidopsis. Plant Physiol **129**: 500–515

Jackson MB (1993) Are Plant Hormones Involved in Root to Shoot Communication? *In* JA Callow, ed, Adv. Bot. Res. Academic Press, pp 103–187

Januszyk K, Lima CD (2014) The eukaryotic RNA exosome. Curr Opin Struct Biol **0**: 132–140

Jensen MK, Lindemose S, de Masi F, Reimer JJ, Nielsen M, Perera V, Workman CT, Turck F, Grant MR, Mundy J, et al (2013) ATAF1 transcription factor directly regulates abscisic acid biosynthetic gene NCED3 in Arabidopsis thaliana. FEBS Open Bio **3**: 321–327

Jiang Z, Zhou X, Tao M, Yuan F, Liu L, Wu F, Wu X, Xiang Y, Niu Y, Liu F, et al (2019) Plant cell-surface GIPC sphingolipids sense salt to trigger Ca 2+ influx. Nature **572**: 341–346

Jojoa-Cruz S, Saotome K, Murthy SE, Tsui CCA, Sansom MS, Patapoutian A, Ward AB (2018) Cryo-EM structure of the mechanically activated ion channel OSCA1.2. eLife **7**: e41845

Joshi-Saha A, Valon C, Leung J (2011) A Brand New START: Abscisic Acid Perception and Transduction in the Guard Cell. Sci Signal **4**: re4–re4

Juenger TE, Verslues PE (2023) Time for a drought experiment: Do you know your plants' water status? Plant Cell **35**: 10–23

Kang W-H, Sim YM, Koo N, Nam J-Y, Lee J, Kim N, Jang H, Kim Y-M, Yeom S-I (2020) Transcriptome profiling of abiotic responses to heat, cold, salt, and osmotic stress of Capsicum annuum L. Sci Data **7**: 17

Kastenmayer JP, Green PJ (2000) Novel features of the XRN-family in Arabidopsis: evidence that AtXRN4, one of several orthologs of nuclear Xrn2p/Rat1p, functions in the cytoplasm. Proc Natl Acad Sci U S A **97**: 13985–13990

Katiyar-Agarwal S, Gao S, Vivian-Smith A, Jin H (2007) A novel class of bacteria-induced small RNAs in Arabidopsis. Genes Dev **21**: 3123–3134

Katsuta S, Masuda G, Bak H, Shinozawa A, Kamiyama Y, Umezawa T, Takezawa D, Yotsui I, Taji T, Sakata Y (2020) Arabidopsis Raf-like kinases act as positive regulators of subclass III SnRK2 in osmostress signaling. Plant J **103**: 634–644

Kawa D, Meyer AJ, Dekker HL, Abd-El-Haliem AM, Gevaert K, Van De Slijke E, Maszkowska J, Bucholc M, Dobrowolska G, De Jaeger G, et al (2020) SnRK2 Protein Kinases and mRNA Decapping Machinery Control Root Development and Response to Salt1 [OPEN]. Plant Physiol **182**: 361–377

Kawa D, Testerink C (2017) Regulation of mRNA decay in plant responses to salt and osmotic stress. Cell Mol Life Sci **74**: 1165–1176

Kawaguchi R, Girke T, Bray EA, Bailey-Serres J (2004) Differential mRNA translation contributes to gene regulation under non-stress and dehydration stress conditions in Arabidopsis thaliana. Plant J **38**: 823–839

Kilian J, Whitehead D, Horak J, Wanke D, Weinl S, Batistic O, D'Angelo C, Bornberg-Bauer E, Kudla J, Harter K (2007) The AtGenExpress global stress expression data set: protocols, evaluation and model data analysis of UV-B light, drought and cold stress responses. Plant J **50**: 347–363

Kim T-H, Böhmer M, Hu H, Nishimura N, Schroeder JI (2010) Guard Cell Signal Transduction Network: Advances in Understanding Abscisic Acid, CO2, and Ca2+ Signaling. Annu Rev Plant Biol **61**: 561–591

Kim Y, Park S, Gilmour SJ, Thomashow MF (2013) Roles of CAMTA transcription factors and salicylic acid in configuring the low-temperature transcriptome and freezing tolerance of Arabidopsis. Plant J Cell Mol Biol **75**: 364–376

Klingler JP, Batelli G, Zhu J-K (2010) ABA receptors: the START of a new paradigm in phytohormone signalling. J Exp Bot **61**: 3199–3210

Knight H, Trewavas AJ, Knight MR (1997) Calcium signalling in Arabidopsis thaliana responding to drought and

salinity. Plant J **12**: 1067–1078

Kramer PJ, Boyer JS (1995) Water Relations of Plants and Soils. Academic Press

Kreps JA, Wu Y, Chang H-S, Zhu T, Wang X, Harper JF (2002) Transcriptome Changes for Arabidopsis in Response to Salt, Osmotic, and Cold Stress,. Plant Physiol **130**: 2129–2141

Kulik A, Anielska-Mazur A, Bucholc M, Koen E, Szymanska K, Zmienko A, Krzywinska E, Wawer I, McLoughlin F, Ruszkowski D, et al (2012) SNF1-related protein kinases type 2 are involved in plant responses to cadmium stress. Plant Physiol **160**: 868–883

Kumar MN, Jane W-N, Verslues PE (2013) Role of the Putative Osmosensor Arabidopsis Histidine Kinase1 in Dehydration Avoidance and Low-Water-Potential Response. Plant Physiol **161**: 942–953

Kumar SV, Wigge PA (2010) H2A.Z-Containing Nucleosomes Mediate the Thermosensory Response in Arabidopsis. Cell **140**: 136–147

Kung C (2005) A possible unifying principle for mechanosensation. Nature **436**: 647–654

Lang I, Sassmann S, Schmidt B, Komis G (2014) Plasmolysis: Loss of Turgor and Beyond. Plants **3**: 583–593

Lee S, Jung HJ, Kang H, Kim SY (2012) Arabidopsis Zinc Finger Proteins AtC3H49/AtTZF3 and AtC3H20/AtTZF2 are Involved in ABA and JA Responses. Plant Cell Physiol **53**: 673–686

Liang W, Li C, Liu F, Jiang H, Li S, Sun J, Wu X, Li C (2009) The Arabidopsis homologs of CCR4-associated factor 1 show mRNA deadenylation activity and play a role in plant defence responses. Cell Res **19**: 307–316

Lindner H, Müller LM, Boisson-Dernier A, Grossniklaus U (2012) CrRLK1L receptor-like kinases: not just another brick in the wall. Curr Opin Plant Biol **15**: 659–669

Liu Q, Greimann JC, Lima CD (2006) Reconstitution, activities, and structure of the eukaryotic RNA exosome. Cell **127**: 1223–1237

Liu Q, Kasuga M, Sakuma Y, Abe H, Miura S, Yamaguchi-Shinozaki K, Shinozaki K (1998) Two Transcription Factors, DREB1 and DREB2, with an EREBP/AP2 DNA Binding Domain Separate Two Cellular Signal Transduction Pathways in Drought- and Low-Temperature-Responsive Gene Expression, Respectively, in Arabidopsis. Plant Cell **10**: 1391–1406

Liu X, Wang J, Sun L (2018) Structure of the hyperosmolality-gated calcium-permeable channel OSCA1.2. Nat Commun **9**: 5060

Lykke-Andersen J, Wagner E (2005) Recruitment and activation of mRNA decay enzymes by two ARE-mediated decay activation domains in the proteins TTP and BRF-1. Genes Dev **19**: 351–361

MacRobbie EAC (2006) Osmotic effects on vacuolar ion release in guard cells. Proc Natl Acad Sci **103**: 1135–1140

Maity K, Heumann JM, McGrath AP, Kopcho NJ, Hsu P-K, Lee C-W, Mapes JH, Garza D, Krishnan S, Morgan GP, et al (2019) Cryo-EM structure of OSCA1.2 from Oryza sativa elucidates the mechanical basis of potential membrane hyperosmolality gating. Proc Natl Acad Sci **116**: 14309–14318

Maldonado-Bonilla LD (2014) Composition and function of P bodies in Arabidopsis thaliana. Front. Plant Sci. 5:

Malecki M, Viegas SC, Carneiro T, Golik P, Dressaire C, Ferreira MG, Arraiano CM (2013) The exoribonuclease Dis3L2 defines a novel eukaryotic RNA degradation pathway. EMBO J **32**: 1842–1854

Malone M (1992) Kinetics of wound-induced hydraulic signals and variation potentials in wheat seedlings. Planta **187**: 505–510

Malone M, Mansfield TA, Davies WJ, Leigh RA (1993) Hydraulic signals. Philos Trans R Soc Lond B Biol Sci **341**: 33–39

Maruyama K, Todaka D, Mizoi J, Yoshida T, Kidokoro S, Matsukura S, Takasaki H, Sakurai T, Yamamoto YY, Yoshiwara K, et al (2012) Identification of Cis-Acting Promoter Elements in Cold- and Dehydration-Induced Transcriptional Pathways in Arabidopsis, Rice, and Soybean. DNA Res Int J Rapid Publ Rep

Genes Genomes **19**: 37–49

McLoughlin F, Galvan-Ampudia CS, Julkowska MM, Caarls L, van der Does D, Laurière C, Munnik T, Haring MA, Testerink C (2012) The Snf1-related protein kinases SnRK2.4 and SnRK2.10 are involved in maintenance of root system architecture during salt stress. Plant J Cell Mol Biol **72**: 436–449

Medina J, Catalá R, Salinas J (2011) The CBFs: three arabidopsis transcription factors to cold acclimate. Plant Sci Int J Exp Plant Biol **180**: 3–11

Mehra P, Pandey BK, Melebari D, Banda J, Leftley N, Couvreur V, Rowe J, Anfang M, Gernier HD, Morris E, et al (2022) Hydraulic flux–responsive hormone redistribution determines root branching. Science. doi: 10.1126/science.add3771

Mielke S, Zimmer M, Meena MK, Dreos R, Stellmach H, Hause B, Voiniciuc C, Gasperini D (2021) Jasmonate biosynthesis arising from altered cell walls is prompted by turgor-driven mechanical compression. Sci Adv **7**: eabf0356

Miller G, Schlauch K, Tam R, Cortes D, Torres MA, Shulaev V, Dangl JL, Mittler R (2009) The Plant NADPH Oxidase RBOHD Mediates Rapid Systemic Signaling in Response to Diverse Stimuli. Sci Signal **2**: ra45–ra45

Mizoguchi M, Umezawa T, Nakashima K, Kidokoro S, Takasaki H, Fujita Y, Yamaguchi-Shinozaki K, Shinozaki K (2010) Two closely related subclass II SnRK2 protein kinases cooperatively regulate drought-inducible gene expression. Plant Cell Physiol **51**: 842–847

Monshausen GB, Bibikova TN, Weisenseel MH, Gilroy S (2009) Ca2+ Regulates Reactive Oxygen Species Production and pH during Mechanosensing in Arabidopsis Roots. Plant Cell **21**: 2341–2356

Mourão MA, Hakim JB, Schnell S (2014) Connecting the Dots: The Effects of Macromolecular Crowding on Cell Physiology. Biophys J **107**: 2761–2766

Nagarajan VK, Jones CI, Newbury SF, Green PJ (2013) XRN 5'→3' exoribonucleases: structure, mechanisms and functions. Biochim Biophys Acta **1829**: 590–603

Nguyen AH, Matsui A, Tanaka M, Mizunashi K, Nakaminami K, Hayashi M, Iida K, Toyoda T, Nguyen DV, Seki M (2015) Loss of Arabidopsis 5'-3' Exoribonuclease AtXRN4 Function Enhances Heat Stress Tolerance of Plants Subjected to Severe Heat Stress. Plant Cell Physiol **56**: 1762–1772

Nishimura N, Kitahata N, Seki M, Narusaka Y, Narusaka M, Kuromori T, Asami T, Shinozaki K, Hirayama T (2005) Analysis of ABA hypersensitive germination2 revealed the pivotal functions of PARN in stress response in Arabidopsis. Plant J Cell Mol Biol **44**: 972–984

Nongpiur RC, Singla-Pareek SL, Pareek A (2020) The quest for osmosensors in plants. J Exp Bot **71**: 595–607

Notaguchi M, Okamoto S (2015) Dynamics of long-distance signaling via plant vascular tissues. Front Plant Sci. doi: 10.3389/fpls.2015.00161

Oertli JJ (1985) The response of Plant Cells to Different Forms of Moisture stress. J Plant Physiol **121**: 295–300

Olmedo G, Guo H, Gregory BD, Nourizadeh SD, Aguilar-Henonin L, Li H, An F, Guzman P, Ecker JR (2006) ETHYLENE-INSENSITIVE5 encodes a 5'-->3' exoribonuclease required for regulation of the EIN3-targeting F-box proteins EBF1/2. Proc Natl Acad Sci U S A **103**: 13286–13293

Osakabe Y, Osakabe K, Shinozaki K, Tran L-S (2014) Response of plants to water stress. Front. Plant Sci. 5:

Parker R, Song H (2004) The enzymes and control of eukaryotic mRNA turnover. Nat Struct Mol Biol **11**: 121–127

Passmore LA, Coller J (2022) Roles of mRNA poly(A) tails in regulation of eukaryotic gene expression. Nat Rev Mol Cell Biol **23**: 93–106

Perea-Resa C, Carrasco-López C, Catalá R, Turečková V, Novak O, Zhang W, Sieburth L, Jiménez-Gómez JM, Salinas J (2016) The LSM1-7 Complex Differentially Regulates Arabidopsis Tolerance to Abiotic

Stress Conditions by Promoting Selective mRNA Decapping. Plant Cell **28**: 505–520

Pirouz M, Du P, Munafò M, Gregory RI (2016) Dis3l2-Mediated Decay Is a Quality Control Pathway for Noncoding RNAs. Cell Rep **16**: 1861–1873

Pomeranz MC, Hah C, Lin P-C, Kang SG, Finer JJ, Blackshear PJ, Jang J-C (2010) The Arabidopsis Tandem Zinc Finger Protein AtTZF1 Traffics between the Nucleus and Cytoplasmic Foci and Binds Both DNA and RNA. Plant Physiol **152**: 151–165

Potuschak T, Vansiri A, Binder BM, Lechner E, Vierstra RD, Genschik P (2006) The Exoribonuclease XRN4 Is a Component of the Ethylene Response Pathway in Arabidopsis. Plant Cell **18**: 3047–3057

Qu J, Kang SG, Wang W, Musier-Forsyth K, Jang J-C (2014) The Arabidopsis thaliana tandem zinc finger 1 (AtTZF1) protein in RNA binding and decay. Plant J Cell Mol Biol **78**: 452–467

Ramanathan A, Robb GB, Chan S-H (2016) mRNA capping: biological functions and applications. Nucleic Acids Res **44**: 7511–7526

Reverdatto SV, Dutko JA, Chekanova JA, Hamilton DA, Belostotsky DA (2004) mRNA deadenylation by PARN is essential for embryogenesis in higher plants. RNA **10**: 1200

Romero-Santacreu L, Moreno J, Pérez-Ortín JE, Alepuz P (2009) Specific and global regulation of mRNA stability during osmotic stress in Saccharomyces cerevisiae. RNA **15**: 1110–1120

Roux ME, Rasmussen MW, Palma K, Lolle S, Regué ÀM, Bethke G, Glazebrook J, Zhang W, Sieburth L, Larsen MR, et al (2015) The mRNA decay factor PAT1 functions in a pathway including MAP kinase 4 and immune receptor SUMM2. EMBO J **34**: 593–608

Rowe J, Grangé-Guermente M, Exposito-Rodriguez M, Wimalasekera R, Lenz MO, Shetty KN, Cutler SR, Jones AM (2023) Next-generation ABACUS biosensors reveal cellular ABA dynamics driving root growth at low aerial humidity. Nat Plants 1–13

Rui Y, Dinneny JR (2020) A wall with integrity: surveillance and maintenance of the plant cell wall under stress. New Phytol **225**: 1428–1439

Rymarquis LA, Souret FF, Green PJ (2011) Evidence that XRN4, an Arabidopsis homolog of exoribonuclease XRN1, preferentially impacts transcripts with certain sequences or in particular functional categories. RNA **17**: 501–511

Sachs AB, Deardorff JA (1992) Translation initiation requires the PAB-dependent poly(A) ribonuclease in yeast. Cell **70**: 961–973

Saedler R, Jakoby M, Marin B, Galiana-Jaime E, Hülskamp M (2009) The cell morphogenesis gene SPIRRIG in Arabidopsis encodes a WD/BEACH domain protein. Plant J Cell Mol Biol **59**: 612–621

Sakuma Y, Maruyama K, Osakabe Y, Qin F, Seki M, Shinozaki K, Yamaguchi-Shinozaki K (2006) Functional analysis of an Arabidopsis transcription factor, DREB2A, involved in drought-responsive gene expression. Plant Cell **18**: 1292–1309

Sarowar S, Oh HW, Cho HS, Baek K-H, Seong ES, Joung YH, Choi GJ, Lee S, Choi D (2007) Capsicum annuum CCR4-associated factor CaCAF1 is necessary for plant development and defence response. Plant J Cell Mol Biol **51**: 792–802

Sato H, Takasaki H, Takahashi F, Suzuki T, Iuchi S, Mitsuda N, Ohme-Takagi M, Ikeda M, Seo M, Yamaguchi-Shinozaki K, et al (2018) Arabidopsis thaliana NGATHA1 transcription factor induces ABA biosynthesis by activating NCED3 gene during dehydration stress. Proc Natl Acad Sci U S A **115**: E11178–E11187

Schäfer IB, Yamashita M, Schuller JM, Schüssler S, Reichelt P, Strauss M, Conti E (2019) Molecular Basis for poly(A) RNP Architecture and Recognition by the Pan2-Pan3 Deadenylase. Cell **177**: 1619-1631.e21

Schoenberg DR, Maquat LE (2012) Regulation of cytoplasmic mRNA decay. Nat Rev Genet **13**: 246–259

Shabala SN, Lew RR (2002) Turgor Regulation in Osmotically Stressed Arabidopsis Epidermal Root Cells. Direct

Support for the Role of Inorganic Ion Uptake as Revealed by Concurrent Flux and Cell Turgor Measurements. Plant Physiol **129**: 290–299

Sharma S, Prasad A, Prasad M (2023) Osmosensing in plants: mystery unveiled. Trends Plant Sci. doi: 10.1016/j.tplants.2023.04.001

Shih H-W, Miller ND, Dai C, Spalding EP, Monshausen GB (2014) The receptor-like kinase FERONIA is required for mechanical signal transduction in Arabidopsis seedlings. Curr Biol CB **24**: 1887–1892

Shinozaki K, Yamaguchi-Shinozaki K (2007) Gene networks involved in drought stress response and tolerance. J Exp Bot **58**: 221–227

Sirichandra C, Gu D, Hu H-C, Davanture M, Lee S, Djaoui M, Valot B, Zivy M, Leung J, Merlot S, et al (2009) Phosphorylation of the Arabidopsis AtrbohF NADPH oxidase by OST1 protein kinase. FEBS Lett **583**: 2982–2986

Soma F, Mogami J, Yoshida T, Abekura M, Takahashi F, Kidokoro S, Mizoi J, Shinozaki K, Yamaguchi-Shinozaki K (2017) ABA-unresponsive SnRK2 protein kinases regulate mRNA decay under osmotic stress in plants. Nat Plants **3**: 16204

Soma F, Takahashi F, Suzuki T, Shinozaki K, Yamaguchi-Shinozaki K (2020) Plant Raf-like kinases regulate the mRNA population upstream of ABA-unresponsive SnRK2 kinases under drought stress. Nat Commun **11**: 1373

Soma F, Takahashi F, Yamaguchi-Shinozaki K, Shinozaki K (2021) Cellular Phosphorylation Signaling and Gene Expression in Drought Stress Responses: ABA-Dependent and ABA-Independent Regulatory Systems. Plants **10**: 756

Somerville C, Bauer S, Brininstool G, Facette M, Hamann T, Milne J, Osborne E, Paredez A, Persson S, Raab T, et al (2004) Toward a Systems Approach to Understanding Plant Cell Walls. Science **306**: 2206–2211

Sorenson RS, Deshotel MJ, Johnson K, Adler FR, Sieburth LE (2018) Arabidopsis mRNA decay landscape arises from specialized RNA decay substrates, decapping-mediated feedback, and redundancy. Proc Natl Acad Sci **115**: E1485–E1494

Sornaraj P, Luang S, Lopato S, Hrmova M (2016) Basic leucine zipper (bZIP) transcription factors involved in abiotic stresses: A molecular model of a wheat bZIP factor and implications of its structure in function. Biochim Biophys Acta BBA - Gen Subj **1860**: 46–56

Stecker KE, Minkoff BB, Sussman MR (2014) Phosphoproteomic Analyses Reveal Early Signaling Events in the Osmotic Stress Response. Plant Physiol **165**: 1171–1187

Steffens A, Bräutigam A, Jakoby M, Hülskamp M (2015) The BEACH Domain Protein SPIRRIG Is Essential for Arabidopsis Salt Stress Tolerance and Functions as a Regulator of Transcript Stabilization and Localization. PLoS Biol **13**: e1002188

Steinhorst L, He G, Moore LK, Schültke S, Schmitz-Thom I, Cao Y, Hashimoto K, Andrés Z, Piepenburg K, Ragel P, et al (2022) A Ca2+-sensor switch for tolerance to elevated salt stress in Arabidopsis. Dev Cell **57**: 2081-2094.e7

Sukharev S, Corey DP (2004) Mechanosensitive Channels: Multiplicity of Families and Gating Paradigms. Sci STKE **2004**: re4–re4

Sun J, Jiang H, Xu Y, Li H, Wu X, Xie Q, Li C (2007) The CCCH-type zinc finger proteins AtSZF1 and AtSZF2 regulate salt stress responses in Arabidopsis. Plant Cell Physiol **48**: 1148–1158

Sussmilch FC, Brodribb TJ, McAdam SAM (2017) Up-regulation of NCED3 and ABA biosynthesis occur within minutes of a decrease in leaf turgor but AHK1 is not required. J Exp Bot **68**: 2913–2918

Suzuki N, Rivero RM, Shulaev V, Blumwald E, Mittler R (2014) Abiotic and biotic stress combinations. New Phytol **203**: 32–43

Symmons MF, Jones GH, Luisi BF (2000) A duplicated fold is the structural basis for polynucleotide phosphorylase catalytic activity, processivity, and regulation. Struct Lond Engl 1993 **8**: 1215–1226

Takahashi F, Shinozaki K (2019) Long-distance signaling in plant stress response. Curr Opin Plant Biol **47**: 106–111

Takahashi F, Suzuki T, Osakabe Y, Betsuyaku S, Kondo Y, Dohmae N, Fukuda H, Yamaguchi-Shinozaki K, Shinozaki K (2018) A small peptide modulates stomatal control via abscisic acid in long-distance signalling. Nature **556**: 235–238

Takahashi Y, Zhang J, Hsu P-K, Ceciliato PHO, Zhang L, Dubeaux G, Munemasa S, Ge C, Zhao Y, Hauser F, et al (2020) MAP3Kinase-dependent SnRK2-kinase activation is required for abscisic acid signal transduction and rapid osmotic stress response. Nat Commun **11**: 12

Thore S, Mauxion F, Séraphin B, Suck D (2003) X-ray structure and activity of the yeast Pop2 protein: a nuclease subunit of the mRNA deadenylase complex. EMBO Rep **4**: 1150–1155

Tomecki R, Kristiansen MS, Lykke-Andersen S, Chlebowski A, Larsen KM, Szczesny RJ, Drazkowska K, Pastula A, Andersen JS, Stepien PP, et al (2010) The human core exosome interacts with differentially localized processive RNases: hDIS3 and hDIS3L. EMBO J **29**: 2342–2357

Towler BP, Jones CI, Harper KL, Waldron JA, Newbury SF (2016) A novel role for the 3′-5′ exoribonuclease Dis3L2 in controlling cell proliferation and tissue growth. RNA Biol **13**: 1286–1299

Tran L-SP, Urao T, Qin F, Maruyama K, Kakimoto T, Shinozaki K, Yamaguchi-Shinozaki K (2007) Functional analysis of AHK1/ATHK1 and cytokinin receptor histidine kinases in response to abscisic acid, drought, and salt stress in Arabidopsis. Proc Natl Acad Sci **104**: 20623–20628

Tucker M, Valencia-Sanchez MA, Staples RR, Chen J, Denis CL, Parker R (2001) The transcription factor associated Ccr4 and Caf1 proteins are components of the major cytoplasmic mRNA deadenylase in Saccharomyces cerevisiae. Cell **104**: 377–386

Umezawa T, Sugiyama N, Takahashi F, Anderson JC, Ishihama Y, Peck SC, Shinozaki K (2013) Genetics and phosphoproteomics reveal a protein phosphorylation network in the abscisic acid signaling pathway in Arabidopsis thaliana. Sci Signal **6**: rs8

Urao T, Miyata S, Yamaguchi-Shinozaki K, Shinozaki K (2000) Possible His to Asp phosphorelay signaling in an Arabidopsis two-component system. FEBS Lett **478**: 227–232

Urao T, Yakubov B, Satoh R, Yamaguchi-Shinozaki K, Seki M, Hirayama T, Shinozaki K (1999) A Transmembrane Hybrid-Type Histidine Kinase in Arabidopsis Functions as an Osmosensor. Plant Cell **11**: 1743–1754

Vaahtera L, Schulz J, Hamann T (2019) Cell wall integrity maintenance during plant development and interaction with the environment. Nat Plants **5**: 924–932

Vishwakarma K, Upadhyay N, Kumar N, Yadav G, Singh J, Mishra RK, Kumar V, Verma R, Upadhyay RG, Pandey M, et al (2017) Abscisic Acid Signaling and Abiotic Stress Tolerance in Plants: A Review on Current Knowledge and Future Prospects. Front. Plant Sci. 8:

Waadt R, Seller CA, Hsu P-K, Takahashi Y, Munemasa S, Schroeder JI (2022) Plant hormone regulation of abiotic stress responses. Nat Rev Mol Cell Biol **23**: 680–694

Walley JW, Kelley DR, Nestorova G, Hirschberg DL, Dehesh K (2010) Arabidopsis Deadenylases AtCAF1a and AtCAF1b Play Overlapping and Distinct Roles in Mediating Environmental Stress Responses. Plant Physiol **152**: 866–875

Wang B, Zhang H, Huai J, Peng F, Wu J, Lin R, Fang X (2022) Condensation of SEUSS promotes hyperosmotic stress tolerance in Arabidopsis. Nat Chem Biol **18**: 1361–1369

Webster MW, Chen Y-H, Stowell JAW, Alhusaini N, Sweet T, Graveley BR, Coller J, Passmore LA (2018)

mRNA Deadenylation Is Coupled to Translation Rates by the Differential Activities of Ccr4-Not Nucleases. Mol Cell **70**: 1089-1100.e8

Wilkinson S, Davies WJ (2002) ABA-based chemical signalling: the co-ordination of responses to stress in plants. Plant Cell Environ **25**: 195–210

Wohlbach DJ, Quirino BF, Sussman MR (2008) Analysis of the Arabidopsis Histidine Kinase ATHK1 Reveals a Connection between Vegetative Osmotic Stress Sensing and Seed Maturation. Plant Cell **20**: 1101–1117

Wolf S (2017) Plant cell wall signalling and receptor-like kinases. Biochem J **474**: 471–492

Xu J, Chua N-H (2009) Arabidopsis Decapping 5 Is Required for mRNA Decapping, P-Body Formation, and Translational Repression during Postembryonic Development. Plant Cell **21**: 3270–3279

Xu J, Chua N-H (2012) Dehydration stress activates Arabidopsis MPK6 to signal DCP1 phosphorylation. EMBO J **31**: 1975–1984

Yamazaki M, Ohshika M, Kashiwagi N, Asano T (1992) Phase transitions of phospholipid vesicles under osmotic stress and in the presence of ethylene glycol. Biophys Chem **43**: 29–37

Yan Y-B (2014) Deadenylation: enzymes, regulation, and functional implications. WIREs RNA **5**: 421–443

Yang M, Zhang B, Jia J, Yan C, Habaike A, Han Y (2013) RRP41L, a Putative Core Subunit of the Exosome, Plays an Important Role in Seed Germination and Early Seedling Growth in Arabidopsis. Plant Physiol **161**: 165–178

Yang Y-Z, Tan B-C (2014) A Distal ABA Responsive Element in AtNCED3 Promoter Is Required for Positive Feedback Regulation of ABA Biosynthesis in Arabidopsis. PLOS ONE **9**: e87283

Yu X, Li B, Jang G-J, Jiang S, Jiang D, Jang J-C, Wu S-H, Shan L, He P (2019) Orchestration of Processing Body Dynamics and mRNA Decay in Arabidopsis Immunity. Cell Rep **28**: 2194-2205.e6

Yuan F, Yang H, Xue Y, Kong D, Ye R, Li C, Zhang J, Theprungsirikul L, Shrift T, Krichilsky B, et al (2014) OSCA1 mediates osmotic-stress-evoked Ca 2+ increases vital for osmosensing in Arabidopsis. Nature **514**: 367–371

Zandalinas SI, Fichman Y, Mittler R (2020) Vascular Bundles Mediate Systemic Reactive Oxygen Signaling during Light Stress. Plant Cell **32**: 3425–3435

Zeller G, Henz SR, Widmer CK, Sachsenberg T, Rätsch G, Weigel D, Laubinger S (2009) Stress-induced changes in the Arabidopsis thaliana transcriptome analyzed using whole-genome tiling arrays. Plant J **58**: 1068–1082

Zhang H, Zhu J, Gong Z, Zhu J-K (2022) Abiotic stress responses in plants. Nat Rev Genet **23**: 104–119

Zhang M, Wang D, Kang Y, Wu J-X, Yao F, Pan C, Yan Z, Song C, Chen L (2018) Structure of the mechanosensitive OSCA channels. Nat Struct Mol Biol **25**: 850–858

Zhang W, Murphy C, Sieburth LE (2010) Conserved RNaseII domain protein functions in cytoplasmic mRNA decay and suppresses Arabidopsis decapping mutant phenotypes. Proc Natl Acad Sci **107**: 15981–15985

Zhang X, Guo H (2017) mRNA decay in plants: both quantity and quality matter. Curr Opin Plant Biol **35**: 138–144

Zhao C, Jiang W, Zayed O, Liu X, Tang K, Nie W, Li Y, Xie S, Li Y, Long T, et al (2020) The LRXs-RALFs-FER module controls plant growth and salt stress responses by modulating multiple plant hormones. Natl Sci Rev **8**: nwaa149

Zhu J-K (2002) Salt and Drought Stress Signal Transduction in Plants. Annu Rev Plant Biol **53**: 247–273

Zhu J-K (2016) Abiotic Stress Signaling and Responses in Plants. Cell **167**: 313–324

Résumé en français

Contexte et objectifs

L'eau est un composant fondamental de la vie, et le déficit en eau limite considérablement la croissance et le développement des plantes ainsi que le rendement des cultures dans le monde entier. Actuellement, le rythme exceptionnel des changements climatiques mondiaux intensifie l'amplitude et la fréquence des événements météorologiques extrêmes qui réduisent la disponibilité de l'eau pour les plantes. Par conséquent, il est devenu essentiel de décrypter comment les plantes perçoivent et réagissent au déficit en eau.

Le déficit en eau est un stress ressenti par les plantes dès que la demande en eau dépasse leur capacité d'absorption. Les chercheurs simulent fréquemment ce stress en induisant un stress osmotique par l'ajout de composés osmotiquement actifs dans l'environnement de croissance des racines des plantes. Cependant, de nombreuses études sur la réponse d'Arabidopsis aux stress osmotiques ont été menées dans des conditions de déficit hydrique sévère (SWD) qui pourraient ne pas refléter la réalité de l'environnement naturel de la plante ou son état physiologique (Claeys et al., 2014; Yuan et al., 2014). Par ailleurs, la diminution du potentiel osmotique externe (Π) due à un déficit hydrique modéré (MWD) réduit généralement le potentiel de turgescence (P) des plantes de manière quantitative, et ces deux paramètres peuvent être perçus par les plantes. Le stress osmotique réduit non seulement Π et P, mais a également d'autres impacts nocifs sur les plantes, qui dépendent des composés osmotiquement actifs spécifiques utilisés. Il est donc très difficile d'identifier précisément les mécanismes de réponse spécifiques et communs aux variations de Π et P (Zhu, 2016). Les études transcriptomiques sont une approche courante pour révéler les transcrits cibles potentiels et les voies de signalisation pour un facteur de stress donné. Cependant, la plupart de ces études n'ont utilisé qu'un ou deux composés osmotiquement actifs, avec une ou deux concentrations, ce qui n'est pas suffisant pour surmonter ce défi. De plus, peu d'études se snont focalisés sur des temps courts (Dinneny et al., 2008), la plupart des recherches utilisant plutôt des transcriptomes obtenus après des heures ou des jours après traitements.

Par conséquent, la question de savoir quels transcrits peuvent être spécifiquement influencés par les changements de Π et/ou P au cours des phases initiales (15 minutes) des conditions de MWD, dans lesquelles les cellules corticales de la racine primaire demeurent turgescentes, reste sans réponse. Le premier objectif principal de la thèse était d'y apporter fournir une réponse.

On sait peu de choses sur les premières étapes des réponses moléculaires des plantes au stress

osmotique, en particulier en ce qui concerne la perception du signal physique. Jusqu'à présent, seul un osmosenseur, OSCA1, a été clairement identifié, tandis que la plupart des voies de signalisation connues n'y ont pas été reliées (Yuan et al., 2014). L'hydrotropisme est une approche émergente pour explorer les sites de perception et de réponse des plantes au déficit en eau. Des études suggèrent que l'hydrotropisme est contrôlé par un mécanisme impliquant de multiples hormones et signaux (Dietrich et al., 2017; Chang et al., 2019; Mielke et al., 2021). Mais cette méthode pourrait ne pas représenter de manière précise la façon dont les racines des plantes répondent au déficit en eau car elle a, jusqu'à présent, utilisé de jeunes plantes (âgées de 7 jours) qui n'ont pas encore développé une architecture racinaire complète. Récemment, Steinhorst et al. ont découvert que le stress au Na+ déclenche rapidement des signaux calciques primaires spécifiques dans un groupe de cellules situé dans la zone de différenciation des racines en utilisant le rapporteur de Ca^{2+} (Steinhorst et al., 2022). Ainsi, les rapporteurs pourraient contribuer à répondre à la question de quand et où les plantes perçoivent les changements de Π et/ou P.

Dans les plantes, deux signaux biophysiques principaux, P et Π, composent un paramètre thermodynamique important, le potentiel hydrique, Ψ, qui permet d'anticiper le mouvement de l'eau entre les différents compartiments du continuum sol/plante/atmosphère. Une étude a rapporté que les baisses de P causées par le MWD peuvent être rétablies après environ 40 minutes à plusieurs heures, en fonction de l'intensité du stress hydrique et de la résistance des plantes (Shabala and Lew, 2002). Il est donc essentiel de tester si les gènes corrélés à Π et/ou P (issus de l'objectif 1) répondent aux changements dynamiques de P provoqués par le MWD. De plus, une différence clé entre le MWD et le SWD en ce qui concerne les paramètres physiques P et Π est que, sous SWD, P restera nulle tandis que Π (qui est approximativement égal à Ψ en hydroponie) peut encore augmenter à mesure que la concentration des solutés augmente. Il est donc également important de tester si ces gènes corrélés à Π et/ou P répondent de manière quantitative aux changements de Π provoqués par le SWD au cours des premières étapes des traitements. Cette question a été abordée dans la section 2 du manuscrit.

La mesure de Ψ et de ses composantes chez les plantes est difficile techniquement: elle est jusqu'à présent obtenue par une combinaison de techniques difficiles et indirectes telles que les chambres à pression, les sondes de pression cellulaire ou les pico-osmomètres (Shabala and Lew,

2002; Boursiac et al., 2022). Il existe un réel besoin de nouveaux outils, car Ψ chez les plantes fluctue constamment (en quelques minutes) en raison de la croissance, de l'humidité du sol et de l'air, ainsi que des variations de lumière. Les rapporteurs sont des outils utiles pour surveiller la santé des plantes, leur statut nutritionnel ou l'activation des voies de signalisation à l'origine de leur adaptation à un environnement difficile. Parmi eux, les constructions rapporteurs intégrées au génome, et en particulier les fusions de gènes promoteurs-rapporteurs, permettent une analyse spatiale et temporelle très précise de certains paramètres. De tels rapporteurs ont été isolés pour l'accumulation de l'ABA et l'état redox de la cellule, ainsi que la visualisation du transport de l'acide borique dans la plante (Christmann et al., 2005; Miller et al., 2009; Fukuda et al., 2018). Dans un autre exemple marquant, après avoir observé que l'expression de HSP70 est quantitativement induite par une température ambiante élevée, Kumar et Wigge ont développé un rapporteur de température en utilisant la construction ProHSP70::luciférase et l'ont utilisé pour isoler un senseur de température, l'histone H2A.Z chez Arabidopsis (Kumar and Wigge, 2010). Par conséquent, pour développer des rapporteurs compétents de Π et P, la principale difficulté réside dans l'obtention d'éléments de régulation de l'expression génique qui répondent de manière quantitative à leur variation. Il a été proposé que l'expression génique est étroitement régulée à la fois au niveau transcriptionnel (activité du promoteur) et au niveau post-transcriptionnel (dégradation de l'ARNm) sous l'effet de stress liés à la sécheresse et à la salinité (Kawa and Testerink, 2017). Pour obtenir les éléments de régulation fiables des candidats corrélés à Π et P, il est indispensable d'examiner à quel niveau leurs expressions sont régulées par le déficit hydrique. Nous avons évalué ces aspects dans la section 2 du manuscrit.

Un autre objectif important est d'utiliser les éléments de régulation des gènes issus des investigations précédentes pour induire l'expression de rapporteurs, permettant ainsi la visualisation de la manière dont les changements de Π ou P sont perçus pendant les conditions de déficit hydrique. Nous avons également examiné si ces rapporteurs rendent effectivement compte des changements de Π et/ou P et s'ils sont régulés par les voies de signalisation dépendant de l'intégrité des parois (CWI) et de l'ABA.

Résultats

L'analyse transcriptomique a révélé qu'ENODL8 était corrélé à P et que *NCED3* était corrélé à Π.

Dans les 15 minutes suivant les traitements de MWD, des concentrations croissantes de NaCl, de

sorbitol et de PEG ont modifié Π et P de façon quantitative dans les cellules corticales de la zone d'élongation de la racine primaire (PR). Les traitements à l'EG, avec une osmolarité similaire à celle des autres osmolytes mais ayant entraîné une réduction moins importante de la turgescence, nous ont permis de distinguer les gènes dont l'expression est corrélée à Π de ceux corrélés à P. Nous avons ainsi obtenu des gènes spécifiques de certains solutés, ou de Π et P, en analysant la corrélation entre l'expression génique dans le transcriptome et la concentration en solutés ou Π ou P. Un gène régulé à la baisse, *At1G64640* (*ENODL8*), de fonction inconnue, et un gène régulé à la hausse, *At3G14440* (*NCED3*), impliqué dans la synthèse de l'ABA, ont été mis en évidence par cette analyse et étudiés plus en détail. Ils ont été initialement identifiés comme, respectivement, corrélés à P et Π.

Les changements de P provoqués par le MWD régulent quantitativement l'expression d'ENODL8 et de NCED3 à la fois au niveau transcriptionnel et post-transcriptionnel, tandis que la plasmolyse causée par le SWD perturbe cette régulation.

Nous avons exposé les racines d'Arabidopsis à des traitements avec différentes concentrations de NaCl, de sorbitol, d'éthylène glycol (EG) et de PEG pendant 15 minutes, incluant le MWD mais en l'étendant également au SWD. Nous avons alors observé un motif en forme de "cloche" pour l'expression de ces deux gènes après 15 minutes de traitements. Tout d'abord, en ce qui concerne *ENODL8*, ses niveaux d'ARNm ont diminué à mesure que les concentrations de NaCl, de sorbitol et de PEG augmentaient, mais seulement jusqu'à des seuils spécifiques (125 mM, 250 mM et 200 g/L, respectivement). De manière surprenante, au-delà de ces seuils, les niveaux d'ARNm ont diminué moins que dans des conditions MWD. Cette corrélation inversée suggère qu'*ENODL8* ne répond pas de manière quantitative aux changements étendus de Π, passant du déficit hydrique modéré au déficit hydrique sévère. Cependant, l'expression d'*ENODL8* est restée relativement stable dans un certain intervalle de concentrations d'EG, laissant entendre une corrélation potentielle avec la turgescence. De manière similaire, *NCED3* a montré un modèle d'expression en forme de cloche régulée à la hausse en réponse aux traitements au NaCl, au sorbitol et au PEG. Cependant, les traitements à l'EG ont entraîné une augmentation continue de l'expression de *NCED3*. Ces résultats suggèrent que la réponse quantitative de *NCED3* pourrait être liée à la Π provoquée par ces traitements. Remarquablement, les concentrations à partir desquelles la plasmolyse a commencé (-0,7 MPa causé par 150 mM de NaCl ou 300 mM de sorbitol) coïncidaient avec les concentrations

qui entraînaient une inversion de la régulation de l'expression d'*ENODL8* et de *NCED3*. Cela indique que la plasmolyse des cellules corticales induit une dynamique différente de régulation transcriptionnelle en réponse au déficit hydrique.

Pour approfondir la dynamique temporelle de l'expression de nos gènes candidats, nous avons prolongé la période de traitement du MWD à 3 heures. Les niveaux d'ARNm d'*ENODL8* ont montré une diminution significative à 15 minutes et jusqu'à 1 heure pour tous les traitements, avec une récupération observée dans les racines après 3 heures. De manière notable, la diminution de l'expression d'*ENODL8* causée par le traitement à l'EG était moins marquée par rapport aux autres traitements à 15 et 30 minutes. Pendant ce temps, *NCED3* était induit par les traitements au PEG, au NaCl et au sorbitol au cours des 30 premières minutes, mais aucun retour au niveau initial n'a été observé après 3 heures. L'EG n'a pas non plus induit l'expression de *NCED3*. Ces résultats laissent penser que le niveau d'expression d'*ENODL8* dans les 3 heures est cohérent avec les changements de P au fil du temps lors des traitements de MWD, tandis que le niveau d'expression de *NCED3* est cohérent avec les changements de P uniquement au cours des 30 premières minutes de traitement.

Nous avons également examiné le rôle des voies de dégradation de l'ARNm en utilisant la cordycépine, un inhibiteur de la transcription. Le traitement cordycépine + NaCl a entraîné une réduction plus rapide et plus marquée de l'abondance de l'ARNm d'*ENODL8*, suggérant que la diminution de la turgescence régulait à la hausse la voie de dégradation de l'ARNm responsable d'*ENODL8*. En ce qui concerne l'expression de *NCED3*, son induction causée par le traitement cordycépine + NaCl était plus élevée que celle par la cordycépine seule, mais plus faible que celle par NaCl seul. Ces résultats suggèrent que le traitement NaCl est capable d'augmenter l'abondance de l'ARNm de *NCED3* en diminuant sa dégradation. De façon inattendue, la cordycépine a initialement réduit les niveaux d'ARNm de *NCED3* mais cela a ensuite été suivi d'une augmentation continue, ce qui suggère des mécanismes de régulation complexes et un contrôle strict des niveaux d'ARN pour ce gène.

Enfin, nous avons examiné l'implication des voies de dégradation de l'ARNm dans la régulation d'*ENODL8* et de *NCED3* en cas de stress osmotique. Des mutants impactés dans la voie de dégradation 5'-3' de l'ARNm (double mutant *lsm1a/1b* et mutants *xrn4*) et une lignée gain de fonction de la voie de dégradation 3'-5' de l'ARNm (WT [Col_SOVLer]) ont été utilisés. Les résultats ont révélé que LSM1A et/ou LSM1B jouent un rôle dans le niveau absolu d'expression

d'*ENODL8*, mais pas dans sa réponse aux stress osmotiques. LSM1A et XRN4 semblent, de plus, indirectement impliqués dans l'induction de *NCED3* en réponse au stress osmotique.

Le signal de luminescence émis par les plantes exprimant *pNCED3::SLuc-3'UTR* peut rendre compte des changements hydrauliques, tandis que *pENODL8::SLuc-3'UTR* ne le peut pas.

Étant donné que les niveaux d'ARNm d'*ENODL8* et de *NCED3* semblent rendre compte quantitativement des variations de Ψ, nous avons tenté de développer des rapporteurs hydrauliques en utilisant leurs promoteurs et leur 3'UTR pour contrôler l'expression d'une version à durée de vie courte de la luciférase (SLuc). L'examen de l'expression de SLuc sous MWD a montré que l'abondance des ARNm de SLuc issus de la construction *pNCED3::SLuc-3'UTR* était significativement corrélée à celle des ARNm endogènes de *NCED3*, tandis que ce n'était pas le cas pour *ENODL8* et la construction *pENODL8::SLuc-3'UTR*. Ces résultats indiquent que les plantes portant une construction *pNCED3::SLuc-3'UTR* semblent être capables de rendre compte avec confiance de l'expression de *NCED3* dans des conditions de déficit hydrique.

Nous avons examiné les signaux de luminescence de SLuc dans les racines et les parties aériennes de lignées de plantes transgéniques (*pNCED3::SLuc-3'UTR*, L7 et L16) exposées à différents traitements osmotiques. De façon reproductible, nous observons une réponse dose-dépendante des signaux de SLuc aux traitements par NaCl, sorbitol, PEG ou EG dans une fenêtre de 2 à 3 heures. Cela suggère que les signaux de SLuc reflètent les changements de Π, faisant de la construction *pNCED3::SLuc-3'UTR* un rapporteur potentiel de Π lors d'un déficit hydrique. Les signaux de SLuc dans les racines de L7 ne sont cependant pas modifiés de manière significative au cours des 15 premières minutes d'un traitement, ce qui a conduit à l'hypothèse d'un délai entre la régulation de l'ARNm et la production d'une protéine luciférase fonctionnelle. La corrélation des cinétiques de SLuc avec les mesures de P (auxquelles ont donc été rajouté un délai de 19 à 31 minutes) se révèle solide également, indiquant la capacité de SLuc à rendre compte des changements de P lors des premiers instants d'un déficit hydrique. Des résultats similaires ont été observés dans les racines de la seconde lignée L16, soutenant la robustesse de la construction en tant que rapporteur de P au cours des 25 à 60 premières minutes de traitement.

Il faut noter, de plus, que les signaux de SLuc dans les parties aériennes réagissent aux traitements osmotiques appliqués aux racines, à l'exception de l'EG. Ces signaux dans les parties aériennes ont montré une corrélation significative avec Π-All (Π sous toutes les conditions) après

30 minutes, persistant pendant plus de 2 heures et indiquant la capacité de SLuc dans les parties aériennes à rendre compte des changements hydrauliques se déroulant dans un premier temps au niveau des racines.

Les sites de perception des changements de P et Π dans les plantes ont été explorés de plusieurs manières.

Tout d'abord, nous avons examiné la régulation de l'expression du gène *ENODL8* et l'activité spécifique de son promoteur dans les tissus racinaires de plantes exprimand la construction *pENODL8 ::eGFP :GUS*. Une forte coloration GUS est apparue dans la zone de transition, dans les racines primaires et latérales, et s'estompant vers leur base. En même temps, une activité GUS a été observée dans les cellules de la coiffe radiculaire de la columelle entièrement différenciées dans les racines latérales. Les signaux GFP ont confirmé ces résultats.

Ensuite, nous avons exploré les sites de perception du déficit hydrique en observant les signaux de luminescence de SLuc dans les plantes (L7/L16) exprimant *pNCED3::SLuc-3'UTR* sous des traitements de déficit hydrique avec diverses concentrations en NaCl, sorbitol, PEG ou EG. Aucun signal n'a été observé dans L7 pendant des conditions de MWD relativement faibles, mais après des traitements de MWD relativement forts pendant 45 minutes, des signaux peuvent être observés dans la partie mature de la racine primaire avec de nombreuses racines latérales. Sous SWD, des signaux lumineux sont d'abord apparus dans l'hypocotyle. Au fil du temps, les signaux se sont intensifiés, se sont étendus le long des racines primaires et latérales, et ont atteint l'hypocotyle et les cotylédons sous des traitements de déficit hydrique relativement forts. Les traitements à l'EG ont produit des signaux faibles, tandis que les traitements au sorbitol ont induit les signaux racinaires les plus forts. Une réponse similaire a eu lieu dans les plantes L16, bien que d'une intensité plus faible et avec un seuil plus élevé.

La capacité de pNCED3::SLuc-3'UTR à percevoir les changements hydrauliques sous un déficit hydrique est indépendante de la signalisation de l'ABA et de la CWI.

Nous avons constaté que l'expression du gène *NCED3* augmentait significativement après une exposition à court terme à l'ABA. L'expression d'*ENODL8* n'est, de son côté, pas sensible à ce traitement. Les signaux SLuc dans les plantes portant la construction *pNCED3::SLuc-3'UTR* ont également montré une réponse dose-dépendante au traitement à l'ABA. Pour comprendre si l'induction de SLuc en réponse au déficit hydrique dépend de la synthèse de l'ABA, nous avons

prétraité les racines avec du fluridone, un inhibiteur de la synthèse d'ABA. Le fluridone a efficacement empêché la synthèse d'ABA et aboli l'induction de Luc dans les plantes portant la construction pHB6::Luc (pHB6, un rapporteur dépendant de l'ABA pour le stress hydrique). Cependant, la construction *pNCED3::SLuc-3'UTR* a montré une réponse précoce au déficit hydrique largement indépendante de l'inhibition de la synthèse de l'ABA par le fluridone.

Nous avons également testé si la CWI est impliquée dans la régulation des signaux de SLuc dans les lignées exprimant *pNCED3::SLuc-3'UTR* (L7) en réponse aux traitements de déficit hydrique. Les plantes portant la construction pHB6::Luc (pHB6) ou *pNCED3::SLuc-3'UTR* (L7) ont été traitées avec du sorbitol et de l'isoxaben (ISX), un agent endommageant la paroi cellulaire. Dans les traitements témoin et ISX, les signaux de SLuc sont restés stables dans les deux lignées, indiquant que l'ISX n'a pas significativement affecté l'accumulation des signaux de SLuc. Dans la plante pHB6, les signaux de SLuc ont été induits après le traitement au sorbitol, avec une différence significative par rapport à ISX + sorbitol observée seulement après 6 heures, suggérant un rôle de la CWI dans l'activation tardive. Dans les racines *pNCED3::SLuc-3'UTR*, la CWI semble ne pas influencer la réponse Sluc précoce, mais joue un rôle dans une phase plus tardive. Dans les parties aériennes, l'ISX retarde et réduit les signaux SLuc induits par le sorbitol chez L7, avec une différence significative après 3-6 heures, ce qui indique que la CWI peut être impliquée dans l'initiation des signaux de SLuc dans les parties aériennes des plantes portant la construction *pNCED3::SLuc-3'UTR*.

La séquence codante d'ENODL8 est essentielle pour sa dégradation rapide en réponse aux changements de P.

Nous avons approfondi l'étude de la régulation du gène *ENODL8* chez les plantes Arabidopsis en conditions de déficit hydrique. Nous avons obtenu un mutant T-DNA *SAIL_603_E07* (L5) et avons confirmé la mutation d'ENODL8 dans cette lignée par génotypage et détection qPCR. Nous avons obtenu des lignées complémentées en transférant la construction *pENODL8::sp-eGFP-ENODL8-3"UTR* dans la plante L5. Sous un déficit hydrique, nous avons surveillé l'expression de trois fragments de séquence de *sp-gGFP-ENODL8*, comprenant les parties N-terminale et C-terminale d'*ENODL8 (*respectivement *ENODL8* et *ENODL8C)*, ainsi qu'une séquence issue de la *GFP*. Étonnamment, *eGFP* et *ENODL8* ont montré seulement de légères réductions en réponse aux traitements de déficit hydrique, tandis qu'un autre fragment, *ENODL8C*, a montré une induction

significative. Par la suite, nous avons constaté que l'expression d'*ENODL8C* était significativement élevée dans le mutant L5 en conditions de contrôle par rapport à Col_0, suggérant l'existence de mécanismes de compensation de l'abondance d'*ENODL8* dans L5 et conduisant probablement à la synthèse d'un transcrit inconnu contenant *ENODL8C*. Ce transcrit peut concurrencer les composants de la voie de dégradation, interférant ainsi avec la dégradation de *sp-eGFP-ENODL8*. Des investigations supplémentaires seront nécessaires pour comprendre pleinement ces mécanismes de régulation. Sans lignée altérée, la recherche de phénotypes déclenchés par une dérégulation de l'expression d'ENODL8 n'a été abordée qu'à la marge.

Discussion

Étant donné le changement climatique en cours et l'augmentation de la fréquence des événements de sécheresse, la compréhension des mécanismes par lesquels les plantes perçoivent le déficit hydrique est devenue d'une importance critique. Dans ce travail, nous avons étudié comment les racines d'Arabidopsis perçoivent le déficit hydrique (DH) et nous nous sommes concentrés sur quatre aspects: l'altération de paramètres hydrauliques des plantes, les transcriptomes, la régulation de l'expression génique et le développement « d'osmo-rapporteurs ». Les trois premiers aspects ont agi de concert pour élucider quel sous-ensembles de gènes était régulé par deux signaux biophysiques : le Π externe et la P des cellules corticales, et quels mécanismes de régulation des ARNm pouvait être impliqué. Le dernier aspect a été développé afin d'approfondir nos connaissances sur le moment et le lieu où les plantes détectent les changements hydrauliques de manière à déclencher une régulation de l'expression génique.

Le déficit hydrique régule l'expression génique à la fois au niveau transcriptionnel et post-transcriptionnel

En analysant la corrélation entre les transcriptomes précoces et Π ou P après des traitements osmotiques, nous avons identifié des gènes spécifiques à chaque soluté, ainsi que des gènes corrélés à Π et P. Ces résultats suggèrent que les cellules végétales ont la capacité de détecter et de répondre spécifiquement aux différents facteurs de stress. Notre analyse des transcriptomes et nos essais avec la cordycépine ont montré que le déficit hydrique peut altérer la demi-vie des ARNm des gènes corrélés à P et Π. Nous avons découvert que LSM1A et/ou 1B interviennent dans la régulation de l'expression absolue d'*ENODL8*, tandis que LSM1A/1B et XRN4 régulent indirectement

l'expression de *NCED3* en réponse au déficit hydrique. Les transcriptomes issus de la littérature ont montré que VCS et RH6/8/12, des composants du complexe de décapage dans la dégradation 5'-3' des ARNm, sont essentiels pour leur expression absolue et/ou la demi-vie de leurs ARNm (Sorenson et al., 2018; Chantarachot et al., 2020). Des études récentes ont révélé que le module "B4 Raf-like MAP kinase kinase kinases (MAPKKKs) - sous-classe I SnRK2s-VCS" est essentiel pour la régulation post-transcriptionnelle de l'expression génique (Soma et al., 2017; Soma et al., 2020). Il serait intéresant d'étudier davantage l'expression des gènes en réponse au déficit hydrique précoce d'un point de vue transcriptomique, tout en manipulant la dégradation des ARNm et l'activité des promoteurs.

La perception du déficit hydrique par les plantes et les « osmo-rapporteurs »

La construction *pNCED3::Sluc-3'UTR* a fidèlement reproduit la régulation native de l'expression de *NCED3*, alors que ce n'était pas la cas avec la construction *pENODL8::Sluc-3'UTR.* Étant donné qu'*ENODL8* est un gène régulé à la baisse, ce qui ne facilite pas une approche par gène rapporteur, une option prometteuse serait de développer un rapporteur de P en utilisant d'autres candidats qui sont régulés à la hausse par le P.

Les signaux Sluc lumineux dans les plantes portant la construction *pNCED3::Sluc-3'UTR* (osmo-rapporteur) sont visibles dans l'hypocotyle et les cotylédons sous des stress hydriques sévères (SWD), ce qui suggère qu'il s'agit d'un rapporteur compétent pour les changements hydrauliques causés par une forte intensité de stress. Son initiation rapide est probablement due à la signalisation hydraulique provoquée par le SWD dans les tissus vasculaires, car son activité promotrice se localise également ici (Christmann et al., 2013; Yang and Tan, 2014). Cet osmo-rapporteur pourrait également être utilisé pour évaluer la disponibilité en eau du sol sans avoir besoin d'accéder aux racines.

L'osmo-rapporteur a répondu rapidement et quantitativement aux changements précoces de P causés par le déficit hydrique modéré (MWD), ce qui suggère qu'il s'agit d'un bon rapporteur pour P. Le site de détection des changements de P causés par le MWD dans les racines d'Arabidopsis pourrait être la partie médiane de la racine principale. Cependant, nous n'avons pas pu visualiser les signaux Sluc avec notre configuration actuelle de caméra CCD sous des traitements avec des concentrations "faibles" de NaCl (<75 mM). Des études ont révélé que la plasmolyse est essentielle pour une accumulation significative d'ABA (Vaahtera et al., 2019), et notre étude a confirmé que la

plasmolyse des cellules corticales à la fin de la zone méristématique de la racine principale perturbait la régulation de l'expression de nos gènes candidats. Étant donné que nous n'avons pas mesuré la pression de turgescence des cellules corticales dans la partie ancienne de la racine principale, il est possible qu'elles aient été plasmolysées par les traitements de MWD avec une concentration relativement élevée. Par conséquent, nous ne pouvons pas exclure que la zone d'expression que nous avons identifiée soit le site de perception de la plasmolyse plutôt que des changements de P. Comme objectif à moyen terme, il serait nécessaire de confirmer si les cellules corticales dans la partie plus ancienne de la racine principale sont plasmolysées sous de tels traitements.

Des études ont montré que la signalisation de l'ABA dans les cellules corticales de la zone d'élongation, et une distribution asymétrique des cytokinines dans la zone méristématique, sont essentielles pour l'hydrotropisme (Dietrich et al., 2017; Chang et al., 2019). De façon coïncidente, l'activité du promoteur *pENODL8* se localise dans les cellules épidermiques et corticales de la partie jeune de la racine principale et des racines latérales, y compris la zone d'élongation et la fin de la zone méristématique. Cependant, nous n'excluons pas la possibilité que la réponse de notre osmo-rapporteur débute également dans ces zones sous MWD ou des conditions similaires, avec une distribution d'eau hétérogène. Néanmoins, ces résultats renforcent l'idée que la zone d'élongation et la zone méristématique sont des sites de perception du déficit hydrique. La fusion d'un rapporteur d'ARN fluorescent indépendant de la protéine, 3WJ-4 × Bro (Bai et al., 2020), avec la structure *pENODL8::sp-GFP-ENODL8-3'UTR* serait bénéfique pour générer un rapporteur de P plus spécifique. Par ailleurs, pour élaborer une carte de perception avec une haute résolution au niveau cellulaire, il serait vivement recommandé de créer de nouveaux vecteurs, tels que *pNCED3::NLS-GFP-3'UTR* (NLS représentant un signal de localisation nucléaire, pour des signaux plus lumineux). Enfin, il sera utile d'explorer les éléments régulateurs minimaux de l'osmo-rapporteur, par une approche de suppression sur les séquences *pNCED3* et 3'-UTR.

Conclusion

Le travail de thèse présenté ici a contribué à un projet initial, appelé "watermarkers", qui visait à développer des marqueurs du potentiel hydrique (Ψ) et/ou du stress hydrique chez Arabidopsis, afin de décrypter la perception et la signalisation précoce du déficit hydrique chez les plantes. Les analyses transcriptomiques ont révélé quelques gènes spécifiquement corrélés à Π et/ou P. Dans les 30 minutes suivant les traitements MWD, l'EG, qui réduit Π comme tout autre osmolyte mais

entraîne une perte de turgescence réduite, a été utilisé pour distinguer les réponses à Π de celles de P. Cette distinction a efficacement délimité la corrélation quantitative entre les réponses transcriptionnelles globales l'une ou l'autre des composantes du potentiel hydrique, ou à leur variation. Plus précisément, nous avons découvert *ENODL8*, un gène corrélé à P et régulé à la baisse, et *NCED3*, un gène corrélé à Π et régulé à la hausse.

En comparant l'expression d'*ENODL8* et de *NCED3* après des traitements MWD et SWD pendant 15 minutes, nous avons constaté que la plasmolyse des cellules corticales dans la zone d'élongation de la racine principale modifiait leur schéma de réponse en matière d'expression. En surveillant leur expression lors d'un traitement à long terme, nous avons découvert qu'*ENODL8* montrait une réponse quantitative correspondant très bien aux variations dynamiques de P, tandis que *NCED3* ne présentait qu'une réponse quantitative aux variations de P dans les 30 minutes. En étudiant leur expression chez Arabidopsis dans différents contextes génétiques en cas de déficit hydrique, ou lors d'un traitement par de la cordycépine, nous avons constaté que le déficit hydrique régulait leur expression à la fois au niveau transcriptionnel et post-transcriptionnel.

Nous avons montré que la construction *pNCED3::Sluc-3'UTR* sert de rapporteur fiable non seulement pour détecter les réductions précoces de P causées par le MWD, mais aussi pour surveiller les variations de Π et de niveaux d'ABA sur quelques heures. Nous l'avons provisoirement appelé un "osmo-rapporteur". L'initiation de sa réponse au déficit hydrique est indépendante de l'ABA et de l'intégrité de la paroi cellulaire. Associées à l'activité promotrice liée au gène corrélé à P *ENODL8*, nos découvertes suggèrent que les sites de perception de la contrainte hydrique pourraient se situer dans les zones d'élongation du méristème, ainsi qu'à la partie médiane de la PR sous MWD, et dans l'hypocotyle et les cotylédons sous SWD. La prochaine étape consisterait à améliorer la luminosité et la résolution de l'imagerie de l'osmo-rapporteur, et d'explorer le mécanisme de régulation de l'expression d'*ENODL8*.

En conclusion, les connaissances acquises grâce à ce projet fournissent un outil utile pour identifier les acteurs moléculaires impliqués dans la perception du déficit hydrique dans les racines, et les intégrer aux réseaux de signalisation du stress déjà connus. Une extension de ce projet consisterait à transposer les résultats issus de nos recherches aux plantes d'intérêt agronomique.

Références

Bai J, Luo Y, Wang X, Li S, Luo M, Yin M, Zuo Y, Li G, Yao J, Yang H, et al (2020) A protein-independent fluorescent RNA aptamer reporter system for plant genetic engineering. Nat Commun 11: 3847

Boursiac Y, Protto V, Rishmawi L, Maurel C (2022) Experimental and conceptual approaches to root water transport. Plant Soil 478: 349–370

Chang J, Li X, Fu W, Wang J, Yong Y, Shi H, Ding Z, Kui H, Gou X, He K, et al (2019) Asymmetric distribution of cytokinins determines root hydrotropism in Arabidopsis thaliana. Cell Res 29: 984–993

Chantarachot T, Sorenson RS, Hummel M, Ke H, Kettenburg AT, Chen D, Aiyetiwa K, Dehesh K, Eulgem T, Sieburth LE, et al (2020) DHH1/DDX6-like RNA helicases maintain ephemeral half-lives of stress-response mRNAs. Nat Plants 6: 675–685

Christmann A, Grill E, Huang J (2013) Hydraulic signals in long-distance signaling. Curr Opin Plant Biol 16: 293–300

Christmann A, Hoffmann T, Teplova I, Grill E, Müller A (2005) Generation of Active Pools of Abscisic Acid Revealed by In Vivo Imaging of Water-Stressed Arabidopsis. Plant Physiol 137: 209–219

Claeys H, Van Landeghem S, Dubois M, Maleux K, Inzé D (2014) What Is Stress? Dose-Response Effects in Commonly Used in Vitro Stress Assays. Plant Physiol 165: 519–527

Dietrich D, Pang L, Kobayashi A, Fozard JA, Boudolf V, Bhosale R, Antoni R, Nguyen T, Hiratsuka S, Fujii N, et al (2017) Root hydrotropism is controlled via a cortex-specific growth mechanism. Nat Plants 3: 17057

Dinneny JR, Long TA, Wang JY, Jung JW, Mace D, Pointer S, Barron C, Brady SM, Schiefelbein J, Benfey PN (2008) Cell Identity Mediates the Response of Arabidopsis Roots to Abiotic Stress. Science 320: 942–945

Fukuda M, Wakuta S, Kamiyo J, Fujiwara T, Takano J (2018) Establishment of genetically encoded biosensors for cytosolic boric acid in plant cells. Plant J 95: 763–774

Kawa D, Testerink C (2017) Regulation of mRNA decay in plant responses to salt and osmotic stress. Cell Mol Life Sci 74: 1165–1176

Kumar SV, Wigge PA (2010) H2A.Z-Containing Nucleosomes Mediate the Thermosensory Response in Arabidopsis. Cell 140: 136–147

Mielke S, Zimmer M, Meena MK, Dreos R, Stellmach H, Hause B, Voiniciuc C, Gasperini D (2021) Jasmonate biosynthesis arising from altered cell walls is prompted by turgor-driven mechanical compression. Sci Adv 7: eabf0356

Miller G, Schlauch K, Tam R, Cortes D, Torres MA, Shulaev V, Dangl JL, Mittler R (2009) The Plant NADPH Oxidase RBOHD Mediates Rapid Systemic Signaling in Response to Diverse Stimuli. Sci Signal 2: ra45–ra45

Shabala SN, Lew RR (2002) Turgor Regulation in Osmotically Stressed Arabidopsis Epidermal Root Cells. Direct Support for the Role of Inorganic Ion Uptake as Revealed by Concurrent Flux and Cell Turgor Measurements. Plant Physiol 129: 290–299

Soma F, Mogami J, Yoshida T, Abekura M, Takahashi F, Kidokoro S, Mizoi J, Shinozaki K, Yamaguchi-Shinozaki K (2017) ABA-unresponsive SnRK2 protein kinases regulate mRNA decay under osmotic stress in plants. Nat Plants 3: 16204

Soma F, Takahashi F, Suzuki T, Shinozaki K, Yamaguchi-Shinozaki K (2020) Plant Raf-like kinases regulate the mRNA population upstream of ABA-unresponsive SnRK2 kinases under drought stress. Nat Commun 11: 1373

Sorenson RS, Deshotel MJ, Johnson K, Adler FR, Sieburth LE (2018) Arabidopsis mRNA decay landscape arises from specialized RNA decay substrates, decapping-mediated feedback, and redundancy. Proc Natl Acad Sci 115: E1485–E1494

Steinhorst L, He G, Moore LK, Schültke S, Schmitz-Thom I, Cao Y, Hashimoto K, Andrés Z, Piepenburg K, Ragel P, et al (2022) A Ca2+-sensor switch for tolerance to elevated salt stress in Arabidopsis. Dev Cell 57: 2081-2094.e7

Vaahtera L, Schulz J, Hamann T (2019) Cell wall integrity maintenance during plant development and interaction with the environment. Nat Plants 5: 924–932

Yang Y-Z, Tan B-C (2014) A Distal ABA Responsive Element in AtNCED3 Promoter Is Required for Positive Feedback Regulation of ABA Biosynthesis in Arabidopsis. PLOS ONE 9: e87283

Yuan F, Yang H, Xue Y, Kong D, Ye R, Li C, Zhang J, Theprungsirikul L, Shrift T, Krichilsky B, et al (2014) OSCA1 mediates osmotic-stress-evoked Ca 2+ increases vital for osmosensing in Arabidopsis. Nature 514: 367–371

Zhu J-K (2016) Abiotic Stress Signaling and Responses in Plants. Cell 167: 313–324